

博士論文

**Evaluation of degradation and evolution of crack-bridging
performance of fibers under flexural fatigue in SFRC structural
beams**

(SFRC梁の曲げ疲労载荷下における繊維架橋効果の減少と
発現の評価)

アデル モーハーメッド

Mohamed Adel Mohamed Abdelnabi

A dissertation submitted to
The University of Tokyo
in partial fulfillment of the requirements for
The Degree of Doctor of Philosophy

Supervisor

Associate Professor: Kohei Nagai

Department of Civil Engineering
The University of Tokyo
Tokyo, Japan

August 2020

Acknowledgments

First of all, I would like to express my profound gratitude to my supervisor associated professor Kohei NAGAI for his relentless support, encouragement, and advice during this research. I am particularly grateful to him for his patience in reviewing the draft chapters. This thesis would not have been completed without his continuous guidance. I sincerely thank him for ensuring uninterrupted support to me.

My thanks are also due to my laboratory colleagues at the Institute of Industrial Science Concrete Laboratory, The University of Tokyo. I would especially like to thank associate professor Koji Matsumoto, DR. Tomohisa Kamada, Dr. Tomohisa Kamada, Mr. Punyawut Jiradilok, Mr. Tanaka Shunsei, Mr. Yokoyama Yuki, Mr. Suzuki, Mr. Gaddam Pruthvi, Mr. Vikas Kuntal, Mr. Ahmed Aki, Mr. Vi Soth, Mr. Abdul Mannan, and Mr. Ahmed Okiel for their assistance and advice during all the tests in past few years.

I am very thankful to the colleagues and friends at the School of Civil and Environmental Engineering for making the research period joyful, especially, Dr. Tomohisa Kamada, Dr. Salim Ibrahim, Mr. Abdul Mannan, Mr. Ahmed Aki, and Mr. Vi Soth. I would also like to thank Mr. Gaddam Pruthvi, Mr. Suzuki and Mr. Tanaka Shunsei for their assistance in the experimental works.

Abstract

Among several modes of failure in reinforced concrete (RC) structural members such as bridge girders and slabs, the fatigue failure is associated with progressive, permanent, and localized internal changes in the material caused by repeated stresses. Consequently, the fatigue design and safety of RC structures give many concerns to sustain millions of repeated cyclic loads over a specified design lifetime, avoiding any kind of structural failure and undesired degradation on the material strength particularly the rupture failure of ordinary reinforcing steel bars. Incorporating steel fibers in concrete, steel fiber reinforced concrete (SFRC) exhibit an improved flexural fatigue performance in a manner of higher strength and longer fatigue life, through the additive toughness strength and fracture energy comparing to normal concrete (NC). Accordingly, the bridging mechanism induced by fibers, that involves the transfer of tensile stress from the matrix to the fibers by interfacial bonding or/and by interlock between the fibers and matrix for the deformed shape fibers, is necessary to be evaluated.

This research focuses on the evaluation of the crack-bridging strength induced by steel fibers from the structural experimental response of SFRC beams subjected to cyclic loading using the sectional analysis calculations inversely. A review of the literature reveals that fatigue is a limiting design consideration for structures. This research work aims to understand the degradation and evolution mechanism of the crack-bridging strength under a wide range of fatigue stress levels with constant and various amplitude cyclic loading through increasing or decreasing the maximum fatigue load levels over the whole fatigue life of SFRC structural beams with different material and steel fibers properties.

Firstly, the degradation in crack-bridging strength of SFRC structural beams with 1.5% by volume of single hooked-end steel fibers under constant amplitude cyclic loading for different flexural fatigue stress levels is evaluated over the fatigue life using an inverse analysis method. The experimental flexural response is monitored during static and fatigue tests, and compared with the calculated one from the section analysis calculations through the execution of the inverse analysis method. Based on the results, the crack-bridging strength is shown to degrade gradually at different flexural fatigue stress levels over the fatigue life. As well, the crack-bridging strength degradation regarding the evolution of the maximum rebar strain relationship is provided, having a constant linear degradation mechanism regardless of the fatigue stress levels. Further, the residual flexural capacity at the end of fatigue life is shown to be little

different from the original capacity obtained in static loading when the flexural fatigue stress level is low.

As structures are subjected to variable amplitude cyclic loading during their service life, in reality, wherein crack-bridging strength induced by steel fibers influences by the preceding loading history and remains unexplored. Secondly, research work is carried out to present an experimental investigation of SFRC structural beams with 1.5% by volume of hooked-end steel fibers under variable amplitude flexural fatigue loading. By utilizing the inverse analysis method with section analysis calculations, a crack-bridging degradation and evolution diagram were captured while increasing and decreasing the fatigue load level over the fatigue life. The result showed that the crack-bridging strength is increasing while increasing the maximum fatigue load level during fatigue life, which indicates the contribution of a new part of fibers in resisting the tensile stress as the crack opening. On the other hand, decreasing the maximum fatigue load level leads to a decrease followed by stabilizing the crack-bridging strength because of lower pullout stresses on the resisting fibers. Further, a crack-bridging degradation and evolution diagram regarding the evolution of maximum rebar strain is proposed, which would be a valuable tool in the flexural fatigue design and assessment of SFRC structural beams.

Finally, a parametric study was carried out to study the effect of changing material properties such as concrete compressive strength, beam's reinforcement ratio, and fiber's geometry and volume fraction on the proposed crack-bridging degradation and evolution diagram. The increased concrete compressive strength resulted in a lower degradation rate of the evaluated crack-bridging strength regarding the evolution of maximum rebar strain. The decreased reinforcement ratio resulted in a lower degradation rate of the evaluated crack-bridging strength regarding the evolution of maximum rebar strain. The lowered volume fraction of double hooked-end steel fibers resulted in a higher degradation rate of the evaluated crack-bridging strength regarding the evolution of maximum rebar strain, with the insignificant effect of the fiber's hooks level. A little change in the degradation rate of crack-bridging was observed due to the enhancement in the material properties.

List of Publications

The following publications has been written as a part of this dissertation:

M. Adel, K. Nagai, K. Matsumoto (2019). Simplified Design Approach of Steel fiber reinforced Concrete under Flexural Fatigue Load, 10th International Conference on Fracture Mechanics of Concrete and Concrete Structures FraMCoS-X, France.

M. Adel, P. Jiradilko, K. Matsumoto, K. Nagai. Evaluation of crack-bridging strength degradation in SFRC structural beams under flexural fatigue, Composite Structures 244 (2020) 112267.

Table of Contents

| | |
|--|-----|
| Acknowledgments..... | i |
| Abstract..... | iii |
| List of Publications | v |
| Table of Contents..... | vii |
| Notation..... | x |
| 1 Introduction | 1 |
| 1.1 General | 1 |
| 1.2 Research Motivation | 4 |
| 1.3 The Hypothesis of the Study | 5 |
| 1.4 Research objectives | 5 |
| 1.5 General outline | 6 |
| 2 Literature Review | 10 |
| 2.1 Introduction | 10 |
| 2.2 Fatigue of Reinforced Concrete | 11 |
| 2.2.1 General..... | 11 |
| 2.2.2 Fatigue of Steel Reinforcing bar | 12 |
| 2.2.3 Fatigue of Plain Concrete..... | 13 |
| 2.2.4 Fatigue of RC at Structural Scale..... | 15 |
| 2.2.5 Design Guidelines for RC Structural Members under Fatigue..... | 15 |
| 2.3 Fatigue of Steel Fiber Reinforced Concrete..... | 16 |
| 2.3.1 General..... | 17 |
| 2.3.2 Fatigue of SFRC at Material Scale | 18 |
| 2.3.3 Fatigue of SFRC at Structural Scale | 20 |
| 2.4 Conclusion..... | 21 |
| 3 Constitutive Flexural Analysis of SFRC Structural Beams..... | 22 |
| 3.1 Introduction | 22 |
| 3.2 Material Constitutive laws | 22 |
| 3.2.1 Steel Rebar in Tension | 22 |
| 3.2.2 SFRC in Compression..... | 23 |

| | | |
|-------|--|-----|
| 3.2.3 | SFRC in Tension (Crack-bridging Strength) | 24 |
| 3.3 | Inverse Analysis Method..... | 30 |
| 3.3.1 | General..... | 30 |
| 3.3.2 | Previous Studies on The Inverse Analysis Method | 30 |
| 3.3.3 | Computation of The Inverse Analysis Method..... | 31 |
| 3.4 | Conclusion..... | 34 |
| 4 | Evaluation of Crack-bridging Strength of SFRC Structural Beams under Flexural Fatigue Constant Load Level | 35 |
| 4.1 | Introduction | 35 |
| 4.2 | Sectional Analysis Calculations | 35 |
| 4.3 | Experimental Program..... | 37 |
| 4.3.1 | Material and Mix Proportion | 39 |
| 4.3.2 | Mixing, Casting and Curing of Concrete..... | 41 |
| 4.3.3 | Specimens | 43 |
| 4.3.4 | Testing Setup and Instrumentations..... | 45 |
| 4.4 | Experimental Results..... | 47 |
| 4.4.1 | Prismatic Specimens under Flexural Static Loading | 48 |
| 4.4.2 | Static Flexural Loading of SFRC Structural Beam..... | 49 |
| 4.4.3 | Fatigue Flexural Loading of SFRC Structural Beams | 53 |
| 4.4.4 | Fatigue Flexural Loading of RC Structural Beams..... | 63 |
| 4.5 | Discussion on The Evaluated Crack-bridging Strength | 67 |
| 4.6 | Conclusion..... | 70 |
| 5 | Evaluation of Crack-bridging Strength of SFRC Structural Beams under Variable Amplitude Flexural Cyclic loading..... | 72 |
| 5.1 | Introduction | 72 |
| 5.2 | Experimental Program..... | 72 |
| 5.2.1 | Material and Mix Proportion | 74 |
| 5.2.2 | Specimens | 75 |
| 5.3 | Experimental Results..... | 75 |
| 5.3.1 | Prismatic Specimens under Flexural Static Loading | 77 |
| 5.3.2 | Fatigue Flexural Loading of SFRC Structural Beams | 78 |
| 5.4 | Discussion on The Evaluated Crack-bridging Strength | 90 |
| 5.4.1 | Evaluated Crack-bridging Strength of The Second Series | 90 |
| 5.4.2 | Crack-bridging Strength Degradation and Evolution diagram | 99 |
| 5.5 | Conclusion..... | 102 |

| | | |
|-------|--|-----|
| 6 | Material Properties Effect on The Crack-bridging Strength Degradation and Evolution of SFRC Structural Beams under Flexural Fatigue..... | 104 |
| 6.1 | Introduction | 104 |
| 6.2 | Experimental Program..... | 105 |
| 6.2.1 | Material and Mix Proportion | 106 |
| 6.2.2 | Specimens | 107 |
| 6.3 | Experimental Results..... | 108 |
| 6.3.1 | Prismatic Specimens under Flexural Static Loading | 108 |
| 6.3.2 | Fatigue Flexural Loading of SFRC Structural Beams | 111 |
| 6.4 | Results Discussion..... | 141 |
| 6.4.1 | Experimental Flexural Fatigue Response | 141 |
| 6.4.2 | Evaluated Crack-bridging Strength of The Third Series | 150 |
| 6.4.3 | Crack-bridging Strength Degradation and Evolution diagram | 160 |
| 6.5 | Conclusion..... | 169 |
| 7 | Fiber’s Volume and Shape Effect on The Crack-bridging Strength Degradation of SFRC Structural Beams under Flexural Fatigue | 171 |
| 7.1 | Introduction | 171 |
| 7.2 | Experimental Program..... | 172 |
| 7.2.1 | Material and Mix Proportion | 173 |
| 7.2.2 | Specimens | 175 |
| 7.2.3 | Testing Setup and Instrumentations..... | 177 |
| 7.3 | Experimental Results..... | 179 |
| 7.3.1 | Dog-bone SFRC Specimens under Uniaxial Tensile Loading | 180 |
| 7.3.2 | Static Flexural Loading of SFRC Structural Beam..... | 184 |
| 7.3.3 | Fatigue Flexural Loading of SFRC Structural Beams | 190 |
| 7.4 | Results Discussion..... | 210 |
| 7.4.1 | Experimental Flexural static Response | 210 |
| 7.4.2 | Experimental Flexural Fatigue Response | 215 |
| 7.4.3 | Evaluated Crack-bridging Strength of The fourth Series | 219 |
| 7.5 | Conclusion..... | 224 |
| 8 | Conclusions | 227 |
| 8.1 | General Conclusions | 227 |
| 8.2 | Recommendations for the Further Study | 232 |
| | References..... | 234 |

Notation

| | |
|-----------------|--|
| FRC | Fiber reinforced concrete |
| f_y | Steel rebar yield stress |
| E_s | Steel modulus of elasticity |
| SFRC | Steel fiber reinforced concrete |
| f_{cm} | Concrete compressive strength |
| E_c | Concrete modulus of elasticity |
| ϵ_{cu} | Ultimate concrete strain |
| G_f | Fracture energy |
| LDP | Load point displacement |
| f_{st} | Concrete first cracking splitting tensile strength |
| P_{crk} | Concrete first cracking load |
| A | Area of specimen interface |
| NC | Normal concrete |
| LVDT | linear variable displacement transducer |
| CTOD | crack tip opening displacement |
| RC | Reinforced concrete |
| M_{ext} | External bending moment |
| M_{int} | Internal bending moment |
| H | Cross-sectional depth |
| Σ | Stress transfer across the crack |
| Ω | Crack opening displacement |

| | |
|------------|--|
| E | Strain |
| L_R | Reference length |
| $F_{int.}$ | Internal force |
| $F_{ext.}$ | External force |
| N.A. | Neutral axis |
| N_1 | The first cycle of flexural fatigue load |
| N_f | The failure cycle of flexural fatigue load |
| α_i | Degradation level of crack-bridging strength at the i th loading cycle |
| β_i | Normalized crack-bridging strength at the i th loading cycle |
| S | Maximum fatigue stress level |
| N | Number of load cycles |
| N_f | Number of cycles until failure |
| M | The stress range exponent |
| K | The fatigue life constant |
| l_{ch} | Characteristics length |
| S | Constant moment loading span |
| L | Span length |
| D | Effective depth |
| D | Nominal diameter |
| JIS | The Japanese industrial standards |
| $P_{max.}$ | The maximum compressive load |
| UTM | Universal testing machine |

Chapter 1

1 Introduction

1.1 General

Reinforced concrete (RC) is the most widely available material used in the construction of structures. Reinforced concrete is a combination of concrete and steel reinforcing bars. Plain concrete has higher compressive strength and durability, however, it is very weak in tension resulting in the development of cracks when load gives rise to tensile stress excess of the tensile strength of concrete. Therefore, steel reinforcing bars that have a higher tensile strength are added in the tensile zone to carry all the developed tensile stresses after concrete cracks. The addition of steel reinforcing bars that bonds strongly to concrete produce a relatively ductile material capable of transmitting tension stress, on the other hand, concrete provides excellent corrosion protection for steel reinforcing bars

Among the different types of failure in reinforced concrete structural members, the fatigue failure is well known as damage in material or structures caused by repeated cyclic loading. From an engineering point of view, fatigue is an important loading condition in terms of assessing the existing structures and in designing the new structures to sustain millions of repeated cyclic loads over a specified design life. Therefore, concerns about the fatigue design and safety of reinforced concrete (RC) structures such as bridge girders, deck slabs, or offshore installations, which are subjected to cyclic loading forces, have recently arisen. These structures are expected to withstand millions of stress cycles resulting from repeated loading during their service life. As a result, the fatigue performance of these structures has to be considered to avoid structural fatigue failure (Schläfli 1998, Barnes 1999, Tong 2016, Loo 2012, Charalambidi 2016) and undesired influence on material characteristics, including static strength, deflection, stiffness, toughness, durability, stress level, etc. (Schläfli 1998, Liu 2018), which might be significant under service loading even in the absence of fatigue failure.

As a result, a wide range of tests have been carried out on the fatigue response of concrete and reinforced concrete, both on material and structural scale, during the 20th century (CEB 1988, Mallett 1991), however, the influence of fatigue on the response of reinforced concrete is yet to be completely understood (Zanuy 2009). The research results show that fatigue in concrete is characterized by:

- Loss of stiffness leading to increased deflection
- Growths in the crack widths and lengths
- Increasing in strain permanently

Fatigue of concrete is a process of progressive changes in the material that may lead to microcracks initiation and propagation, followed by the formation of macrocracks that grow, until the resisting sectional area is reduced and concrete stress is permanently reduced. This eventually leads to failure (Gao 1998, Horii 1992, Kolluru 2000). The mechanism of concrete under repeated cyclic loading starts with the loss of the bond between cement paste and aggregate. Cracks then propagate through the mortar until they are arrested by the presence of aggregate. As this process repeats, failure ultimately occurs when the strain energy released overcomes the remaining cohesive strength of the concrete (CEB 1988, Mallett 1991). In the case of reinforced concrete (RC), cyclic loads cause microcracking that affects the stress concentration around the steel reinforcing bars, followed by crack propagation, and finally leading in most cases to rupture of the rebar (Schläfli 1998, Barnes 1999, Tong 2016, Loo 2012, Charalambidi 2016, Liu 2018).

Additionally, the performance of an RC structural member is affected by the composite interaction between steel reinforcing bars and the surrounding concrete (Lee 2011). Experimental results have shown that the governing fatigue failure mode of RC structural members is a brittle rupture of the steel reinforcing bars even in the case of higher compressive stresses (Loo 2012, Johansson 2004) because of concrete's capacity to redistribute stresses to less-fatigued regions inside the compression zone (Schläfli 1998, Barnes 1999, Heffernan 2004, Zanuy 2007, 2009). As a consequence, for the equilibrium condition to be maintained, the rebars suffer higher stresses, eventually leading to rebar fracture. In contrast, increasing the rebar area in RC beams to reduce rebar stress levels leads to over-reinforced beams, and this can eventually lead to compressive fatigue failure of the concrete, especially under higher stress levels (Zanuy 2009).

Steel fiber reinforced concrete (SFRC) is a composite material reinforced with discrete, uniformly distributed, and randomly oriented steel fibers. By adding fibers, the mechanical properties of quasi-brittle cement-based materials, including ductility, durability, energy absorption, fatigue, and toughness, can be improved at the material scale through their ability to arrest cracks growth and transfer tensile stress (Bentur 2007, Olivito 2010, Tejchman 2010). In particular, the flexural fatigue performance is improved with SFRC material beams exhibiting improved strength and longer fatigue life as a function of fibers volume fraction and aspect ratio (Lee 2004, Singh 2008, Goel 2014).

Additionally, the performance of SFRC structural members is affected by the tensile stresses developed in rebars, tensile stress-induced from steel fibers by bridging cracks, and the bond mechanism between the rebars and the concrete matrix (Lee 2013). Numerous experimental studies have explored the behavior of SFRC members at the structural scale under monotonic and static loading and shown them to have higher capacity than RC members (Meda 2012, Özcan 2009, Altun 2007). Recently, a few studies have been carried out to investigate the fatigue performance of SFRC structural beams (Kormeling 1980, Parvez 2015), which concluded that there is a substantial reduction of average tensile stresses in the rebar compared with the RC member, contributing to the observed increase in fatigue life. This phenomenon is explained by the crack-bridging ability of the steel fibers, by which they carry a portion of the load in the tensile zone. However, this crack-bridging strength degraded over the fatigue life under cyclic loading, leading to an incremental increase in rebar stress level, eventually leading to rebar rupture (Parvez 2015).

It is worthwhile noting that an understanding of post-cracking behavior in tension – the crack-bridging strength – and toughness properties is essential when optimizing the structural design of SFRC members (RILEM 2002). As a result, standard procedures and specifications are well established at a material-level under static tests, resulting in a tension softening curve that expresses the stress-crack opening relationship (JCI 2003, EN 2007, ASTM 2010, Su-Tae 2010). In contrast, the fatigue tensile behavior of SFRC structural members is determined by the degradation of the fiber's contribution in carrying tensile stress during the fatigue life. A few studies have been carried out to investigate the degradation in SFRC constitutive laws under fatigue compression and direct tension tests at the material scale have been performed (Zhang 2000, Otter 1988). However, these studies do not reflect the mechanical response at the structural scale through changes in bond mechanics due to composite interaction between

rebars, the surrounding concrete, and fibers in tensile stress zone (Lee 2013), nor concrete's capacity to redistribute stresses in the compression stress zone (Heffernan 2004, Zanuy 2007, 2009).

In this research study, a model of crack-bridging strength degradation during cyclic loading is derived to obtain a rational understanding of the mechanical response of SFRC structural beams under flexural cyclic loading at each set of cycles during the fatigue life. The basis of the model is inverse sectional analysis calculations.

1.2 Research Motivation

To promote wide use of steel fiber reinforced concrete in the construction of structures, an accurate understanding of the fatigue behavior for fiber reinforced concrete structural members is crucial. Nevertheless, the degradation level of crack-bridging strength induced by fibers that are incorporated in the tensile zone with steel reinforcing bars is still unknown. Also, there is a lack of guidelines for the fatigue design of fiber reinforced concrete beams. It is because the influence of steel fibers on the fatigue resisting mechanism of FRC beams with steel reinforcing bars have not been completely understood.

While numerous research works have been carried out for material and structural scale reinforced concrete beams with steel fibers. The experimental investigations have focused exclusively on the static and fatigue response of the material scale beams (Bentur 2007, Olivito 2010, Tejchman 2010, Lee 2004, Singh 2008, Goel 2014). Besides, a few studies have been carried out to investigate the static and fatigue performance of SFRC structural beams (Meda 2012, Özcan 2009, Altun 2007, Kormeling 1980, Parvez 2015). The available studies; however, have been performed without understanding and providing a degradation mechanism of the crack-bridging strength of fiber reinforced concrete leading mostly to an evolution in the rebar strain level, ending by a rupture failure of the steel reinforcing bars. As a result, fatigue design guidelines have not been satisfactorily quantified yet. To overcome this shortcoming, the experimental flexural response is monitored during static and fatigue tests, and compared with the calculated one from the section analysis calculations through the execution of the inverse analysis method to evaluate the degradation of crack-bridging strength over the fatigue life.

Also, the investigations on the steel reinforcing bars stress level evolution concerning the degradation of the crack-bridging strength over the fatigue life have been conducted. Such a

relationship would be helpful for the assessment of the fatigue response of the existing SFRC structures with the monitoring of the surface concrete cracks. Finally, to cover the effect of different parameters such as concrete compressive strength, beam reinforcement ratio, fiber volume, and fibers shapes, that may influence on the degradation crack-bridging model, to be considered.

1.3 The Hypothesis of the Study

Unlike direct sectional analysis, which aims at a prediction of structural response using specified constitutive material laws, the inverse analysis method has the objective of determining the degradation model of crack-bridging strength from the experimental response of actual structures. The principles of the inverse technique for deriving stress-averaged strain relationships of tensile concrete using experimental data of flexural members. The initial crack-bridging strength (tension softening curve) is assumed to degrade proportionally with a certain level (α) during the fatigue life of an SFRC structural beam under flexural cyclic loading.

Computations are iterated for the incremental set of fatigue cycles (N_i) until reaching the fatigue life (N_f), which is marked by fatigue rupture or two million cycles. After each increment (N_i), a certain degradation (α_i) of equivalent crack-bridging strength is assigned to adjust the balance between the experimental and calculated results. If the calculated and experimental results agree within the set threshold, the degree of degradation of crack-bridging strength (α_i) is derived. Finally, the degradation of crack-bridging strength normalized to the initial crack-bridging strength.

The proposed degradation model can be set up to predict the same average experimental response as obtained in tests, leading to accurate estimation of the rebar stress level that controls fatigue rupture of the SFRC structural beam, through a simplified design methodology, and ensuring compatibility with the evolution of strain levels and deformations during the fatigue life of the SFRC structure.

1.4 Research objectives

The main objectives of this study are:

To evaluate the crack-bridging strength degradation model of SFRC structural beams under flexural cyclic loading for several fatigue stress levels over the fatigue life.

To evaluate the crack-bridging strength degradation model concerning the maximum steel reinforcing bar strain evolution of SFRC structural beams under flexural cyclic loading for different fatigue stress levels.

To evaluate the crack-bridging strength recovery rate of SFRC structural beams by increasing the flexural load monotonically after a certain degradation by flexural fatigue loading from different fatigue stress levels over the fatigue life.

To investigate the effect of concrete compressive strength, beam's reinforcement ratio, hooked level, and fiber's volume fraction of steel fibers on the crack-bridging strength degradation model over the fatigue life for different fatigue stress levels.

To propose appropriate recommendations for the fatigue design and assessment of SFRC structural beams under different fatigue stress levels.

1.5 General outline

It is obvious from the above discussion that the main aim of this research study is to provide a degradation and recovery model for the crack-bridging strength induced by hooked steel fibers in the tensile stress zone of SFRC structural beams under flexural cyclic loads. Moreover, it is a fact that the structures subjected to cyclic loading such as bridges are experienced different fatigue load stress levels where the crack-bridging strength is expected to change related to loading levels that have to be evaluated and captured. The proposed models cover a wide range of the experimental data that counted the effect of concrete compressive strength, beam's reinforcement ratio, hooked level, and fiber's volume fraction of steel fibers on the crack-bridging strength degradation models. The general scheme for this study is shown in [Fig. 1.1](#).

The outline of the research can be mentioned as followed:

Chapter 1

In this chapter, a brief introduction to motivations and the hypothesis of this research are given. Also, the objectives of this research work were provided.

Chapter 2

Through this chapter, the current literature has been reviewed on the fatigue in general, fatigue behavior of plain concrete, reinforced concrete, and steel fiber reinforced concrete. Relevant

design guidelines for RC structures under fatigue loads are also presented. A knowledge gap in the current understanding of the fatigue behavior of SFRC structural beams is identified, leading to providing a simplified model for fatigue design of the structures through the presented research work.

Chapter 3

In this chapter, the methodology for the evaluation of the crack-bridging strength of SFRC structural beams under flexural fatigue loading is provided. Firstly, the material level tests are introduced to investigate the material constitutive laws from the tensile strength of steel reinforcing bars to the tensile and compressive strength of FRC following the current design guidelines. Secondly, the sectional analysis calculations method is discussed that could be used to analyze the flexural response of concrete structural beams using the material constitutive laws. Finally, the execution of the inverse analysis method is explained to evaluate the crack-bridging strength induced by steel fibers over the fatigue life of SFRC structural beams under flexural cyclic loading.

Chapter 4

Through this chapter, the experimental program for the first series of NC and SFRC beams on material and structural scale under static and fatigue loading conditions is presented. Firstly, the material properties, mix proportion, specimen's geometry, testing setup, and measuring instruments are explained. Secondly, the experiment fatigue response data of structural beams are captured to be used in the execution of the inverse analysis calculation method. Finally, the crack-bridging strength is evaluated for the first series of SFRC structural beams under a single flexural fatigue load level over their fatigue life varying from a low, medium, to high fatigue stress level.

Chapter 5

In this chapter, the experimental program for the second series of SFRC beams on the structural scale under flexural cyclic loading conditions is presented. Through this series, the structural SFRC beam is tested under different flexural fatigue load levels during its fatigue life ranging from low, medium, high, to ultrahigh stress levels in an increasing or decreasing manner. Then, the experiment fatigue response data of structural beams are captured to be used in the execution of the inverse analysis calculation method. Finally, the crack-bridging strength is

evaluated for the second series of SFRC structural beams, and the changing mechanism of the proposed crack-bridging strength is captured by increasing or decreasing the fatigue load levels.

Chapter 6

Through this chapter, the experimental program for the third series of SFRC beams on the structural scale under flexural cyclic loading conditions is presented. In this series, the effect of higher concrete compressive strength and lower beam's reinforcement ratio on the proposed degradation model of crack-bridging strength is countered. Structural SFRC beams are tested under single and different flexural fatigue load levels during its fatigue life ranging from low, medium, high, to ultrahigh stress levels in an increasing manner. Then, the experiment fatigue response data of structural beams are captured to be used in the execution of the inverse analysis calculation method. Finally, the crack-bridging strength is evaluated for the third series of SFRC structural beams, and the changing mechanism of the proposed crack-bridging strength is captured and compared with the first and second series.

Chapter 7

Through this chapter, the experimental program for the fourth series of SFRC beams on the structural scale under flexural cyclic loading conditions is presented. In this series, the effect of lower fiber's volume fraction with a double hooked level of steel fibers on the proposed degradation model of crack-bridging strength is countered. Structural SFRC beams are tested under static and single flexural fatigue load levels during its fatigue life ranging from low, medium, high, to ultrahigh stress levels in an increasing manner. Then, the experiment fatigue response data of structural beams are captured to be used in the execution of the inverse analysis calculation method. Finally, the crack-bridging strength is evaluated for the fourth series of SFRC structural beams, and the changing mechanism of the proposed crack-bridging strength is captured and compared with the first and second series.

Chapter 8

Finally, the major conclusions from the presented study are drawn together and recommendations for further studies are given.

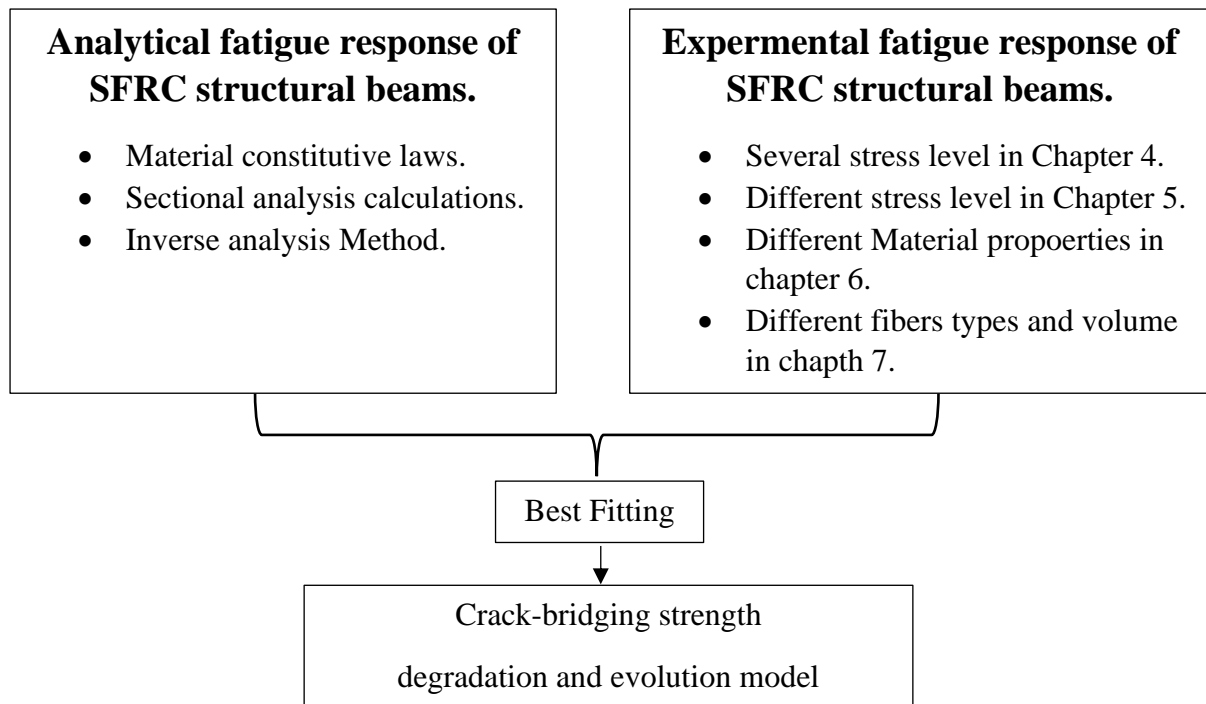


Fig. 1.1 Research strategy.

Chapter 2

2 Literature Review

2.1 Introduction

The fatigue process is referred to as the damage in the materials or the structures caused by the exposure to repeated cyclic loading during the structural life. From the engineering point of view, the fatigue behavior of the structures plays an important role in the assessing process of the existing structures and the design process of the new structures to sustain repeated cycles of loading over the structures designed lifetime. Therefore, many Concerns about the fatigue design and safety of RC structures such as bridge girders and deck slabs, which are subjected to cyclic loading forces, have recently arisen. These structures are expected to withstand millions of stress cycles resulting from repeated loading during their service life. The fatigue performance of these structures has to be considered to avoid structural fatigue failure and undesired influence on material characteristics, including static strength, deflection, stiffness, toughness, durability, stress level, etc., which might be significant under service loading even in the absence of fatigue failure (Schläfli 1998, Barnes 1999, Tong 2016, Loo 2012, Charalambidi 2016, Liu 2018).

Fiber reinforced concrete (FRC) is a composite material between a plain concrete, that defined as a brittle material, reinforced with discrete, uniformly distributed, and randomly oriented fibers. Fibers can be made of steel, polymers, carbon, glass, or natural materials. By adding fibers, the mechanical properties of quasi-brittle cement-based materials, including ductility, durability, energy absorption, flexural strength, impact resistance, fatigue, and toughness, can be improved and the deflection, crack width, shrinkage, and creep can be decreased through their ability to arrest cracks growth and transfer tensile stress between cracks (Bentur 2007, Olivito 2010, Tejchman 2010, Lee 2004). In particular, the current research work interest is limited to the fatigue performance of steel fiber reinforced concrete (SFRC).

The flexural fatigue performance is improved with SFRC material beams exhibiting improved strength and longer fatigue life as a function of fibers volume fraction and aspect ratio. Several experimental research works were carried out on the SFRC at the material scale to investigate the enhanced fatigue performance compared to normal plain concrete (Lee 2004, Singh 2008, Goel 2014). Recently, a few studies have been undertaken with SFRC beams at structural scale to evaluate its fatigue performance (Kormeling 1980, Parvez 2015), which their results showed a substantial reduction in the rebar stress level compared with RC structural, leading to the observed longer fatigue life. This phenomenon is explained by the ability of the steel fibers in crack-bridging, by which they carry a portion of the tensile stress in the tensile zone. However, this crack-bridging strength degraded over the fatigue life under cyclic loading, leading to an incremental increase in rebar stress level, eventually leading to rebar rupture (Parvez 2015).

This chapter summarizes the previous research work in the field of fatigue behavior of both normal and steel fiber reinforced concrete at material and structural scale to assess a better understanding and to identify the effect of fiber's crack-bridging strength over the fatigue life of SFRC structural beams.

2.2 Fatigue of Reinforced Concrete

Fatigue of the structural element is declared as a tendency of a material deterioration process to fracture through a progressive cracking under repeated stress cycles that have a lesser intensity than the normal strength. The mechanism of concrete under repeated cyclic loading starts with the loss of the bond between cement paste and aggregate. Followed by crack propagation through the mortar until they are arrested by the presence of aggregate. As this process repeats, failure ultimately occurs when the strain energy released overcomes the remaining cohesive strength of the concrete (CEB 1988, Mallett 1991). In the case of reinforced concrete, repeated loads cause microcracking that affects the stress concentration around the rebar, followed by crack propagation, and finally leading in most cases to rupture of the rebar (Schläfli 1998, Barnes 1999, Tong 2016, Loo 2012, Charalambidi 2016, Liu 2018).

2.2.1 General

The fatigue features of the reinforced concrete structural members have a wide variance across the structural element as fatigue is influenced by the stress level of its components such as the steel reinforcing bars and concrete across each section (CEB 1988). Besides, the effect of the

composite interaction between the steel reinforcing bar and the surrounding concrete has a great effect on the fatigue response of reinforced concrete (Mallett 1991). Depending on the design concern of the reinforced concrete members, the failure mechanism under the flexural cyclic loading could be ranging from the brittle rupture failure of the steel reinforcing bars for the under reinforced structural members (Johansson 2004; Loo et al. 2012) to flexural or shear failure for the over reinforced structural members.

2.2.2 Fatigue of Steel Reinforcing bar

The fatigue resistance capacity of the steel reinforcing bar strongly depends on the stress range ($\Delta\sigma$), that indicates the difference between the maximum stress (σ_{\max}) and the minimum stress (σ_{\min}), rather than the level of σ_{\max} . The fatigue behavior of steel reinforcing bar passes through three stages: crack initiation, steady crack propagation, and brittle rupture failure (Schläfli 1998). The cracking process under cyclic loading starts with micro-cracks that grow to macro-cracks by the application of the load. At a critical crack length, the cracking process becomes unstable leading to sudden rupture.

Two different tests are used to investigate the fatigue performance of the steel reinforcing bar through by either testing it axially in the air or by bending in concrete (CEB 1988). However, carrying out the bending tests in concrete is closer to the practical performance, the axial tests are more convenient. The fatigue failure in the steel reinforcing bar is initiated by stress concentration on the rebar-matrix interface, resulting in loss of the bond between rebar and concrete (Mallet 1991).

Several research works were carried out to investigate the fatigue performance of steel reinforcing bars in air and concrete as well, also the parametric study was carried out to capture the most important factor affecting the crack initiation process (Tilly 1988; Moss 1982). The results showed that the rib pattern and the bar diameter are the most governing parameters, where the larger bars having less fatigue resistance due to the higher probability of flaws being present in the material (CEB 1988). The fatigue life of the reinforcing steel bar could be expressed in terms of S-N relationship as:

$$(\Delta\sigma)^m N_f = K \quad (2.1)$$

Where N_f is the number of cycles until failure, $\Delta\sigma$ is the stress range for a constant amplitude loading, m is the stress range exponent, and K is the fatigue life constant.

2.2.3 Fatigue of Plain Concrete

Fatigue of concrete is a process of progressive changes in the material that may lead to micro-cracks initiation and propagation, followed by the formation of macrocracks that grow, until the resisting sectional area is reduced and concrete stress is permanently reduced. This eventually leads to failure (Gao 1998, Horii 1992, Kolluru 2000). The mechanism of concrete under repeated cyclic loading starts with the loss of the bond between cement paste and aggregate. Cracks then propagate through the mortar until they are arrested by the presence of aggregate. As this process repeats, failure ultimately occurs when the strain energy released overcomes the remaining cohesive strength of the concrete (CEB 1988, Mallett 1991).

The stress-strain behavior of concrete under several repetitive loading, changing from concave towards the strain axis to a straight line and then to a convex form as shown in Fig. 2.1 (Holmen 1982). The degree of convexity indicates the higher probability of concrete to failure (CEB 1988). The strain evolution during the fatigue life consists of three stages, the first stage shows a rapid increase in strains up to 10% of fatigue life. In this stage, the micro-crack initiation starts with a deterioration of the bond between the mortar and the aggregate, followed by a uniform increase of the strain from 10% to 80% of the fatigue life due to steady growth of cracks indicating the end of the second stage. The third stage shows a rapid increase in strain until failure.

Concrete is a non-homogenous material due to the heterogeneity of its constituents, inherently concrete contains flaws. As a result, repeated loading initiate and accelerate the cracking process, leading to the failure of the material below its static strength. Stress concentration in concrete is caused by pores, inclusions, or an interface between distinct material phases. There are three fracture modes of failure: the opening mode or mode I, in-plane shear or mode II, and out-of-plane shear or mode III, where the most common mode for concrete is the mode I because of its inherent weakness in tension.

The fictitious crack model is used for the description of the fracture process of concrete including a process zone at the tip of the visible crack. At the visible crack location, there are no tensile stress is transmitted, however at the micro-cracking zone the tensile stress could be transmitted that so-called fictitious crack. The fictitious crack model is shown in Fig. 2.2 (Van Mier 2013). The pre-peak relationship of stress-strain is stated for an uncracked zone where the concrete is expected to exhibit linear elastic behavior. The concrete cracks as soon as the

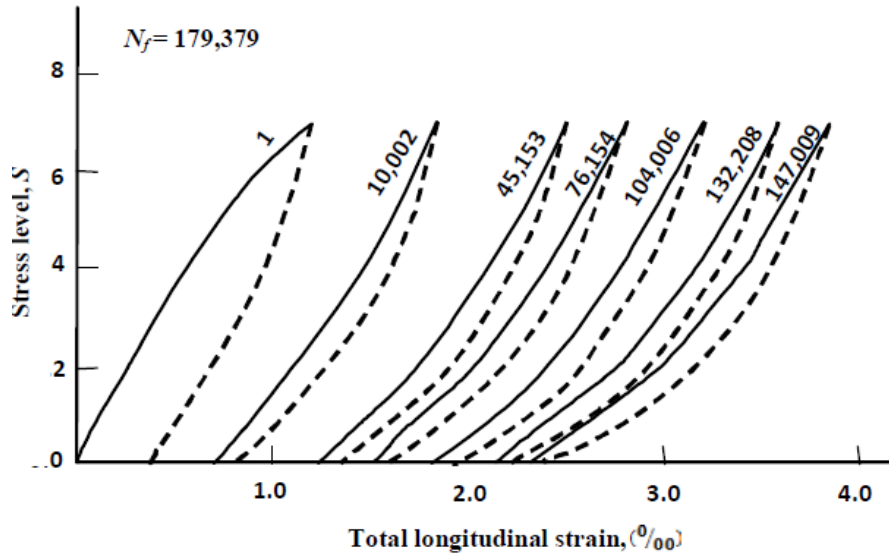


Fig. 2.1 Cyclic stress-strain curve for concrete in compression (Holmen 1982).

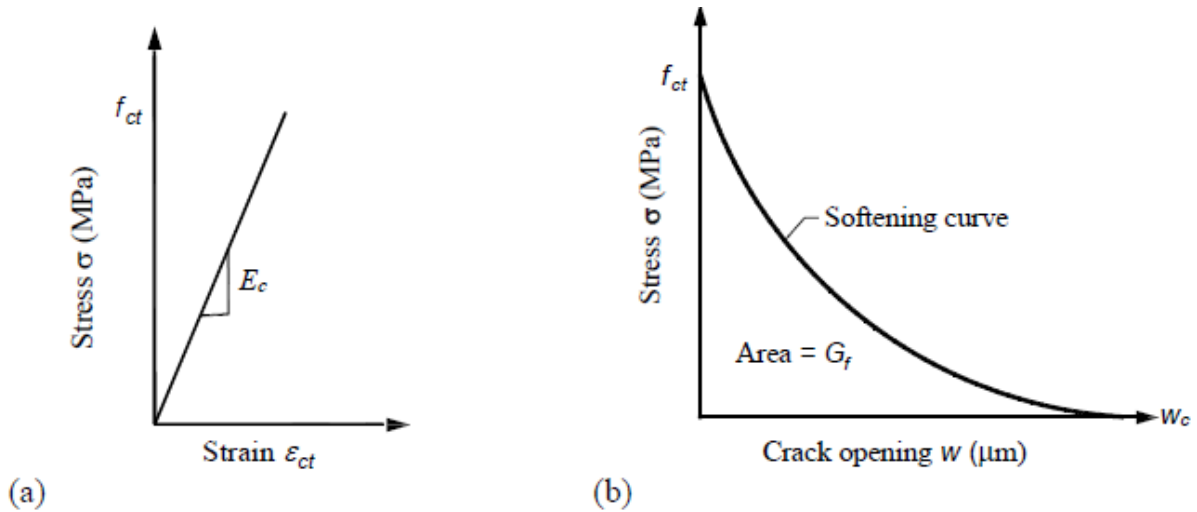


Fig. 2.2 Fictitious crack model: (a) pre-peak stress-strain curve (b) post-peak stress-crack opening diagram (Van Mier 2013).

tensile strength reached and then followed by a softening regime depending on the degree of fracture energy (G_f).

The two important quantities of the fictitious crack model are the fracture energy (G_f) and the characteristic length (l_{ch}). The fracture energy is defined as the amount of energy needed to create one unit crack area and is equal to the area under the softening curve of Fig. 2.2b where higher fracture energy indicates higher ductility. On the other hand, the characteristic length (l_{ch}) is a measurement of the brittleness of the concrete, that I would depend on the ratio between the fracture energy and concrete tensile strength for constant stiffness. Kolluru et al. (2000) reported that the rate of fatigue crack growth in concrete exhibits a deceleration stage followed by an acceleration stage. In the first stage, the rate of crack growth decreases with

increasing crack length, whereas in the second stage there is a steady increase in crack growth rate up to failure. Several factors affecting the rate of fatigue crack growth in concrete such as concrete composition variables, maximum and minimum stress level, load amplitude, loading frequency, and the size of the specimen (CEB 1988, Mallett 1991, Zhang 2001).

2.2.4 Fatigue of RC at Structural Scale

For reinforced concrete structural members, after cracking the steel reinforcing bar carries the tensile stress. Concrete under service conditions has different stresses ranging from compression stress up to their ultimate tensile strength level. As a result, the fatigue tendency will vary throughout the structure depending upon stress level. Cracks resulting from fatigue will propagate and lead to excessive deformations and redistribution of stresses, resulting in different types of failure under fatigue in comparison to that of failure obtained under static load. According to (CEB 1988), if the quality of steel and concrete is uniform, their fatigue performance can be estimated quite precisely by testing them independently and the same performance should be observed while they are tested as a composite material.

Several tests have been carried out to understand the fatigue behavior of reinforced concrete structural members (CEB 1988, Mallett 1991, Moss 1982, Loo 2012). That research work was aimed to study the effect of different parameters on the fatigue performance of RC structural beams such as span length, cross-section, reinforcement ratio, and compression reinforcement ratio. The result showed that under fatigue loading concrete compressive strains increase, with a significant softening of concrete due to racking effects from progressive growth of microcracks. This leads to an increase in tensile strain in steel. The average concrete strain at the level of the reinforcing steel increases with the increasing number of cycles and the rate of change accelerated to near the end of the test. Also, it was noted that fatigue life increases as the stress range in the reinforcing steel reduces.

2.2.5 Design Guidelines for RC Structural Members under Fatigue

Most of the design guidelines such as the fib Model Code 2010 (Fib 2013) provides design recommendations for the fatigue of reinforced concrete structural members based on the individual performance of concrete and steel reinforcing bar using S-N curves and their equations. But, an accurate model could be accomplished by understanding the interaction between the steel reinforcing bar and the surrounding concrete under fatigue loading. Experiments have shown that brittle rupture of the steel reinforcing bar is the dominant failure

mechanism for fatigue in reinforced concrete structural beams, even though for the over reinforced structural members (Schläfli 1998; Mallett 1991) different than the one under static loading. This highlights how the failure mechanism that is observed in static failure can be different from that produced in fatigue failure.

2.3 Fatigue of Steel Fiber Reinforced Concrete

Steel fiber reinforced concrete (SFRC) is a composite material reinforced with discrete, uniformly distributed, and randomly oriented steel fibers. The introduction of fibers into concrete was originally intended to enhance the tensile strength of the concrete matrix, by delaying the widening of micro-cracks but without consideration for material toughness (Li 2002). As a result, the mechanical properties of quasi-brittle cement-based materials, including ductility, durability, energy absorption, fatigue, and toughness, can be improved at the material scale through their ability to arrest cracks growth and transfer tensile stress (Bentur 2007, Olivito 2010, Tejchman 2010).

In particular, the flexural fatigue performance is improved with SFRC material beams exhibiting improved strength and longer fatigue life as a function of fibers volume fraction and aspect ratio (Lee 2004, Singh 2008, Goel 2014). The gained advantages in FRC over plain concrete depend on the size, shape, aspect ratio, volume fraction, concentration, orientation and surface characteristics of fibers, the ratio between fiber length and maximum aggregate size, and the concrete strength (Zollo 1997).

Additionally, the performance of SFRC structural members is affected by the tensile stresses developed in rebars, tensile stress-induced from steel fibers by bridging cracks, and the bond mechanism between the rebars and the concrete matrix (Lee 2013). Several experimental research works have investigated the behavior of SFRC members at the structural scale under monotonic and static loading and with a higher capacity than RC members (Meda 2012, Özcan 2009, Altun 2007).

Recently, a few studies have been carried out to investigate the fatigue performance of SFRC structural beams (Kormeling 1980, Parvez 2015), which concluded that there is a substantial reduction of average tensile stresses in the rebar compared with the RC member, contributing to the observed increase in fatigue life. This phenomenon is explained by the crack-bridging ability of the steel fibers, by which they carry a portion of the load in the tensile zone. However,

this crack-bridging strength degraded over the fatigue life under cyclic loading, leading to an incremental increase in rebar stress level, eventually leading to rebar rupture (Parvez 2015).

Understanding the post-cracking tensile strength – the crack-bridging strength – and toughness properties is important while utilizing it in the structural design of SFRC members (RILEM 2002). As a result, standard procedures and specifications are well established at a material-level under static tests, resulting in a tension softening curve that expresses the stress-crack opening relationship (JCI 2003, EN 2007, ASTM 2010, Su-Tae 2010). In contrast, the fatigue tensile behavior of SFRC structural members is determined by the degradation of the fiber's contribution in carrying tensile stress during the fatigue life. A few studies have been carried out to estimate the degradation in SFRC constitutive laws under fatigue compression and direct tension tests at the material scale (Zhang 2000, Otter 1988). However, these studies do not reflect the mechanical response at the structural scale through changes in bond mechanics due to composite interaction between rebars, the surrounding concrete, and fibers in tensile stress zone (Lee 2013), nor concrete's capacity to redistribute stresses in the compression stress zone (Heffernan 2004, Zanuy 2007, 2009).

2.3.1 General

Fiber reinforced concrete (FRC) is a composite material that has a cement matrix and discrete, uniformly distributed, and randomly oriented fibers. The fiber's material could be steel, polymers, carbon, glass, or natural materials. The mechanism of the fibers involves the transfer of stress from the matrix to the fibers by interfacial bonding or by interlock between the fibers and matrix for the deformed shape fibers. The tensile stress is shared between fibers and matrix at the pre-cracking stage. Once the concrete matrix cracked when the tensile stress reached to the tensile strength limit, the tensile stress transfers over the crack through fibers. The failure mode of FRC is either bond failure between fibers and matrix in a pullout mode of the fibers from the matrix or material failure in a rupture mode of fibers, as shown in Fig. 2.2 (Zollo 1997).

During the fiber pull-out process, the resistance to crack propagation and widening depends primarily on the transmission of forces between the fiber and the matrix. This is achieved through the bond, and this characterizes the interface mechanics between the fiber and the surrounding matrix. Alwan et al. (Alwan 1999) listed the constituents of the fiber-matrix bond as chemical adhesion, frictional resistance, and bond due to mechanical anchorage.

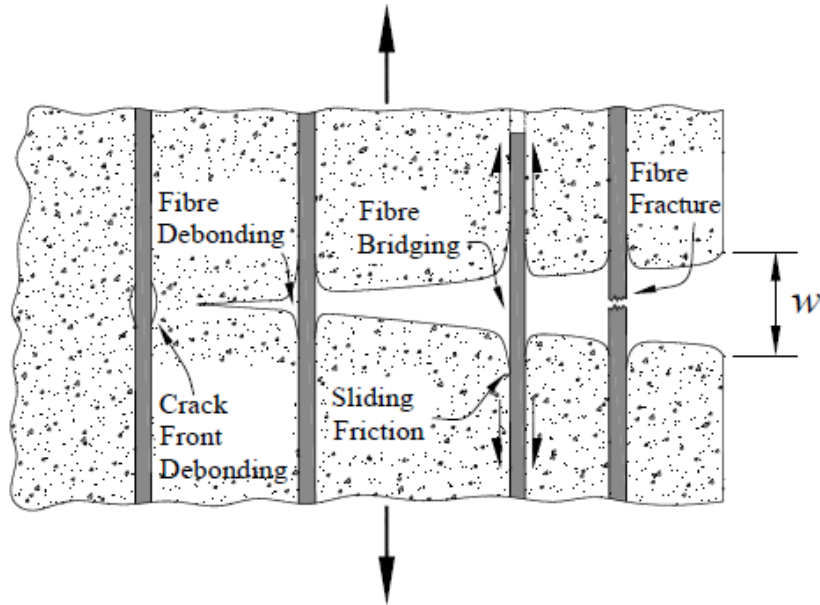


Fig. 2.3 Fiber-Matrix pullout mechanism (Zollo 1997).

The mechanical properties of a cementitious matrix are improved when the fibers are added especially the tensile strength that increased by almost 40 percent. The fibers can improve the post-cracking behavior and modify the brittle behavior to ductile behavior. There is a great improvement in the fracture energy and toughness, however, it depends on the fiber types and volume fraction. To predict the behavior of FRC members, a wide range of experiments have been conducted and are discussed in the following section.

2.3.2 Fatigue of SFRC at Material Scale

The use of FRC in engineering applications has furthered the need for the study of its behavior under fatigue loading, which endures significant cyclic loading during their service life. Within these areas of application, the fatigue characteristics of FRC are important performance and design parameters. However, there are a lot of influencing variables such as type of loading cycle, strain rates, and fiber parameters. Generally, it has been observed that the addition of steel fibers can significantly improve the bending fatigue performance of concrete members. The extent of improvement in the fatigue capacity of FRC can be expected to depend upon the fiber volume content, fiber type, and geometry. Various combinations of these parameters will give rise to different fatigue characteristics.

In this section, the results of fatigue experiments on the concrete specimens with the addition of steel fibers are described in detail. The experiments have been carried out mainly in the last

20 years by different researchers. The attention is given to the advantageous properties of SFRC in fatigue as compared to plain concrete.

Zhang et al. (2000)

Zhang et al. investigated the crack bridging behavior of SFRC with two types of commercially available steel fibers under uniaxial fatigue tensile load with constant amplitude between a minimum and maximum crack width. In this study, two types of commercially available steel fibers, smooth and hooked-end, with circular cross-sections, 0.4 and 0.5 mm in diameter, 25 and 30 mm in length, respectively, were used separately in the same matrix.

The experimental results show that the bridging stress decreases with the number of load cycles, and this phenomenon is termed bridging degradation. The general behavior of the bridging degradation with the number of cycles in SFRC is represented by a fast dropping stage (reduction in bridging stress within the first 10–15 cycles) with a decelerated degradation rate, followed by a stable stage with an almost constant degradation rate for straight SFRC, or by several periods with a decelerated rate in each period for hooked SFRC. Although fiber deformation, such as in hooked end fiber, can improve the monotonic crack bridging significantly, faster bridging degradation is found in hooked SFRC than in straight SFRC with the same maximum crack width (>0.1 mm) and minimum load condition.

Lee and Barr (2004)

Lee and Barr provided a general overview of recent developments in the study of the fatigue behavior of plain concrete and FRC and commented that the understanding of fatigue failure in cementitious composites is still lacking in comparison to that of ferrous materials. The parameters like loading conditions, load frequency, boundary conditions, stress level, number of cycles, matrix composition, stress ratio influence the fatigue performance of concrete specimens. However, the quantitative and qualitative nature of these parameters on the fatigue performance of concrete is yet to be agreed in the literature.

Singh et al. (2006)

Singh et al. carried out an extensive experimental program to study the fatigue performance of SFRC containing fibers of mixed aspect ratio. They conducted 90 flexural fatigue tests on SFRC specimens with fiber contents 1.0, 1.5, and 2.0 percent. Each volume fraction of fibres

incorporated corrugated mixed steel fibers of size 0.6 x 2.0 x 25 mm and 0.6 x 2.0 x 50 mm in the ratio of 50:50 by weight. The specimens were cast in 9 batches, each batch consisting of 14 fiber concrete prisms of size 100 x 100 x 500 mm, four of which were tested under static flexural load and the remaining 10 were tested under flexural fatigue load at different stress levels.

Singh et al. (2006) used their data to plot the S-N diagram and derived fatigue equations for predicting the flexural fatigue strength of SFRC. It was observed that an increase in fiber content improves fatigue strength significantly. The two-million-cycle fatigue strength for plain concrete was 58 percent of static strength, whereas, for SFRC containing fibers of mixed aspect ratio the fatigue life for 2×10^6 cycles were 72 percent, 65 percent and 62 percent of the static flexural strength for 1.0, 1.5, and 2.0 percent fibers (by volume), respectively. The best performance (24 percent increase over plain concrete) was given by SFRC containing 1.0 percent by volume fibers. When the fatigue performance is examined in terms of actually applied fatigue stress, increasing fiber volumetric content from 0 to 2.0 percent seems to improve the performance in terms of the applied maximum fatigue stress. For example, the 2×10^6 fatigue strengths were 5.3, 5.5, and 5.5 MPa for fiber contents 1.0, 1.5, and 2.0 percent by volume, respectively, whereas it was 3.1 MPa for plain concrete.

2.3.3 Fatigue of SFRC at Structural Scale

The fatigue performance of SFRC at the structural level has not received much attention. Kormeling et al. (1980) conducted the only study found in the journal literature on the fatigue of reinforced concrete beams with fibers. The objective of their tests was to study the influence of steel fibers on the fatigue performance of conventionally reinforced concrete beams. The experimental program of Kormeling et al. (1980) included 46 beams (27 of them tested in fatigue and 19 in static) of 2200 mm in length and a span of 2000 mm. The cross-section was 100 x 152 mm. The beams were reinforced with three different reinforcement ratios, 0.17, 0.75, and 2.09 percent, and were provided by using two-4 mm, four-6 mm, and four-10 mm diameter bars, respectively. Three different types of steel fibers were used: straight fibers, hooked-end fibers, and paddle-end fibers with the fiber contents of 1.27, 0.89, and 1.54 percent, respectively. Beams without fibers were taken as control specimens for each group of tests. The fatigue test results of the beams containing four longitudinal bars with a diameter of 10 mm. In all cases, failure was due to the fracturing of the longitudinal steel reinforcement.

It was observed that the addition of steel fibers increased the number of cycles to failure and that the general characteristics of the fiber performance exhibited in the static tests were valid for the fatigue tests. The addition of fibers resulted in improved ductility, reduced deflections, smaller crack widths, and lower stresses in longitudinal reinforcement.

The recent research work was done by Ahsan (2015) where his research work looks into the behavior of SFRC beams and sleepers subjected to cyclic loading. In the experimental program, twelve (out of sixteen) reinforced concrete beams with fiber volume fractions 0.4 and 0.8 percent, and eight prestressed sleepers with fiber volume fractions 0.25 and 0.5 percent were tested under constant amplitude cyclic loading. Steel and concrete strains, crack widths, and deflections were measured. The results of the SFRC specimens were compared to that of non-fiber reinforced specimens. The steel fibers prolonged the fatigue life in SFRC beams and sleepers by reducing the stress level in the tensile reinforcement. The SFRC beams and sleepers also demonstrated smaller deflections and crack widths than that of reinforced concrete beams and prestressed sleepers without fibers, respectively.

2.4 Conclusion

It is worthwhile noting that an understanding of post-cracking behavior in tension – the crack-bridging strength – and toughness properties is essential when optimizing the structural design of SFRC members (RILEM 2002). As a result, standard procedures and specifications are well established at a material-level under static tests, resulting in a tension softening curve that expresses the stress-crack opening relationship (JCI 2003, EN 2007, ASTM 2010, Su-Tae 2010). In contrast, the fatigue tensile behavior of SFRC structural members is determined by the degradation of the fiber's contribution in carrying tensile stress during the fatigue life. A few studies have been carried out to investigate the degradation in SFRC constitutive laws under fatigue compression and direct tension tests at the material scale have been performed (Zhang 2000, Otter 1988). However, these studies do not reflect the mechanical response at the structural scale through changes in bond mechanics due to composite interaction between rebars, the surrounding concrete, and fibers in tensile stress zone (Lee 2013), nor concrete's capacity to redistribute stresses in the compression stress zone (Heffernan 2004, Zanuy 2007, 2009).

Chapter 3

3 Constitutive Flexural Analysis of SFRC Structural Beams

3.1 Introduction

Fiber reinforced concrete (FRC) has been used over the last decades for the aim of improving the tensile strength of concrete, as the presence of closely spaced, discrete, uniformly distributed and randomly oriented fibers helps in the enhancement of the tensile load-crack width of concrete, that shows the brittle behavior in tension. The parameters proposed to describe the gaining fracture energy after cracking of the concrete (i.e. tension softening curve and crack-bridging strength) are used in this study. This chapter explains the constitutive flexural analysis of steel fiber reinforced concrete structural beams, through implementing the inverse analysis method based on sectional analysis calculations using the material constitutive laws for both concrete and steel rebar in tension and compression. Finally, the crack-bridging strength of hooked-end steel fibers in SFRC structural beams under flexural cyclic loading is proposed over the fatigue life.

3.2 Material Constitutive laws

For the execution of the sectional analysis calculation of the structural SFRC beams under flexural loading, material constitutive laws for steel rebar, and SFRC in compression and tension are required to be derived from the material-scale test.

3.2.1 Steel Rebar in Tension

The behavior of the steel rebar under tension is idealized as an elastoplastic material for examination as shown in [Fig 3.1](#). The yield strength (f_y) and the modulus of elasticity (E_s) are determined from the stress-strain curve. The specified strength used in the sectional analysis calculations is based on the yield stress (f_y) and with a modulus of elasticity (E_s) of 200 Gpa.

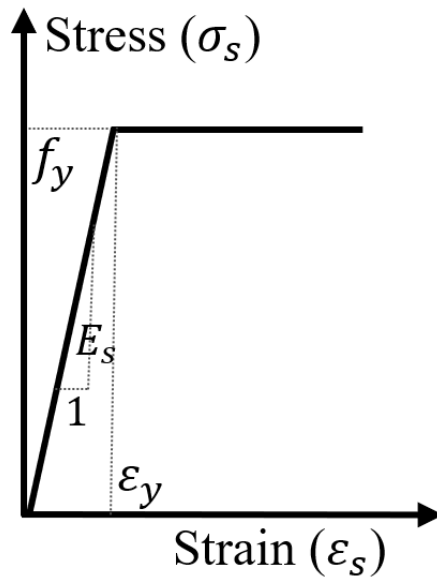


Fig. 3.1 Steel constitutive law in tension.

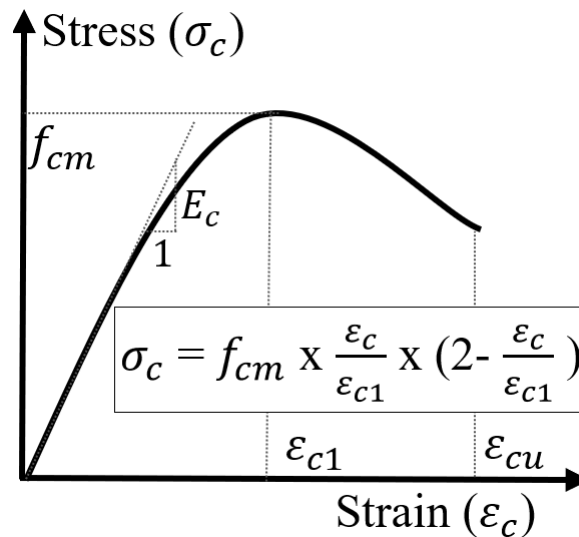


Fig. 3.2 Fiber reinforced concrete constitutive law in compression.

3.2.2 SFRC in Compression

Typical idealized stress-strain curves for steel fiber reinforced concrete in compression are shown in Fig. 3.2 following the Japanese standard specification for concrete structures (JSCE 2007). In these curves, a substantial increase in the strain at the peak stress (ϵ_{cu}) can be noted, and the slope of the descending portion is less steep than that of control specimens without fibers. The specified strength used in the sectional analysis calculations is based on the concrete compressive strength (f_{cm}) and concrete modulus of elasticity (E_c) measured by compression tests on 100 mm x 200 mm cylinders tested after 28 days of moist curing.

3.2.3 SFRC in Tension (Crack-bridging Strength)

The crack-bridging strength (tension softening curve) is one of the fracture mechanics parameters of fiber reinforced concrete (FRC). It is a relationship between tensile stress and crack-opening displacement in the fracture zone. The total area under the tension softening curve is defined as the fracture energy (G_f). The crack-bridging strength (tension softening curve) can describe the post-cracking behavior and express the concrete resistance against crack development of SFRC in the tensile zone, and used in the sectional analysis calculations to understand the response of structural beams to loading.

3.2.3.1 Splitting Tensile Strength of Fiber Reinforced Concrete

The splitting tensile test configuration used for the study is shown in Fig. 3.3(a). Using a loading strip with an 8.0 mm width to limit the size effect, as the size of the compression zone depends on the size of the loading strip (Denneman 2011). Two pi-gauges with 100 mm length attached in the center of both faces of the cylinder to record the transversal deformation perpendicular to the load direction during the test (Denneman 2011). Consequently, the experimental load-transversal deformation curves were obtained, that having two peaks, an initial one reflecting the tensile cracking load (P_{crk}) and a second peak due to secondary cracking as shown in Fig. 4. Finally, the first cracking tensile strength (f_{st}) obtained from the first cracking load that derived using Eq. (3.1). Differences in failure modes for both normal concrete (NC) and steel fiber reinforced concrete (SFRC) under splitting test from a complete separation for NC case and no separation for SFRC case because of fiber as shown in Fig. 3.3(b,c).

$$f_{st} = \frac{2 P_{crk}}{\pi A} \quad (3.1)$$

Where f_{st} is the first cracking splitting tensile strength (MPa), P_{crk} is the first cracking load (N), and A is the area of the specimen interface (mm^2).

3.2.3.2 Crack-bridging Strength from notched Beam Bending Test

The crack-bridging strength (tension softening curve) of fiber reinforced concrete with various types of fibers and fiber volume fraction were determined by notched beam test following JCI standard (2003a) (JCI 2003a) using a poly-linear approximation analysis method. Figure 3.5 shows the determination procedures of the crack-bridging strength (tension softening curve) from a 3-point bending test of the notched beams.

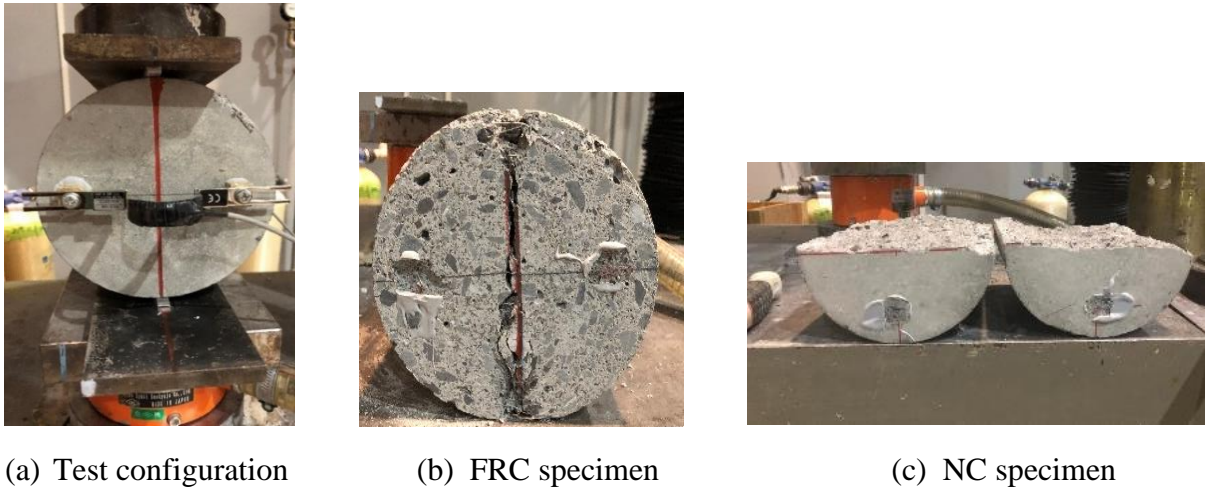


Fig. 3.3 Splitting tensile test.

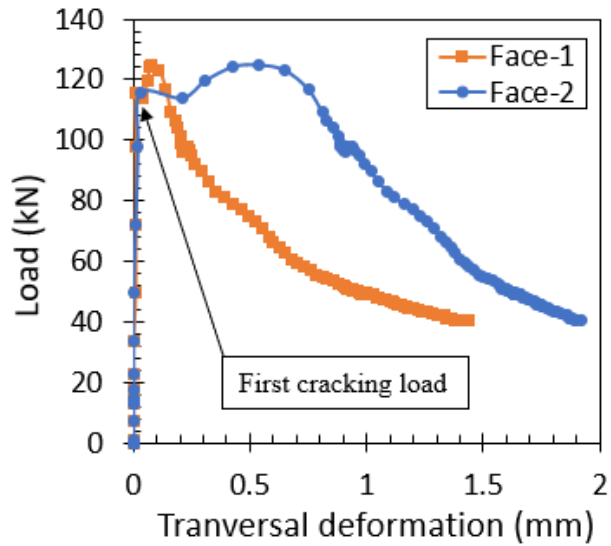


Fig. 3.4 Splitting tensile test result.

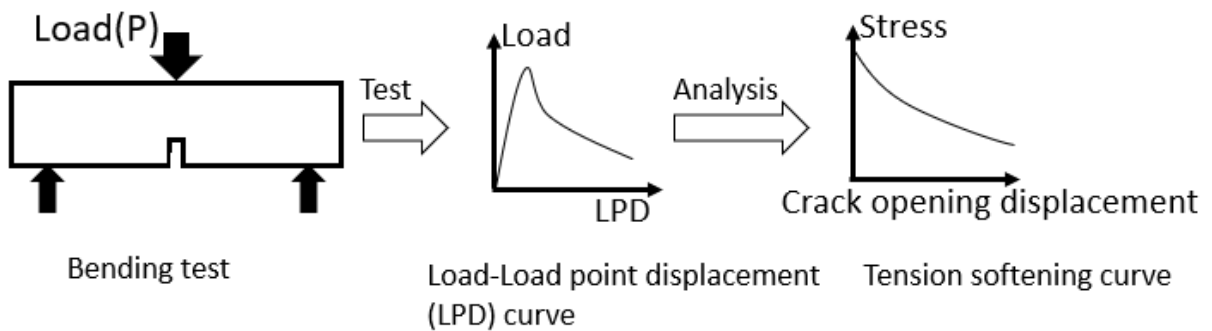


Fig. 3.5 Tension softening curve analyzed from the bending test

Specimens were a prismatic rectangular cross-section with a notch at a mid-length. The detail of the notched beams is illustrated in Fig. 3.6. the beams have a dimension of 100x100x400 mm with a notch of 5 mm width, 30 mm height, and span length of 300mm. six specimens of

notched beams were cast for one test series. For each series, cylinders with dimensions of 150 mm diameter and 300 mm height were cast and cured with the same condition as notched beam specimens to determine the splitting tensile strength of concrete (f_{st}).

Three-point loading tests of notched beams were conducted according to the JCI standard (2003a) (JCI 2003a). Both supports were hinged supports having rollers. The supports were horizontally movable to avoid any restraint on the deformation until the specimen completely ruptures. Figure 3.7 shows a notched beam under a 3-point flexural loading test. Two linear variable displacement transducers (LVDT) were used to measure the vertical displacement under the load point on the two specimen faces. The transducers were mounted on a rigid yoke accurately set up on the specimen to minimize the effect of rotation during the test. Two further pi-gauges were placed at the tip of the notch on the two faces of the specimen to measure the crack tip opening displacement (CTOD) as shown in Fig. 3.7.

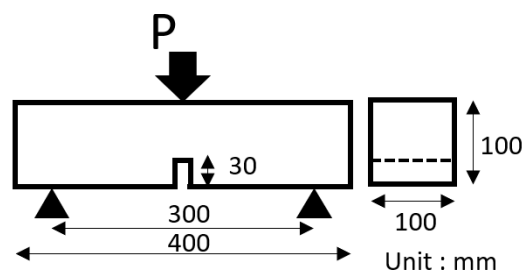
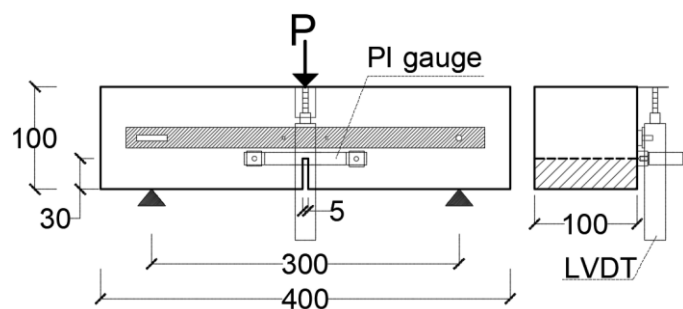


Fig. 3.6 Geometry of the notched beam specimen.



(a) Actual test setting



(b) Prismatic specimens geometry

Fig. 3.7 Bending test on the prismatic notched beam specimen.

The fracture behavior of concrete is related to the fracture process zone that consists of a microcracking and bridging zone as shown in Fig. 3.8. the bridging zone is a kind of macrocracking that the stress transfer across the cracks by partial matrix through the aggregate bridging. The crack-bridging strength (tension softening curve) is a material property describing the effect of fibers to transmit tensile stress across the cracks to the crack opening

displacement as shown in Fig. 3.5. The crack-bridging strength (tension softening curve) can be investigated from poly-linear approximation using the load-displacement curve obtained from mode I stable failure testing on notched specimens.

The JCI standard (2003a) (JCI 2003a) has recommended a program with confirmed reliability for the analysis of the crack-bridging strength (tension softening curve). The tension softening curve was estimated by using the program proposed by JCI (2003a), which has been developed by Prof. Uchida. The tension softening curve was estimated by poly-linear approximation using the average data of load-displacement curves obtained from six notched specimens following the analysis flow as shown in Fig. 3.9. the nonlinear finite element method (FEM) analysis was performed and obtained the analytical results.

The poly linear approximation method was carried out through modeling of a specimen and the elastic modulus of concrete was calculated from the initial slope of load-displacement obtained from the test results, then the FEM analysis was carried out. The initial tensile stress in the tension softening curve from the agreement between the analytical and experimental load-displacement curve. Next, the slope of the tip of the tension softening curve was assumed and changed to determine the optimum slope depending on the agreement between the analytical and experimental load-displacement curve. Finally, the final tension softening curve has been used as a constitute model for the FRC in tension.

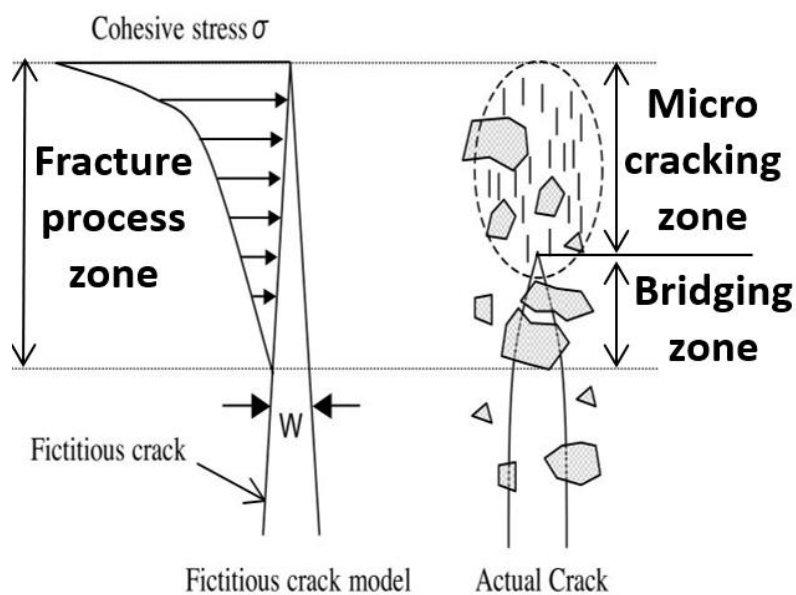


Fig. 3.8 Fracture process zone of concrete.

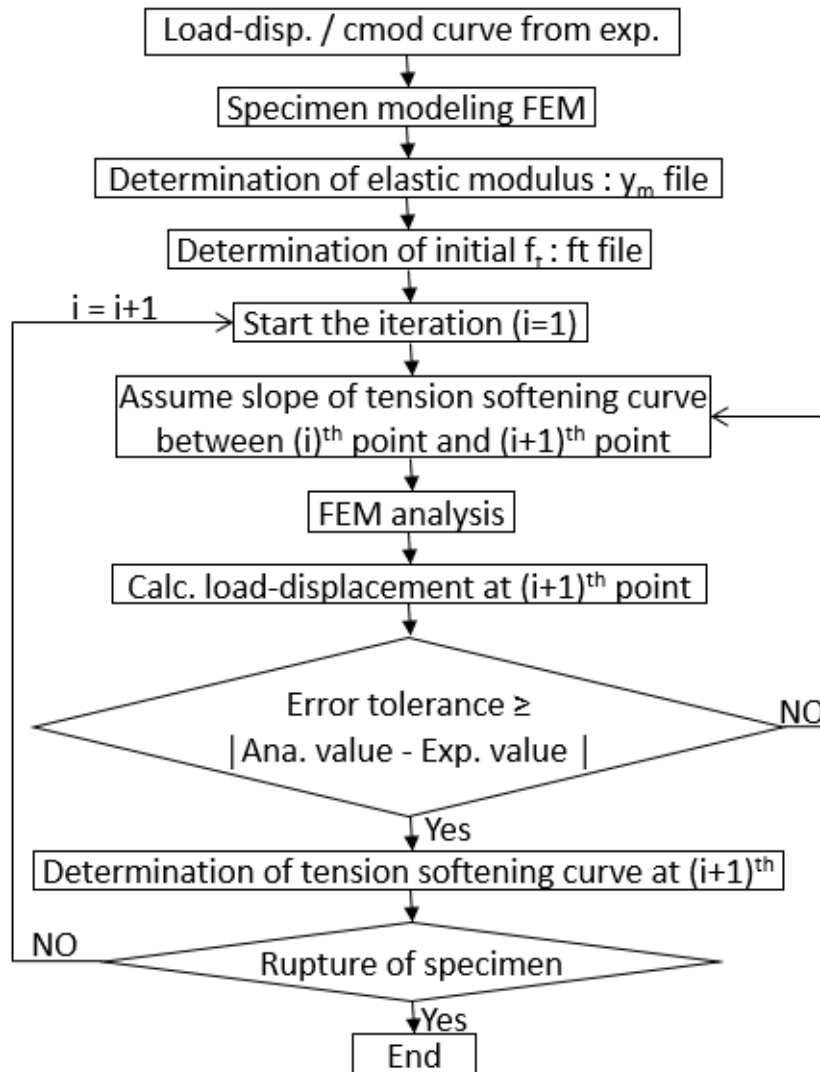


Fig. 3.8 Fracture process zone of concrete.

3.2.3.3 Crack-bridging Strength from dog-bone uniaxial tensile Test

Theoretically, the uniaxial tensile test is the ideal test to determine the post cracking characteristics of SFRC. The results of the test do not require an inverse analysis and can be directly processed into design models. There are, however, drawbacks of running direct tension tests on SFRC. The first is the nature of the test set up. Due to the heterogeneity of the material, a fracturing of the matrix starts at the weakest spot along the perimeter of the specimen. Consequently, the boundary conditions of the test play an important role. The type of boundary conditions that should be applied to a uniaxial tension test continues to be an ongoing matter of discussion in the scientific community. The categories of boundary conditions are limited to rotating and/or fixed boundary conditions. Rotating boundaries allow the specimen ends to freely rotate during the test; fixed boundaries prevent rotation of the specimen ends by the bending stiffness of the test setup. By including a universal joint at one end of the specimen,

the accidental residual tensions that develop as a result of gripping the specimen can be eliminated. The testing arrangement is illustrated in Fig. 3.9.

The characteristic behavior of SFRC in direct tension can be expressed by the tensile stress-strain response before cracking and in terms of nominal stress versus crack opening displacement after cracking. It is well known that the inclusion of fibers within a concrete matrix significantly enhances its post cracking strength. The degree of residual post cracking tensile strength attained by SFRC is dependent on the mechanical and geometrical properties of the fibers. In the analysis of the dogbone specimens, the following assumptions were made: (i) the elastic deformations of the concrete near the vicinity of the crack are negligible relative to the opening of the crack, (ii) shape induced tensile stress concentrations are small and can be ignored, and (iii) the uncracked concrete undergoes elastic unloading.

The stress transferred across the crack is determined from a tension softening curve corresponding to the post-peak stress-displacement obtained from the direct tension test. To determine the crack opening displacement, the average of the four transducers is taken; no further manipulation of the data is required as all cracking, for all specimens tested in the study, occurred within the gauged length. The tensile stresses presented in the analysis are in terms of equivalent tensile stress, which is the resultant of the applied tensile load divided by the cross-sectional area at the most narrow cross-section.



Fig. 3.9 Dog-bone uniaxial tensile test.

3.3 Inverse Analysis Method

In the present study, the purpose is to evaluate the crack-bridging contribution induced by steel fibers in the tensile stress zone during cyclic loading over the fatigue life. The inverse analysis method is an analytical model used to investigate the crack bridging strength by achieving a complete agreement between the experimental and analytical structural response for rebar and surface concrete strain.

3.3.1 General

The response of an SFRC structural member is determined by the tensile stresses developed in rebars, crack-bridging steel fibers, and the bond mechanism between rebars and concrete matrix (which is assumed not to be degraded during fatigue loading). However, direct sectional analysis calculations are difficult to implement in this case, because the degradation model of crack-bridging strength during cyclic loading is unknown. For this reason, an inverse technique is used here to obtain the degradation of crack-bridging strength of SFRC in tension, deriving it from rebar tensile strain, surface concrete maximum compression strain, and the N.A. position measurements of SFRC structural beams during application of a flexural fatigue load.

Incidentally, this approach is not necessary in the case of RC structural beams because post-cracking concrete tensile strength is ignored (it is treated as a brittle material). On the other hand, in the case of SFRC, the steel fibers bridge cracks during loading (it is treated as a ductile material), so the contribution induced by the steel fibers is more important and should be investigated. Unlike direct sectional analysis, which aims at a prediction of structural response using specified constitutive material laws, the inverse analysis method has the objective of determining the degradation model of crack-bridging strength from the experimental response of actual structures.

3.3.2 Previous Studies on The Inverse Analysis Method

The principles of the inverse technique for deriving stress-averaged strain relationships of tensile concrete using test data for RC flexural members were formulated by Kaklauskas and Ghaboussi (kakulauskas 2001,2004). The method was based on the smeared crack approach. Average stress-strain relations for concrete in tension (including the descending branch) and compression are computed from experimental moment-average strain and/or moment-curvature curves. Computation of stress-strain relations is performed incrementally for the

extreme surface fibers and is based on a novel idea of using the previously computed portions of the stress-strain relations at each load increment to compute the current increments of the stress-strain relations.

Recently, the inverse technique was modified by Gribniak and Kaklauskas (Gribniak 2011, KaKulauskas 2012) to eliminate the shrinkage effect from the test data of flexural reinforced concrete elements. The shrinkage effect was eliminated by assuming in the direct technique a positive (expansion) free shrinkage strain. Based on the proposed procedure, free-of-shrinkage tension-stiffening and moment-curvature relationships were derived by using test data of shrunk RC beams.

Finally, the inverse analysis was used by Kakulauskas (KaKulauskas 2012) to derive the stress-strain relationships for steel fiber concrete in tension from tests of beams with ordinary reinforcement. The analysis utilized the layer section model as shown in Fig. 3.12 and based on the concept of a progressive calculation of the stress-strain relationship for the extreme tension layer of the section.

3.3.3 Computation of The Inverse Analysis Method

In this study, the initial crack-bridging strength, as shown by the straight line in Fig. 3.11(c), is assumed to degrade proportionally with a factor (α) during the fatigue life of an SFRC structural beam under flexural cyclic loading, as presented in Fig. 3.10 and Fig. 3.11(c). As a result, no need for the layer section model to be used in the inverse analysis procedure, but with validity limits until the yielding point of rebar. The proposed degradation model can be set up to predict the same average experimental response as obtained in tests, leading to accurate estimation of the rebar stress level that controls fatigue rupture of the SFRC structural beam, through a simplified design methodology, and ensuring compatibility with the evolution of strain levels and deformations during the fatigue life of the SFRC structure.

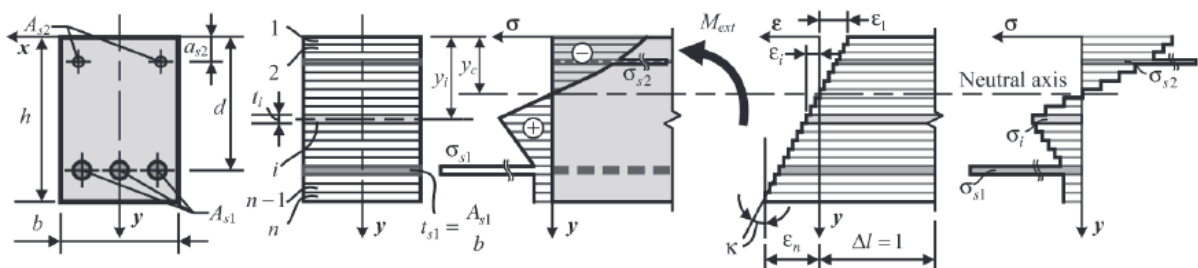


Fig. 3.12 Layer section model.

The computation for the inverse analysis method is performed incrementally during cyclic loading, as presented in the form of a flow chart in Fig. 3.13. Under the first cycle flexural load (N_1), the material constitutive laws of SFRC are used to perform the direct sectional analysis calculations at the maximum fatigue stress level with zero degradation ($\alpha_1 = 0$) of the initial crack-bridging strength (tension softening curve), as shown in Fig. 3.11(c), to calculate rebar strain, ultimate compressive concrete strain, and N.A. position. Then, the calculated and average experimental results within the constant moment region are compared, and if they differ, a certain degree of degradation (α_1) of initial crack-bridging strength is set to minimize the difference between the two. Accordingly, the crack-bridging strength used in the first cycle (N_1), after a certain level of degradation (α_1), is an equivalent initial crack-bridging strength that predicts the same structural response of the SFRC beam at the first cycle (KaKulauskas 2012), since under flexural loading cracks are initiated in the weakest section inside the constant moment region. This region may have a lower fiber dosage or different fiber orientation, giving rise to lower fracture energy than obtained from the notched prismatic specimen results (tension softening curve) for a predefined crack location. Incidentally, crack-bridging strength degradation obtained in this study concurs with the experiment from the first cycle (N_1) till the fatigue life (N_f).

Thereafter, computations are iterated for the incremental set of fatigue cycles (N_i) until reaching the fatigue life (N_f), which is marked by fatigue rupture or two million cycles. After each increment (N_i), a certain degradation (α_i) of equivalent crack-bridging strength is assigned to adjust the balance between the experimental and calculated results, as represented by the dotted line in Fig. 3.11(c). If the calculated and experimental results agree within the set threshold, the degree of degradation of crack-bridging strength (α_i) is derived. Finally, the degradation of crack-bridging strength normalized to the initial crack-bridging strength using Eq. (3.4), as shown in Fig. 3.11(d).

$$\beta_i = 1 - \alpha_i \quad (3.4)$$

where, β_i is normalized crack-bridging strength at the i th loading cycle and α_i is the reduction in crack-bridging strength at the i th loading cycle (see Figs. 2(c) and (d)).

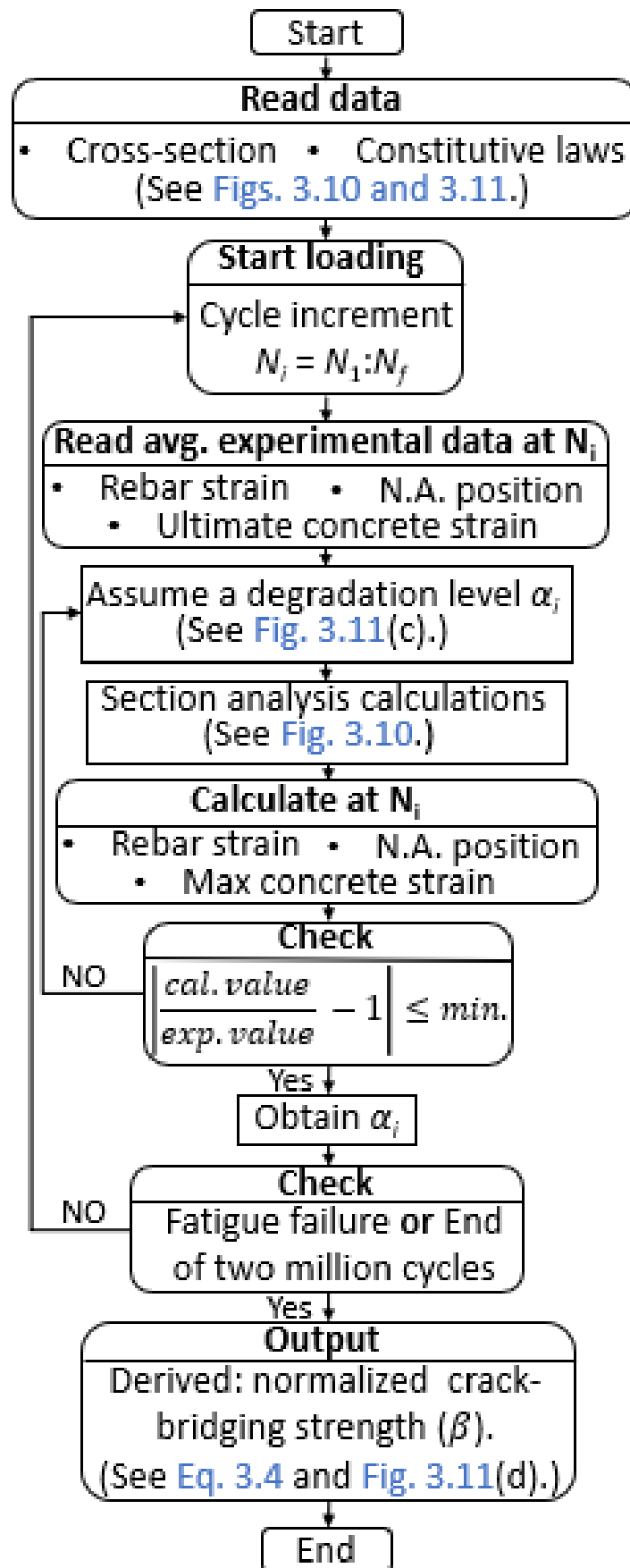


Fig. 3.13 Flow chart of the inverse analysis method.

3.4 Conclusion

In this chapter, a model for the evaluation of the crack-bridging strength degradation during cyclic loading is derived to obtain a rational understanding of the mechanical response of SFRC structural beams under flexural cyclic loading at each set of cycles over the whole fatigue life from the experimental response of SFRC structural beams. The basis of the model is inverse sectional analysis calculations.

Material-level experimental tests are carried out to identify the mechanical and fracture properties of SFRC, with the results consequently used in the sectional analysis calculations. Also, structure-level experimental tests are carried out on RC and SFRC beams under static and fatigue 4-point bending loading while simultaneously monitoring mid-span deflection, rebar strain, surface concrete strain, and neutral axis (N.A.) position. Finally, in the inverse analysis, certain levels of degradation in the crack-bridging strength were derived in each set of cycles during the fatigue life at maximum fatigue stress level. A model such as the one proposed for the degradation of crack-bridging strength induced by fibers might be used to accurately estimate fatigue capacity and rebar stress level through a simplified design methodology that is compatible with the evolution of stresses and deformations during the fatigue life of SFRC structures.

Chapter 4

4 Evaluation of Crack-bridging Strength of SFRC Structural Beams under Flexural Fatigue Constant Load Level

4.1 Introduction

This chapter examines the influence of hooked-end steel fibers on the reinforced concrete structural beams subjected to flexural cyclic loading, as well the inverse analysis method is used to evaluate the crack-bridging strength degradation over the fatigue life for SFRC structural beams. A degradation model for the crack-bridging strength is proposed over the fatigue life and also a model for that crack-bridging strength degradation is related to the evolution of the maximum rebar strain for several fatigue stress levels ranging from low, medium to high. The experimental program for the first series of NC and SFRC beams on material and structural scale under static and fatigue loading conditions is presented. Firstly, the material properties, mix proportion, specimen's geometry, testing setup, and measuring instruments are explained. Secondly, the experimental fatigue response data of structural beams are captured to be used in the execution of the inverse analysis calculation method. Finally, the crack-bridging strength is evaluated for the first series of SFRC structural beams under a constant flexural fatigue load level over their fatigue life varying from a low, medium, to high fatigue stress level.

4.2 Sectional Analysis Calculations

The flexural structural behavior of SFRC members is investigated utilizing a sectional analysis. The sectional analysis is developed in the cracked section, where the stress level is higher and, thus, it is the weakest section from the fatigue sensibility. The basic assumptions are the same as for RC beams, consisting of:

- (a) The hypothesis of beam bending in a plane section and the resulting linear distribution of strain over the depth of the beam section is adopted.
- (b) The strain in rebars and concrete at the same depth in the beam is assumed to be the same.
- (c) Stresses in concrete and rebars can be calculated using the idealized stress-strain curves for concrete and steel, respectively.

A single SFRC member subjected to an external bending moment (M_{ext}) is considered. The cross-section of such a member is presented in Fig. 3.10, with strain and stress distributions across the cross-sectional depth (h). For this kind of sectional analysis, material constitutive laws for rebar, and SFRC in compression and tension are required, and here they are derived from material-scale tests, as shown in Figs. 3.11 (a),(b) and (c). The post-cracking constitutive law of SFRC in tension, known as the tension softening curve, is obtained from a material-scale flexural test of a notched prismatic SFRC specimen. It describes the relationship between decreasing transfer stress (σ) and increasing crack opening displacement (ω) in the fracture process zone (JCI 2003a). The transforming of ω into a strain (ϵ) can be carried out by dividing ω by a reference length (L_R) that is equal to the average crack spacing measured in the constant moment region of flexural structural beams (Montaignac 2012). Finally, the sectional analysis calculations can be carried out by assuming the ultimate compressive concrete strain and N.A. position, and satisfying equilibrium conditions between internal (int.) and external (ext.) forces (F) using Eq. (3.2) and moments (M) using Eq. (3.3), respectively. However, the external forces ($F_{ext.}$) in the case of simply supported beams are zero.

$$\Sigma F_{int.} = \Sigma F_{ext.} \quad (3.2)$$

$$\Sigma M_{int.} = \Sigma M_{ext.} \quad (3.3)$$

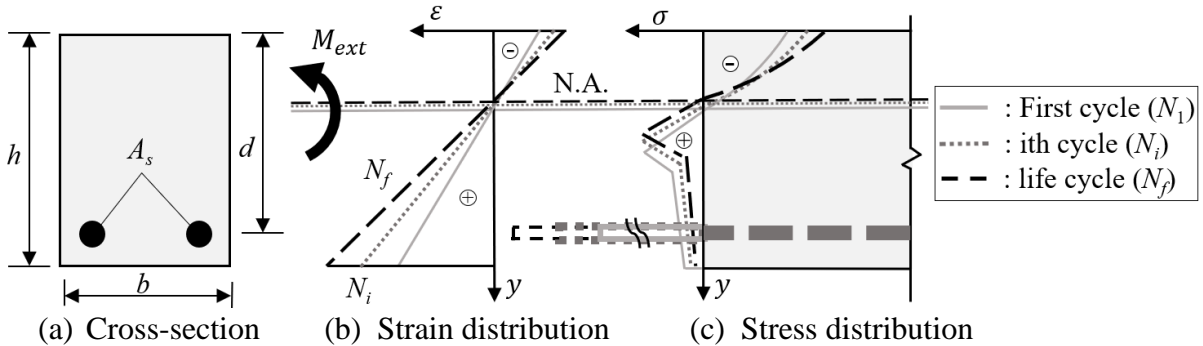


Fig. 3.10 Stress and strain distribution of a flexural member during fatigue.

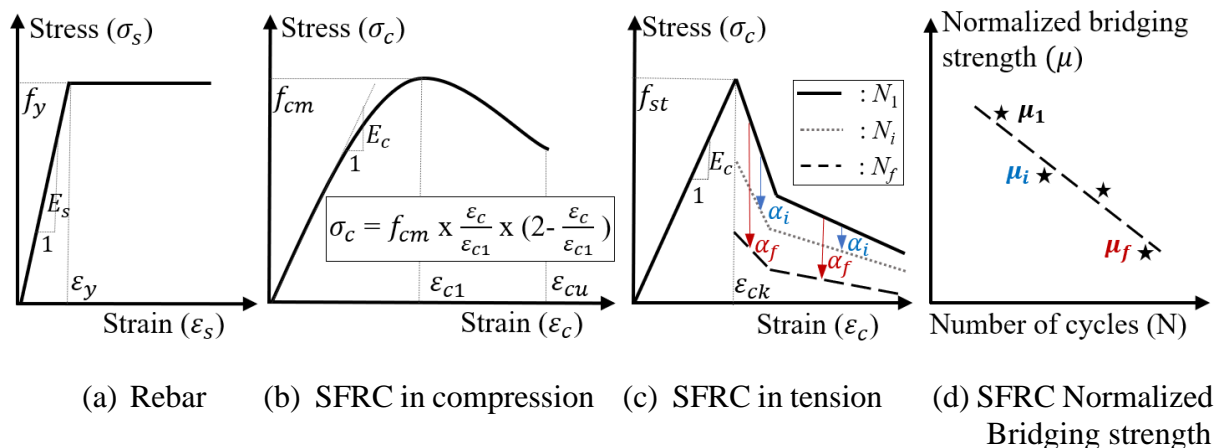


Fig. 3.11 Material constitutive laws.

4.3 Experimental Program

The experimental program of the first series consisted of several NC and SFRC specimens that are tested on both material and structural scale, with the proportions and testing set up as described in the following sections.

Material level tests were carried out to evaluate the material properties such as concrete compressive strength (f_{cm}), concrete first cracking tensile strength (f_{ct}), concrete modulus of elasticity (E_c), and the steel fiber reinforced concrete's tension softening curve and fracture energy (G_f) as listed in [Table 4.1](#). The results of the tests are presented and evaluated with particular emphasis on the effects of steel fibers on the fatigue response of the beams.

Besides, structural scale tests consist of seven structural scale beams, three beams are NC structural beams and the other remaining four beams are SFRC structural beams with 1.5% hooked-end steel fibers (Dramix 3D 65/35 BG), having a cross-section area of 150 mm x 200 mm and a span length (l) of 1700 mm with 300 mm of constant moment loading span (s) and effective depth (d) of 170 mm, each had two conventional rebars with a nominal diameter (D) of 16 mm as listed in [Table 4.2](#). The beams were instrumented to measure the rebar strains, surface concrete strains, and mid-span deflections having testing configurations as shown in [Fig. 4.1](#). The structural beams are labeled as follows: $\phi B\delta_\Omega$, in which, ϕ reflects whether the material of the beam is NC or SFRC, δ reflects whether the flexural test is under static or fatigue loading, and Ω reflects the maximum fatigue load in kN.

Table 4.1: Test program of material scale specimens.

| Specimen | Description | NC | SFRC |
|--|-------------------------------|------|------|
| Cylinder (D =100 mm) (L=200 mm) | Number of specimens | 3 | 9 |
| | Compressive strength (MPa) | 51.0 | 35.0 |
| | Young's modulus (GPa) | 31.0 | 25.0 |
| Cylinder (D =150 mm) (L=150 mm) | Number of specimens | 3 | 7 |
| | Tensile strength (MPa) | 3.7 | 3.4 |
| Prismatic specimen (100 x 100 x 400 mm) | Number of specimens | – | 6 |
| | Flexural strength (kN) | – | 11.1 |
| | Fracture energy (N/mm) | – | 12.9 |

Table 4.2: Test program of structural scale beams.

| Beam ID | Test type | Fiber volume (%) | Flexural capacity (kN) | Min. fatigue load (kN) | Max. fatigue load (kN) | Fatigue life | Residual flexural capacity (kN) |
|---------|-----------|------------------|------------------------|------------------------|------------------------|--------------|---------------------------------|
| FBS_01 | Static | 1.5 | 85.2 | – | – | – | – |
| FBF_30 | Fatigue | 1.5 | – | 5.0 | 30.0 | 2,000,000 ↑ | 88.2 |
| FBF_40 | Fatigue | 1.5 | – | 5.0 | 40.0 | 2,000,000 ↑ | 80.5 |
| FBF_50 | Fatigue | 1.5 | – | 5.0 | 50.0 | 380,116 | – |
| NBF_30 | Fatigue | – | – | 5.0 | 30.0 | 2,000,000 ↑ | 76.4 |
| NBF_40 | Fatigue | – | – | 5.0 | 40.0 | 2,000,000 ↑ | 76.8 |
| NBF_50 | Fatigue | – | – | 5.0 | 50.0 | 766,087 | – |

Note: The structural beams were tested under a four-point bending static and fatigue test. the arrow in fatigue life cells indicates the end of the fatigue test without fatigue failure.

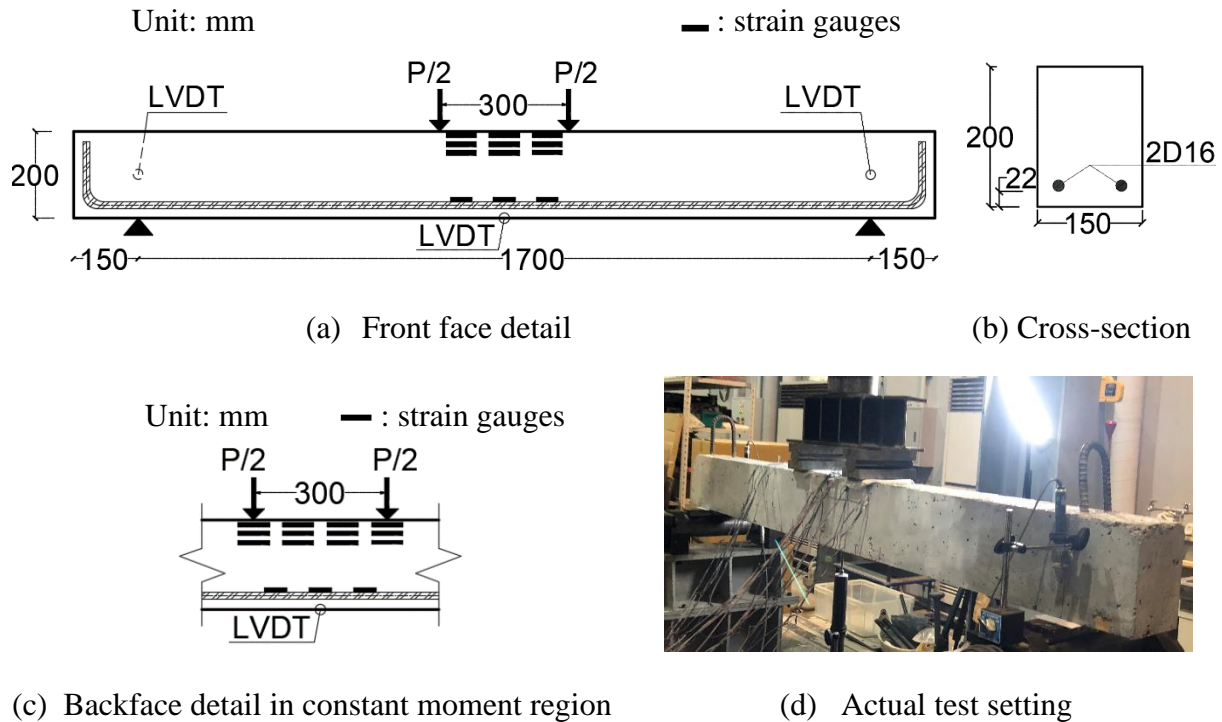


Fig. 4.1 Details of tested structural scale beams.

4.3.1 Material and Mix Proportion

The concrete used in the first series for both NC and SFRC was a normal grade concrete with a target mean strength (f_{cm}) of 40 MPa. The concrete mixes were designed and prepared at the concrete laboratory of the institute of industrial science, the University of Tokyo. The following materials were used in the first series in mixing and production of concrete: cement, coarse aggregate, fine aggregate, steel fibers, water, and superplasticizer. Table 4.3 shows the mix proportions of NC and SFRC. Ordinary portland cement meeting the Japanese industrial standards (JIS) was used as the binding material, with a specific gravity of 3.15. Crushed coarse and fine aggregates were used with maximum aggregate sizes of 13.0 mm and 4.75 mm and specific gravities of 2.66 and 2.65, respectively. The steel fibers were gradually sprinkled into the mix by hand to a 1.5% volume fraction of the full SFRC volume, and care was taken to obtain a homogenous and workable mixture. Furthermore, a high-performance air-entraining water-reducing agent (Type: SP8SV) was used in SFRC in a range of 1.5% to the weight of the cement for each concrete mix as a superplasticizer to obtain an average 120 mm slump value, while a normal water-reducing agent (Type: AE.70) was used for NC. The water to cement ratio was 55% for both NC and SFRC. Finally, the NC and SFRC batches were introduced into their molds and compacted, then the specimens were removed from the molds after 3 days and cured for 28 days.

The steel fibers, that were used in the first series, were Dramix 3D 65/35 BG with an aspect ratio of 65, a length of 35 mm, having a rounded cross-section with a smooth surface, and a hooked-end shape as shown in Fig. 4.2. The properties of steel fibers are given in Table 4.4 and with an ultimate tensile strength of 1050 MPa as reported by the manufacturer.

Table 4.3: Mix proportion of the first series for NC and SFRC.

| Ingredient | Amount (kg/m ³) | |
|-------------------------|-----------------------------|-------|
| | NC | SFRC |
| Portland cement | 318 | 336 |
| Water | 175 | 185 |
| Fine aggregate | 828 | 1055 |
| Coarse aggregate | 1015 | 706 |
| Hooked-end steel fibers | – | 117.8 |
| Superplasticizer | 3.18 | 5.05 |

Table 4.4: Hooked-end steel fibers properties.


| Description | Value |
|------------------------------|--|
| Length (mm) | 35 |
| Diameter (mm) | 0.55 |
| Density (kg/m ³) | 7850 |
| Tensile strength (MPa) | 1050 |
| Aspect ratio | 65 |
| Fiber shape |  |



Fig. 4.2 Hooked-end steel fibers.

The structural beams were reinforced with tensile reinforcement consisted of two 16 mm nominal diameter bars, resulting in a tensile reinforcement ratio of 1.34 percent for the first series. The longitudinal reinforcing bars were hot rolled deformed steel bars, all from the same batch with a nominal yield strength of 357 MPa and Young's modulus of 200 GPa. The structural beams were designed to be failed under flexural loading conditions, using an appropriate concrete cross-section of structural beams to resist the shear stress during loading without any need for shear reinforcement and compression reinforcement.

4.3.2 Mixing, Casting and Curing of Concrete

A 50-liter capacity of mixing machine was used for concrete production. First, cement and fine aggregate were mixed in a dry condition for 30 seconds. Then, the all mount of water including the superplasticizer were inserted within 30 seconds and continued mixing for 60 seconds. The amount and the type of superplasticizer were slightly different depending on the concrete types from NC to SFRC. The addition of the superplasticizer was aimed to obtain a similar slump average value of 120 mm for concrete. Next, fibers were added to the mixer and mixed for another 60 seconds to ensure that the fibers were dispersed properly as presented in [Fig. 4.3](#). After that, the coarse aggregate was added and mixed for 120 seconds. [Figure 4.4](#) shows the fresh concrete and the slump of SFRC. Satisfactory workability was achieved in all specimens for both NC and SFRC. From the observation, the distribution of steel fibers was found to be uniformly distributed and randomly oriented in all batches of concrete casting without any observation of fiber's balling.

The concrete was carefully cast into the formwork move-filling method to insure the random orientation of fibers. In this move-filling method, concrete was filled continuously in the longitudinal direction along the axis of the formwork. Previous research work was carried out by Zhou and Uchida ([Zhou 2013](#)) showing the effectiveness of using the move-filling method in casting the concrete to confirm the random distribution of fibers inside the concrete matrix.

By the end of the casting of the NC and SFRC in both material and structural scales, the specimens were covered with polyethylene sheets and cured for 48 hours. After 48 hours, the formwork was removed and the beam was covered again by moistened cloths and polyethylene sheets as shown in [Fig. 4.5](#). Moist-curing was continued until the 28th day after casting then the specimens were uncured and prepared for testing.



Fig. 4.3 Addition of steel fibers during the concrete mixing process.



Fig. 4.4 Fresh properties of SFRC.



Fig. 4.5 Moist-curing.



Fig. 4.6 Structural level specimens.

4.3.3 Specimens

The test program consisted of several NC and SFRC specimens that were tested on both material and structural scale for the first series test set. The first series aims to capture the fatigue response of SFRC over the fatigue life with a comparison with the NC. Besides, the execution of the inverse analysis calculations method requires detailed information about the material properties of both NC and SFRC, as a result, material level tests were carried out to identify the materials constitutive laws, targeting finally in the evaluation of crack-bridging strength over the fatigue life of SFRC structural beams.

Seven structural scale beams reinforced with two ordinary steel reinforcing bars and made of normal and steel fiber reinforced concrete were tested under 4-points bending test monotonically and under cyclic loading. The details of the tested structural beams of the first series are discussed in [Table 4.2](#). All structural beams have a rectangular cross-section with a dimension of 150 x 200 mm and a length of 2000 mm. The structural beams were tested under flexural loading test with a span length (l) of 1700 mm, with 300 mm of constant moment loading span (s), and an effective depth (d) of 170 mm as shown in [Fig. 4.1](#). All structural beams were reinforced with two ordinary steel reinforcing bars with a diameter (D) of 16 mm with a tensile longitudinal reinforcement ratio of 1.34 percent to be failed inside the constant moment region in a flexural failure mode as shown in [Fig. 4.6](#).

The concrete material properties were determined for the first series by testing several specimens at a material scale as shown in [Fig. 4.7](#). Tests for compressive strength (f_{cm}), concrete modulus of elasticity (E_c), concrete first cracking tensile strength (f_{ct}), and the steel

fiber reinforced concrete's tension softening curve and fracture energy (G_f) were carried out as listed in Table 4.1. Nine cylinders of SFRC and three cylinders of NC with a length of 200 mm and a diameter of 100 mm were tested under compression loading to measure the compressive strength (f_{cm}), concrete modulus of elasticity (E_c) as shown in Fig. 4.8. Also, seven cylinders of SFRC and three cylinders of NC with a length of 150 mm and a diameter of 150 mm were tested under indirect tensile stress by the Brazilian test to measure the concrete first cracking tensile strength (f_{ct}) (Denneman 2011) as shown in Fig. 4.9. Finally, six notched prismatic SFRC specimens with a cross-section dimension of 100 x 100 mm and length of 400 mm with loading span 300 mm were tested under a 3-points bending test to measure the steel fiber reinforced concrete's tension softening curve and fracture energy (G_f) (JCI 2003a) as shown in Fig. 4.10.



Fig. 4.7 Material level specimens.



Fig. 4.8 Concrete compressive test.



Fig. 4.9 Splitting tensile test.

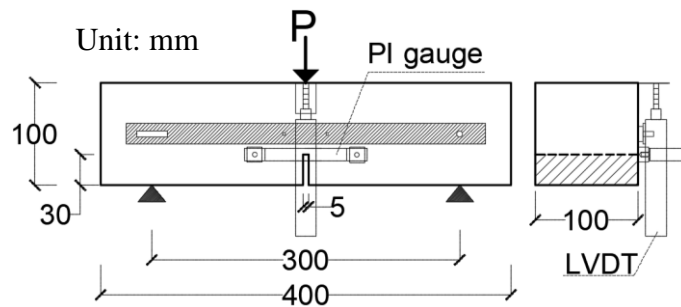


Fig. 4.10 Bending test on prismatic SFRC specimens.

4.3.4 Testing Setup and Instrumentations

The compressive test was carried out to measure both concrete compressive strength (f_{cm}), concrete modulus of elasticity (E_c) using a load cell to monitor the load, and 30 mm electronic strain gauges were attached on both sides of cylinders to record longitudinal deformation parallel to the loading direction during the test as shown in Fig. 4.8. The concrete compressive strength (f_{cm}) was calculated by dividing the maximum compressive strength to the cross-section of the concrete cylinder using Eq. (4.1). The concrete modulus of elasticity (E_c) was calculated by measuring the slope of compression load-longitudinal deformation from 50 micro-strain of the longitudinal deformation to one-third of the maximum compressive load.

$$f_{cm} = \frac{4 P_{max.}}{\pi D^2} \quad (4.1)$$

Where f_{cm} is the compressive strength, $P_{max.}$ is the maximum compressive load, and D is the diameter of the specimen.

The splitting tensile test was carried out to measure cracking tensile strength (f_{st}) using a loading strip 8 mm in width to limit the size effect, as the size of the compression zone depends on the size of the loading strip (Denneman 2011). A pi-gauge of length 100 mm length was

attached to each face of the cylinder to record transversal deformation perpendicular to the loading direction during the test (Denneman 2011) as shown in Fig. 4.9. Consequently, experimental load-transversal deformation curves were obtained for SFRC cylinders with two peaks of load, an initial one reflecting the tensile cracking load ($P_{crk.}$) and a second peak due to secondary cracking. Finally, the cracking tensile strength (f_{st}) is obtained from the first cracking load and is derived in Table 4.1 by using Eq. (4.2).

$$f_{st} = \frac{2 P_{crk.}}{\pi L D} \quad (4.2)$$

Where f_{st} is the cracking splitting tensile strength, $P_{crk.}$ is the first cracking load, L is the length of the specimen, and D is the diameter of the specimen.

The notched prismatic specimens were tested under 3-point loading with a span of 300 mm following the JCI-S-001-2003 standard (JCI 2003a), as shown in Fig. 4.10, to obtain the tension softening curve and measure the fracture energy (G_f) for SFRC. For this flexural static test, 300 kN capacity loading actuator was used to apply a monotonic load under deflection control at 0.06 mm/min up to the peak load, then at a rate of 0.6 mm/min until the specimen completely ruptured. Two linear variable displacement transducers (LVDT) were used to measure the vertical displacement under the load point on the two specimen faces. The transducers were mounted on a rigid yoke accurately set up on the specimen to minimize the effect of rotation during the test. Two further pi-gauges were placed at the tip of the notch on the two faces of the specimen to measure the crack tip opening displacement (CTOD).

The structural beams were tested under 4-point loading with a span of 1700 mm, as shown in Fig. 4.1. Steel plates were placed on the pin-hinge supports and loading points. Displacements at mid-span and the supporting points were measured using three linear variable displacement transducers (LVDTs). Rebar strain was measured using six 2 mm electrical resistance strain gauges attached to the rebars in the constant moment region before concrete casting with a spacing 100 mm. Besides, for measuring surface concrete strains, 60 mm electronic strain gauges were attached in the constant moment region at several sections (50, 150, 250) at a spacing of 100 mm on both sides (right side and left side) and three heights (10, 30, and 50 mm) from the top of the beam, as shown in Figs. 4.1(a) and (c) and Fig. 4.11.

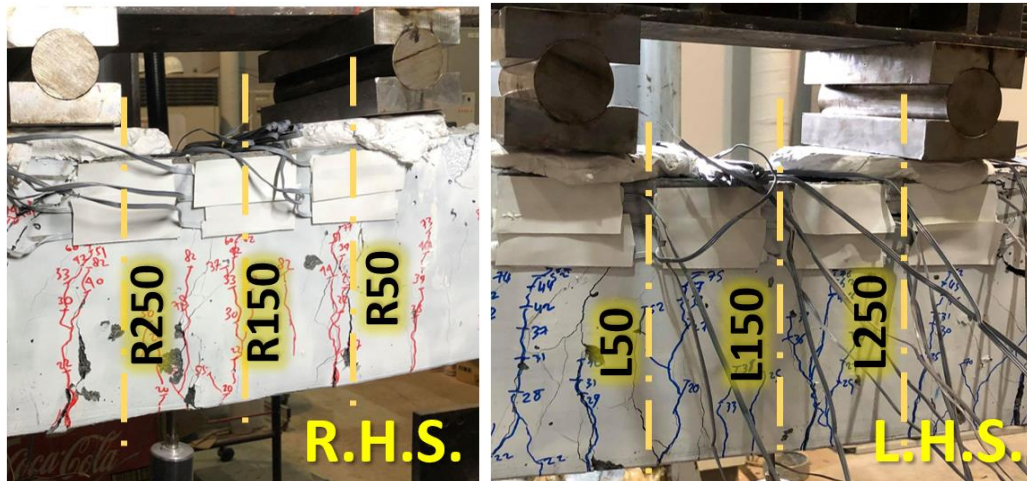


Fig. 4.11 Constant moment region of structural beams.

The static flexural loading was applied by a monotonic load under deflection control at 0.6 mm/min up to the peak load, then at a rate of 1.8 mm/min to completion. For the fatigue flexural loading, the cyclic load was applied in a sinusoidal manner under load control at a frequency of 5.0 Hz with a constant amplitude. Fatigue stress levels were selected to reflect low, medium, and high-stress scenarios (0.35, 0.47, and 0.59) thereby covering a wide range of flexural fatigue behavior of SFRC structural beams. Three NC structural beams were tested as controls under the same flexural cyclic loading to identify the improvement in fatigue response resulting from the addition of hooked-end steel fibers, as summarized in [Table 4.2](#). However, the NC structural beams have higher compressive strength (f_{cm}) than the SFRC structural beams, the NC structural beams were used as a control beam as the compression failure is not the organized failure for the structural beams and there is no big difference in young's modulus to change the beam response, as summarized in [Table 4.1](#). The actuator was programmed to pause at certain intervals during fatigue loading to enable data recording and observation. Testing continued 24 hours a day until either rupture or completion of two million cycles. For uncollapsed structural beams, after two million cycles of fatigue loading, a monotonic static flexural test was carried out to measure the residual flexural capacity of the beam.

4.4 Experimental Results

In the first series, several specimens were tested under the material and structural level to capture and analyze the fatigue response of SFRC beams under flexural loads and to evaluate the crack-bridging strength degradation over the fatigue life. Firstly, a 3-point bending test was carried out on notched prismatic SFRC specimens to calculate the crack-bridging strength –

tension softening curve – to be used in sectional analysis calculations. Secondly, one SFRC structural beam was tested under static loading to determine the ultimate flexural load capacity and confirm a constant crack-bridging strength during the monotonical application of load without any degradation through the utilization of the inverse analysis calculation method. Finally, six structural beams were tested under fatigue loading for different stress levels ranging from low to high-stress levels. Considering, the time consuming for testing each beam, three beams for NC and three beams for SFRC have been tested cyclically. The following sections discuss the test results of the individual beams. As a result, the results of inverse analysis calculations are presented in the next section in a model of degradation of the crack-bridging strength induced by hooked-end steel fibers over the fatigue life of different flexural fatigue stress levels.

4.4.1 Prismatic Specimens under Flexural Static Loading

The crack-bridging strength – or the tension softening curve – is a fracture mechanics parameter that describes post-cracking behavior, represents the fracture energy (G_f) of SFRC in the tensile stress zone, and is used in the sectional analysis calculations to understand the response of structural beams to loading. It is obtained from the material scale flexural test results obtained in the bending test of notched prismatic specimens until complete rupture as shown in Figs. 4.10 and 4.12 using the poly-linear approximation analysis method following the JCI-S-001-2003 standard (JCI 2003a).

The average static flexural capacity of the six SFRC notched prismatic specimens ranging from Sp-01 to Sp-06 was 11.1 kN with a standard deviation of 2.38 kN, as shown in Fig. 4.13(a). Based on this result, the fracture energy (G_f) was calculated following (JCI 2003a) as 12.94 N/mm on average with a standard deviation of 3.71 N/mm, as summarized in Table 4.1. Using a least-squares data-fitting procedure, the shape of the tension softening diagram can be obtained from the calculated results; this is plotted in Fig. 4.13(b) and summarized as Eq. (4.3). This tension softening curve can be divided into three zones. The first zone is immediately after cracking, where the stress abruptly decreases at a crack opening (ω) of less than 0.004 mm; this initial softening branch is assumed to be neglected. This is followed by a fiber bridging plateau (plastic region), where the cohesive stress is constant at 3.4 MPa until a crack opening (ω) of 0.42 mm. Finally, the cohesive stress decreases following a softening branch, as shown in Fig. 4.13(b).

$$\begin{aligned} \sigma &= f_{st} && (MPa) && \text{for } \omega = 0.0 \\ \sigma &= 3.4 && (MPa) && \text{for } 0 < \omega \leq 0.42 \text{ mm} \\ \sigma &= 3.7 - 0.72 \omega && (MPa) && \text{for } 0.42 \text{ mm} < \omega \end{aligned} \quad (4.3)$$



Fig. 4.12 Fracture of SFRC prismatic specimen at the end of the bending test.

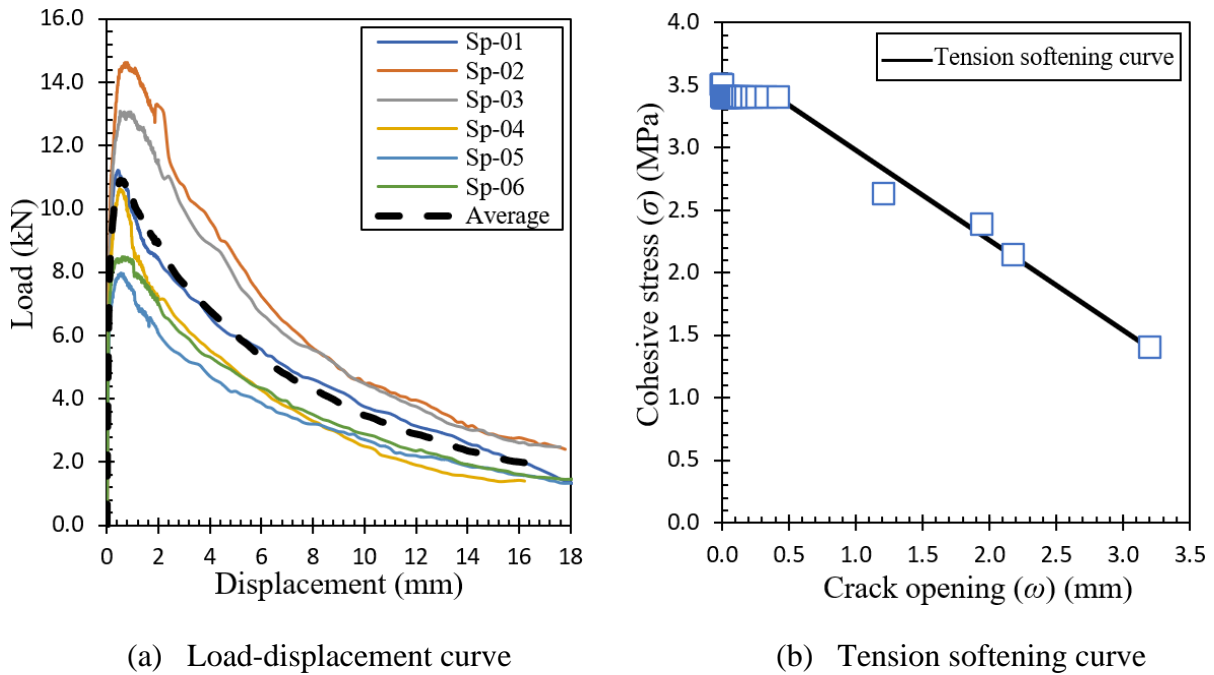


Fig. 4.13 Three-point bending test on SFRC prismatic specimens.

4.4.2 Static Flexural Loading of SFRC Structural Beam

The static flexural test was carried out on an SFRC structural beam to estimate the flexural capacity of SFRC structural beams, identify the yielding load, and confirm the experimental structural response of SFRC beams against the calculated response obtained by direct sectional analysis calculations using the initial crack-bridging strength over the whole loading process. The SFRC structural beam (FBS_01) exhibited a flexural capacity of 85.2 kN and the flexural

load corresponding to yielding of the rebar in the constant moment region was 80.0 kN, as shown in Fig. 4.14, with an average crack spacing – or reference length (L_R) – of 80 mm, as shown in Fig. 4.15.

As explained in section 4.3.4, the surface concrete strain was measured at several sections on both faces of the SFRC structural beams within the constant moment region. Further, rebar strains were measured at three points on the two rebars and the load versus rebar strain curves for the specified locations inside the constant moment region is given in Fig. 4.16. After testing, the experimental strain distributions were plotted for these three sections of the SFRC structural beam to estimate the ultimate compressive concrete strain at the extreme compression fiber and the N.A. position. Figure 4.17 shows the strain distribution at midspan on the front face of the beam (L150), showing the strain evolution for both rebar and concrete throughout the application of flexural monotonic loading until tensile ductile failure of the steel rebars followed by concrete crushing in the compression zone, as shown in Fig. 4.15.

All experimental measurements within the constant moment region of the three sections, in which rebar strain gauges were attached, between the front and back faces, were averaged and plotted versus flexural load (shown as a solid line) to reflect the average response of a structural beam, as shown in Fig. 4.18. The applied load was divided into increments and the computation was performed incrementally. During load application, the rebar strain, the ultimate compressive concrete strain, and the N.A. position are calculated from the direct sectional analysis calculations using the initial crack-bridging strength that was derived from the bending test of notched prismatic specimens on the material scale over the whole loading process, as explained in Section 3.3. Finally, the calculated results using the method of sectional analysis for the region before the rebar yielding point are also plotted in Fig. 4.18. The calculated flexural response of SFRC structural beam from the sectional analysis calculation method achieves a good fit with the experiment flexural response. The error is small, as represented in the R squared values given in Fig. 4.18.

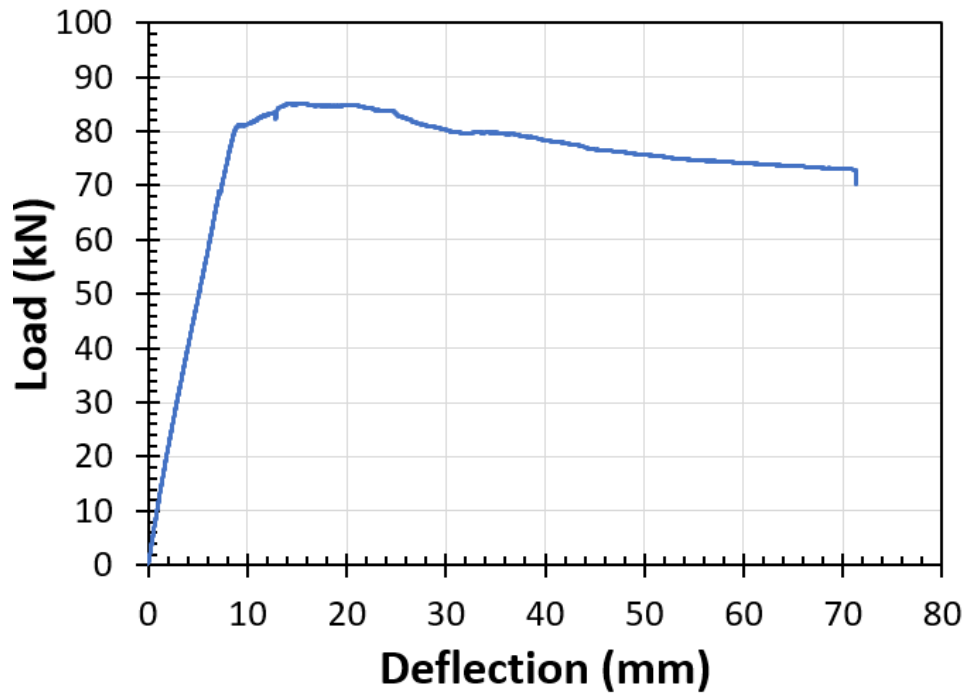


Fig. 4.14 Load versus deflection under static loading for beam FBS_01.



Fig. 4.15 Beam FBS_01 after failure under static loading.

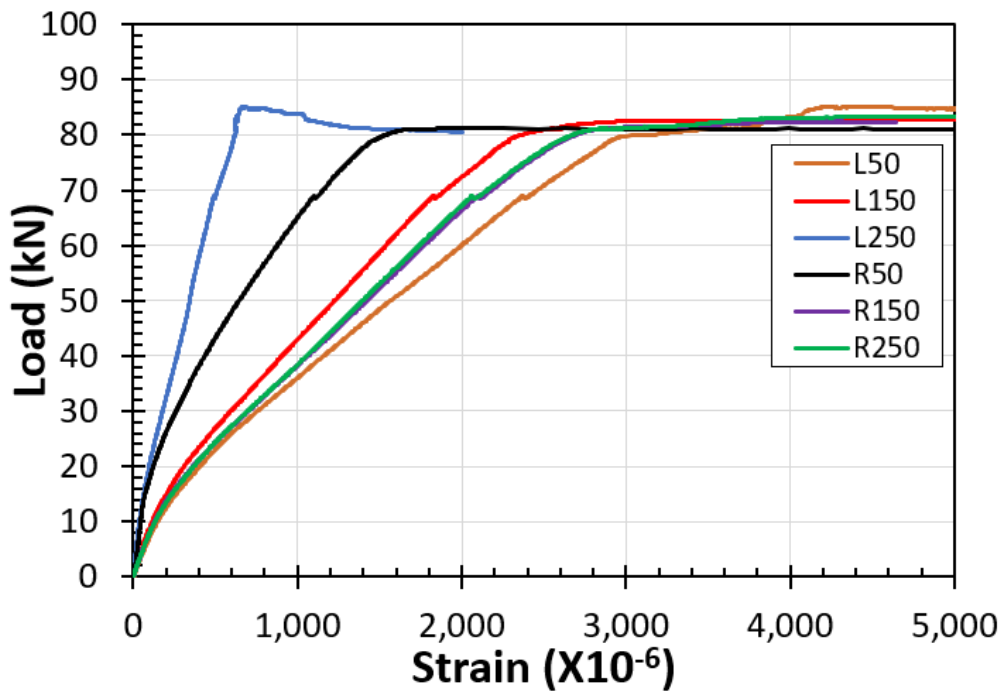


Fig. 4.16 Load versus rebar strain under static loading for beam FBS_01.

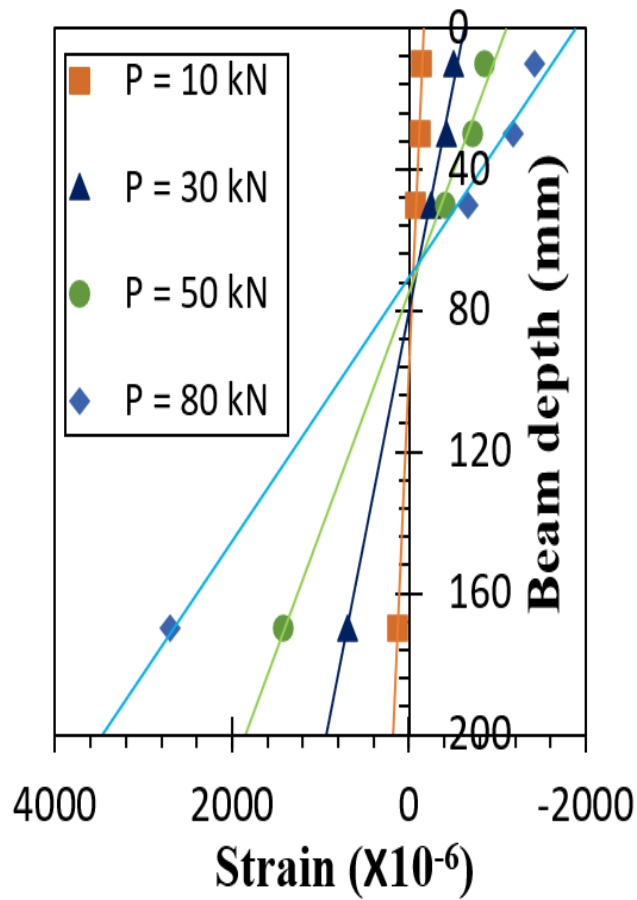


Fig. 4.17 Strain distribution of the mid-span section for beam FBS_01.

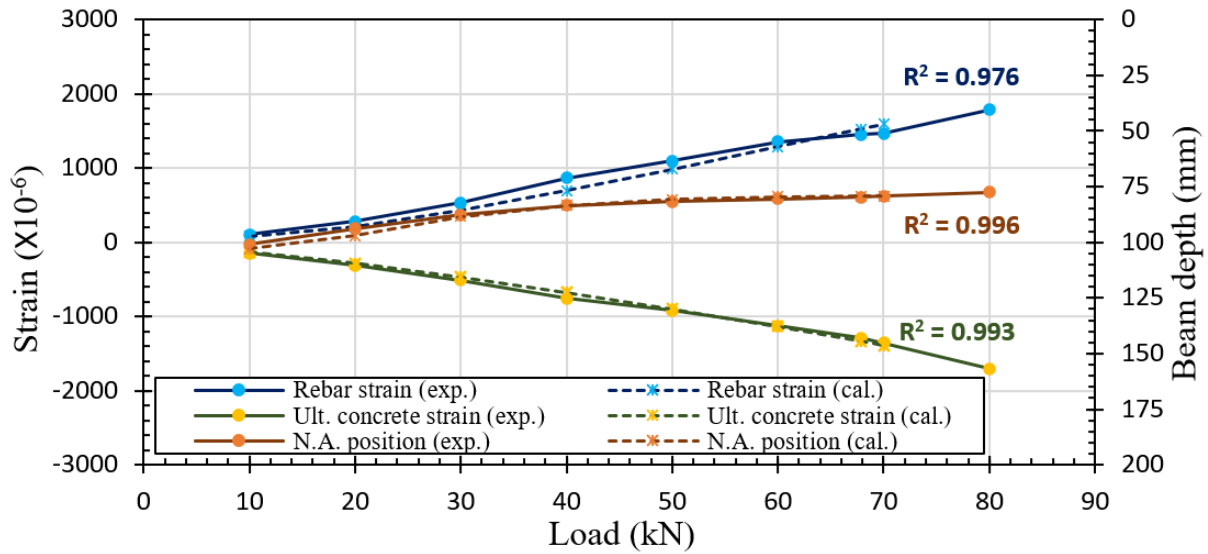


Fig. 4.18 Experimental versus calculated response under static loading for beam FBS_01.

4.4.3 Fatigue Flexural Loading of SFRC Structural Beams

A flexural cyclic loading test was carried out on three SFRC structural beams for measuring the flexural fatigue response to evaluate the degradation of crack-bridging strength over fatigue life using the inverse analysis method, as explained in section 3.4.3. Also, residual flexural capacity after completion of two million cycles was evaluated in the case of beams that survived without fatigue failure, as summarized in Table 4.2. During fatigue loading, as the number of loading cycles increases, an evolution of both the rebar and concrete strain was observed for the SFRC structural beams, resulting in increasing mid-span deflection and crack length and width and decreasing structural stiffness as noted from the decrease of the inclination of the load-deflection curve and N.A. position, as illustrated in the following paragraphs, with an average crack spacing – or reference length (L_R) – of 60 mm, as shown in Figs. 4.19, 4.23, and 4.27.

Beam FBF_30

For the low fatigue stress level ($S = 0.35$), one SFRC structural beam – FBF_30 – was tested under flexural cyclic loading with 5 kN as a minimum flexural load and 30 kN as a maximum flexural load, as shown in Fig. 4.19. Figure 4.20 shows the load versus mid-span deflection relationship over fatigue life under a low-stress level of flexural fatigue load showing an increase in mid-span deflection as cycles progress. Figure 4.21 shows the strain distribution at midspan on the front face of the beam (L150), showing the strain evolution for both rebar and concrete throughout the application of flexural cyclic loading until the end of fatigue life. The

average rebar strain within the constant moment region of FBF_30 is also plotted against the maximum and minimum flexural cyclic load for the three fatigue stress levels during the fatigue life, starting from the first flexural cyclic loading (N_1) and showing the evolution of average rebar strain, as shown in Fig. 4.22. After a complete of two million cycles of flexural loading, SFRC beam FBF_30 was subjected to residual flexural static tests to measure their residual capacity, as shown in Figs. 4.23 and 4.24. The result is listed in Table 4.2. Residual flexural capacity is a little different from the original capacity of the beams under static loading, even after the fatigue loading.



Fig. 4.19 Beam FBF_30 over fatigue life under flexural cyclic loading.

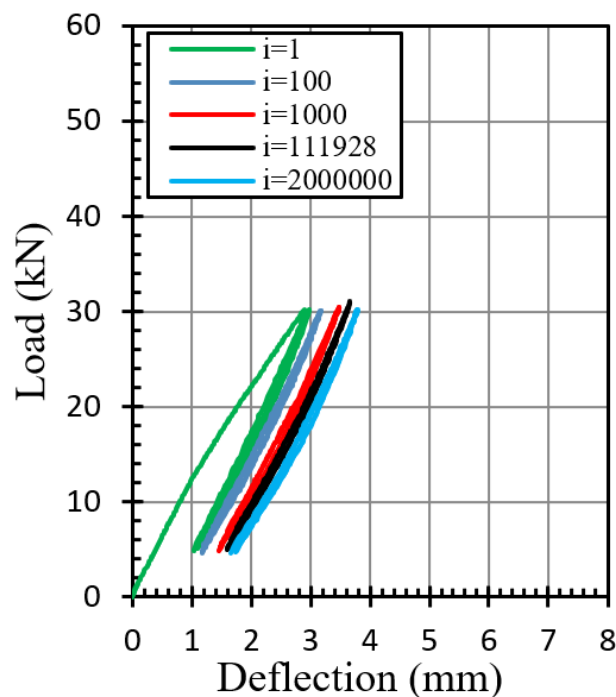


Fig. 4.20 Load versus deflection under flexural cyclic loading for beam FBF_30.

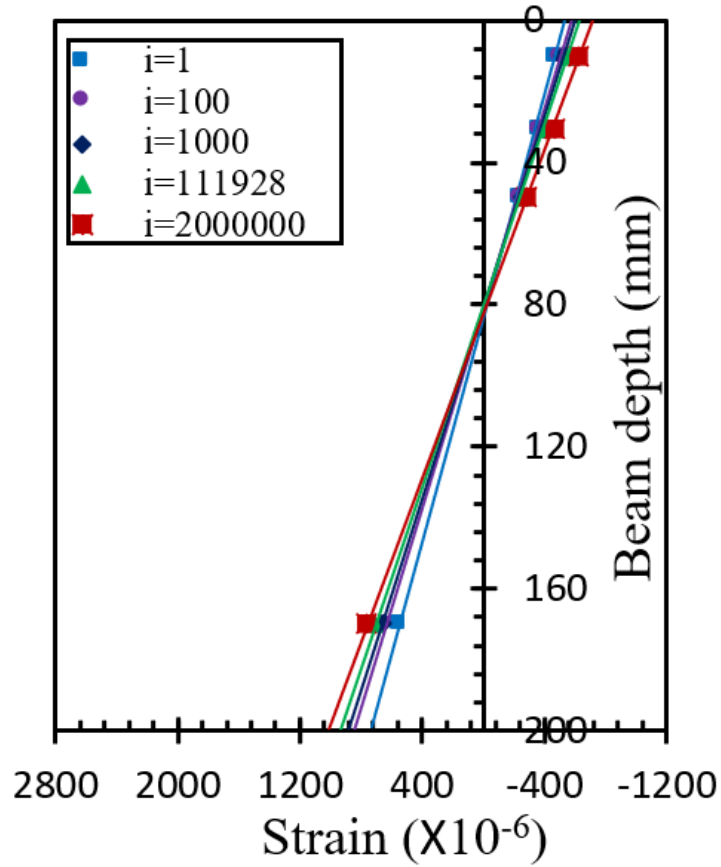


Fig. 4.21 Mid-span strain distribution under flexural cyclic loading for beam FBF_30.

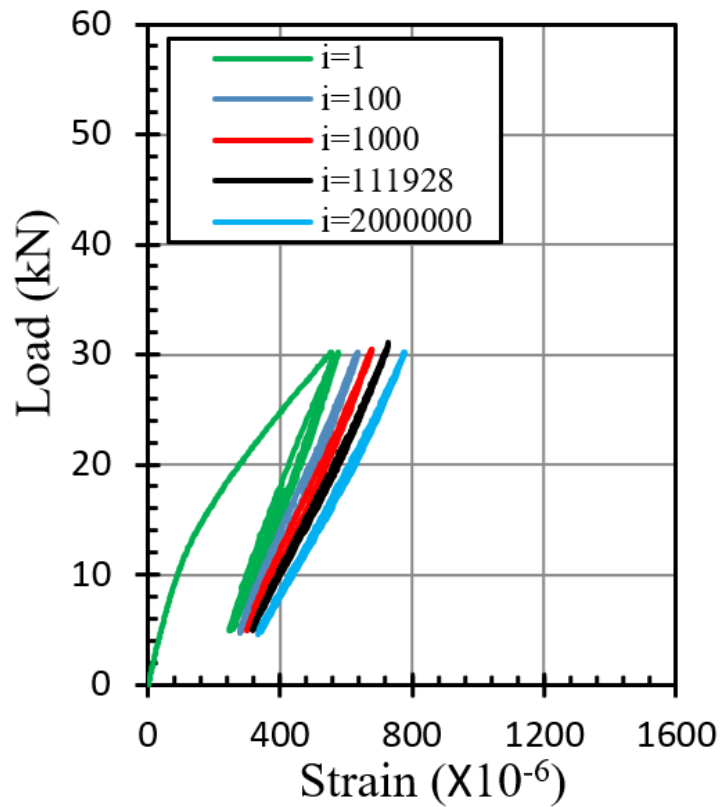


Fig. 4.22 Load versus average rebar strain under flexural cyclic loading for beam FBF_30.

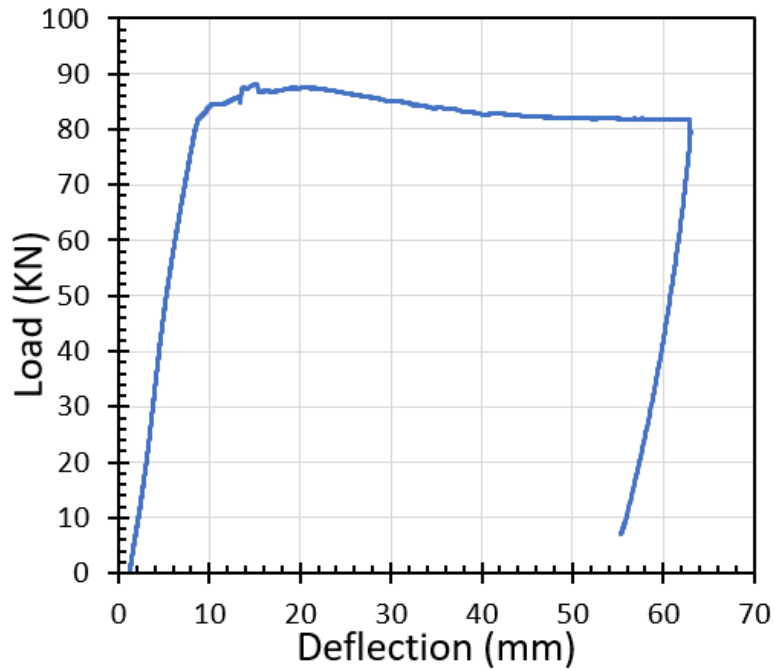


Fig. 4.23 Load versus deflection under residual flexural static loading for beam FBF_30.

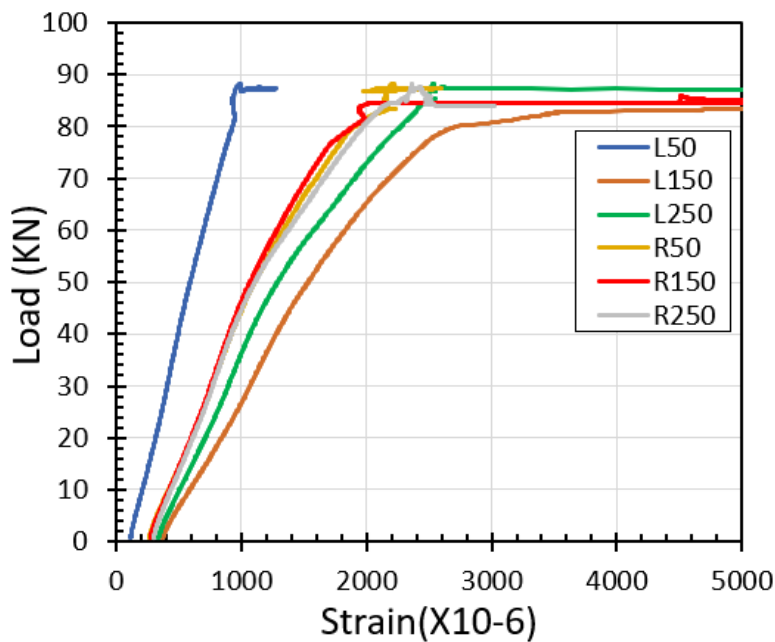


Fig. 4.24 Load versus rebar strain under residual flexural static loading for beam FBF_30.

Beam FBF_40

For the medium fatigue stress level ($S = 0.47$), one SFRC structural beam – FBF_40 – was tested under flexural cyclic loading with 5 kN as a minimum flexural load and 40 kN as a maximum flexural load, as shown in Fig. 4.25. Figure 4.26 shows the load versus mid-span deflection relationship over fatigue life under a medium-stress level of flexural fatigue load showing an increase in mid-span deflection as cycles progress and compared to FBF_30. Figure

4.27 shows the strain distribution at midspan on the front face of the beam (L150), showing the strain evolution for both rebar and concrete throughout the application of flexural cyclic loading until the end of fatigue life. The average rebar strain within the constant moment region of FBF_40 is also plotted against the maximum and minimum flexural cyclic load for the medium fatigue stress levels during the fatigue life, starting from the first flexural cyclic loading (N_1) and showing the evolution of average rebar strain, as shown in Fig. 4.28. After a complete of two million cycles of flexural loading, SFRC beam FBF_40 was subjected to residual flexural static tests to measure their residual capacity, as shown in Figs. 4.29 and 4.30. The result is listed in Table 4.2. Residual flexural capacity is a little different from the original capacity of the beams under static loading, even after the fatigue loading.

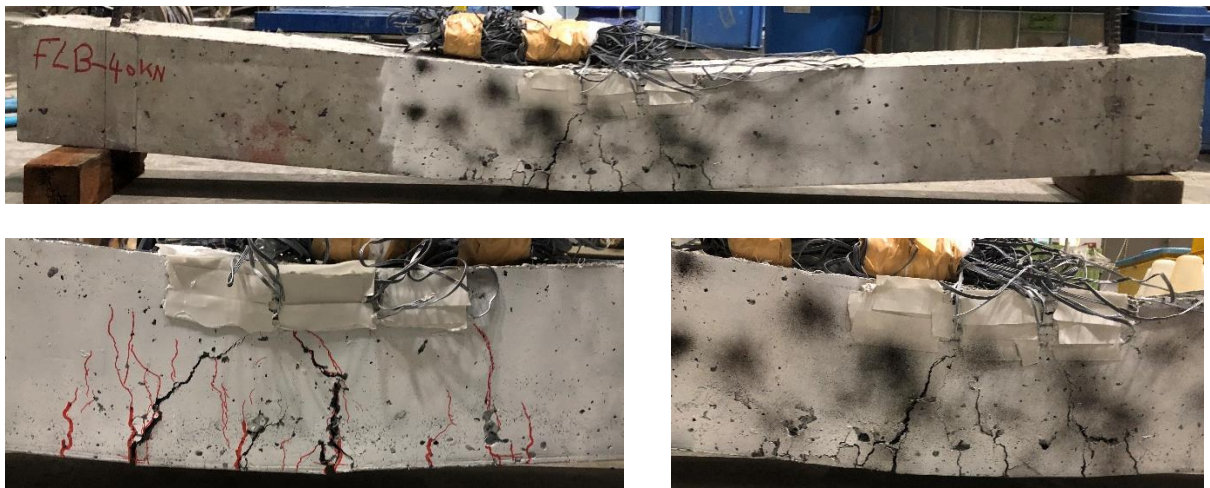


Fig. 4.25 Beam FBF_40 over fatigue life under flexural cyclic loading.

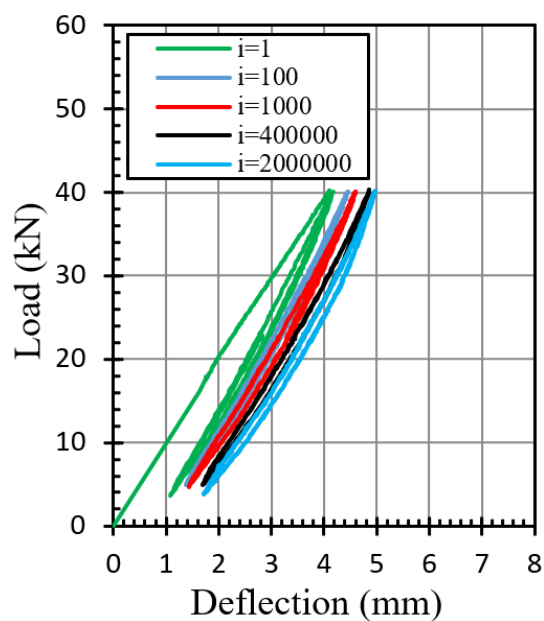


Fig. 4.26 Load versus deflection under flexural cyclic loading for beam FBF_40.

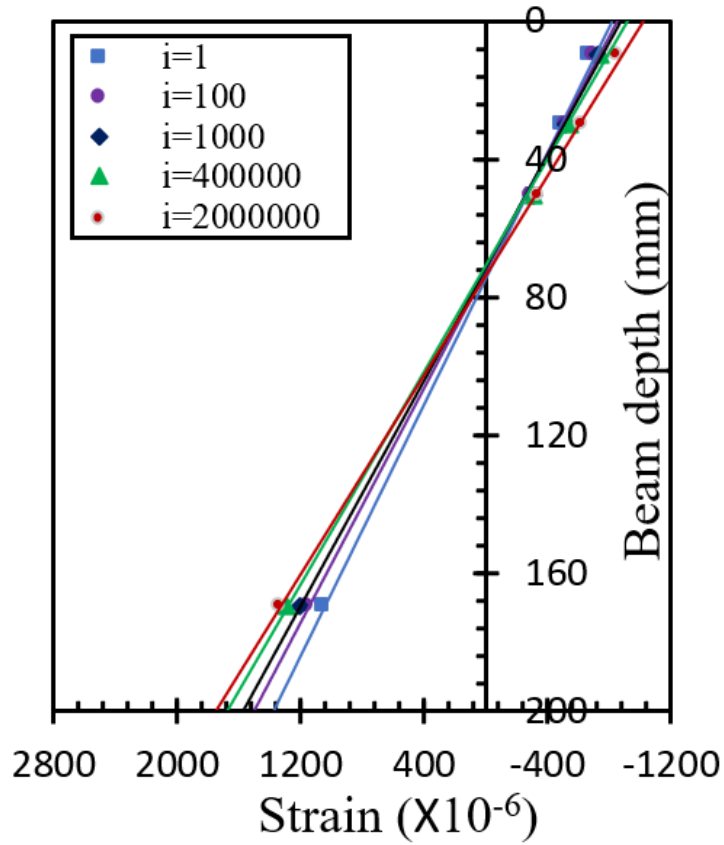


Fig. 4.27 Mid-span strain distribution under flexural cyclic loading for beam FBF_40.

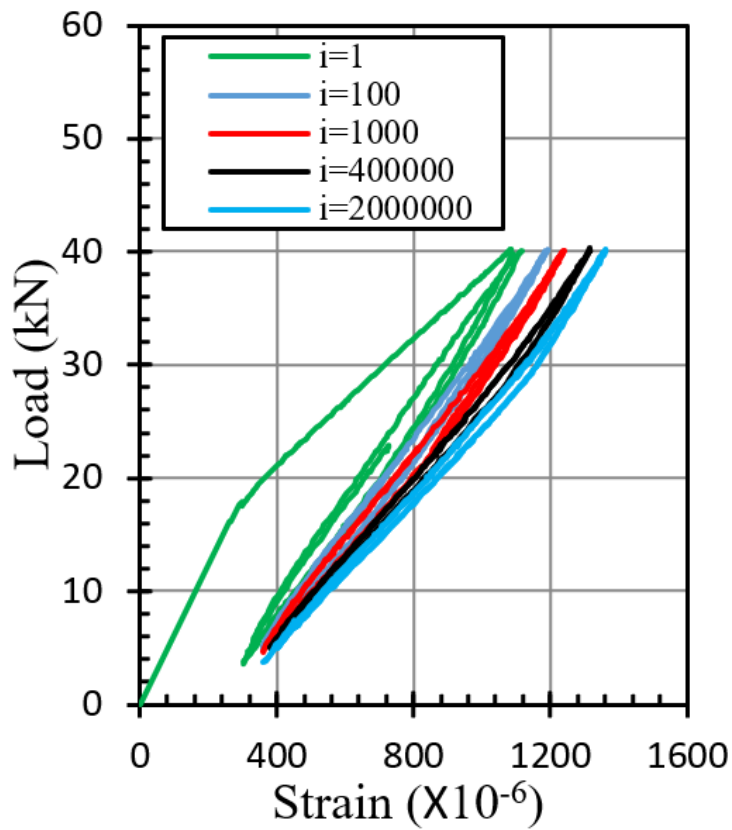


Fig. 4.28 Load versus average rebar strain under flexural cyclic loading for beam FBF_40.

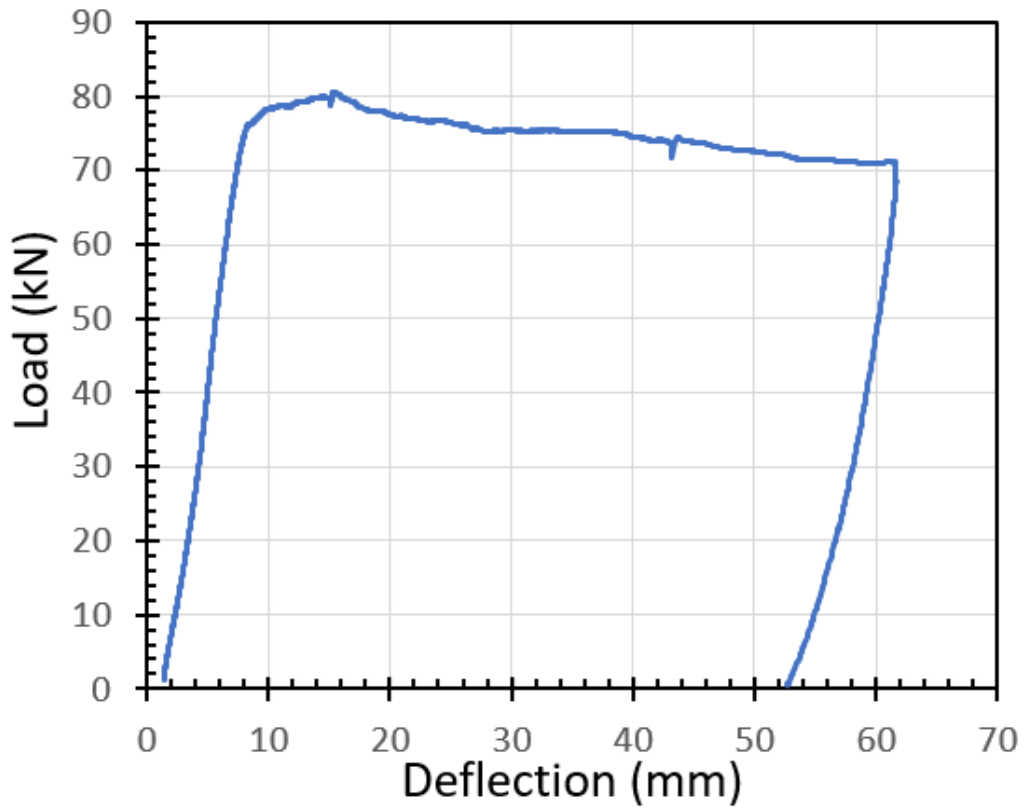


Fig. 4.29 Load versus deflection under residual flexural static loading for beam FBF_40.

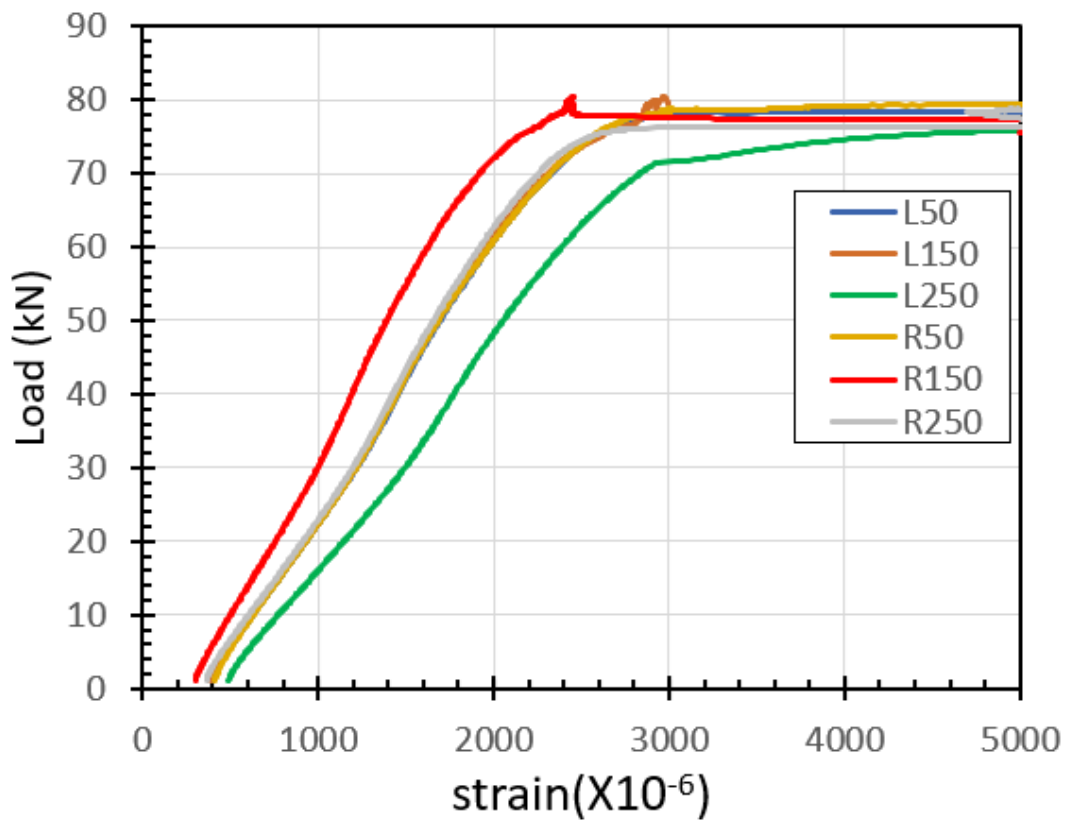


Fig. 4.30 Load versus rebar strain under residual flexural static loading for beam FBF_40.

Beam FBF_50

For the high fatigue stress level ($S = 0.59$), one SFRC structural beam – FBF_50 – was tested under flexural cyclic loading with 5 kN as a minimum flexural load and 50 kN as a maximum flexural load, as shown in Fig. 4.31. Figure 4.32 shows the load versus mid-span deflection relationship over fatigue life under a high-stress level of flexural fatigue load showing an increase in mid-span deflection as cycles progress and compared to FBF_30 and FBF_40. Figure 4.33 shows the strain distribution at midspan on the front face of the beam (L150), showing the strain evolution for both rebar and concrete throughout the application of flexural cyclic loading until fatigue failure. The average rebar strain within the constant moment region of FBF_50 is also plotted against the maximum and minimum flexural cyclic load for the high fatigue stress levels during the fatigue life, starting from the first flexural cyclic loading (N_1) and showing the evolution of average rebar strain until rebar brittle rupture at 380116 cycles, as shown in Figs. 4.34 and 4.31.



Fig. 4.31 Beam FBF_50 over fatigue life under flexural cyclic loading.

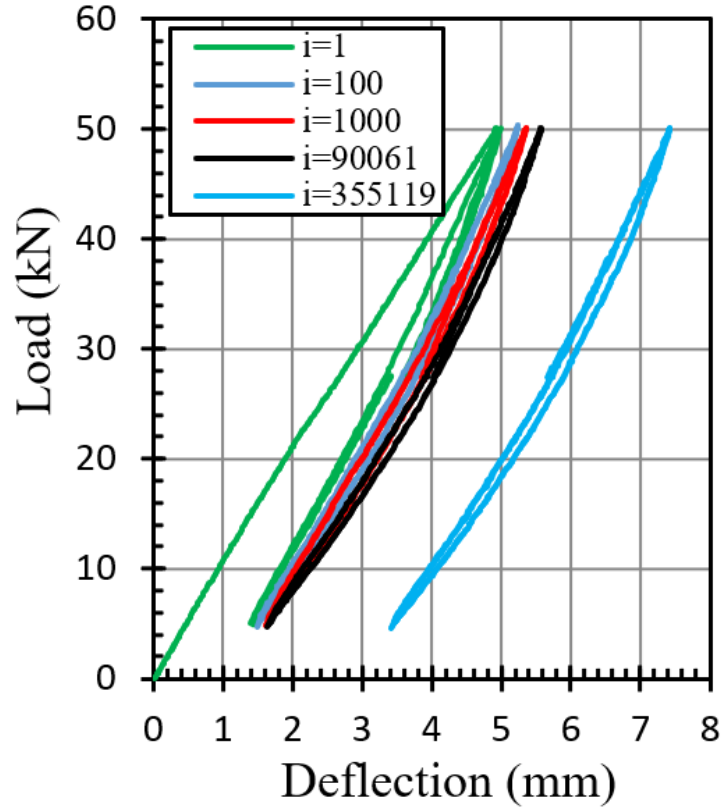


Fig. 4.32 Load versus deflection under flexural cyclic loading for beam FBF_50.

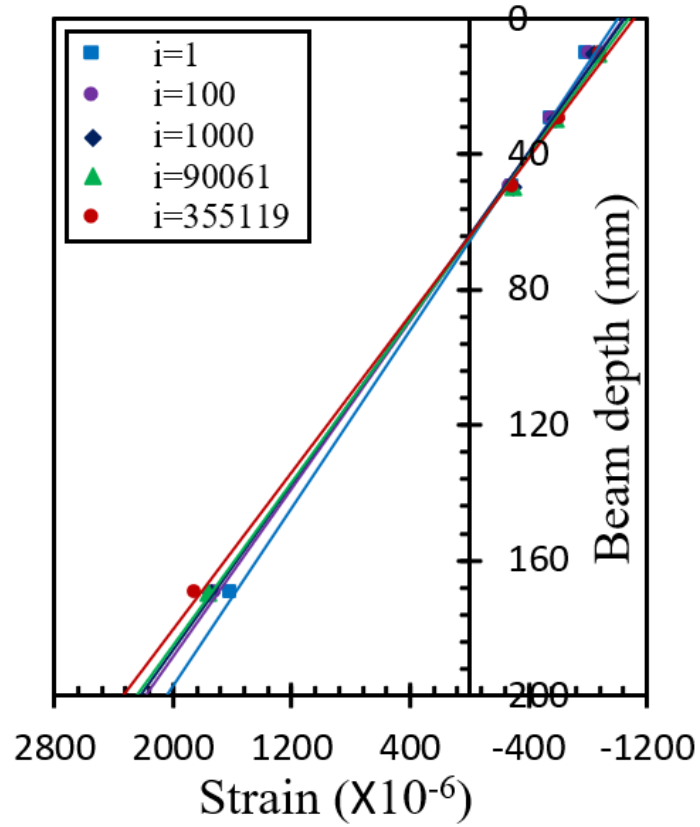


Fig. 4.33 Mid-span strain distribution under flexural cyclic loading for beam FBF_50.

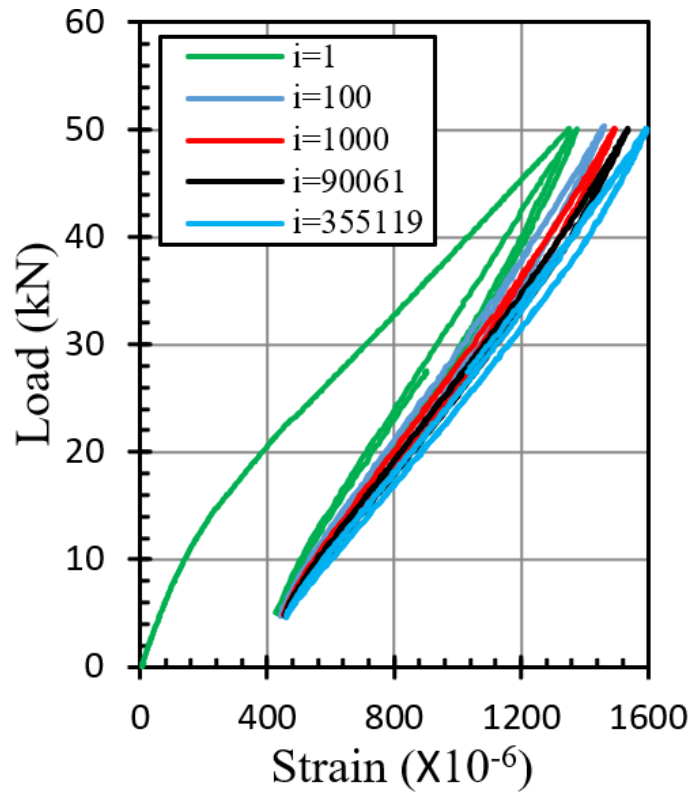


Fig. 4.34 Load versus average rebar strain under flexural cyclic loading for beam FBF_50.

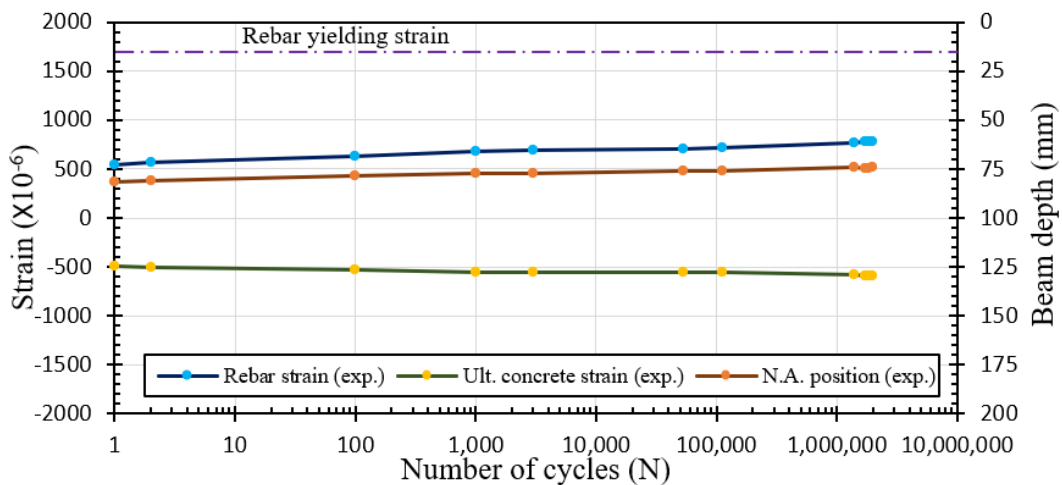


Fig. 4.35 Average experimental fatigue response of beam FBF_30 over the fatigue life.

Finally, the average experimental data of the fatigue response of the SFRC structural beams over the fatigue life to be used in the inverse analysis calculation method. The degradation of the crack-bridging strength would be evaluated by achieving a good fitting between the experimental and calculated fatigue response of the tested structural SFRC beams. As a result, the average experimental rebar strain, ultimate surface concrete strain, and N.A. position were monitored and plotted in [Figure 4.35](#) for the FBF_30 beam, [Figure 4.36](#) for the FBF_40 beam, and [Figure 4.37](#) for the FBF_50 beam over the flexural fatigue life.

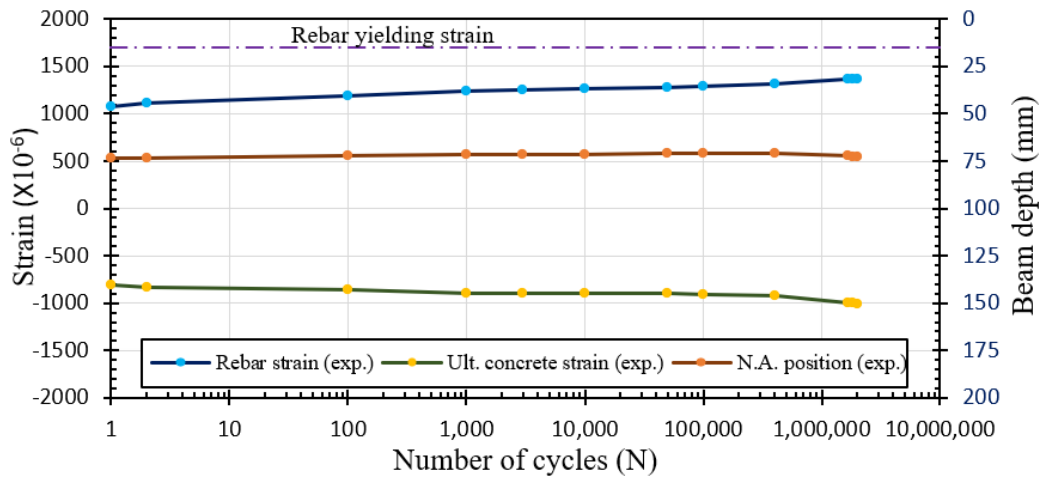


Fig. 4.36 Average experimental fatigue response of beam FBF_40 over the fatigue life.

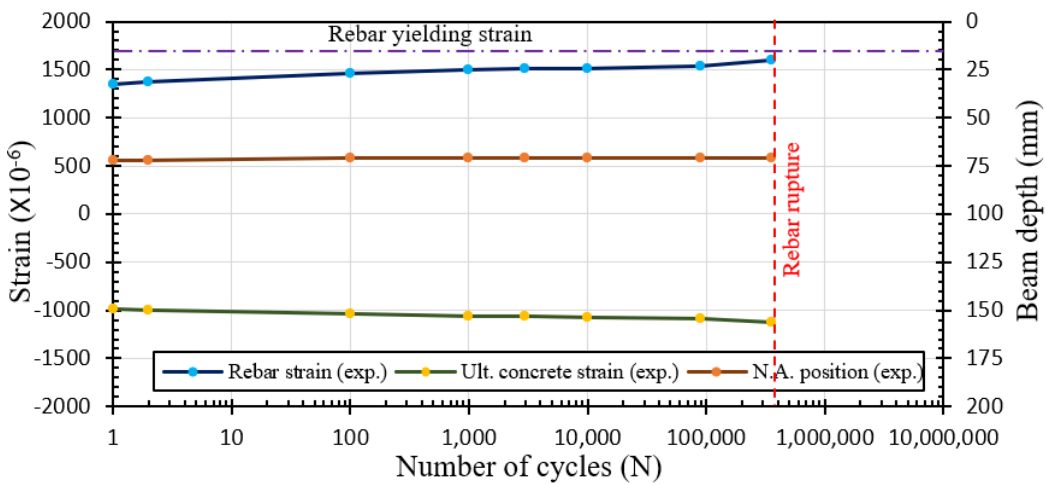


Fig. 4.37 Average experimental fatigue response of beam FBF_50 over the fatigue life.

4.4.4 Fatigue Flexural Loading of RC Structural Beams

On the other hand, a flexural cyclic loading test was carried out on three NC structural beams for measuring the flexural fatigue response and comparing it with the SFRC flexural fatigue response. Through this comparison, the steel fiber's contribution to bridging the cracks opening and resisting the tensile stress with ordinary rebar could be emphasized. As a result, the three NC structural beams were tested under 30 kN, 40 kN, and 50 kN maximum load level of flexural fatigue as same as SFRC structural beams. The tested beams labeled as followed NBF_30, NBF_40, and NBF_50. Beams NBF_30 and NBF_40 survived until the end of two million cycles and after that, they were tested under residual flexural static test, however, beam NBF_50 were failed at 766087 cycles in a rupture brittle failure of rebar, as listed in [Table 4.2](#).

Over the fatigue life, the load versus deflection relationship for the three NC structural beams are shown in the following [Figures 4.38,4.39](#), and [4.40](#) for NBF_30, NBF_40, and NBF_50 respectively. Also, the load versus average rebar strain relationship for the three NC structural beams are shown in the following [Figures 4.41,4.42](#), and [4.43](#) for NBF_30, NBF_40, and NBF_50 respectively.

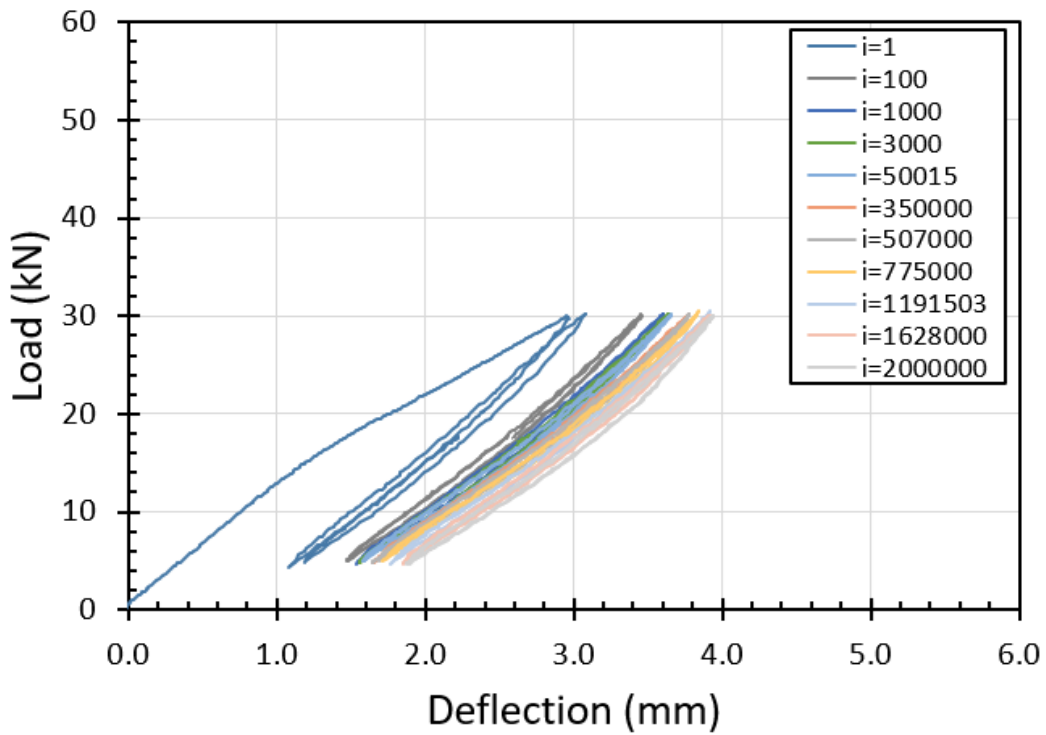


Fig. 4.38 Load versus deflection under flexural cyclic loading for beam NBF_30.

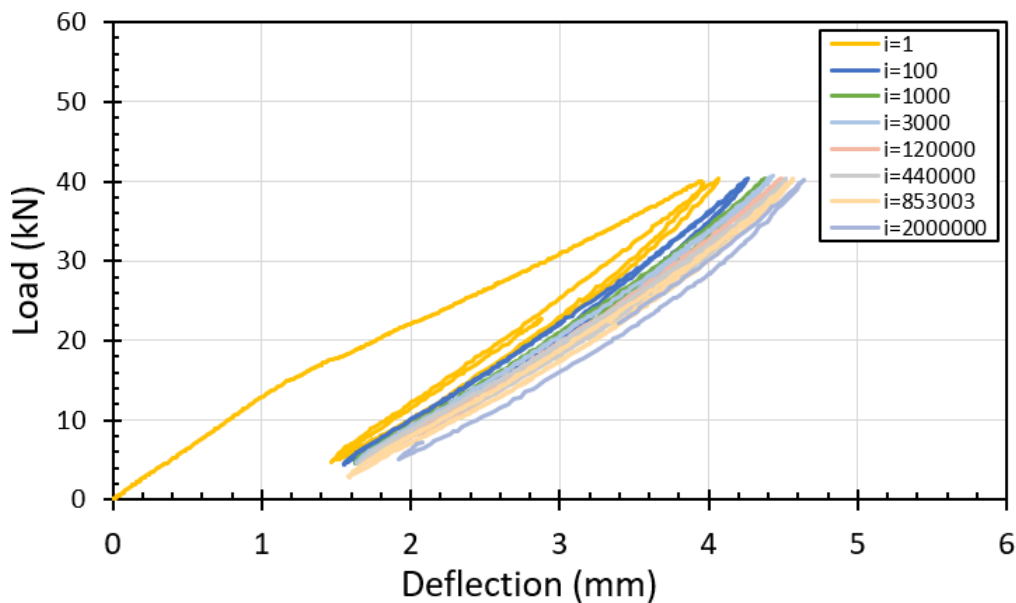


Fig. 4.39 Load versus deflection under flexural cyclic loading for beam NBF_40.

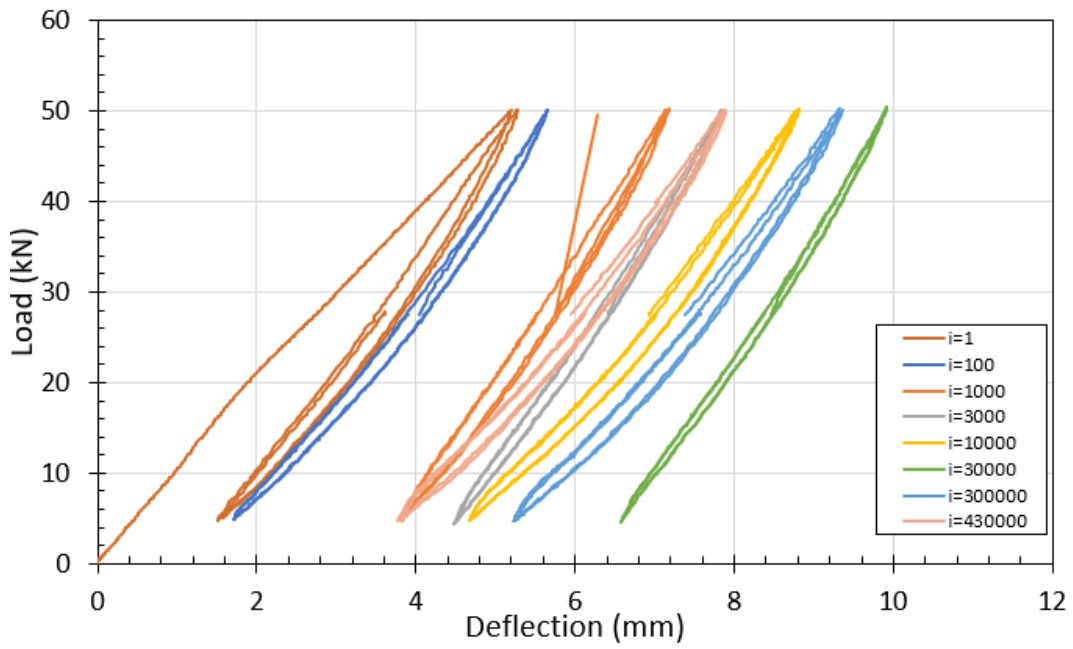


Fig. 4.40 Load versus deflection under flexural cyclic loading for beam NBF_50.

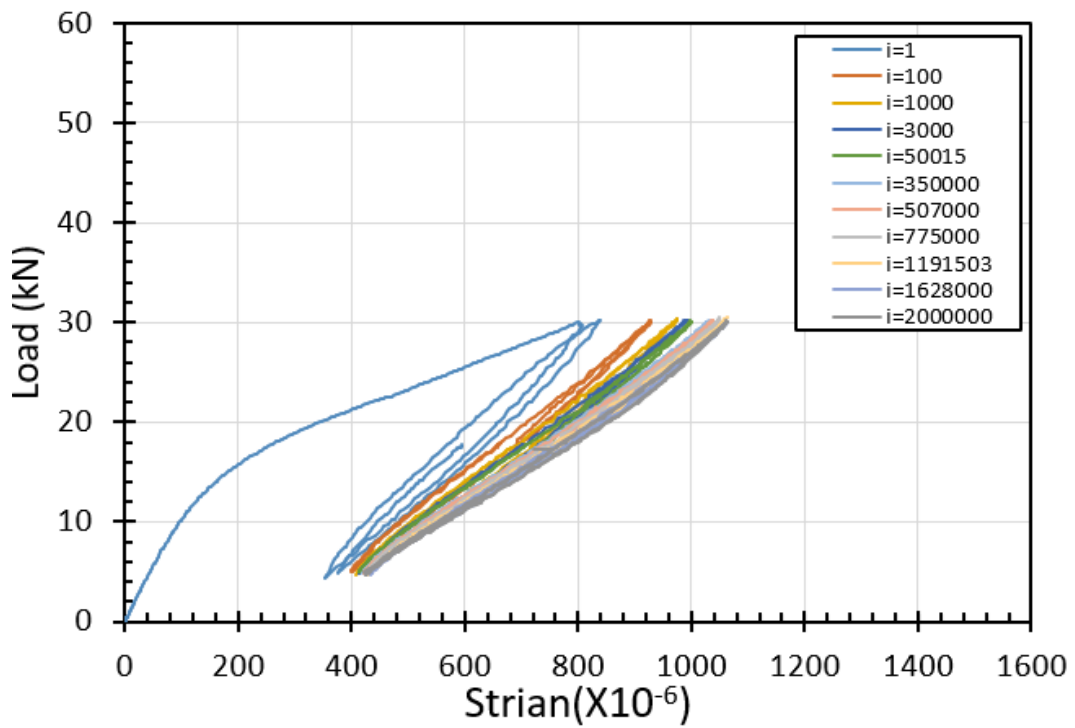


Fig. 4.41 Load versus average rebar strain under flexural cyclic loading for beam NBF_30.

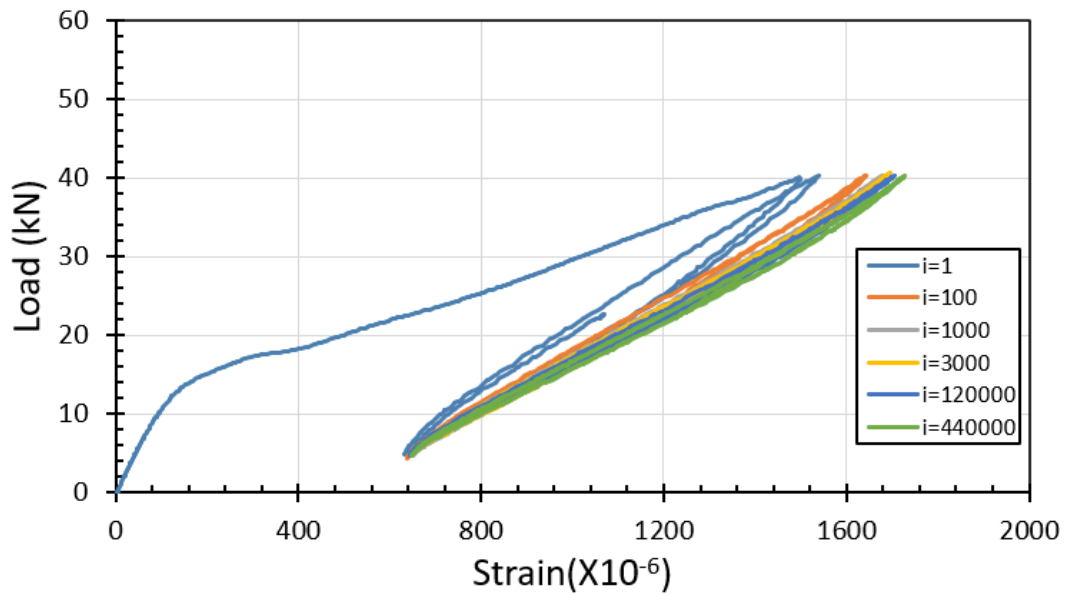


Fig. 4.42 Load versus average rebar strain under flexural cyclic loading for beam NBF_40.

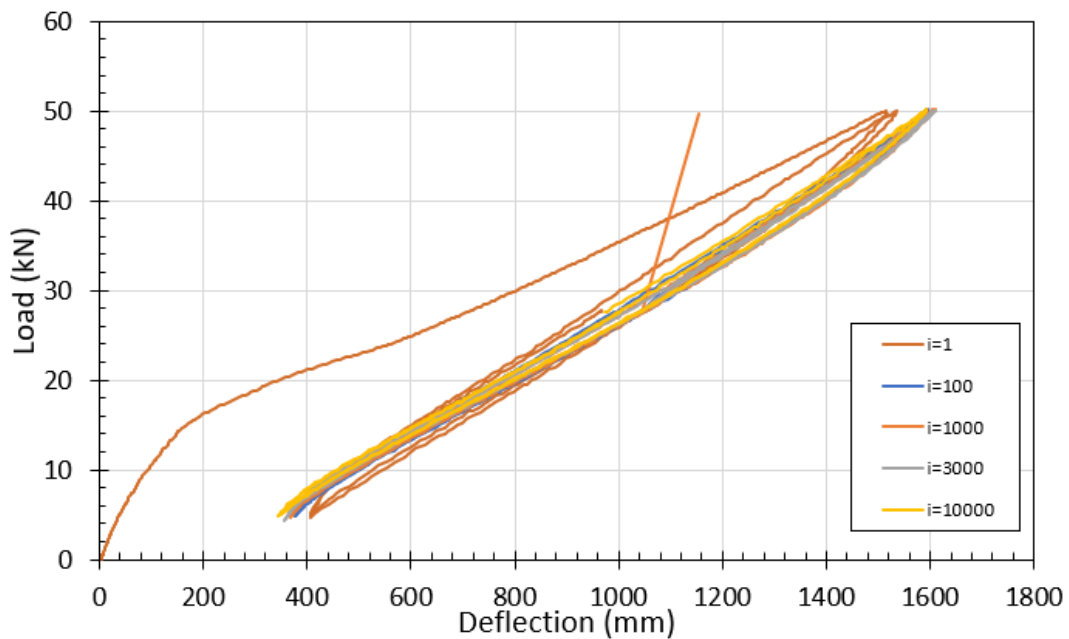


Fig. 4.43 Load versus average rebar strain under flexural cyclic loading for beam NBF_50.

In [Figure 4.44](#), the maximum rebar strains within the constant moment region at the maximum flexural fatigue load are plotted over the whole fatigue life for both NC and SFRC structural beams. These experimental results show that the rebar strain in NC structural beams is higher than in SFRC structural beams from the first cycle load of loading (N_1), indicating the influence of the steel fibers in bridging the cracks and carrying tensile strength. Further, the maximum rebar strain of SFRC structural beams increased faster than that of NC Structural beams, with the two becoming closer over the fatigue life, confirming the degradation of crack-bridging strength induced by the steel fibers, as shown in [Fig. 4.44](#).

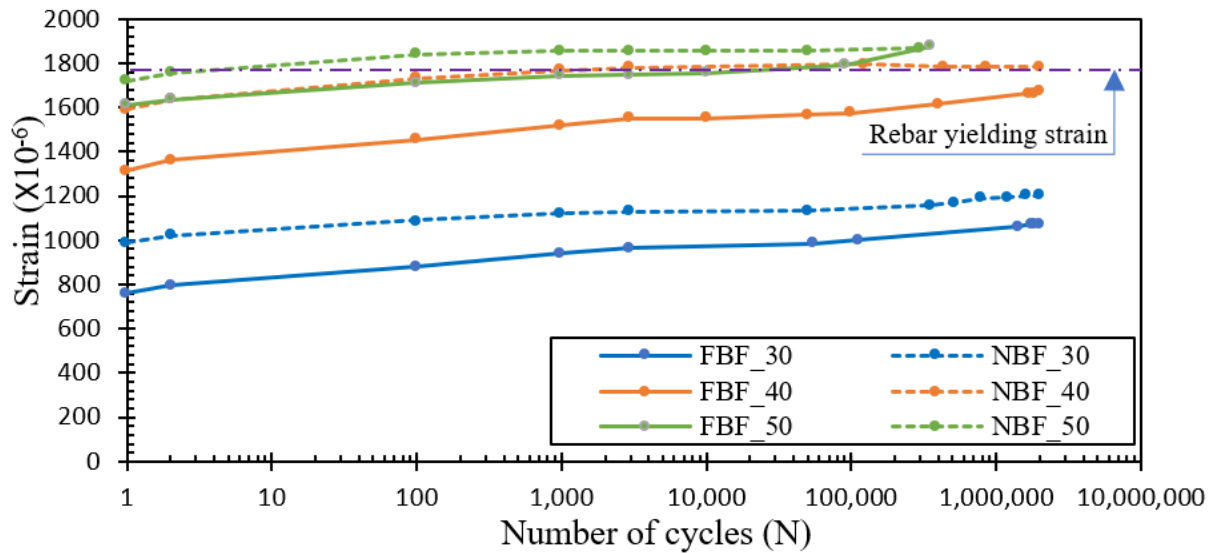


Fig. 4.44 Average experimental fatigue response of beam FBF_50 over the fatigue life.

4.5 Discussion on The Evaluated Crack-bridging Strength

The inverse analysis method of computation involves incremental calculations during fatigue loading as the number of cycles increases, as explained in section 3.4.3. The computations are performed iteratively for the incremental set of fatigue cycles (N_i) until fatigue ruptures or the completion of two million cycles (N_f). At each increment N_i , a certain degradation level (α_i) of initial crack-bridging strength is proposed to adjust the balance between the experimentally measured results and the calculated values; if the agreement between the calculated and experimental results is not within the set threshold, the analysis is repeated using a different level of degradation until the threshold is met, as illustrated in Figs. 3.13, 4.45, 4.46, and 4.47.

The normalized crack-bridging strength (β_i) is derived using Eq. (3.4) and plotted in Fig. 4.48, illustrating the degradation of crack-bridging strength over the fatigue life of the three SFRC structural beams. Note, however, that the normalized crack-bridging strength at the first cycle (N_1) of fatigue loading does not necessarily start at 1.0 because cracking is initiated at the weakest section in the constant moment region of an SFRC structural beam, as compared to the predefined crack in a specific location on the notched prismatic specimen.

Figures 4.45, 4.46, and 4.47 compare the calculated and averaged experimental results for rebar strain, ultimate compressive concrete strain, and N.A. position for the three different fatigue stress levels. The fit is acceptable in all cases, as illustrated by the R squared value. In all cases, there is a clear increase in average strain levels for both rebar and concrete and a decrease in

the N.A. position as the number of cycles increases. The normalized crack-bridging strength at all fatigue stress levels tends to decrease with the number of loading cycles, as shown in Fig. 4.48. Further, at the high fatigue stress level of FBF_50, crack-bridging strength degrades rapidly, followed by a plateau for the rest of the fatigue life; when the rebar strain is close to the yield strain. The conclusion from these results is that the proposed inverse analysis method could predict the degradation of crack-bridging strength provided by fibers as flexural fatigue loading continues.

Besides, the normalized crack-bridging strength at all fatigue stress levels is plotted versus the evolution of the experimental maximum rebar strain, as shown in Fig. 4.49. By cyclic progress of flexural fatigue loading, the repeated tensile stress resulted in increasing the width of the cracks. That would lead to loss of the bond between fibers and matrix where degradation of crack-bridging strength took place. Simultaneously, an increase in the level of rebar strain over the fatigue life is achieved. Figure 4.49 shows an interesting linear constant relationship between the degradation of the crack-bridging strength and the evolution of the maximum rebar strain over the fatigue life regardless of the fatigue stress level, that it would be a helpful tool for design and assessment of SFRC structural beams under fatigue loading by controlling the rebar strain level through avoiding the brittle rupture of steel reinforcing bars.

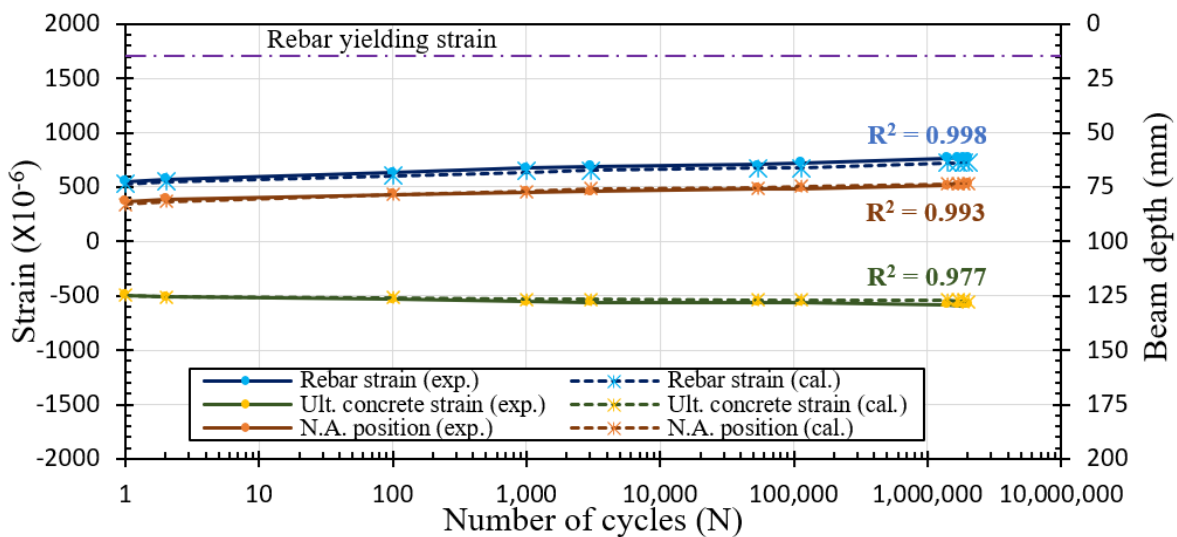


Fig. 4.45 Calculated versus experimental fatigue response of FBF_30 over the fatigue life.

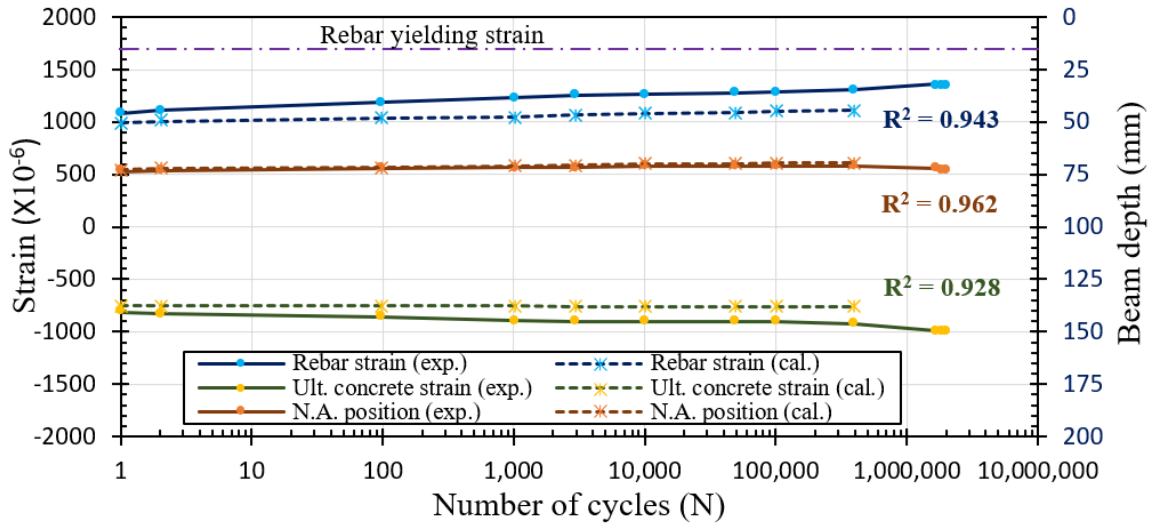


Fig. 4.46 Calculated versus experimental fatigue response of FBF_40 over the fatigue life.

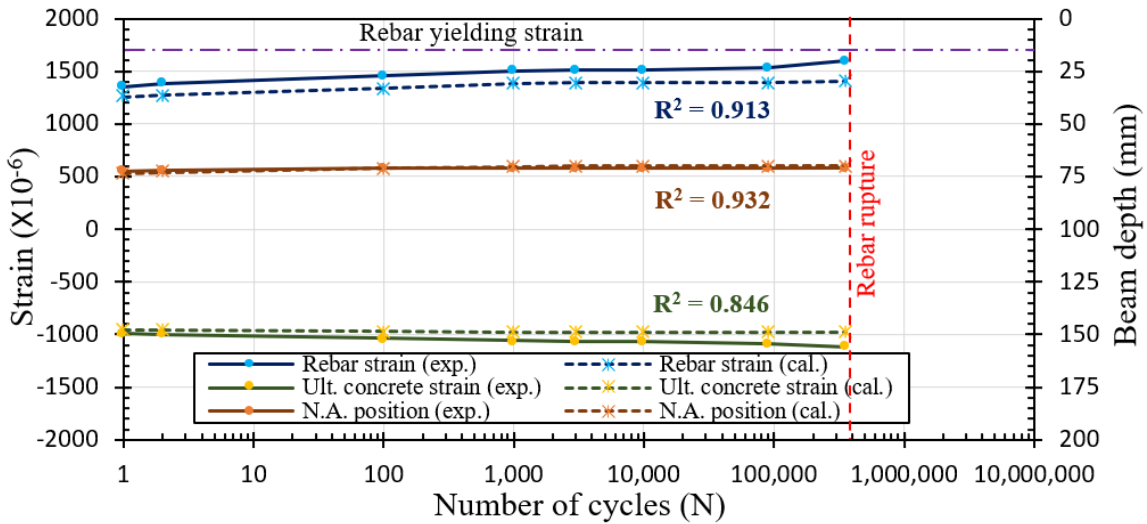


Fig. 4.47 Calculated versus experimental fatigue response of FBF_50 over the fatigue life.

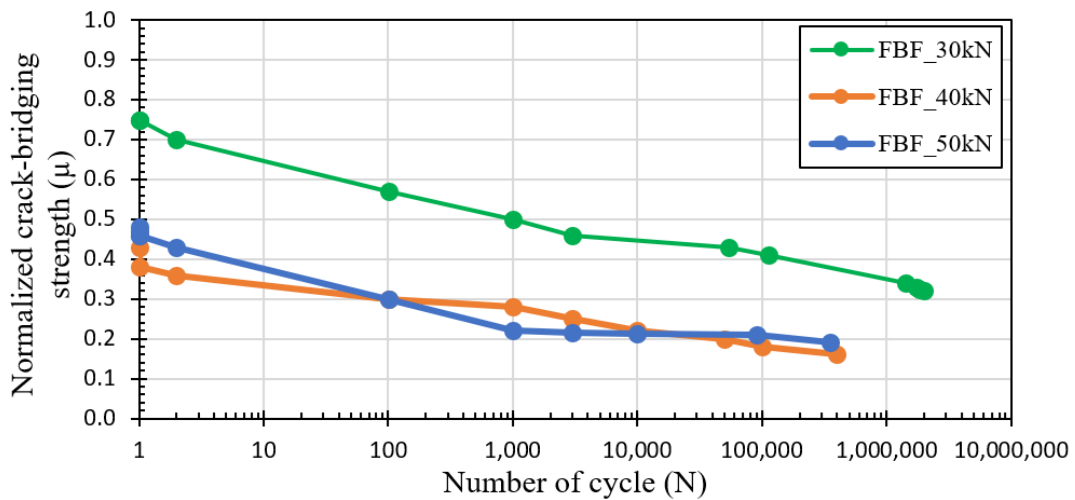


Fig. 4.48 Normalized crack-bridging strength degradation over flexural fatigue life.

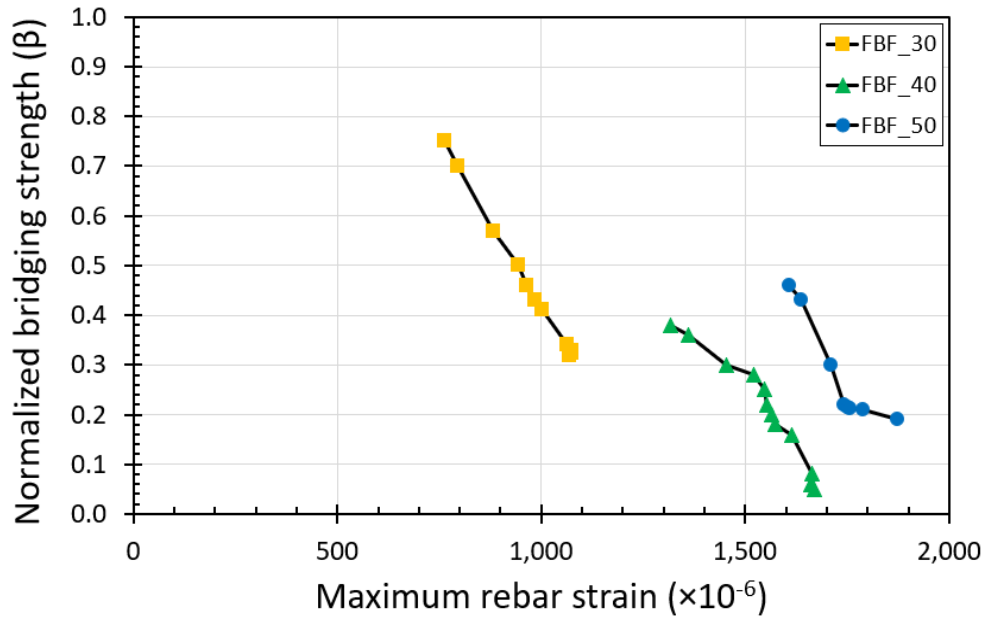


Fig. 4.49 Normalized crack-bridging strength degradation versus maximum rebar strain.

4.6 Conclusion

The research work of the first series presented in this chapter aimed at evaluating the degradation of crack-bridging strength provided by hooked-end steel fibers over the whole fatigue life of structural beams under cyclic loading with a constant amplitude between a minimum and maximum flexural load. An inverse analysis method is used to derive a degradation model for crack-bridging strength from the experimental response of SFRC structural beams. The degradation model is then used to evaluate degradation for three different levels of fatigue stress. The main conclusions that can be drawn from this work are as follow:

1. It is confirmed, by tracing the evolution of maximum rebar strain for both NC and SFRC structural beams, that crack-bridging strength degrades as the number of cycles of flexural loading increases.
2. The residual capacity of an SFRC structural beam subjected to flexural cyclic loading at lower stress levels (0.35 and 0.47) was unchanged after two million cycles, indicating that the ultimate capacity of an SFRC structural beam is determined by its static capacity.
3. The good fit obtained with the proposed degradation model for the crack-bridging strength provided by steel fibers confirms the applicability of inverse analysis assuming

a plane strain distribution since no strain redistributions in the compressive stress zone was observed.

4. The normalized crack-bridging strength, which is proposed for each different level of flexural fatigue stress of SFRC structural beams, monotonically decreases with the number of loading cycles for all fatigue stress levels, except in the case of high fatigue stress when there is a rapid initial degradation followed by a plateau when the rebar stress reaches close to the yield point.
5. The normalized crack-bridging strength, which is proposed for each different level of flexural fatigue stress of SFRC structural beams, monotonically linearly decreases with the evolution of rebar strain level for all fatigue stress levels, with almost same inclination regardless the fatigue stress level.
6. Using the degraded crack-bridging strength obtained from material level tests (the tension softening curve) and the proposed degradation model based on direct sectional analysis calculations over a certain number of fatigue loading cycles, an accurate full design procedure for the whole fatigue life of SFRC beams under flexural fatigue loading is expected to be developed.

Chapter 5

5 Evaluation of Crack-bridging Strength of SFRC

Structural Beams under Variable Amplitude Flexural

Cyclic loading

5.1 Introduction

This chapter examines the influence of hooked-end steel fibers on the reinforced concrete structural beams subjected to flexural cyclic loading in bridging the crack's opening under several fatigue stress levels in an increasing or decreasing manner. As well, this chapter aims to understand the mechanism of crack-bridging strength evaluated from the inverse analysis calculation method based on changing the fatigue load levels in an increasing or decreasing manner. Furthermore, by the end of this chapter, a diagram of the crack-bridging strength degradation and evolution over the fatigue life of SFRC structural beams under flexural cyclic loading under several fatigue stress levels would be proposed based on inverse analysis calculation methods. The experimental program for the second series of SFRC beams on the structural scale under fatigue loading conditions is presented. Firstly, the experimental fatigue response data of structural beams are captured to be used in the execution of the inverse analysis calculation method in case of increasing and decreasing flexural fatigue load level. Finally, the crack-bridging strength is evaluated for the second series of SFRC structural beams under a variable flexural fatigue load level over their fatigue life varying from a low, medium, to high fatigue stress level.

5.2 Experimental Program

The experimental program of the second series consisted of SFRC specimens that are tested on both material and structural scale, with the same proportions and testing set up as the first series as described in chapter four.

Material level tests were carried out to evaluate the material properties such as concrete compressive strength (f_{cm}), concrete first cracking tensile strength (f_{ct}), concrete modulus of elasticity (E_c), and the steel fiber reinforced concrete's tension softening curve and fracture energy (G_f) as listed in [Table 5.1](#). The results of the tests are presented and evaluated with particular emphasis on the effects of steel fibers on the fatigue response of the beams.

Besides, structural scale tests consist of two structural scales SFRC beams with 1.5% hooked-end steel fibers (Dramix 3D 65/35 BG), having the same cross-section area of 150 mm x 200 mm and a span length (l) of 1700 mm with 300 mm of constant moment loading span (s) and effective depth (d) of 170 mm, each had two conventional rebars with a diameter (D) of 16 mm as listed in [Table 5.2](#). The beams were instrumented to measure the rebar strains, surface concrete strains, and mid-span deflections having testing configurations as shown in [Fig. 4.1](#).

Table 5.1: Test program of material scale specimens.

| Specimen | Description | SFRC |
|--|-------------------------------|-------|
| Cylinder (D =100 mm) (L=200 mm) | Number of specimens | 9 |
| | Compressive strength (MPa) | 32.65 |
| | Young's modulus (GPa) | 25.17 |
| Cylinder (D =150 mm) (L=150 mm) | Number of specimens | 7 |
| | Tensile strength (MPa) | 3.2 |
| Prismatic specimen (100 x 100 x 400 mm) | Number of specimens | 6 |
| | Flexural strength (kN) | 13.7 |
| | Fracture energy (N/mm) | 10.0 |

Table 5.2: Test program of structural scale beams.

| Beam ID | Fiber volume (%) | Min. fatigue load (kN) | Max. fatigue load (kN) | Fatigue life |
|-----------------------|------------------|------------------------|------------------------|--------------|
| FBF_30-40-50-60 | 1.5 | 5.0 | 30→40→50→60 | 4,397,844 |
| FBF_50-40-30-40-50-60 | 1.5 | 5.0 | 50→40→30→40→50→60 | 6,481,200 |

Note: The structural beams were tested under a four-point bending fatigue test. the arrow in maximum fatigue load cells indicates the changing of the fatigue load within the fatigue life.

5.2.1 Material and Mix Proportion

The concrete used in the second series for SFRC was a normal grade concrete with a target mean strength (f_{cm}) of 35 MPa. The following materials were used as same as the first series in mixing and production of concrete: cement, coarse aggregate, fine aggregate, steel fibers, water, and superplasticizer. Table 5.3 shows the mix proportions of SFRC. Ordinary portland cement meeting the Japanese industrial standards (JIS) was used as the binding material, with a specific gravity of 3.15. Crushed coarse and fine aggregates were used with maximum aggregate sizes of 13.0 mm and 4.75 mm and specific gravities of 2.66 and 2.65, respectively. The steel fibers - Dramix 3D 65/35 BG - were gradually sprinkled into the mix by hand to a 1.5% volume fraction of the full SFRC volume, and care was taken to obtain a homogenous and workable mixture. Furthermore, a high-performance air-entraining water-reducing agent (Types: SP8SV and SBsX3) were used in SFRC in a range of 1.0% per each to the weight of the cement for each concrete mix as a superplasticizer to obtain an average 120 mm slump value. The water to cement ratio was 55% for SFRC. Finally, the SFRC batches were introduced into their molds and compacted, then the specimens were removed from the molds after 3 days and cured for 28 days.

The structural beams were reinforced with tensile reinforcement consisted of two 16 mm nominal diameter bars as same as the first series. The longitudinal reinforcing bars were hot rolled deformed steel bars, all from the same batch with a nominal yield strength of 346 MPa and Young's modulus of 200 GPa. The structural beams were designed to be failed under flexural loading conditions without any need for shear reinforcement and compression reinforcement.

Table 5.3: Mix proportion of the first series for NC and SFRC.

| Ingredient | Amount (kg/m³) SFRC |
|-------------------------|---|
| Portland cement | 336 |
| Water | 185 |
| Fine aggregate | 1055 |
| Coarse aggregate | 706 |
| Hooked-end steel fibers | 117.8 |
| Superplasticizer | 5.05 |

5.2.2 Specimens

The test program consisted of several SFRC specimens that were tested on both material and structural scales for the second series test set. The second series aims to capture the fatigue response of SFRC over the fatigue life under variable fatigue load levels in an increasing and decreasing manner. Besides, as same as the first series the execution of the inverse analysis calculations method requires detailed information about the material properties of SFRC, as a result, material level tests were carried out to identify the materials constitutive laws, targeting finally in the evaluation of the degradation and evolution in the crack-bridging strength over the fatigue life of SFRC structural beams.

Two structural scale beams of steel fiber reinforced concrete were tested under a 4-points bending test under cyclic loading. The details of the tested structural beams of the second series are discussed in [Table 5.2](#). All structural beams have a rectangular cross-section with a dimension of 150 x 200 mm and a length of 2000 mm. The structural beams were tested under flexural loading test with a span length (l) of 1700 mm, with 300 mm of constant moment loading span (s), and an effective depth (d) of 170 mm as shown in [Fig. 4.1](#). All structural beams were reinforced with two ordinary steel reinforcing bars with a diameter (D) of 16 mm with a tensile longitudinal reinforcement ratio of 1.34 percent to be failed inside the constant moment region in a flexural failure mode.

The concrete material properties were determined from the material tests of the second series that were carried out as listed in [Table 5.1](#). The material level specimen's details were as same as the first series as discussed in section 4.2.3 and the results of compressive strength (f_{cm}), concrete modulus of elasticity (E_c), first cracking tensile strength (f_{ct}), the steel fiber reinforced concrete's tension softening curve, and fracture energy (G_f) are listed in [Table 5.1](#).

5.3 Experimental Results

In the second series, several specimens were tested under the material and structural level to capture and analyze the fatigue response of SFRC beams under flexural loads and to evaluate the crack-bridging strength degradation and evolution over the fatigue life while increasing and decreasing the fatigue load levels. Firstly, a 3-point bending test was carried out on notched prismatic SFRC specimens to calculate the crack-bridging strength – tension softening curve – to be used in sectional analysis calculations. Finally, two structural beams were tested under

different stress levels of fatigue loading ranging from low to high-stress levels and vice versa. Considering, the time consuming for testing each beam, two beams of SFRC have been tested cyclically under variable flexural fatigue stress levels, as shown in Figs. 5.1 and 5.2. The following sections discuss the test results of the individual beams. As a result, the results of inverse analysis calculations are presented in the next section in a model of degradation and evolution of the crack-bridging strength induced by hooked-end steel fibers over the fatigue life of variable flexural fatigue stress levels.

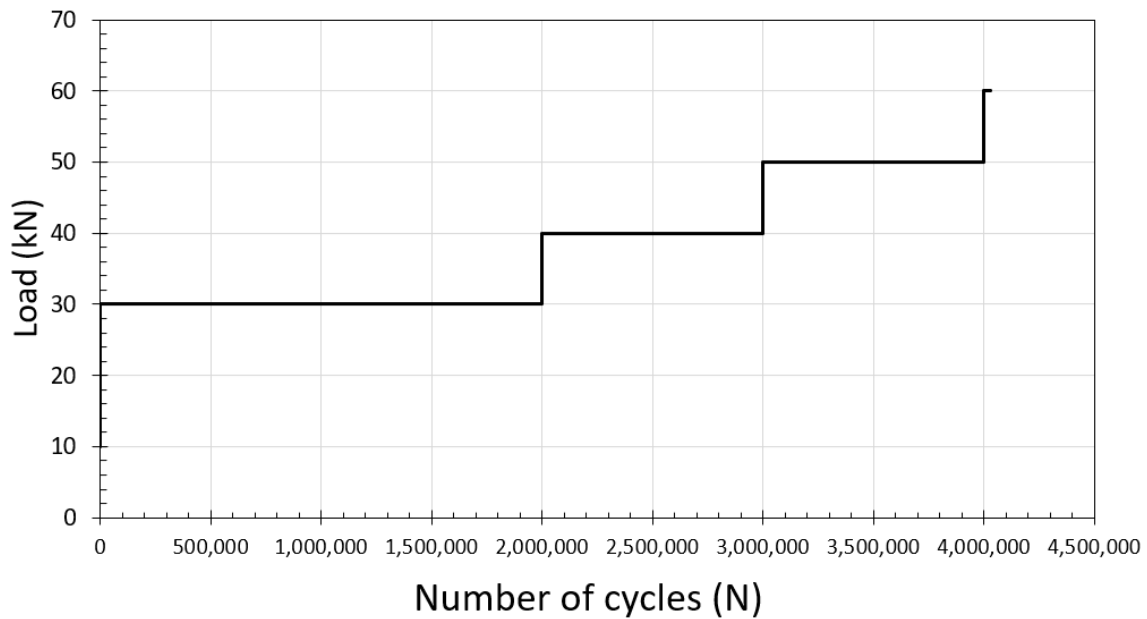


Fig. 5.1 Maximum fatigue load level over the fatigue life of FBF_30-40-50-60.

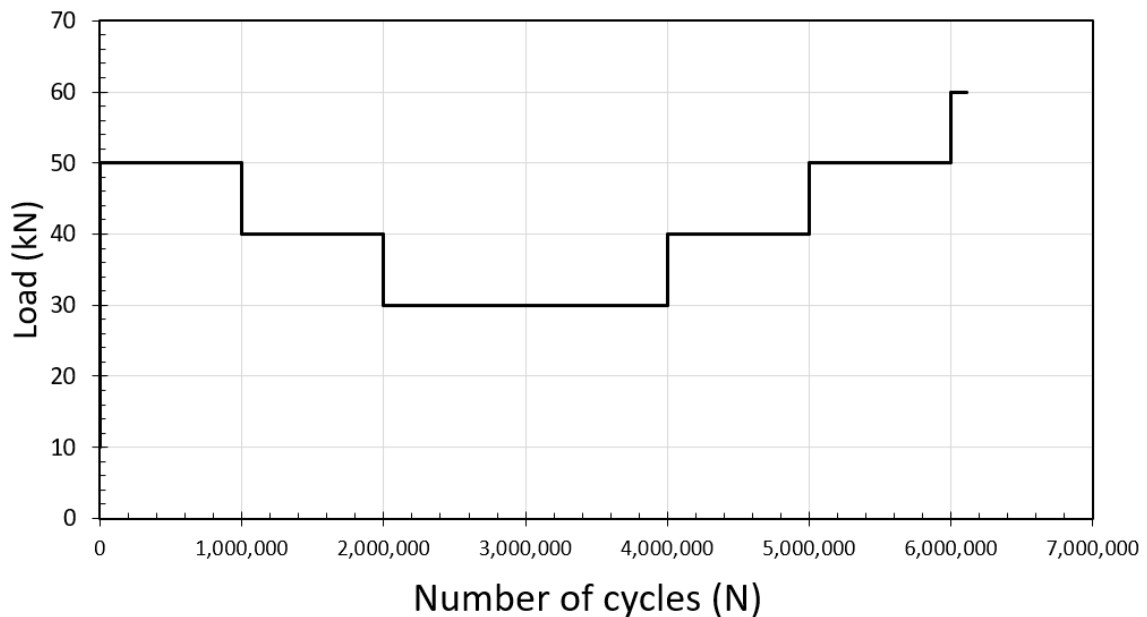


Fig. 5.2 Maximum fatigue load level over the fatigue life of FBF_50-40-30-40-50-60.

5.3.1 Prismatic Specimens under Flexural Static Loading

The crack-bridging strength – or the tension softening curve – is a fracture mechanics parameter that describes post-cracking behavior, represents the fracture energy (G_f) of SFRC in the tensile stress zone, and is used in the sectional analysis calculations to understand the response of structural beams to loading. It is obtained from the material scale flexural test results obtained in the bending test of notched prismatic specimens until complete rupture as shown in Fig. 5.3 using the poly-linear approximation analysis method following the JCI-S-001-2003 standard (JCI 2003a).

The average static flexural capacity of the six SFRC notched prismatic specimens ranging from Sp-01 to Sp-06 was 13.7 kN with a standard deviation of 1.51 kN, as shown in Fig. 5.4. Based on this result, the fracture energy (G_f) was calculated following (JCI 2003a) as 10.00 N/mm on average with a standard deviation of 0.94 N/mm, as summarized in Table 5.1. Using a least-squares data-fitting procedure, the shape of the tension softening diagram can be obtained from the calculated results, having the same tension softening curve of the first series and summarized as Eq. (4.3). This tension softening curve can be divided into three zones. The first zone is immediately after cracking, where the stress abruptly decreases at a crack opening (ω) of less than 0.004 mm; this initial softening branch is assumed to be neglected. This is followed by a fiber bridging plateau (plastic region), followed by the cohesive stress decreases following a softening branch, as shown in Fig. 4.13(b).



Fig. 5.3 Fracture of SFRC prismatic specimen at the end of the bending test.

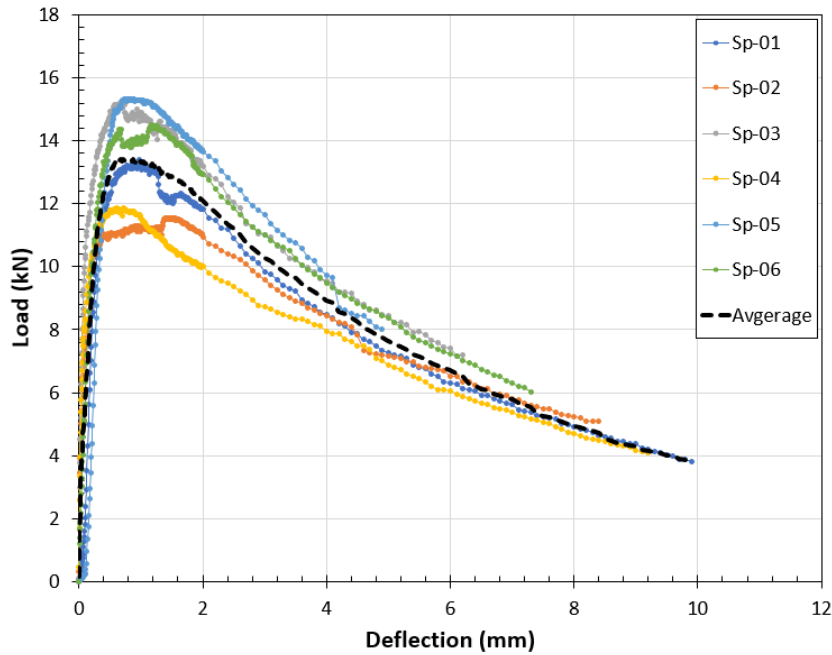


Fig. 5.4 Three-point bending test on SFRC prismatic specimens.

5.3.2 Fatigue Flexural Loading of SFRC Structural Beams

A flexural variable cyclic loading test was carried out on two SFRC structural beams for measuring the flexural fatigue response to evaluate the degradation and evolution of crack-bridging strength over fatigue life using the inverse analysis method, as explained in section 3.4.3 Also, as summarized in [Table 5.2](#). During fatigue loading, as the number of loading cycles increases, an evolution of both the rebar and concrete strain was observed for the SFRC structural beams, resulting in increasing mid-span deflection and crack length and width and decreasing structural stiffness as noted from the decrease of the inclination of the load-deflection curve and N.A. position, as illustrated in the following paragraphs, with an average crack spacing – or reference length (L_R) – of 70 mm, as shown in [Figs. 5.5](#), and [5.13](#).

Beam FBF_30-40-50-60

For the increasing study case of the fatigue stress levels ($S = 0.35 \rightarrow 0.47 \rightarrow 0.59 \rightarrow 0.70$), one SFRC structural beam – FBF_30-40-50-60 – was tested under flexural cyclic loading with 5 kN as a minimum flexural load and 30 kN, 40 kN, 50 kN, 60 kN as a maximum flexural load for two, one, one, one million cycles, respectively and sequentially, as shown in [Figs. 5.1](#), [5.5](#), and [5.8](#). [Figure 5.6](#) shows the load versus mid-span deflection relationship over fatigue life under a low to a high-stress level of flexural fatigue load showing an increase in mid-span deflection as cycles progress. [Figure 5.7](#) shows the strain distribution at midspan on the front

face of the beam (L150), showing the strain evolution for both rebar and concrete throughout the application of flexural cyclic loading until the end of fatigue life. The average rebar strain within the constant moment region is plotted against the maximum and minimum flexural cyclic load for the variable fatigue stress levels during the fatigue life, starting from the first cyclic loading (N_1) and showing the evolution of average rebar strain, as shown in Fig. 5.8.

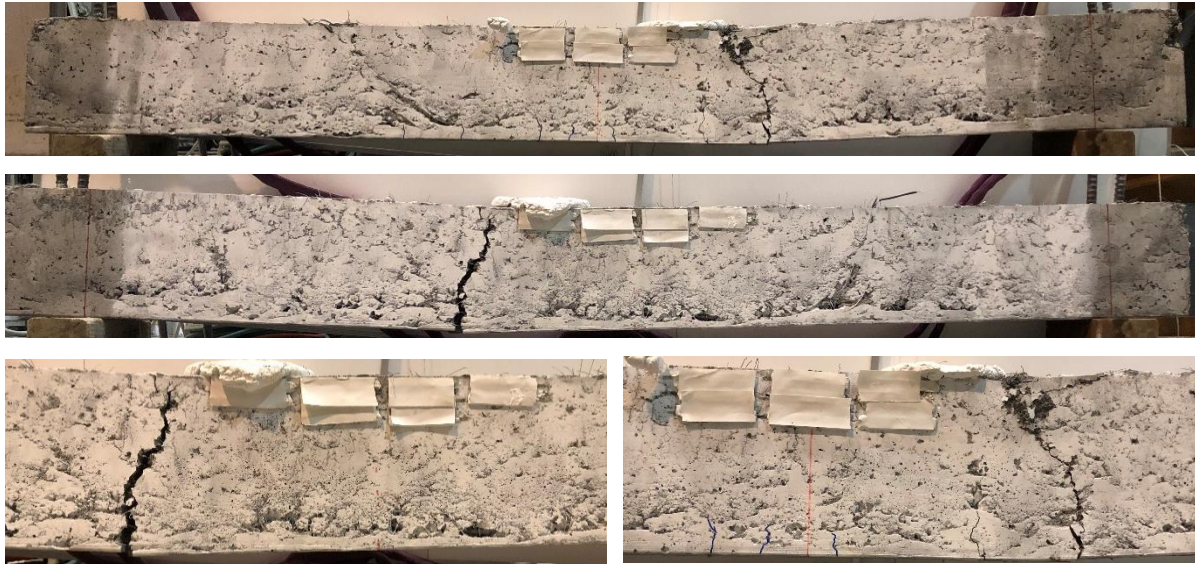


Fig. 5.5 Beam FBF_30-40-50-60 over fatigue life under flexural fatigue.

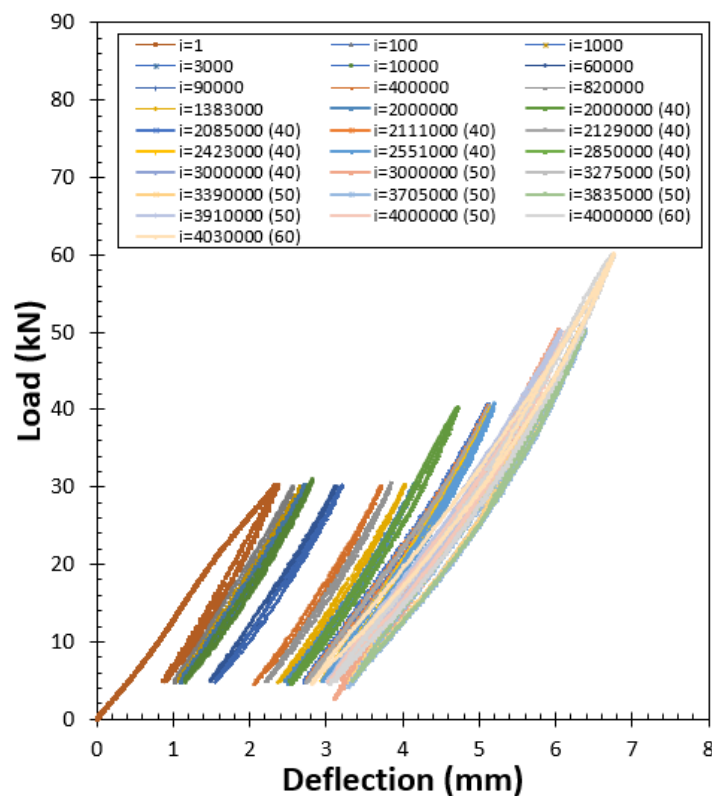


Fig. 5.6 Load versus deflection under flexural fatigue for beam FBF_30-40-50-60.

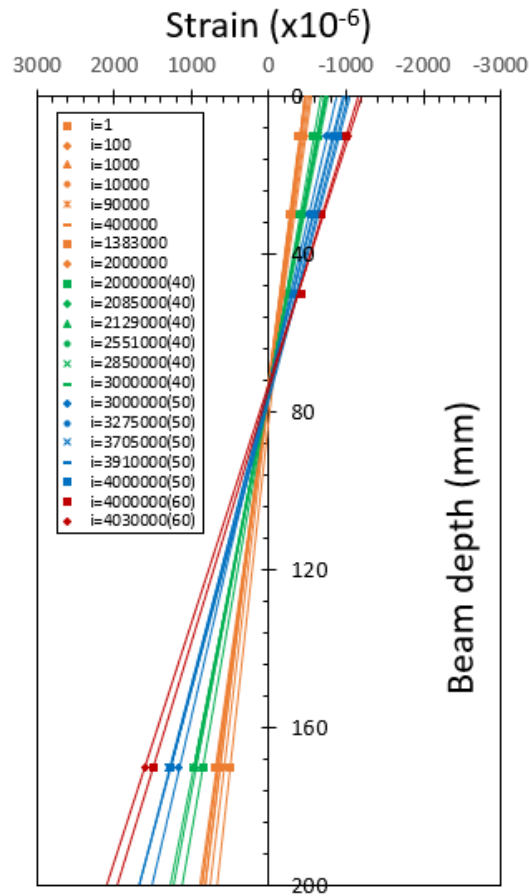


Fig. 5.7 Mid-span strain distribution under flexural fatigue for beam FBF_30-40-50-60.

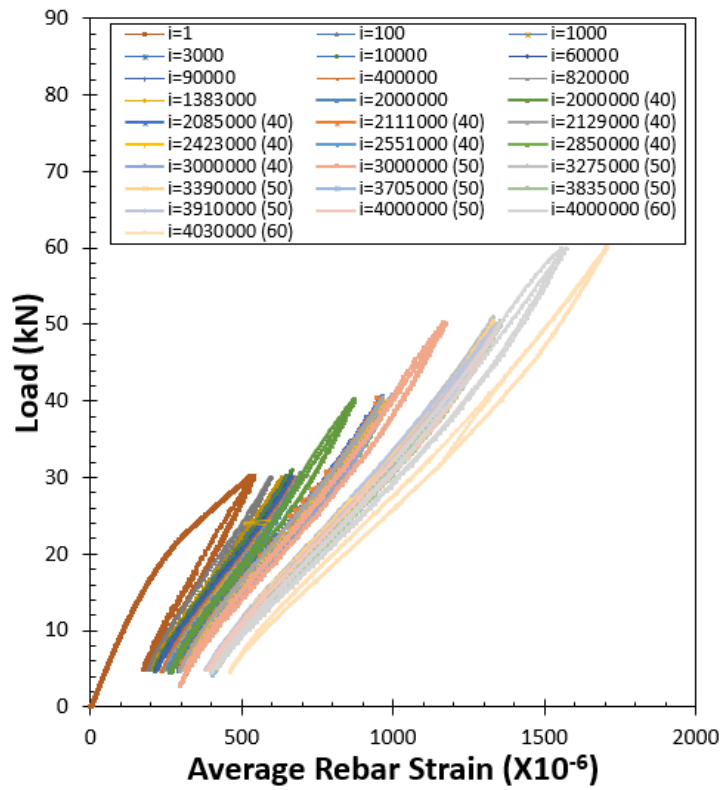


Fig. 5.8 Load versus average rebar strain under flexural fatigue for beam FBF_30-40-50-60.

During the fatigue life of the tested beam – FBF_30-40-50-60 – a higher flexural fatigue load level was applied by increasing the flexural load monotonically then the cyclic flexural load was applied between 5 kN as a minimum fatigue load level and the increased flexural load as a maximum fatigue load level. While the flexural applied load was increased monotonically, the mid-span deflection and the crack length and width were increased and structural stiffness was decreased as noted from the decrease of the inclination of the load-deflection curve and N.A. position, as shown in Figs. 5.6, 5.7, 5.8, and 5.12. As a result, an evolution of both the rebar and concrete strain was observed for the SFRC structural beams, as shown in Figs. 5.7, 5.8, 5.10, and 5.11.

After increasing the flexural load monotonically, the cyclic flexural load was applied under the desired higher flexural fatigue load level. During that application of repeated cyclic loading, again an increase on both the rebar and concrete strain was observed for the SFRC structural beams, resulting in increasing mid-span deflection and crack length and width and decreasing structural stiffness as noted from the decrease of the inclination of the load-deflection curve and N.A. position, as shown in Figs. 5.9, 5.10, 5.11, and 5.12. finally, at a higher fatigue load level ($S=0.7$) where a 60 kN of flexural maximum load level was applying, a rupture fatigue failure took place in a manner of rebar rupture achieving 4397844 cycles of fatigue life, as summarized in Table 5.2.

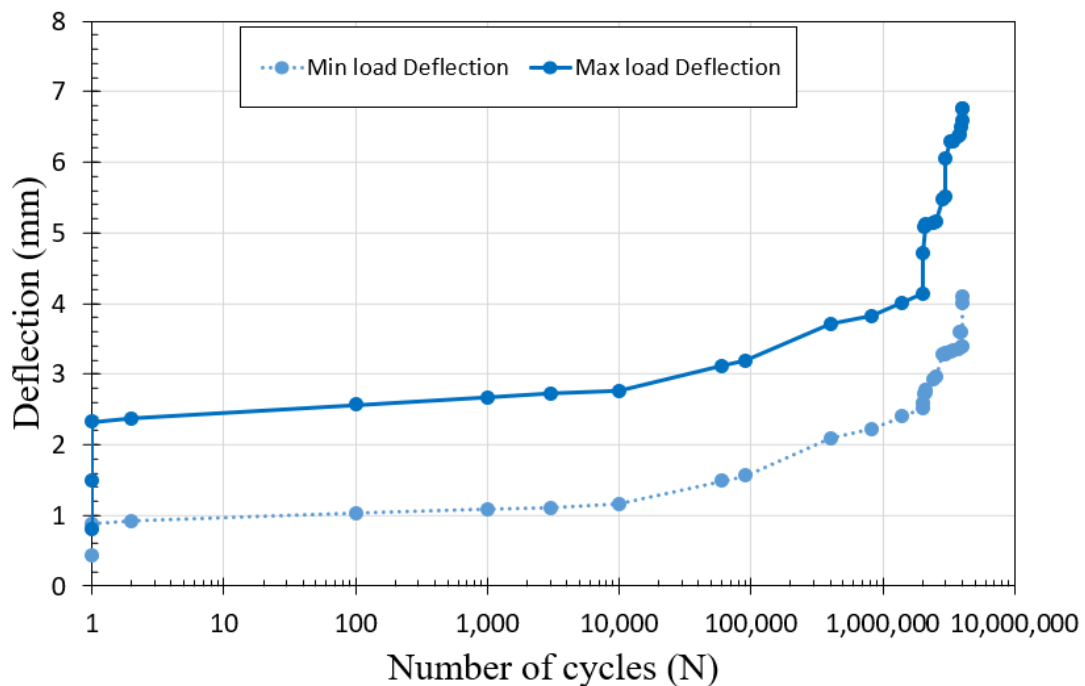


Fig. 5.9 Mid-span deflection at maximum and minimum load level under flexural fatigue for beam FBF_30-40-50-60.

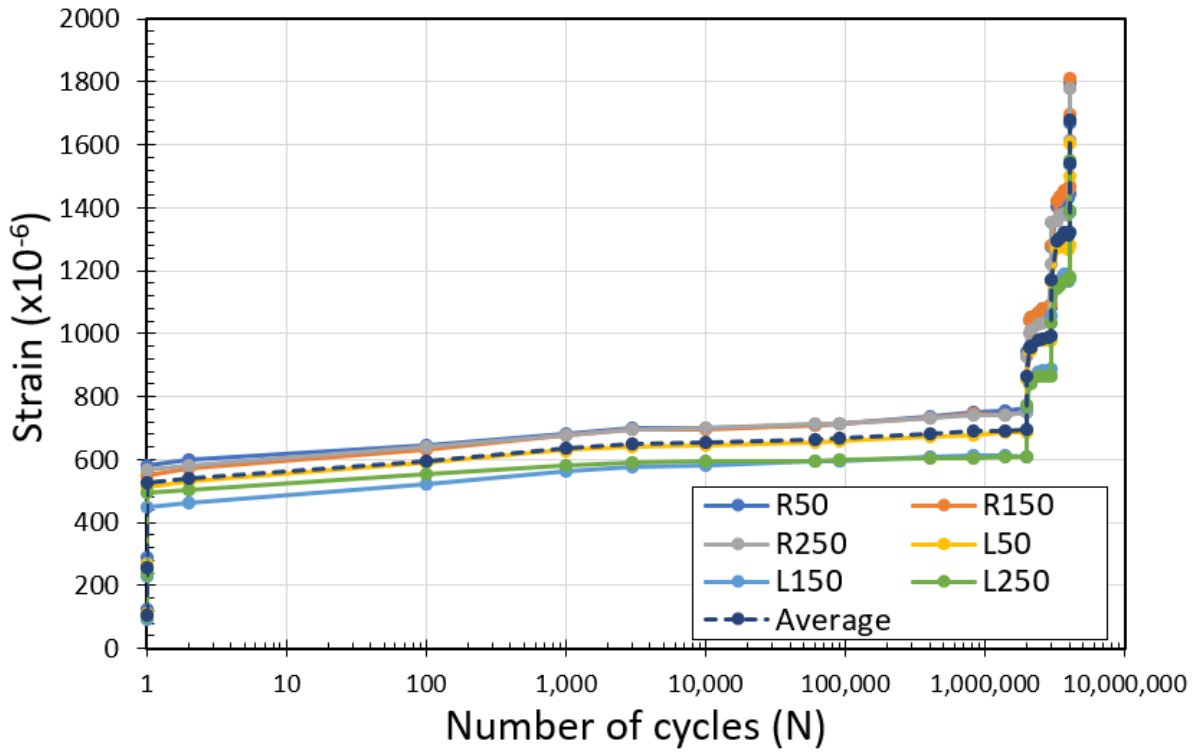


Fig. 5.10 Rebar strain evolution under flexural fatigue for beam FBF_30-40-50-60.

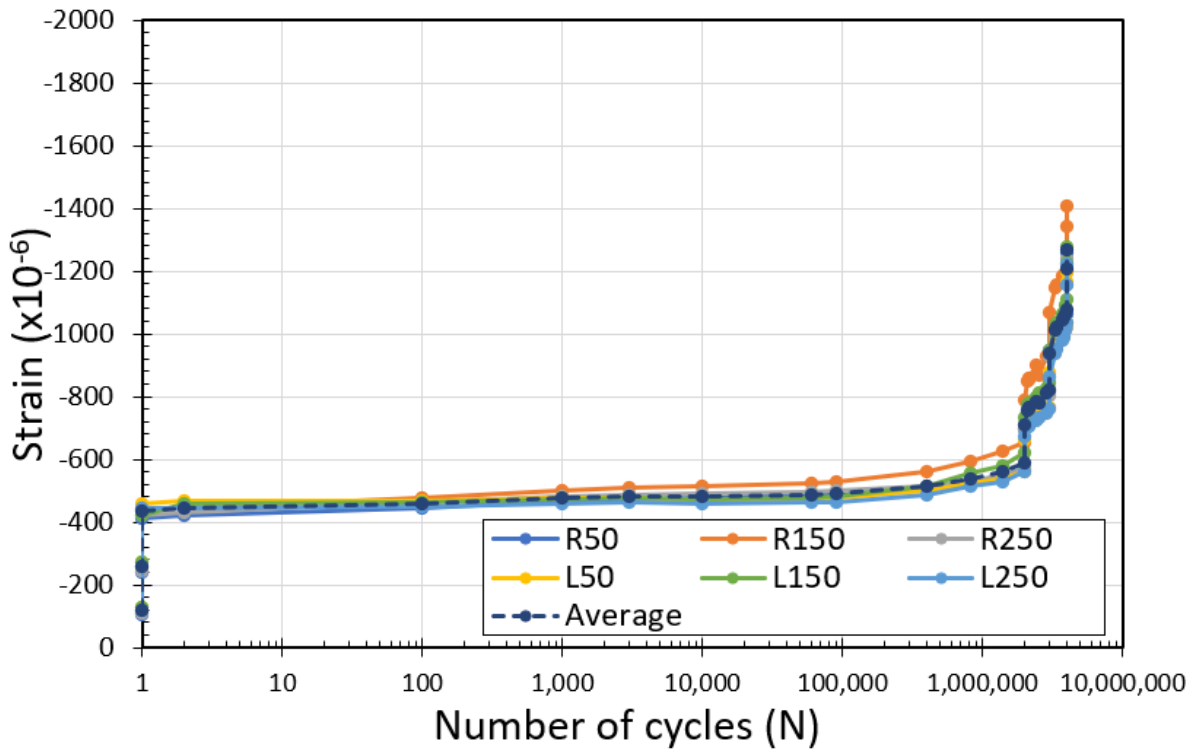


Fig. 5.11 ultimate concrete strain evolution under flexural fatigue for beam FBF_30-40-50-60.

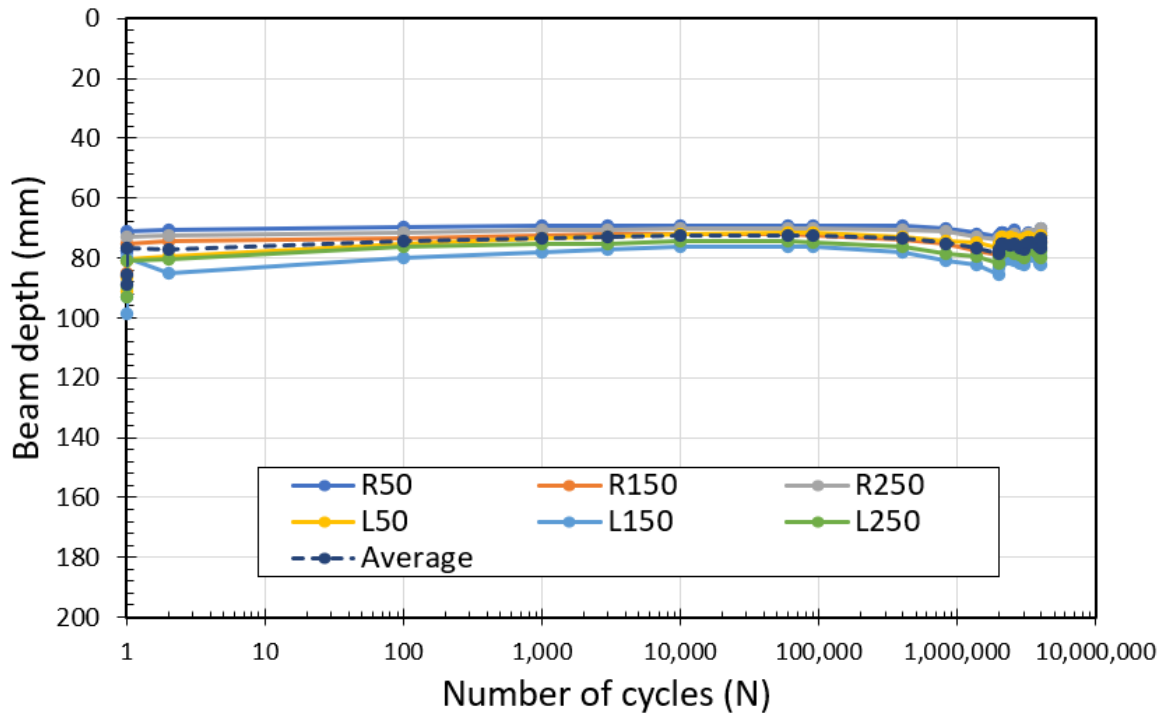


Fig. 5.12 Neutral axis position evolution under flexural fatigue for beam FBF_30-40-50-60.

Beam FBF_50-40-30-40-50-60

For the decreasing case of the fatigue stress levels ($S = 0.59 \rightarrow 0.47 \rightarrow 0.35 \rightarrow 0.47 \rightarrow 0.59 \rightarrow 0.70$), one SFRC structural beam – FBF_50-40-30-40-50-60 – was tested under flexural cyclic loading with 5 kN as a minimum flexural load and 50 kN, 40 kN, 30 kN, 40 kN, 50 kN, 60 kN as a maximum flexural load for one, one, two, one, one, one million cycles, respectively and sequentially, as shown in Figs. 5.2, 5.13, and 5.14. Figure 5.14 shows the load versus mid-span deflection relationship over fatigue life under a high to a low to a high-stress level of flexural fatigue load, showing an increase, decrease, and stabilizing in mid-span deflection as cycles progress within the application of the variable flexural cyclic loading by increasing and decreasing the fatigue load level over the fatigue life.

Figure 5.15 shows the strain distribution at midspan on the front face of the beam (L150), showing an increase and decrease in strain level for both rebar and concrete throughout the application of flexural cyclic loading until the end of fatigue life. The average rebar strain within the constant moment region is also plotted against the maximum and minimum flexural cyclic load for the variable fatigue stress levels during the fatigue life, starting from the first flexural cyclic loading (N_1) until the end of the fatigue life, showing the evolution of average rebar strain from increasing to decreasing and stabilizing within the application of the variable

flexural cyclic loading by increasing and decreasing the fatigue load level over the fatigue life, as shown in Fig. 5.16.

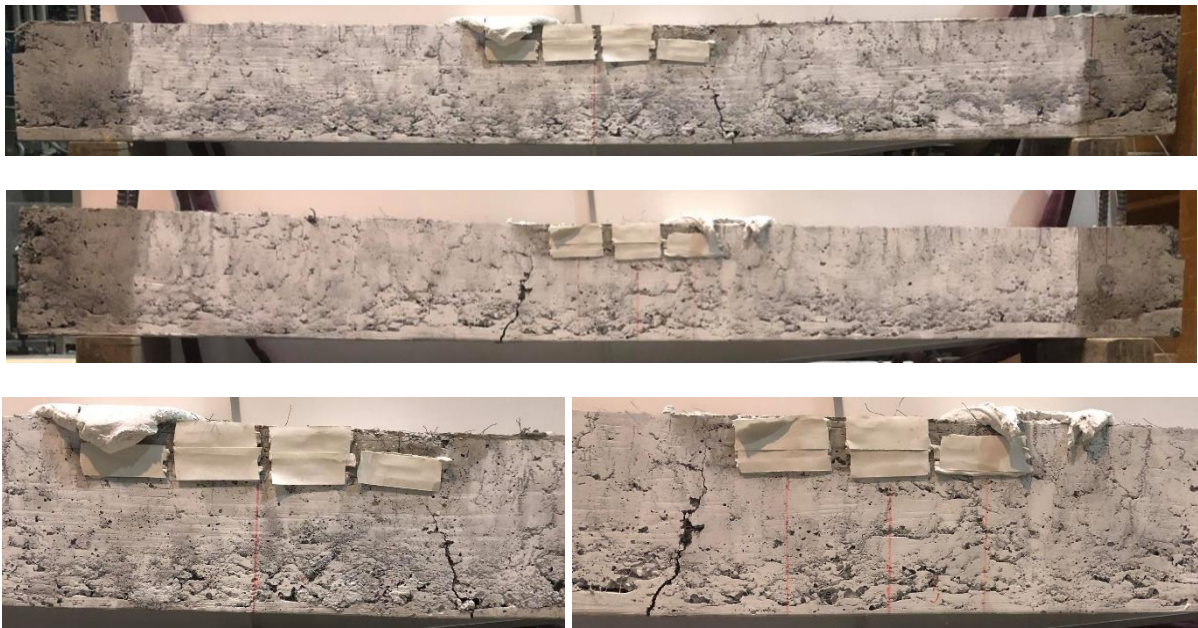


Fig. 5.13 Beam FBF_50-40-30-40-50-60 over fatigue life under flexural fatigue.

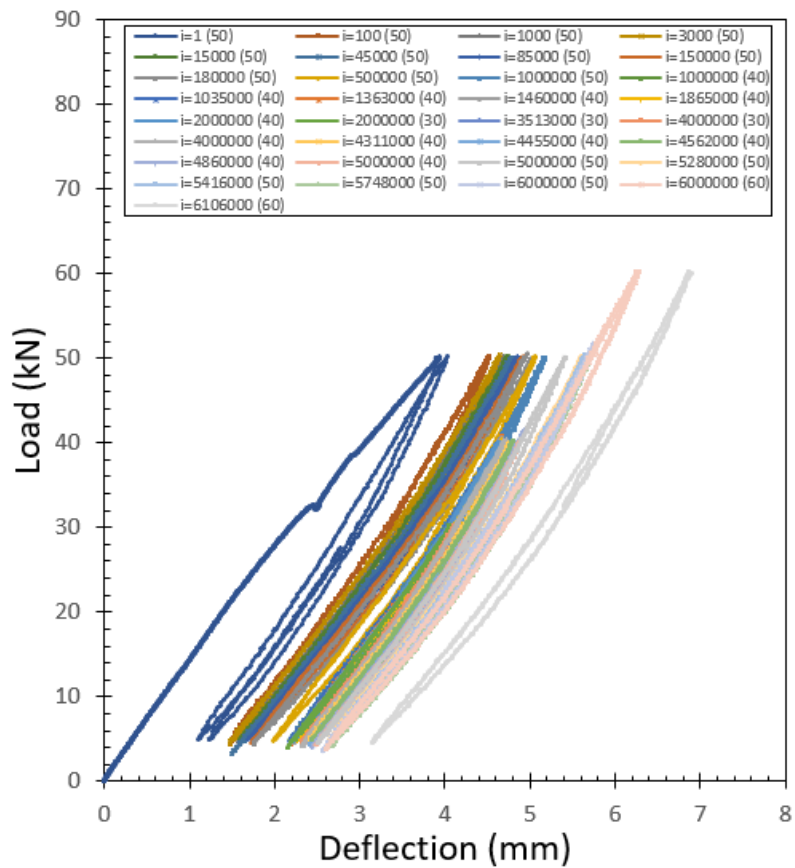


Fig. 5.14 Load versus deflection under flexural fatigue for beam FBF_50-40-30-40-50-60.

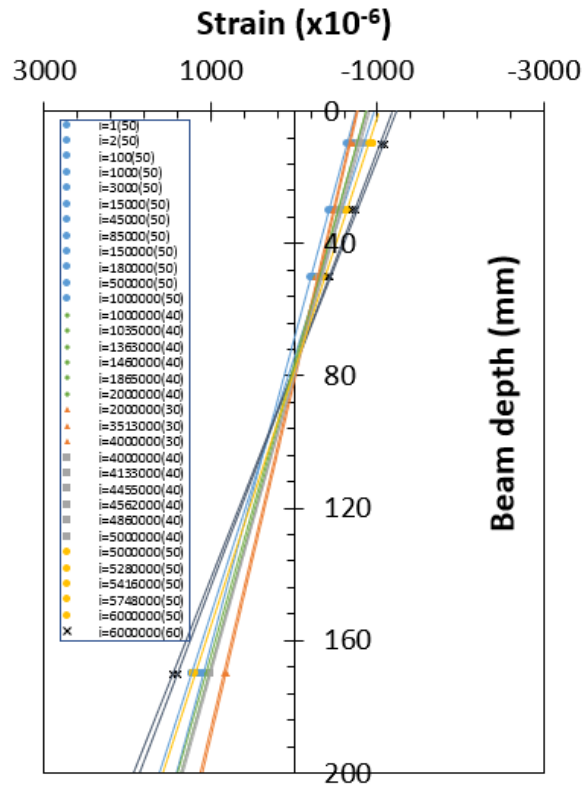


Fig. 5.15 Mid-span strain distribution under flexural fatigue for beam FBF_50-40-30-40-50-60.

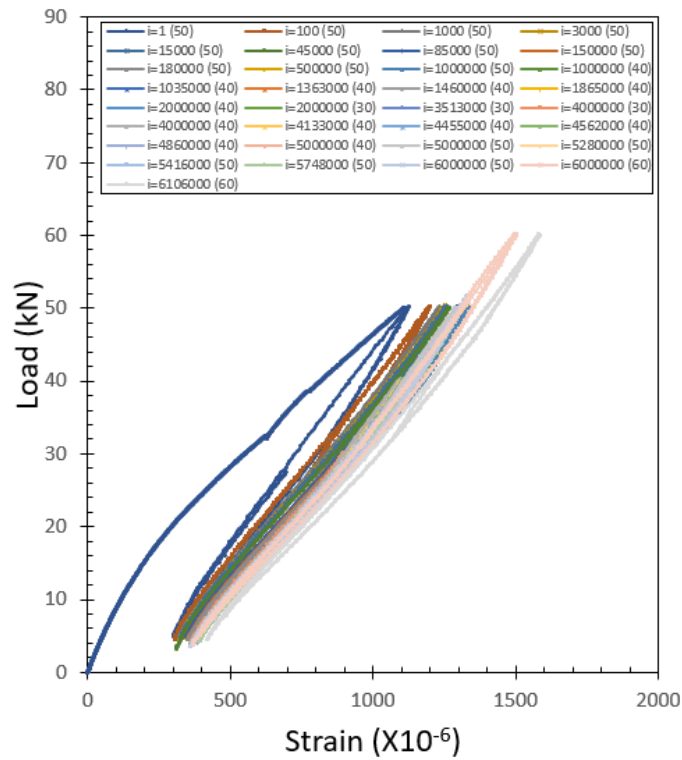


Fig. 5.16 Load versus average rebar strain under flexural fatigue for beam FBF_50-40-30-40-50-60.

During the fatigue life of the tested beam – FBF_50-40-30-40-50-60 – a lower flexural fatigue load level was applied by decreasing the flexural load monotonically then the cyclic flexural load was applied between 5 kN as a minimum fatigue load level and the decreased flexural load as a maximum fatigue load level. While the flexural applied load was decreased monotonically, the mid-span deflection and the crack width were decreased and structural stiffness was increased as noted from the increase of the inclination of the load-deflection curve and N.A. position, as shown in Figs. 5.15, 5.17, and 5.20. As a result, a decrease of both the rebar and concrete strain was observed for the SFRC structural beam, as shown in Figs. 5.18 and 5.19.

After decreasing the flexural load monotonically, the cyclic flexural load was applied under the desired lower flexural fatigue load level. During that application of repeated cyclic loading, a stabilization on both the rebar and concrete strain level was observed for the SFRC structural beams, resulting in an almost stabilizing mid-span deflection and crack length and width and an almost stabilizing structural stiffness as noted from the stabilizing of the inclination of the load-deflection curve and N.A. position, as shown in Figs. 5.17, 5.18, 5.19, and 5.20.

Furthermore, after a certain number of cycles during the fatigue life, the tested SFRC structural beam – FBF_50-40-30-40-50-60 – has experienced an increase in flexural fatigue load level, that had been experienced before during the fatigue life of a 40 kN and 50 kN of flexural maximum load level. While the flexural applied load was increased monotonically, the mid-span deflection and the crack length and width were increased and structural stiffness was decreased as noted from the decrease of the inclination of the load-deflection curve and N.A. position, also the rebar and concrete strain level increased, as shown in Figs. 5.17, 5.18, 5.19, and 5.20. During the application of the flexural cyclic loading, the mid-span deflection and the crack length and width were stabilized and structural stiffness was stabilized as noted from the stabilized of the inclination of the load-deflection curve and N.A. position, also the rebar and concrete strain level stabilized, as shown in Figs. 5.17, 5.18, 5.19, and 5.20.

Finally, a higher fatigue load level ($S=0.7$) where a 60 kN of flexural maximum load level was applied on the tested beam – FBF_50-40-30-40-50-60 – that had not been experienced before during the fatigue life. During the application of the flexural cyclic loading, the mid-span deflection and the crack length and width were increased and structural stiffness was decreased as noted from the decrease of the inclination of the load-deflection curve and N.A. position, as shown in Figs. 5.17, 5.18, 5.19, and 5.20. After a certain number of fatigue cycles, a rupture

fatigue failure took place in a manner of rebar rupture achieving 6481200 cycles of fatigue life, as summarized in Table 5.2.

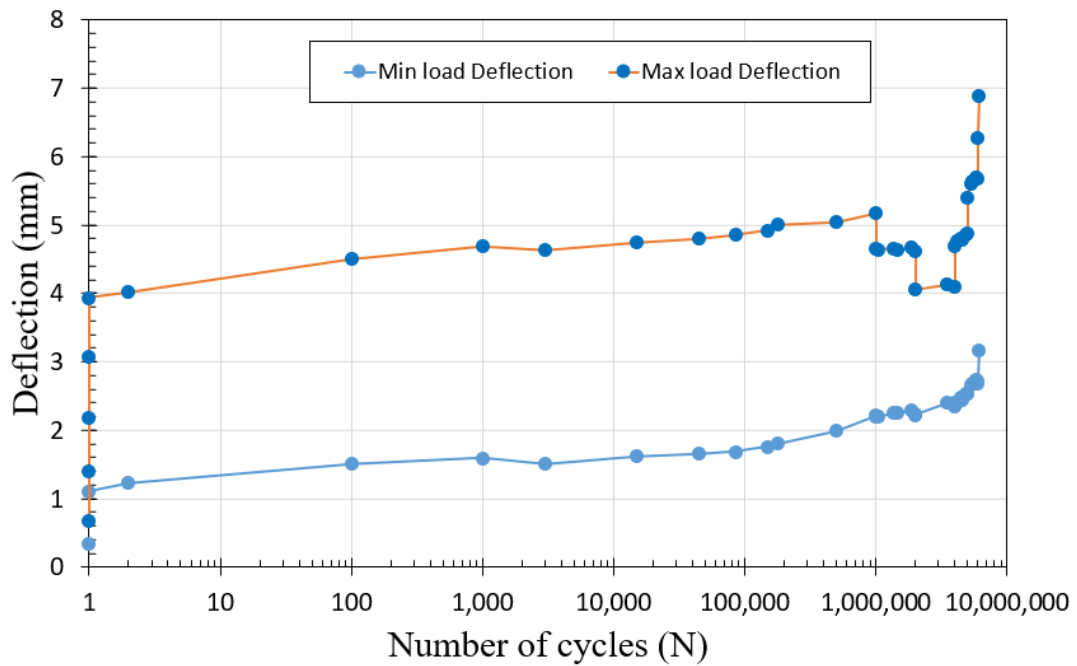


Fig. 5.17 Mid-span deflection at maximum and minimum load level under flexural fatigue for beam FBF_50-40-30-40-50-60.

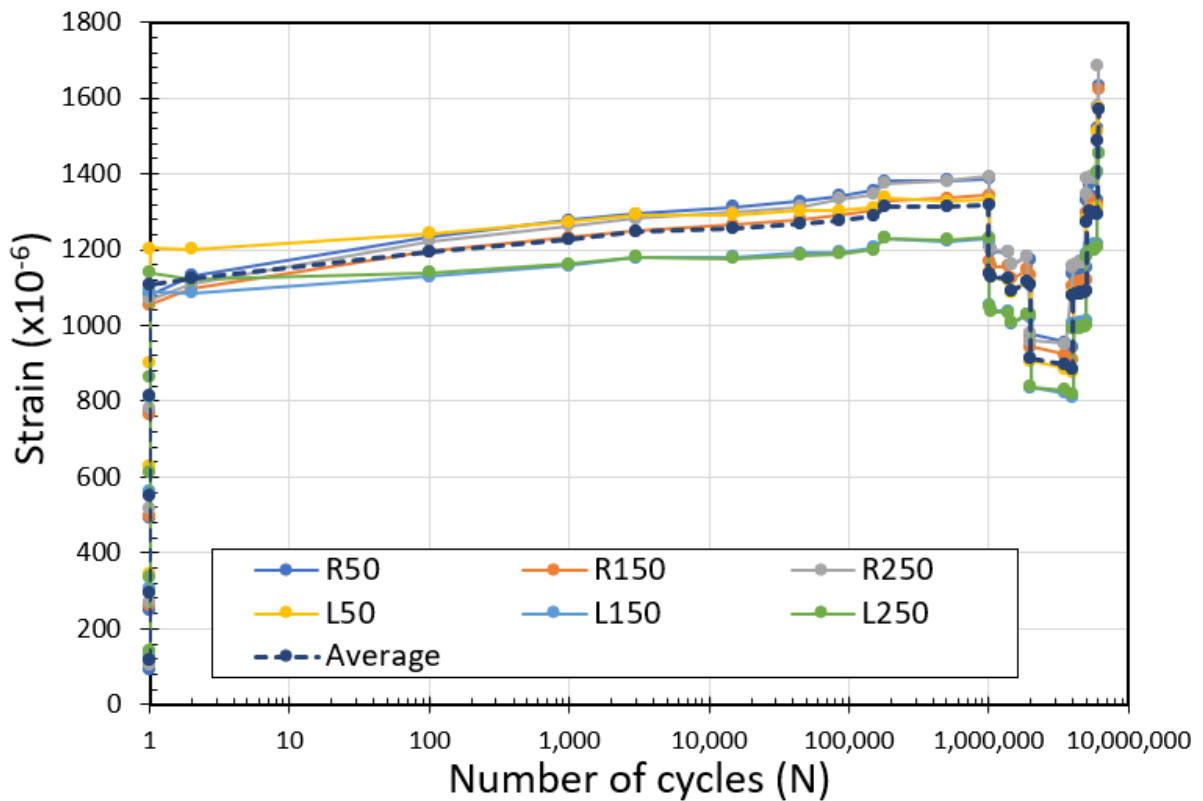


Fig. 5.18 Rebar strain evolution under flexural fatigue for beam FBF_50-40-30-40-50-60.

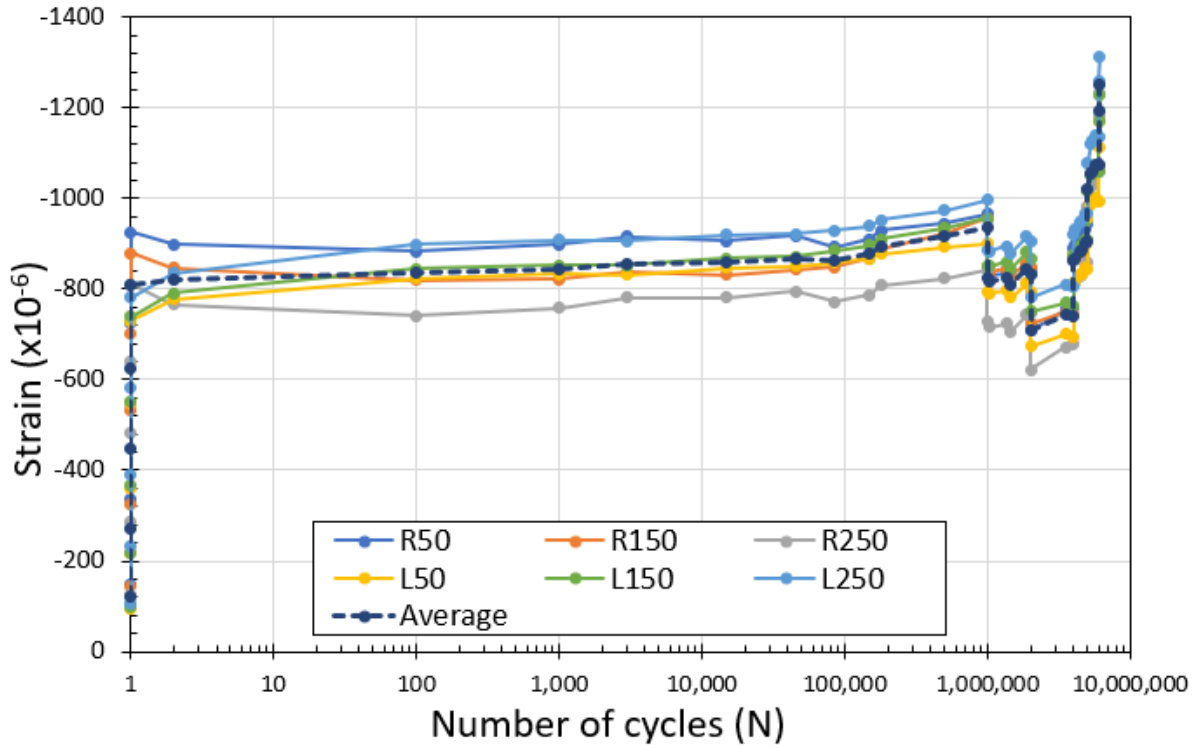


Fig. 5.19 ultimate concrete strain evolution under flexural fatigue
for beam FBF_50-40-30-40-50-60.

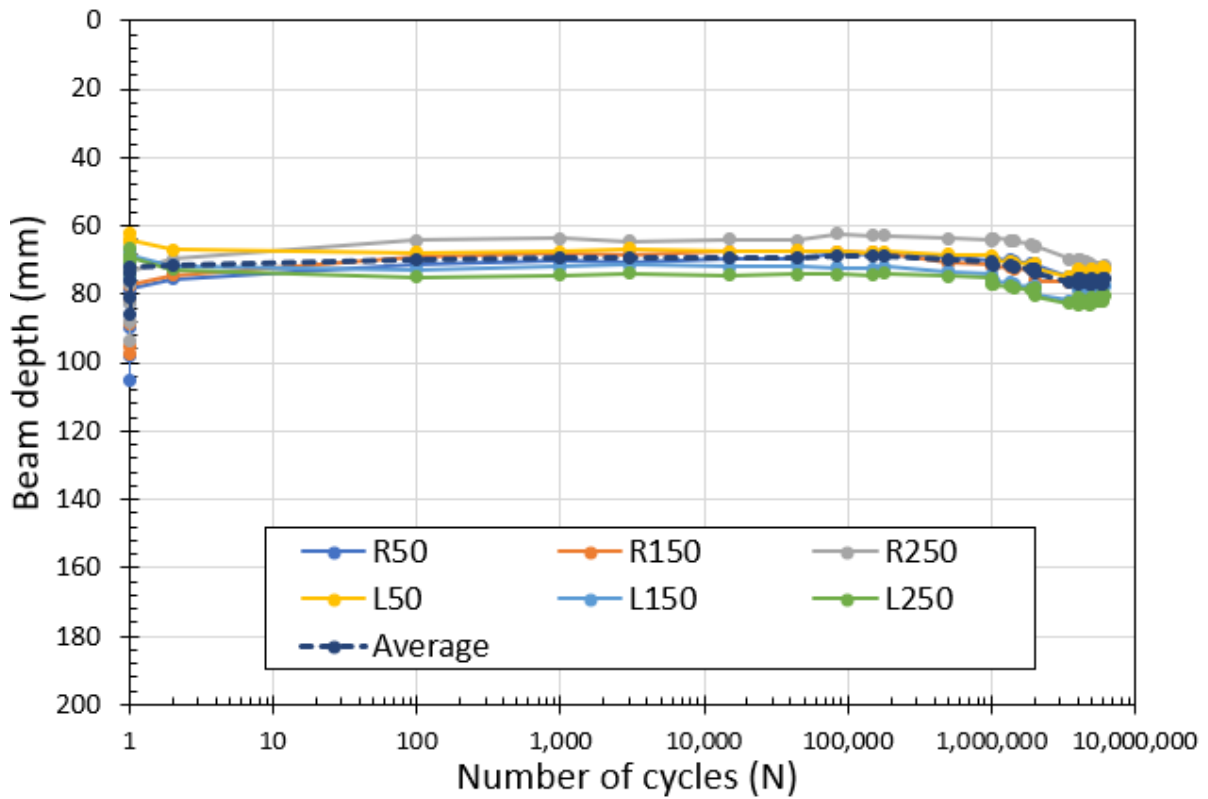


Fig. 5.20 Neutral axis position evolution under flexural fatigue
for beam FBF_50-40-30-40-50-60.

Finally, the average experimental data of the fatigue response of the SFRC structural beams over the fatigue life to be used in the inverse analysis calculation method. The degradation and evolution of the crack-bridging strength would be evaluated by achieving a good fitting between the experimental and calculated fatigue response of the tested structural SFRC beams. As a result, the average experimental rebar strain, ultimate surface concrete strain, and N.A. position were monitored and plotted in Figure 4.21 for the FBF_30-40-50-60 beam, and Figure 4.22 for the FBF_50-40-30-40-50-60 beam over the flexural fatigue life.

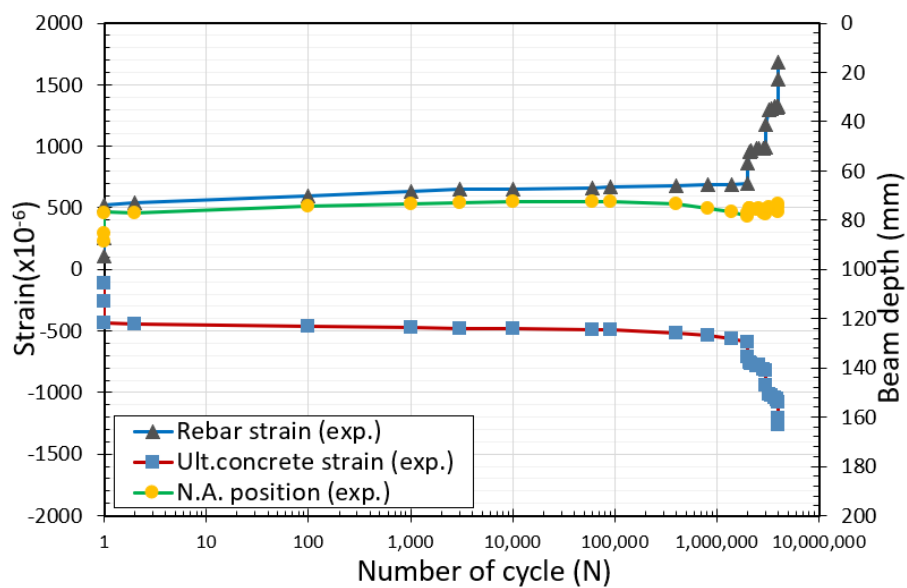


Fig. 5.21 Average experimental fatigue response of beam FBF_30-40-50-60 over fatigue life.

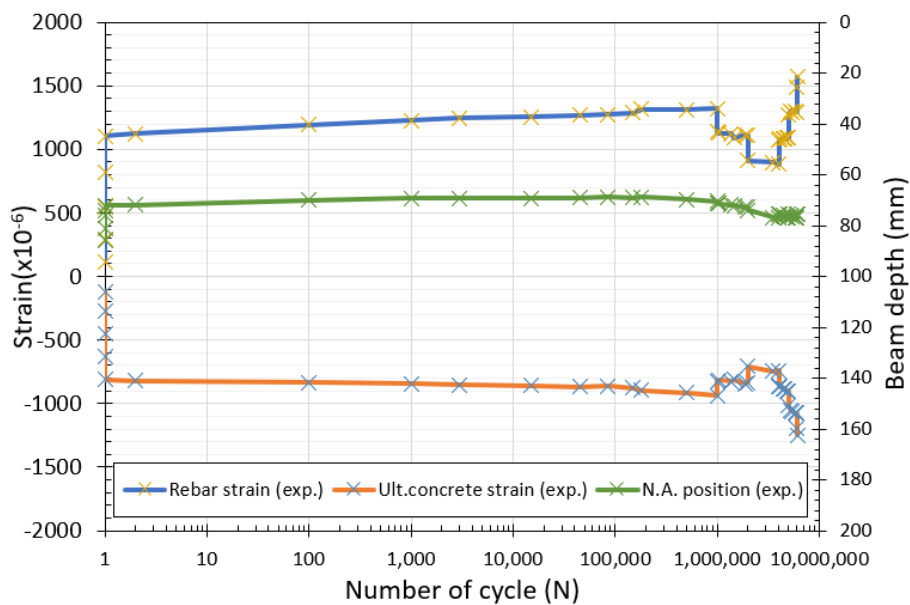


Fig. 5.22 Average experimental fatigue response of beam FBF_50-40-30-40-50-60 over fatigue life.

5.4 Discussion on The Evaluated Crack-bridging Strength

5.4.1 Evaluated Crack-bridging Strength of The Second Series

The inverse analysis method of computation involves incremental calculations during fatigue loading as the number of cycles increases, as explained in section 3.4.3. The computations are performed iteratively for the incremental set of fatigue cycles (N_i) until fatigue rupture failure of rebar (N_f). At each increment N_i , a certain degradation or evolution level (α_i) of initial crack-bridging strength is proposed to adjust the balance between the experimentally measured results and the calculated values; if the agreement between the calculated and experimental results is not within the set threshold, the analysis is repeated using a different level of degradation or evolution until the threshold is met, as illustrated in Figs. 3.13, 5.23, and 5.26.

The normalized crack-bridging strength (β_i) is derived using Eq. (3.4) and plotted in Figs. 5.24, and 5.27, illustrating the degradation and evolution of crack-bridging strength over the fatigue life of the two SFRC structural beams for FBF_30-40-50-60 and FBF_50-40-30-40-50-60. The effect of changing the maximum fatigue load level during the fatigue life in an increasing or decreasing manner had been captured on the evaluated crack-bridging strength, the maximum rebar strain evolution and crack propagation mechanics. Note, however, that the normalized crack-bridging strength at the first cycle (N_1) of fatigue loading does not necessarily start at 1.0 as discussed in section 4.4.

Beam FBF_30-40-50-60

Figure 5.23 shows a comparison between the calculated and averaged experimental results for rebar strain, ultimate compressive concrete strain, and N.A. position for the increasing case of the maximum fatigue load level of beam FBF_30-40-50-60. The fit is acceptable in fatigue load levels with a minimum error. For all fatigue load levels, there is a clear increase in average strain levels for both rebar and concrete and a decrease in the N.A. position as the number of cycles increases. The normalized evaluated crack-bridging strength during the fatigue life of beam FBF_30-40-50-60 tends to decrease with the increase of the number of loading cycles during cyclic loading, as shown in Fig. 5.24. However, at the stage of increasing the load level monotonically, the normalized crack-bridging strength increases with the increase of the load level monotonically from lower to higher fatigue load level, as shown in Fig. 5.24. The conclusion from these results is that the proposed inverse analysis method could predict the

degradation and evolution of crack-bridging strength provided by fibers as flexural fatigue loading continues.

Besides, the normalized crack-bridging strength at all fatigue load levels is plotted versus the evolution of the experimental maximum rebar strain, as shown in Fig. 5.25. Figure 5.25 shows an interesting zigzag linear relationship of the degradation and evolution of the crack-bridging strength regarding the evolution of the maximum rebar strain over the fatigue life regardless of the fatigue stress levels, that could be a useful relationship for design and assessment of SFRC structural beams under fatigue loading by controlling the rebar strain level through avoiding the brittle rupture of steel reinforcing bars. The degradation model of the crack-bridging strength regarding the evolution progress of maximum rebar strain has a constant linear relationship regardless of the fatigue stress levels. On the other hand, the evolution increase model of the crack-bridging strength regarding the evolution progress of maximum rebar strain through increasing the load level monotonically has a decreasing linear relationship with the increase of fatigue stress levels, as shown in Fig. 5.25.

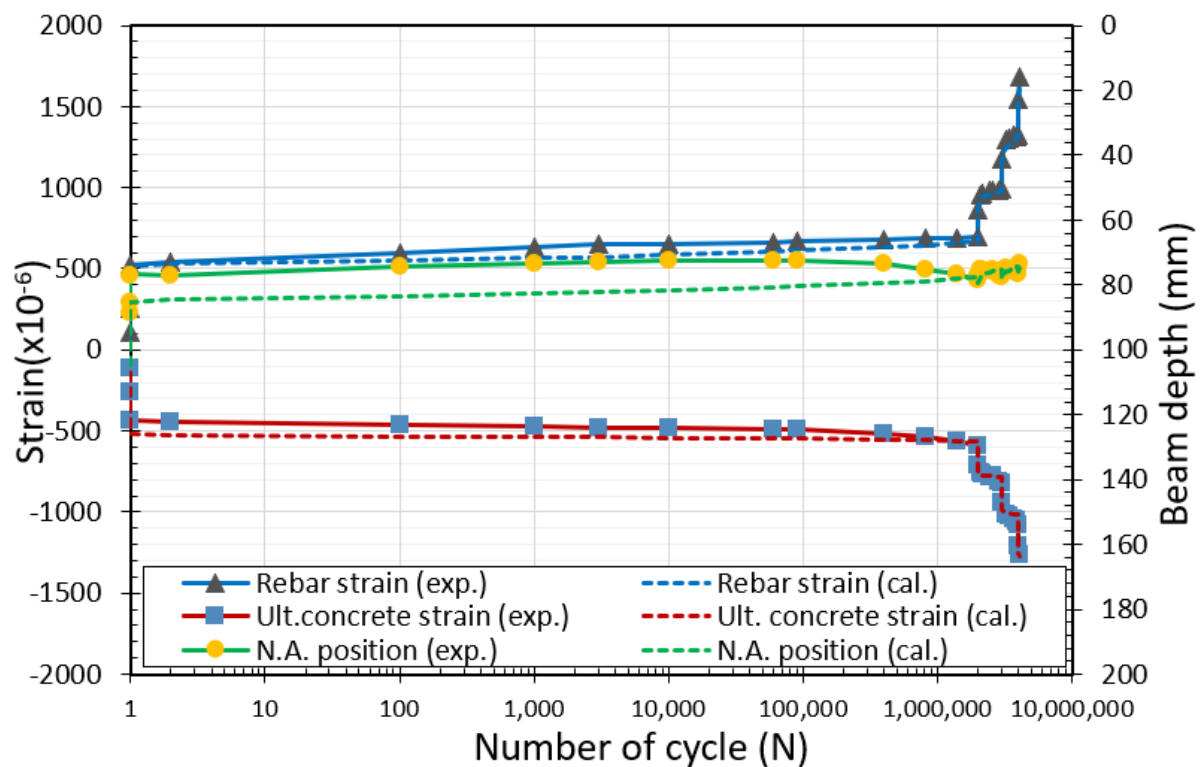


Fig. 5.23 Calculated versus experimental fatigue response of FBF_30-40-50-60 over the fatigue life.

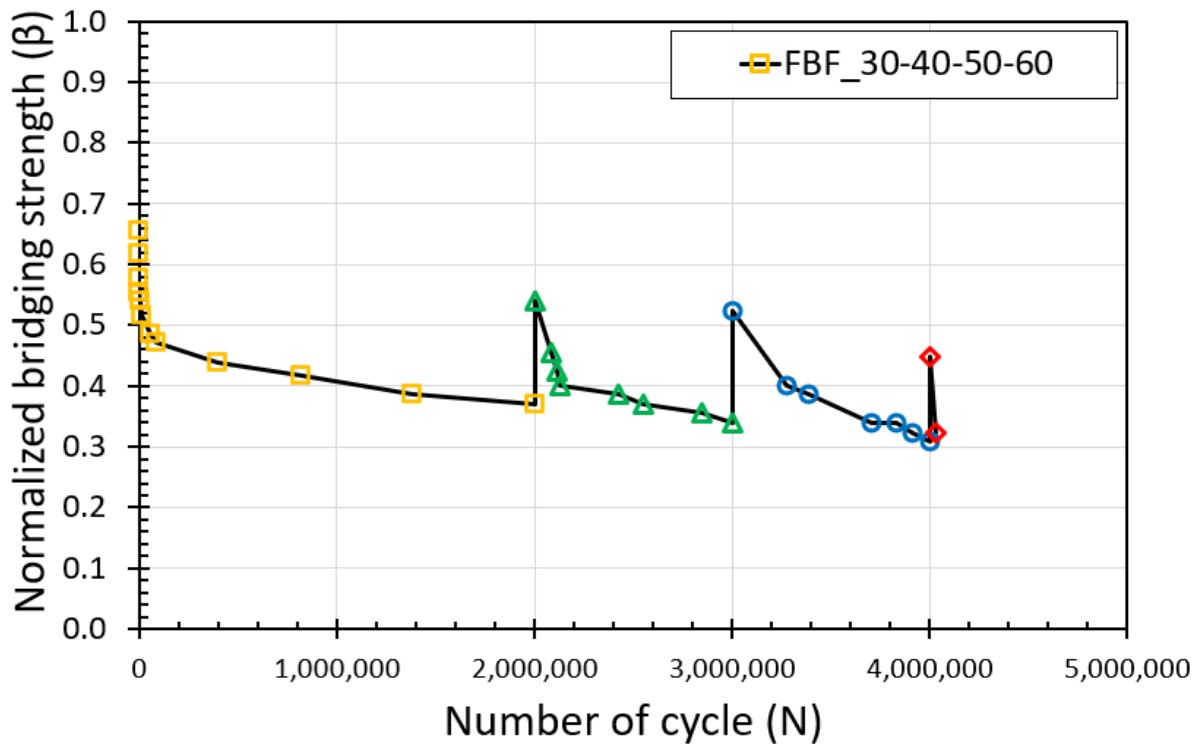


Fig. 5.24 Normalized crack-bridging strength degradation and evolution of FBF_30-40-50-60 over flexural fatigue life.

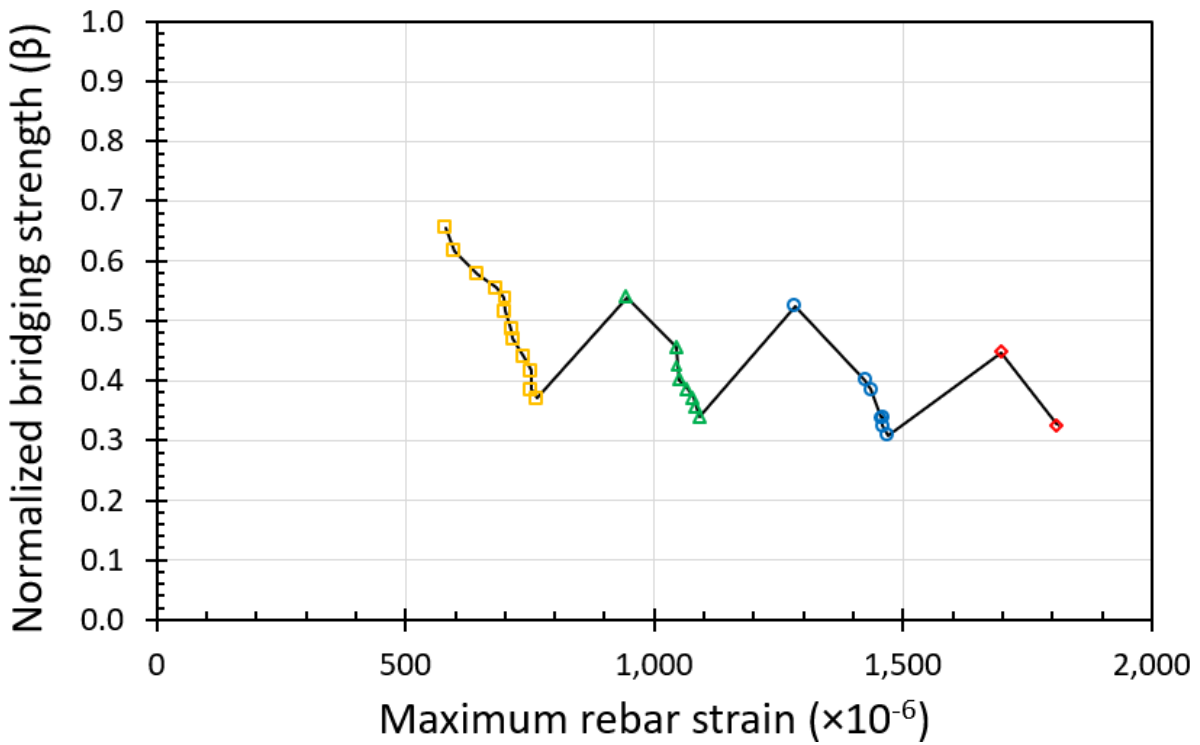


Fig. 5.25 Normalized crack-bridging strength degradation and evolution versus maximum rebar strain of FBF_30-40-50-60 over flexural fatigue life.

By cyclic progress of flexural fatigue loading of the first lower fatigue load level of 30 kN as a maximum fatigue flexural load, the repeated tensile stress resulted in increasing the width of the cracks. That would lead to loss of the bond between fibers and matrix where degradation of crack-bridging strength took place, as shown in Fig. 5.24 and illustrated in Fig. 5.26(a). Simultaneously, an increase in the level of rebar strain over the fatigue life is achieved, as shown in Fig. 5.25 as a square yellow dots.

After two million cycles under 30 kN maximum load level of fatigue life for beam – FBF_30-40-50-60 – a higher flexural fatigue load level of 40 kN was applied by increasing the flexural load monotonically then the cyclic flexural load was applied between 5 kN and 40 kN as a minimum and maximum fatigue load level. While the flexural applied load was increased monotonically, the mid-span deflection and the crack length and width were increased and structural stiffness was decreased, noticing a new contribution of steel fibers in bridging the cracks by transmitting tensile stress in tensile stress zone below the N.A., as shown in Fig. 5.26(b) as indicated by green color fibers. As a result, an increase in the crack-bridging strength was observed for the SFRC structural beams with the evolution of the maximum rebar strain level, as shown in Figs. 5.25, and 5.24 as a black line started by a square yellow dot and ended by a triangle green dot.

After increasing the flexural load monotonically, the cyclic flexural load was applied for one million cycles under the desired higher flexural fatigue load level. During that application of repeated cyclic loading, an increase in the width of the cracks took place, leading to a loss in the bond between fibers and matrix where degradation of crack-bridging strength took place again, as shown in Fig. 5.24 and illustrated in Fig. 5.26(b). Simultaneously, an increase in the level of rebar strain over the fatigue life is achieved, as shown in Fig. 5.25 as a triangle green dots.

As cycles progress, other higher fatigue load levels were tested for 50 kN and 60 kN of the maximum flexural load by increasing monotonically first, then a cyclic loading was applied for one million cycles. The same mechanism of degradation and evolution in crack-bridging strength were observed over the fatigue life and with the maximum rebar strain evolution, as shown in Figs. 5.24, 5.25, 5.26(c), and 5.26(d). Finally, at a higher fatigue load level ($S=0.7$) where a 60 kN of flexural maximum load level was applying, a rupture fatigue failure took place in a manner of rebar rupture achieving 4397844 cycles of fatigue life, as summarized in Table 5.2 and shown in Fig. 5.26(d).

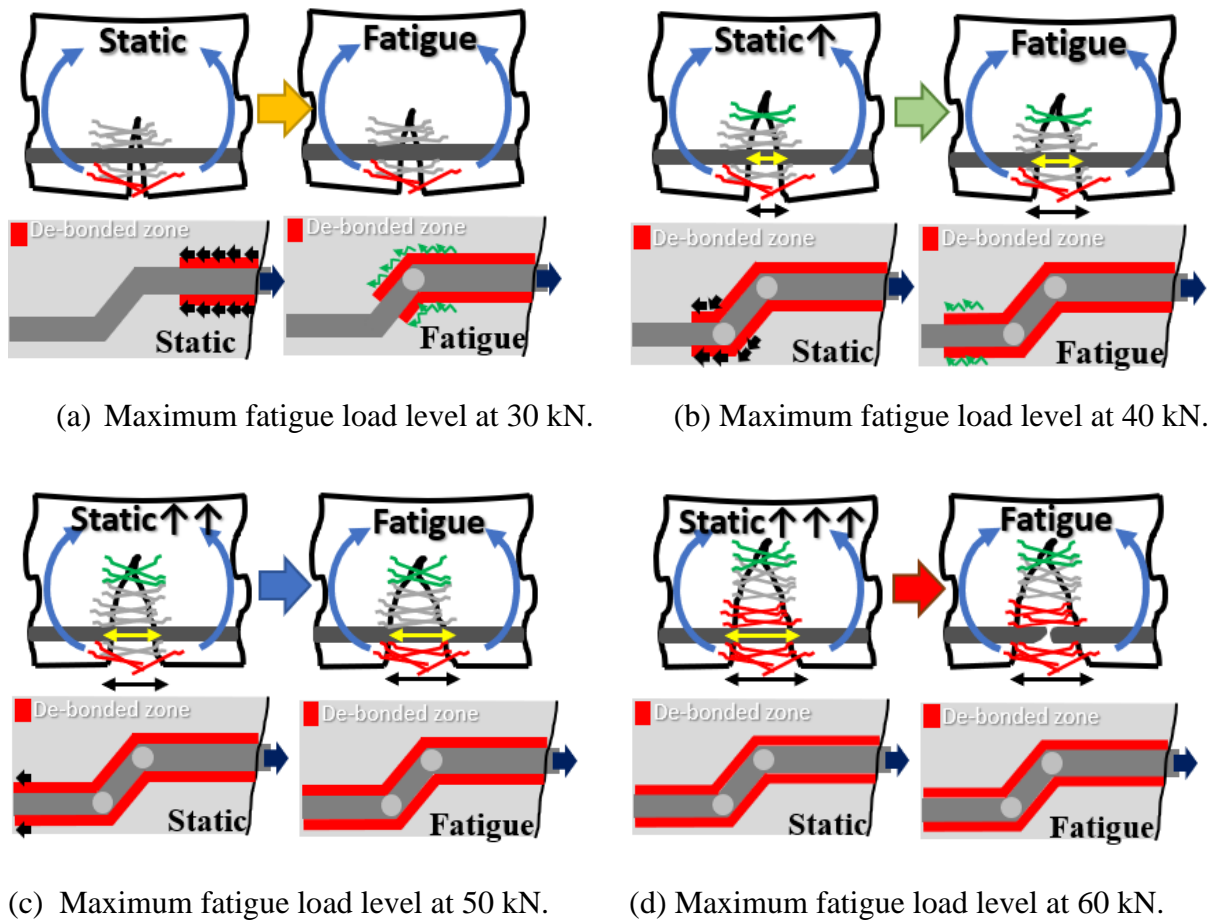


Fig. 5.26 Schematic damage in the tensile stress zone and at the fiber-matrix interface of fibers and rebar of FBF_30-40-50-60 over flexural fatigue life.

Beam FBF_50-40-30-40-50-60

Figure 5.26 shows a comparison between the calculated and averaged experimental results for rebar strain, ultimate compressive concrete strain, and N.A. position for the increasing case of the maximum fatigue load level of beam FBF_50-40-30-40-50-60. The fit is acceptable in fatigue load levels with a minimum error. Over different fatigue load levels, there is a clear increase, decrease, and stabilize in average strain levels for both rebar and concrete, and the N.A. position as the number of cycles increases. The normalized evaluated crack-bridging strength during the fatigue life of beam FBF_50-40-30-40-50-60 tends to change regarding the fatigue load level with the increase of the number of loading cycles during cyclic loading, as shown in Fig. 5.27. Especially, at the stage of decreasing the load level monotonically, the normalized crack-bridging strength decreases with the decrease of the load level monotonically from higher to lower fatigue load level, as shown in Fig. 5.27. Likewise beam FBF_30-40-50-60, at the stage of increasing the load level monotonically, the normalized crack-bridging strength increases with the increase of the load level monotonically from lower to higher

fatigue load level, as shown in Fig. 5.27. The conclusion from these results is that the proposed inverse analysis method could predict the degradation and evolution of crack-bridging strength provided by fibers as flexural fatigue loading continues.

Besides, the normalized crack-bridging strength at all fatigue load levels is plotted versus the evolution of the experimental maximum rebar strain, as shown in Fig. 5.28. Figure 5.28 shows a broken linear relationship of the degradation and evolution of the crack-bridging strength regarding the increase and decrease of the maximum rebar strain over the fatigue life regardless of the fatigue stress levels, that could be a useful relationship for design and assessment of SFRC structural beams under fatigue loading by controlling the rebar strain level. The degradation model of the crack-bridging strength regarding the increase and decrease progress of maximum rebar strain has a constant linear relationship regardless of the fatigue stress levels. On the other hand, the evolution increase model of the crack-bridging strength regarding the evolution progress of maximum rebar strain through increasing the load level monotonically has a decreasing linear relationship with the increase of fatigue stress levels, as shown in Fig. 5.28.

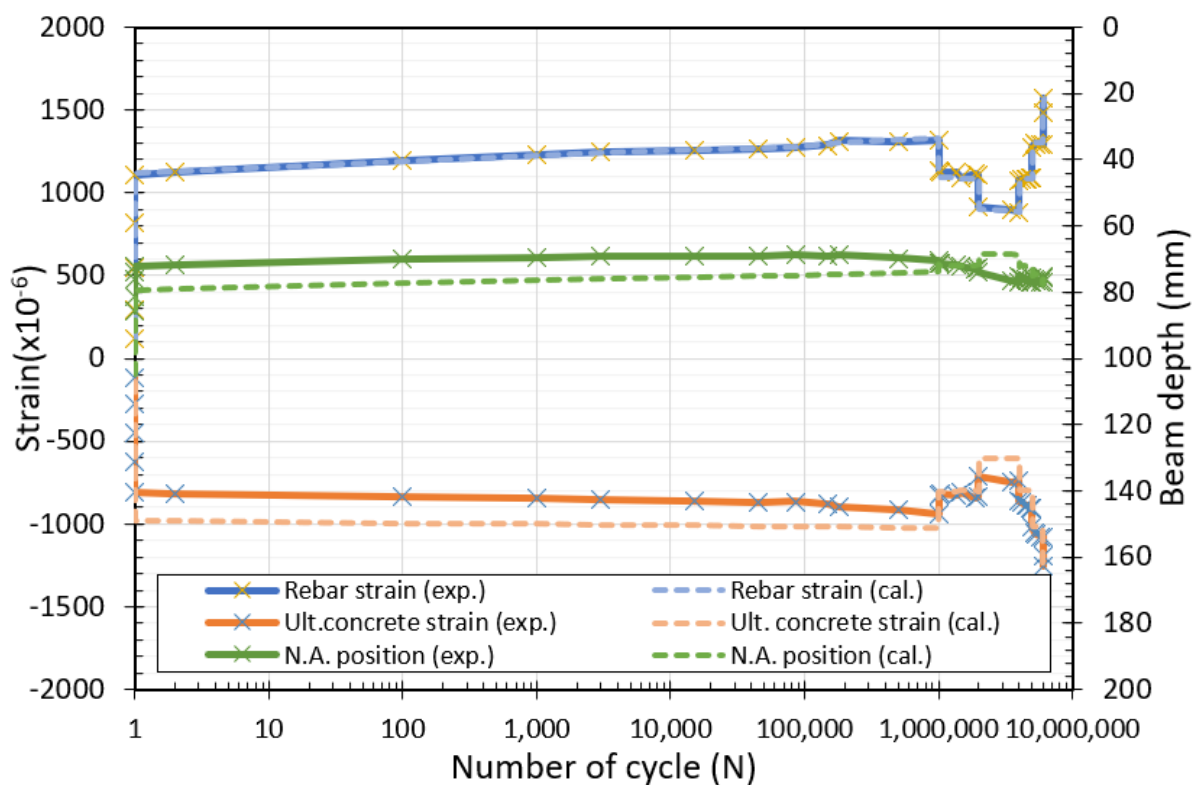


Fig. 5.26 Calculated versus experimental fatigue response of FBF_50-40-30-40-50-60 over the fatigue life.

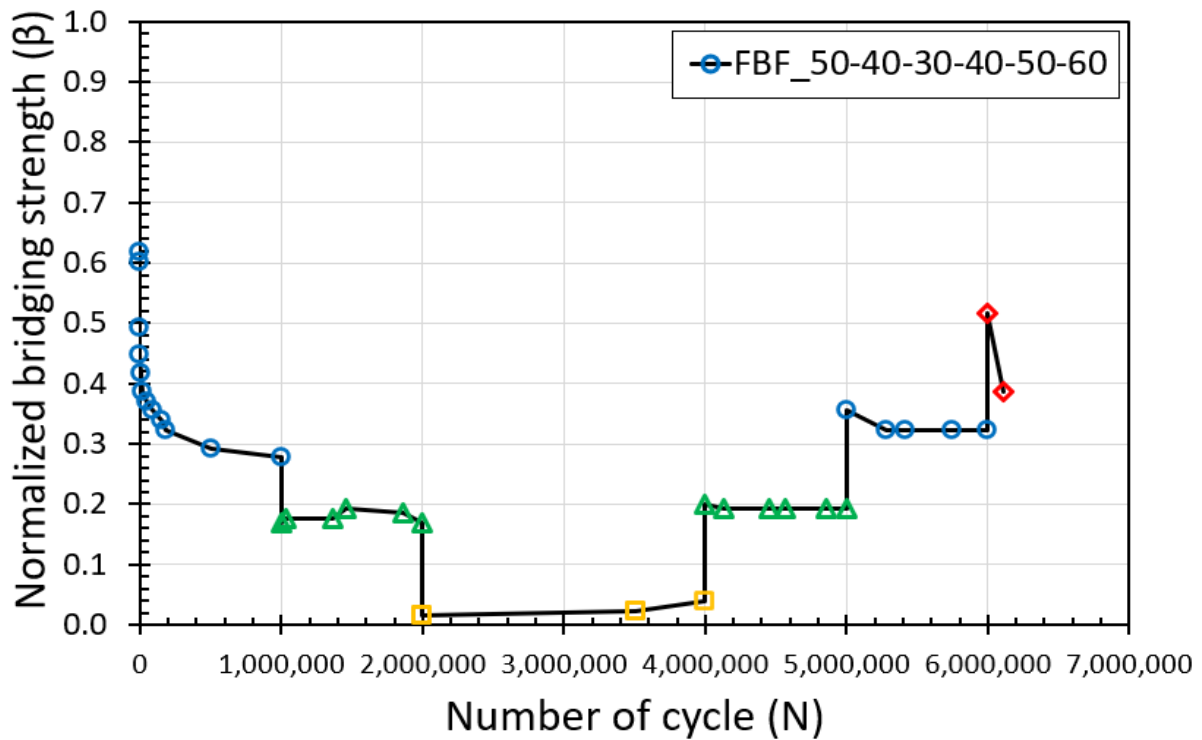


Fig. 5.27 Normalized crack-bridging strength degradation and evolution of FBF_50-40-30-40-50-60 over flexural fatigue life.

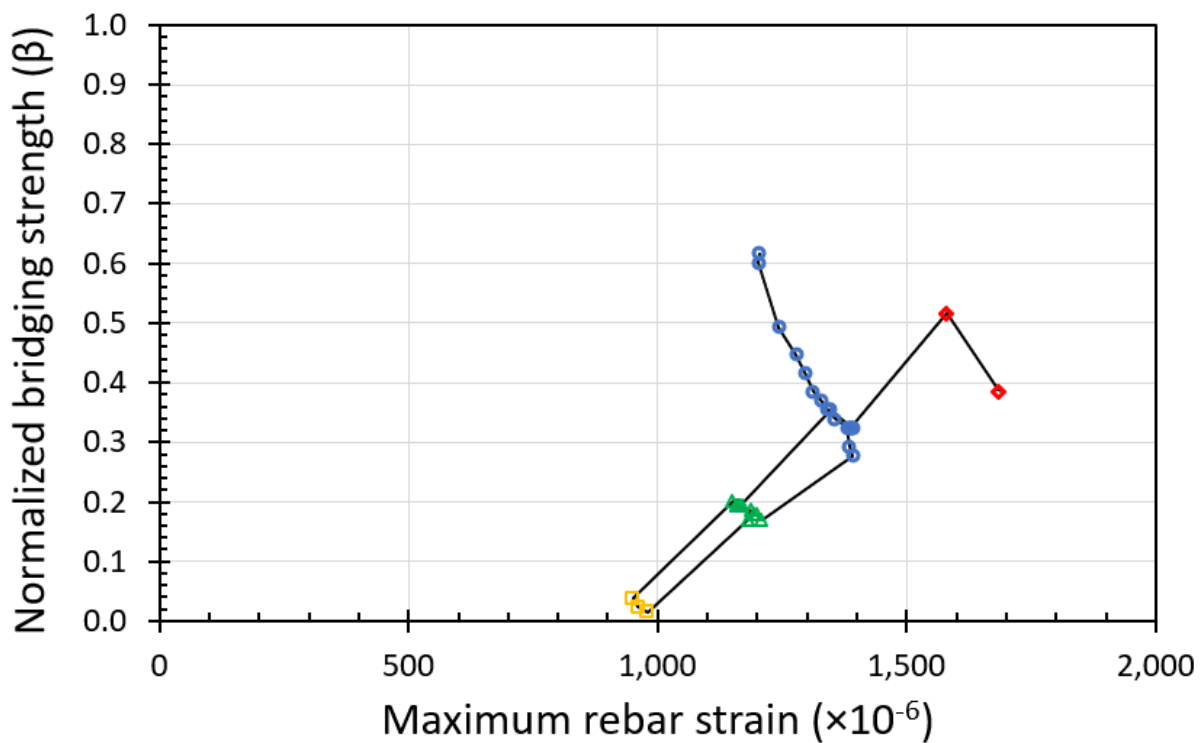


Fig. 5.28 Normalized crack-bridging strength degradation and evolution versus maximum rebar strain of FBF_30-40-50-60 over flexural fatigue life.

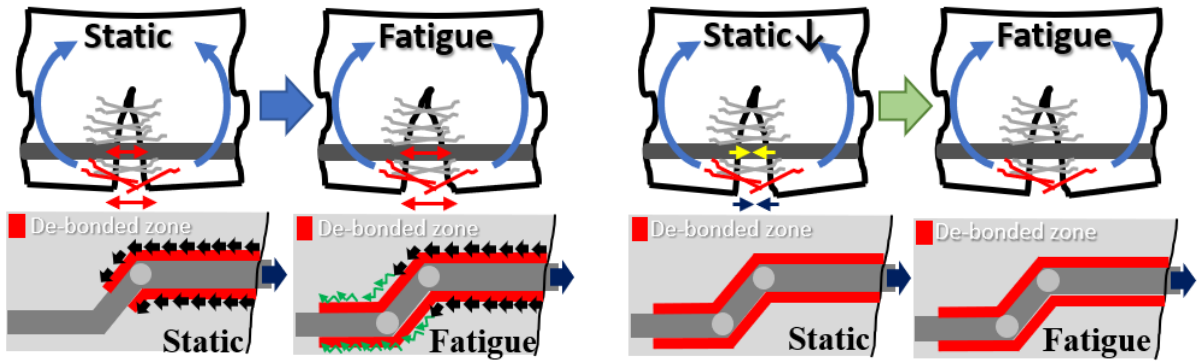
By cyclic progress of flexural fatigue loading of the first higher fatigue load level of 50 kN as a maximum fatigue flexural load, the repeated tensile stress resulted in increasing the width of

the cracks. That would lead to loss of the bond between fibers and matrix where degradation of crack-bridging strength took place, as shown in Fig. 5.27 as a circle blue dots and illustrated in Fig. 5.29(a). Simultaneously, an increase in the level of rebar strain over the fatigue life is achieved, as shown in Fig. 5.28 as a circle blue dots.

After one million cycles under 50 kN maximum load level of fatigue life for beam – FBF_50-40-30-40-50-60 – a lower flexural fatigue load level of 40 kN was applied by decreasing the flexural load monotonically then the cyclic flexural load was applied between 5 kN and 40 kN as a minimum and maximum fatigue load level, respectively. While the flexural applied load was decreased monotonically, the mid-span deflection and the crack width were decreased with the same structural stiffness, having as same bond damage level at the fiber-matrix interface as that was achieved by the 50 kN fatigue load level, as shown in Fig. 5.29(b). Under a lower flexural load level of 40 kN, the applied pullout forces applied to fibers would be less under a higher bond damage level at the fiber-matrix interface, leading to a lower fiber's ability to bridging cracks and carrying tensile stress. As a result, a decrease in the normalized evaluated crack-bridging strength was observed for the SFRC structural beams with a decrease in the maximum rebar strain level, as shown in Figs. 5.28, and 5.27 as a black line started by a circle blue dot and ended by a triangle green dot.

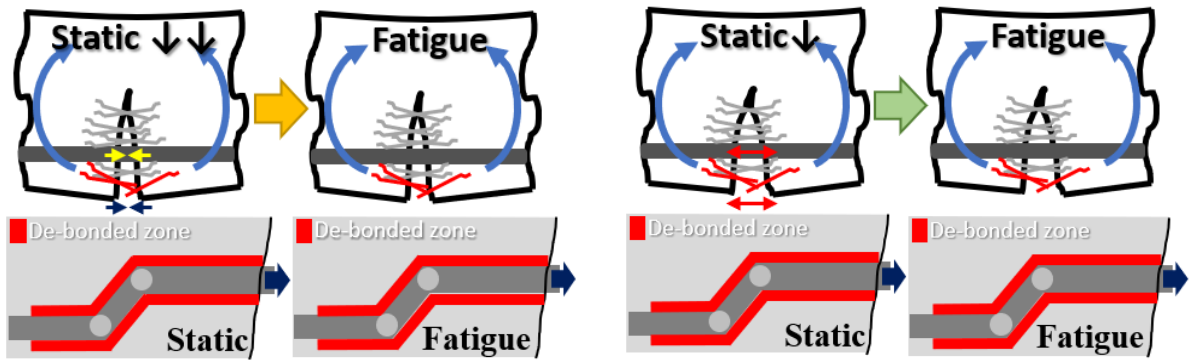
After decreasing the flexural load monotonically, the cyclic flexural load was applied for one million cycles under the desired lower flexural fatigue load level. During that application of repeated cyclic loading, Neither increase nor decrease in the width of the cracks took place, leading to a stabilization in the bond between fibers and matrix where degradation process of crack-bridging strength paused, as shown in Fig. 5.27 and illustrated in Fig. 5.29(b). Simultaneously, the level of rebar strain over fatigue life did not change, as shown in Fig. 5.28 as a triangle green dots.

As cycles progress, another lower fatigue load level was tested for 30 kN of the maximum flexural load by decreasing monotonically first, then a cyclic loading was applied for two million cycles. The same mechanism of decreasing followed by stabilizing in crack-bridging strength was observed over the fatigue life and with the maximum rebar strain evolution because of lower pullout forces on the fibers at the crack location, as shown in Figs. 5.27, 5.28, and 5.29(c) as a square yellow dots.



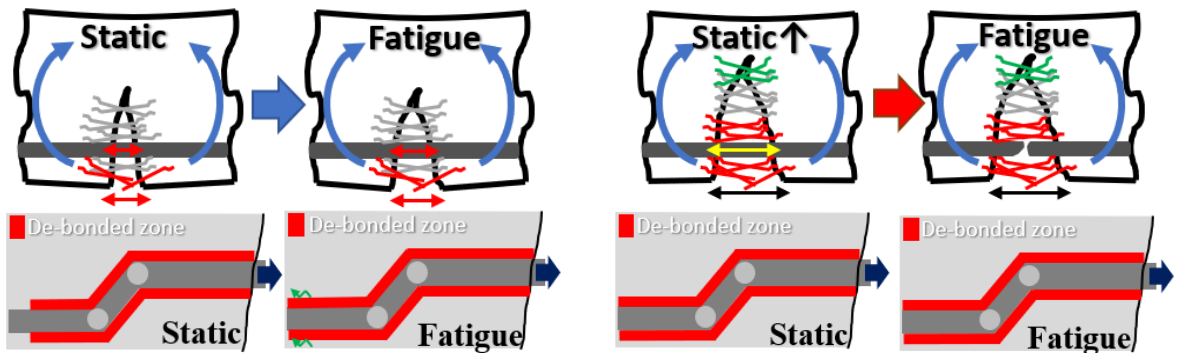
(a) Maximum fatigue load level at 50 kN.

(b) Maximum fatigue load level at 40 kN.



(c) Maximum fatigue load level at 30 kN.

(d) Maximum fatigue load level at 40 kN.



(e) Maximum fatigue load level at 50 kN.

(f) Maximum fatigue load level at 60 kN.

Fig. 5.29 Schematic damage in the tensile stress zone and at the fiber-matrix interface of fibers and rebar of FBF_50-40-30-40-50-60 over flexural fatigue life.

Furthermore, the beam – FBF_50-40-30-40-50-60 – had been experienced an increase in fatigue load level for 40 kN of the maximum flexural load by increasing from 30 kN monotonically first, then a cyclic loading was applied for one million cycles. The mechanism of increasing followed by stabilizing in crack-bridging strength was observed over the fatigue life and with the maximum rebar strain evolution because of lower pullout forces on the fibers at the crack location, as shown in Figs. 5.27, 5.28, and 5.29(d). while increasing the load level

monotonically to 40 kN again, the normalized crack-bridging strength and the maximum rebar strain level return to the same level that has been achieved while decreasing the load level from 50 kN to 40 kN during the fatigue life of the tested beam, as shown in Figs. 5.27, and 5.28 a triangle green dot.

After that, the beam – FBF_50-40-30-40-50-60 – had been experienced a higher fatigue load level of 50 kN as a maximum flexural load by increasing from 40 kN monotonically first, then a cyclic loading was applied for one million cycles. The mechanism of increasing followed by degradation in crack-bridging strength was observed over the fatigue life and with the maximum rebar strain evolution as degradation process was resumed by application of 50 kN, as shown in Figs. 5.27, 5.28, and 5.29(e). while increasing the load level monotonically to 50 kN again, the normalized crack-bridging strength and the maximum rebar strain level return to the same level that has been achieved by the end of the first one million cycles of the fatigue life for the tested beam, as shown in Figs. 5.27, and 5.28 a circle blue dot.

Finally, at a higher fatigue load level ($S=0.7$) where a 60 kN of flexural maximum load level was applying, a rupture fatigue failure took place in a manner of rebar rupture achieving 4397844 cycles of fatigue life, as summarized in Table 5.2 and shown in Fig. 5.26(d).

5.4.2 Crack-bridging Strength Degradation and Evolution diagram

The normalized crack-bridging strength is derived using the inverse analysis calculation method for the first and second series, testing the effect of single and variable flexural fatigue load levels and plotted in Fig. 5.30, illustrating the degradation of crack-bridging strength over the fatigue life of the five SFRC structural beams. Besides, the evolution process of the crack-bridging strength was captured while increasing the flexural load level monotonically during the fatigue life of SFRC structural beams for the second series or after the end of the two million cycles for the first series, as shown in Fig.5.31 as black solid lines. Finally, a diagram of the normalized crack-bridging strength degradation and evolution induced by hooked-end steel fibers for SFRC structural beams under flexural fatigue loading was plotted in Fig. 5.31 depending on results-driven from the first and second series. The proposed diagram of the crack-bridging strength degradation and evolution could be a useful relationship for the design and assessment of SFRC structural beams under fatigue loading by controlling the rebar strain level through avoiding the brittle rupture of steel reinforcing bars.

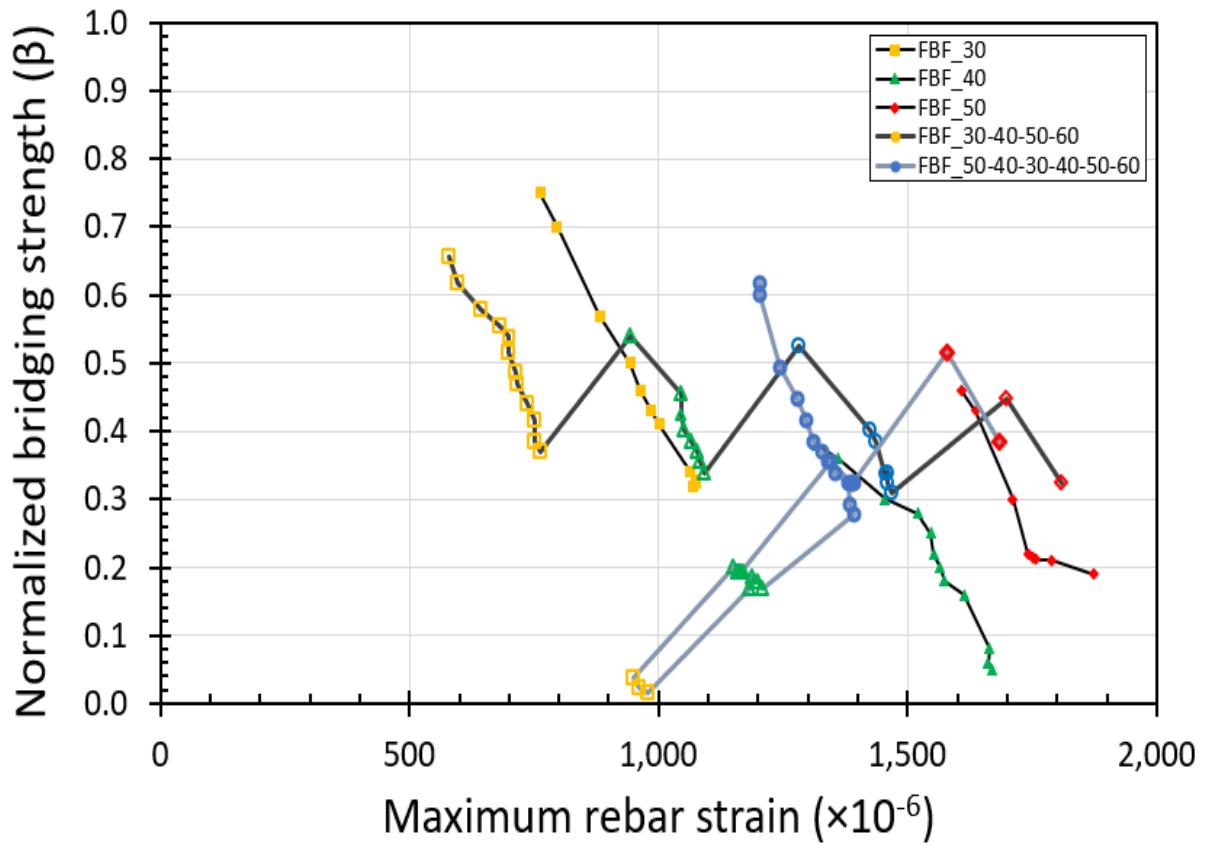


Fig. 5.30 Normalized crack-bridging strength degradation versus maximum rebar strain under various flexural fatigue load level.

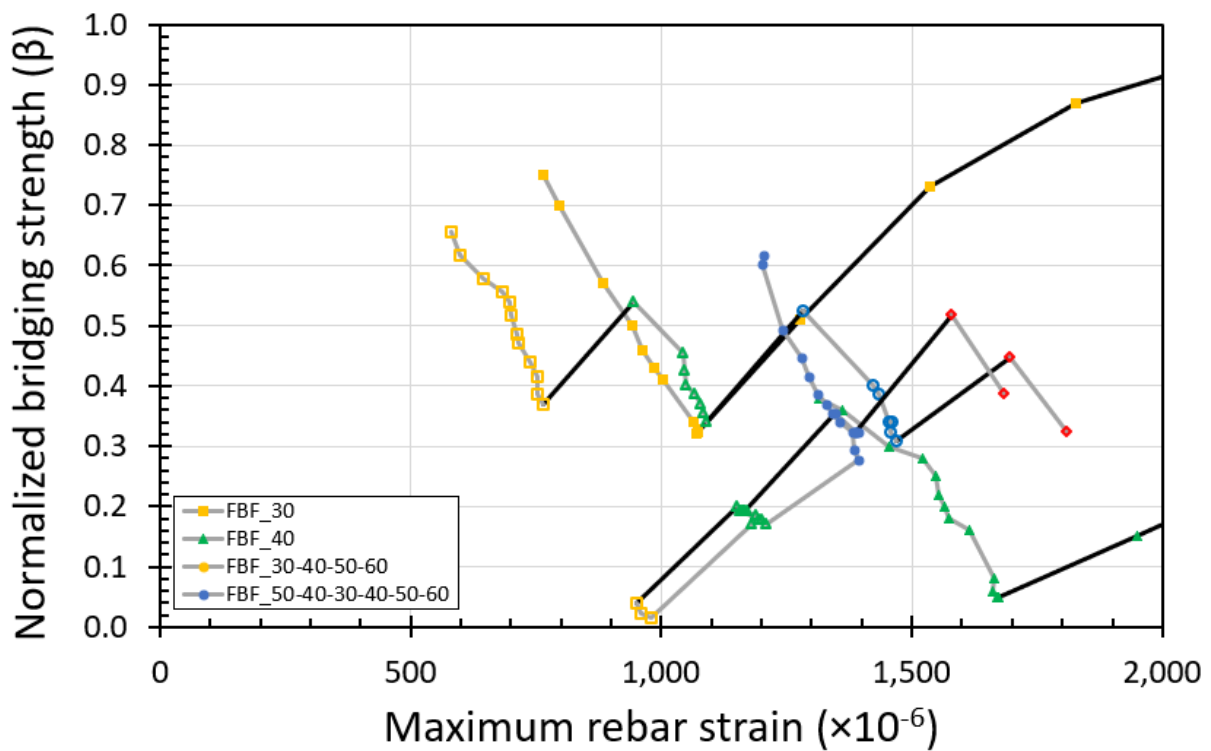


Fig. 5.31 Normalized crack-bridging strength evolution versus maximum rebar strain under various flexural fatigue load level.

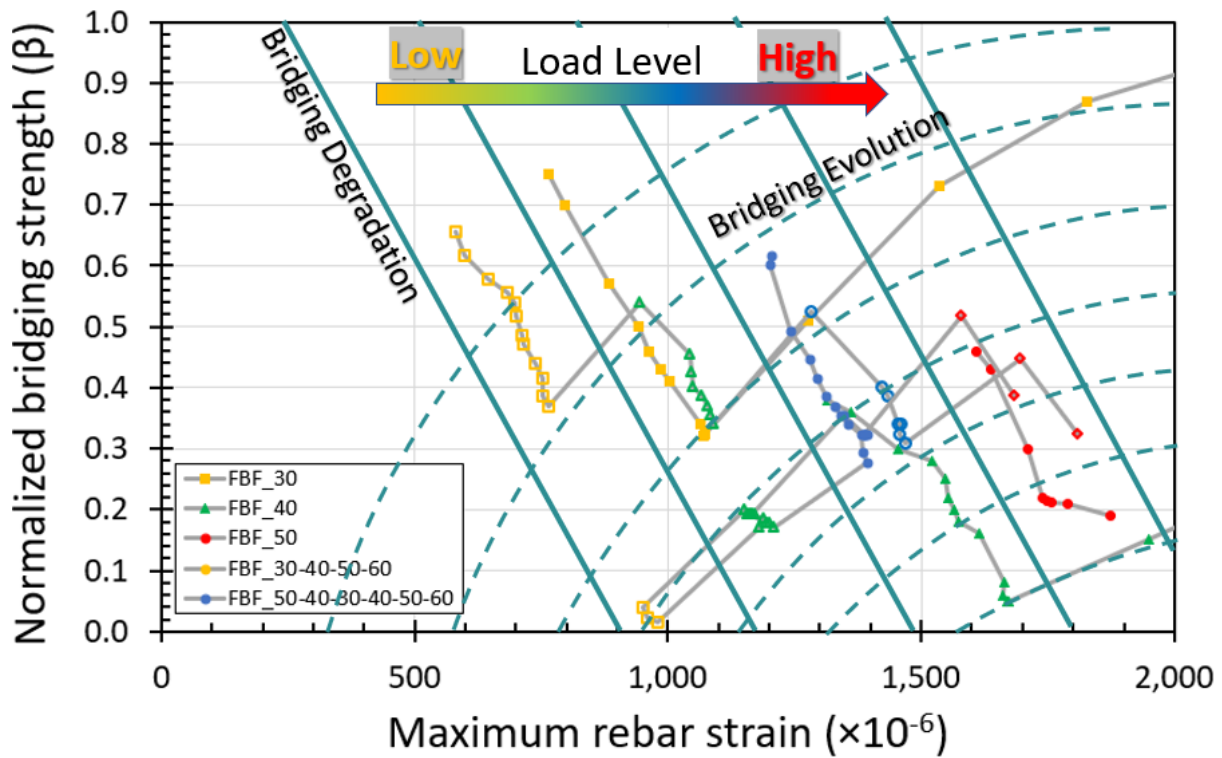


Fig. 5.32 Normalized crack-bridging strength degradation and evolution diagram versus maximum rebar strain under various flexural fatigue load level.

The proposed diagram of the crack-bridging strength degradation resulted from different tested beams from the first and second series shows that the degradation mechanism has a constant linear relationship over a wide range of fatigue load level regarding the maximum rebar strain level evolution, as shown in Fig.5.31 as parallel inclined solid lines. As cycles progress, the repeated cyclic loading leads to crack growth that would lead to loss of bond between the matrix and the fibers, as well as increasing in rebar strain level, simultaneously. Also, while decreasing the fatigue load level during the fatigue life i.e. beam FBF_50-40-30-40-50-60, the normalized crack-bridging strength versus the rebar strain evolution relationship returns to the same zone of the lower load level, as shown in Fig.5.31. The diagram of the crack-bridging strength degradation proposed for a 1.5% volume fraction of hooked-end steel fibers, and normal compressive strength of 35 MPa that may affect the inclination of degradation diagram, as it will be discussed in the next chapter.

The proposed diagram of the crack-bridging strength evolution resulted from different tested beams from the first and second series shows that the evolution increase mechanism has a linear relationship over fatigue life with a decreased slope for a higher fatigue load level regarding the maximum rebar strain level evolution depending on the damaged level, as shown in Fig.5.31 as circular dotted curves. As cycles progress, the repeated cyclic loading leads to crack

growth that would lead to loss of bond between the matrix and the fibers and increasing in the damage level, as well as increasing in rebar strain level. By increasing the flexural load level monotonically, new fibers contribute to bridging cracks with old fibers that have a damaged level at the fiber-matrix interface. As the damaged level increased by a higher fatigue load level, the crack-bridging strength ability to recover would be reduced indicating a lower increased slope in the evolution curves, as shown in Fig.5.31. The diagram of the crack-bridging strength evolution might be affected by material properties, as would be discussed in the next chapter.

5.5 Conclusion

The research work of the second series presented in this chapter aimed at evaluating the degradation and evolution of crack-bridging strength provided by hooked-end steel fibers over the whole fatigue life of structural beams under cyclic loading with a variable flexural load in an increasing or decreasing manner until a rupture fatigue failure. An inverse analysis method is used to derive a degradation and evolution model for crack-bridging strength from the experimental fatigue response of SFRC structural beams. The degradation and evolution model was captured for a wide range of fatigue load levels and the main conclusions that can be drawn from this work are as follow:

1. The good fit obtained with the proposed degradation and evolution model for the crack-bridging strength provided by steel fibers confirms the applicability of inverse analysis assuming a plane strain distribution since no strain redistributions in the compressive stress zone was observed.
2. The normalized crack-bridging strength was proposed for each different level of flexural fatigue stress of each SFRC structural beam during the fatigue life, that monotonically changes by increasing or decreasing or stabilizing regarding the changing in the fatigue load level over the fatigue life and regarding the evolution of rebar strain level.
3. The normalized crack-bridging strength tends to monotonically degrade under flexural fatigue loading over the fatigue life, except for if the SFRC beam was tested under a higher fatigue loading level in the fatigue loading history, where the crack-bridging strength tends to stabilize because of lower pullout force applied on fibers at the crack location with a higher damage level at fiber-matrix interface.

4. The normalized evaluated crack-bridging strength monotonically linearly decreases regarding the evolution of rebar strain level for all fatigue stress levels, with almost the same inclination regardless of the fatigue stress level and the fatigue loading level history, whether the SFRC beam was tested under the desired fatigue load level in the past or not.
5. The normalized evaluated crack-bridging strength increased by increasing the flexural load level monotonically with the contribution of the new fibers in bridging the cracks inside the tensile stress zone and the contribution of the old fibers with the desired damage level.
6. The normalized evaluated crack-bridging strength monotonically linearly increased regarding the evolution of the rebar strain level for all fatigue stress levels, with almost the decreased inclination regarding the fatigue stress level and the bond damage level at the fiber-matrix interface, resulting in an evolution model of crack-bridging strength.
7. Using the proposed degradation and evolution diagram of crack-bridging strength with the material constitutive laws based on direct sectional analysis calculations over of fatigue loading cycles, an accurate full design and assessment procedure for the whole fatigue life of SFRC beams under flexural fatigue loading is expected to be accomplished.

Chapter 6

6 Material Properties Effect on The Crack-bridging Strength Degradation and Evolution of SFRC Structural Beams under Flexural Fatigue

6.1 Introduction

This chapter examines the influence of changing material properties (i.e. concrete compressive strength and the beam's reinforcement ratio) on the flexural fatigue experimental response and the crack-bridging strength induced by hooked-end steel fibers on the reinforced concrete structural beams subjected to flexural cyclic loading under single and variable fatigue stress levels. As well, this chapter aims to understand the mechanism of crack-bridging strength evaluated from the inverse analysis calculation method based on changing the material properties under various fatigue load levels. Furthermore, by the end of this chapter, a diagram of the crack-bridging strength degradation and evolution over the fatigue life of SFRC structural beams under flexural cyclic loading regarding fatigue stress levels would be proposed based on inverse analysis calculation methods and to be compared with the one proposed in chapter 5. The experimental program for the third series of SFRC beams on the structural scale under fatigue loading conditions is presented. Firstly, the experimental fatigue response data of structural beams are captured to be compared with the first and the second series and to be used in the execution of the inverse analysis calculation method under various flexural fatigue load level. Finally, the crack-bridging strength is evaluated for the third series for the changed material properties of SFRC structural beams under various flexural fatigue load level over their fatigue life varying from a low, medium, to high fatigue stress level and compared with the proposed crack-bridging strength degradation and evolution diagram in the previous chapter.

6.2 Experimental Program

The experimental program of the third series consisted of SFRC specimens that are tested on both material and structural scale, with a higher compressive strength of 0.40 water to cement ratio for one set and with a lower reinforcement ratio of two steel reinforcing bars of 13 mm diameter for another set as compared with the first series as described in chapter four.

Material level tests were carried out to evaluate the material properties such as concrete compressive strength (f_{cm}), concrete first cracking tensile strength (f_{ct}), concrete modulus of elasticity (E_c), and the steel fiber reinforced concrete's tension softening curve and fracture energy (G_f) as listed in Table 6.1. The results of the tests are presented and evaluated with particular emphasis on the effects of steel fibers on the fatigue response of the beams.

Besides, structural scale tests consist of six structural scales SFRC beams with 1.5% hooked-end steel fibers (Dramix 3D 65/35 BG), having the same cross-section area of 150 mm x 200 mm and a span length (l) of 1700 mm with 300 mm of constant moment loading span (s) and effective depth (d) of 170 mm. Three SFRC structural beams had two conventional rebars with a diameter (D) of 16 mm and a higher concrete compressive strength of 62.80 MPa, but the other Three SFRC structural beams had two conventional rebars with a diameter (D) of 13 mm and a normal concrete compressive strength of 32.65 MPa, as listed in Table 6.2. The beams were instrumented to measure the rebar strains, surface concrete strains, and mid-span deflections having testing configurations as shown in Fig. 4.1.

Table 6.1: Test program of material scale specimens.

| Specimen | Description | SFRC (C60) | SFRC (C35) |
|--|-------------------------------|------------|------------|
| Cylinder (D =100 mm) (L=200 mm) | Number of specimens | 9 | 9 |
| | Compressive strength (MPa) | 62.80 | 32.65 |
| | Young's modulus (GPa) | 33.08 | 25.17 |
| Cylinder (D =150 mm) (L=150 mm) | Number of specimens | 7 | 7 |
| | Tensile strength (MPa) | 3.55 | 3.2 |
| Prismatic specimen (100 x 100 x 400 mm) | Number of specimens | 6 | 6 |
| | Flexural strength (kN) | 20.80 | 13.7 |
| | Fracture energy (N/mm) | 14.62 | 10.0 |

Table 6.2: Test program of structural scale beams.

| Beam ID | Fiber volume (%) | Min. fatigue load (kN) | Max. fatigue load (kN) | Fatigue life | Residual flexural capacity (kN) |
|---------------------|------------------|------------------------|------------------------|--------------|---------------------------------|
| C60_FBF_30-45-55-65 | 1.5 | 5.0 | 30→45→55→65 | 4,981,386 | – |
| C60_FBF_45 | 1.5 | 5.0 | 45.0 | 2,000,000 ↑ | 115.79 |
| C60_FBF_55 | 1.5 | 5.0 | 55.0 | 979,605 | – |
| D13_FBF_25-36-40 | 1.5 | 5.0 | 25→36→40 | 3,685,131 | – |
| D13_FBF_36 | 1.5 | 5.0 | 36.0 | 2,000,000 ↑ | 69.17 |
| D13_FBF_40 | 1.5 | 5.0 | 40.0 | 714,580 | – |

Note: The structural beams were tested under a four-point bending fatigue test. the horizontal arrow in maximum fatigue load cells indicates the changing of the fatigue load over fatigue life and the vertical arrow in fatigue life cells indicates the end of the fatigue test without fatigue failure.

6.2.1 Material and Mix Proportion

The concrete used in the third series for SFRC was a high and normal-grade concrete with a target mean strength (f_{cm}) of 60 MPa and 35 MPa, respectively by which they were labeled as C60 and C35. The following materials were used as same as the first series in mixing and production of concrete: cement, coarse aggregate, fine aggregate, steel fibers, water, and superplasticizer. [Table 6.3](#) shows the mix proportions of both SFRC (C60) and SFRC (C35). Ordinary portland cement meeting the Japanese industrial standards (JIS) was used as the binding material, with a specific gravity of 3.15. Crushed coarse and fine aggregates were used with maximum aggregate sizes of 13.0 mm and 4.75 mm and specific gravities of 2.66 and 2.65, respectively. The steel fibers - Dramix 3D 65/35 BG - were gradually sprinkled into the mix by hand to a 1.5% volume fraction of the full SFRC volume, and care was taken to obtain a homogenous and workable mixture. Furthermore, a high-performance air-entraining water-reducing agent (Types: SP8SV and SBsX3) were used in SFRC in a range of 1.0% per each to the weight of the cement for each concrete mix as a superplasticizer to obtain an average 120 mm slump value. The water to cement ratio was 55% for SFRC (C35) as a normal strength

concrete and 40% for SFRC (C60) as a high strength concrete. Finally, the SFRC batches were introduced into their molds and compacted, then the specimens were removed from the molds after 3 days and cured for 28 days.

Three structural beams were reinforced with tensile reinforcement consisted of two 16 mm nominal diameter bars as same as the first series and another three structural beams were reinforced with two 13 mm nominal diameter bars by which they were labeled as D13, as listed in Table 6.2. The longitudinal reinforcing bars were hot rolled deformed steel bars, all from the same batch with a nominal yield strength of 346 MPa and Young's modulus of 200 GPa. The structural beams were designed to be failed under flexural loading conditions without any need for shear reinforcement and compression reinforcement.

Table 6.3: Mix proportion of the first series for NC and SFRC.

| Ingredient | Amount (kg/m ³) | |
|-------------------------|-----------------------------|------------|
| | SFRC (C60) | SFRC (C35) |
| Portland cement | 463 | 336 |
| Water | 185 | 185 |
| Fine aggregate | 990.8 | 1055 |
| Coarse aggregate | 663 | 706 |
| Hooked-end steel fibers | 117.8 | 117.8 |
| Superplasticizer | 5.05 | 5.05 |

6.2.2 Specimens

The test program consisted of several SFRC specimens that were tested on both material and structural scales for the third series test set. The third series aims to capture the fatigue response of SFRC over the fatigue life under variable fatigue load levels by changing the concrete compressive strength and the beam's reinforcement ratio as compared with the first and second series. Besides, as same as the first and second series the execution of the inverse analysis calculations method requires detailed information about the material properties of SFRC, as a result, material level tests were carried out to identify the materials constitutive laws, targeting finally in the evaluation of the degradation and evolution in the crack-bridging strength over the fatigue life of SFRC structural beams.

Two sets of structural scale beams of steel fiber reinforced concrete were tested under a 4-points bending test under cyclic loading. The details of the tested structural beams of the third

series are discussed in [Table 6.2](#). All structural beams have a rectangular cross-section with a dimension of 150 x 200 mm and a length of 2000 mm. The structural beams were tested under flexural loading test with a span length (l) of 1700 mm, with 300 mm of constant moment loading span (s), and an effective depth (d) of 170 mm as shown in [Fig. 4.1](#). Two sets of structural beams were reinforced with a tensile longitudinal reinforcement ratio of 1.34 percent and 0.885 percent to be failed inside the constant moment region in a flexural failure mode.

The concrete material properties were determined from the material tests of the third series that were carried out as listed in [Table 6.1](#). The material level specimen's details were as same as the first series as discussed in section 4.2.3 and the results of compressive strength (f_{cm}), concrete modulus of elasticity (E_c), first cracking tensile strength (f_{ct}), the steel fiber reinforced concrete's tension softening curve, and fracture energy (G_f) are listed in [Table 6.1](#).

6.3 Experimental Results

In the third series, several specimens were tested under the material and structural level to capture and analyze the fatigue response of SFRC beams under flexural loads and to evaluate the crack-bridging strength degradation and evolution over the fatigue life under variable fatigue load levels. Firstly, a 3-point bending test was carried out on notched prismatic SFRC (C60) and SFRC (C35) specimens to calculate the initial crack-bridging strength – tension softening curve – to be used in sectional analysis calculations. Finally, two sets of structural beams were tested under different stress levels of fatigue loading ranging from low to high-stress levels. Considering, the time consuming for testing each beam, one beam of SFRC has been tested cyclically under variable flexural fatigue stress levels, as shown in [Figs. 6.3](#), and [6.4](#), and two beams of SFRC have been tested cyclically under a single flexural fatigue medium and high load level. The following sections discuss the test results of the individual beams. As a result, the results of inverse analysis calculations are presented in the next section in a model of degradation and evolution of the crack-bridging strength induced by hooked-end steel fibers over the fatigue life of various flexural fatigue stress levels.

6.3.1 Prismatic Specimens under Flexural Static Loading

The crack-bridging strength – or the tension softening curve – is a fracture mechanics parameter that describes post-cracking behavior, represents the fracture energy (G_f) of SFRC in the tensile stress zone, and is used in the sectional analysis calculations to understand the

response of structural beams to loading. It is obtained from the material scale flexural test results obtained in the bending test of notched prismatic specimens until complete rupture as shown in Fig. 6.1 using the poly-linear approximation analysis method following the JCI-S-001-2003 standard (JCI 2003a).

The average static flexural capacity of the six SFRC (C60) notched prismatic specimens ranging from Sp-01 to Sp-06 was 20.80 kN with a standard deviation of 1.21 kN, as shown in Fig. 6.2. Based on this result, the fracture energy (G_f) was calculated following (JCI 2003a) as 14.62 N/mm on average with a standard deviation of 1.13 N/mm, as summarized in Table 6.1. Using a least-squares data-fitting procedure, the shape of the tension softening diagram can be obtained from the calculated results and summarized as Eq. (6.1). On the other hand, the shape of the tension softening diagram of SFRC (C35) can be obtained from the calculated results of the second series, having the same tension softening curve of the second series and summarized as Eq. (4.3). This tension softening curve can be divided into three zones. The first zone is immediately after cracking, where the stress abruptly increases at a crack opening (ω) of less than 0.1 mm. This is followed by a fiber bridging plateau (plastic region), followed by the cohesive stress decreases following a softening branch, as illustrated in Eq. (6.1).

$$\begin{aligned} \sigma &= f_{st} && (MPa) && \text{for } \omega = 0.0 \\ \sigma &= \left(\frac{6.4 - f_{st}}{0.1} \right) \omega + f_{st} && (MPa) && \text{for } 0 < \omega \leq 0.1 \text{ mm} \\ \sigma &= 6.4 && (MPa) && \text{for } 0.1 < \omega \leq 0.88 \text{ mm} \\ \sigma &= 6.4 - 2.34 \omega && (MPa) && \text{for } 0.88 < \omega \text{ mm} \end{aligned} \quad (6.1)$$



Fig. 6.1 Fracture of SFRC prismatic specimen at the end of the bending test.

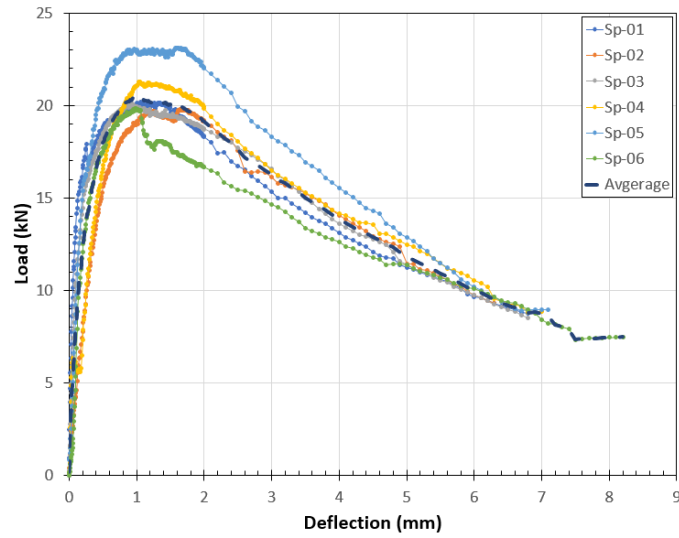


Fig. 6.2 Three-point bending test on SFRC (C60) prismatic specimens.

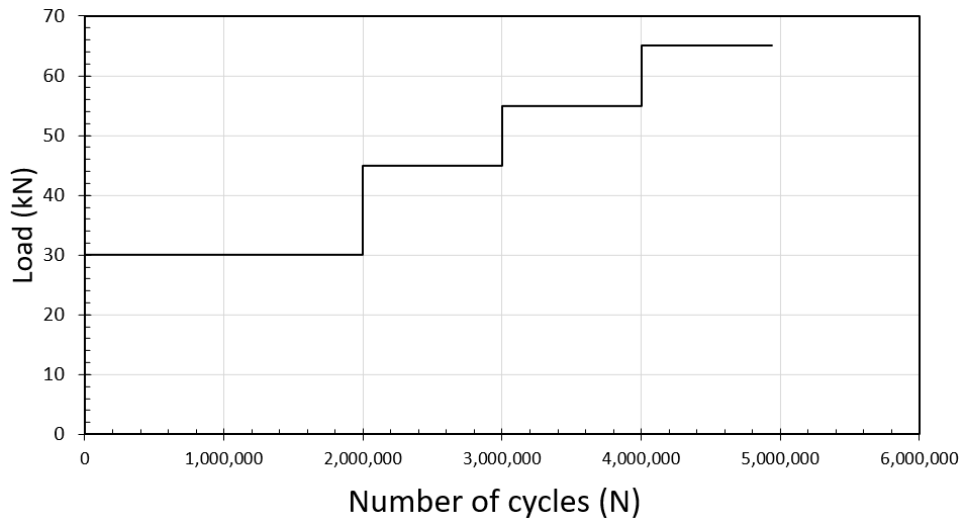


Fig. 6.3 Maximum fatigue load level over the fatigue life of C60_FBF_30-45-55-65.

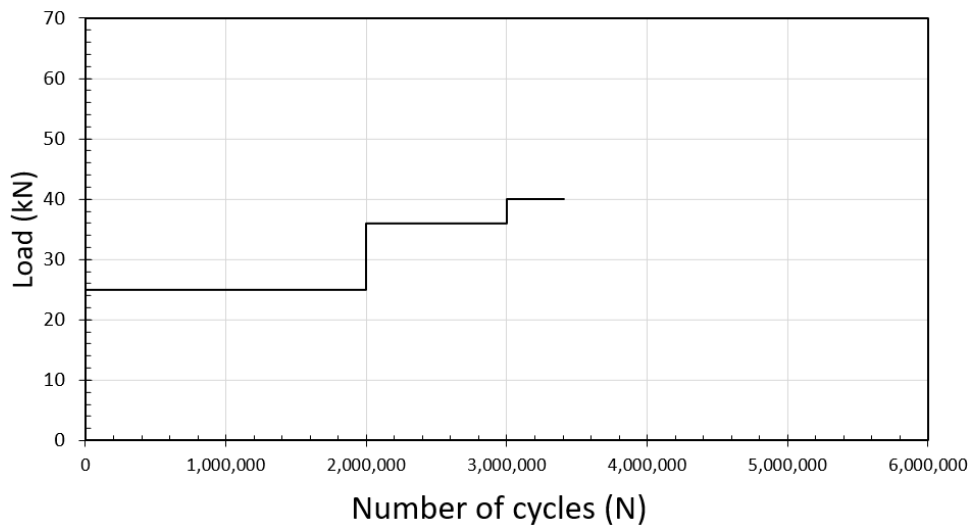


Fig. 6.4 Maximum fatigue load level over the fatigue life of D13_FBF_25-36-40.

6.3.2 Fatigue Flexural Loading of SFRC Structural Beams

A flexural variable cyclic loading test was carried out on two sets of SFRC structural beams for measuring the effect of higher concrete strength and lower reinforcement ratio on the flexural fatigue response and the evaluated degradation and evolution model of crack-bridging strength over fatigue life using the inverse analysis method, as explained in section 3.4.3 Also, as summarized in [Table 6.2](#). During fatigue loading, as the number of loading cycles increases, an evolution of both the rebar and concrete strain was observed for the SFRC structural beams, resulting in increasing mid-span deflection and crack length and width and decreasing structural stiffness as noted from the decrease of the inclination of the load-deflection curve and N.A. position, as illustrated in the following paragraphs, with an average crack spacing – or reference length (L_R) – of 70 mm, as shown in [Figs. 6.5, 6.5, 6.5, 6.5, 6.5, and 5.13](#).

6.3.2.1 Concrete Compressive Strength Effect

A flexural cyclic loading test was carried out on three SFRC structural beams, with higher compressive strength compared with the beams set in the first and second series, aiming to capture the difference in the flexural fatigue response and the influence degree on the evaluate degradation and evolution model of crack-bridging strength over fatigue life using the inverse analysis method, as explained in section 3.4.3. Also, residual flexural capacity after completion of two million cycles was evaluated in the case of beams that survived without fatigue failure, as summarized in [Table 6.2](#). As the higher concrete compressive strength would enhance the bond strength between fibers and matrix. As a result, The first SFRC structural beam – C60_FBF_30-45-55-65 – was tested for variable fatigue load levels starting with a low-stress level and the maximum fatigue load level increased over the fatigue life until failure in a mode of rebar rupture by 4981386 flexural fatigue cycles, as shown in [Figs. 6.5, 6.6, 6.8, and 6.9](#). The second SRFC structural beam – C60_FBF_45 – was tested under a medium fatigue load level of 45 kN as a maximum fatigue load level until the end of the fatigue life by two million cycles and then the residual flexural capacity was tested through a flexural static test, as shown in [Figs. 6.13, 6.14, and 6.16](#). The third SRFC structural beam – C60_FBF_55 – was tested under a high fatigue load level of 55 kN as a maximum fatigue load level until the end of the fatigue life of 979605 cycles by brittle rupture of rebar, as shown in [Figs. 6.22, 6.23, and 6.25](#). The fatigue load levels were selected to have the same rebar strain level in the first cycle at the maximum fatigue load level, aiming to have an appropriate comparison with the first and second series, as listed in [Table 6.2](#).

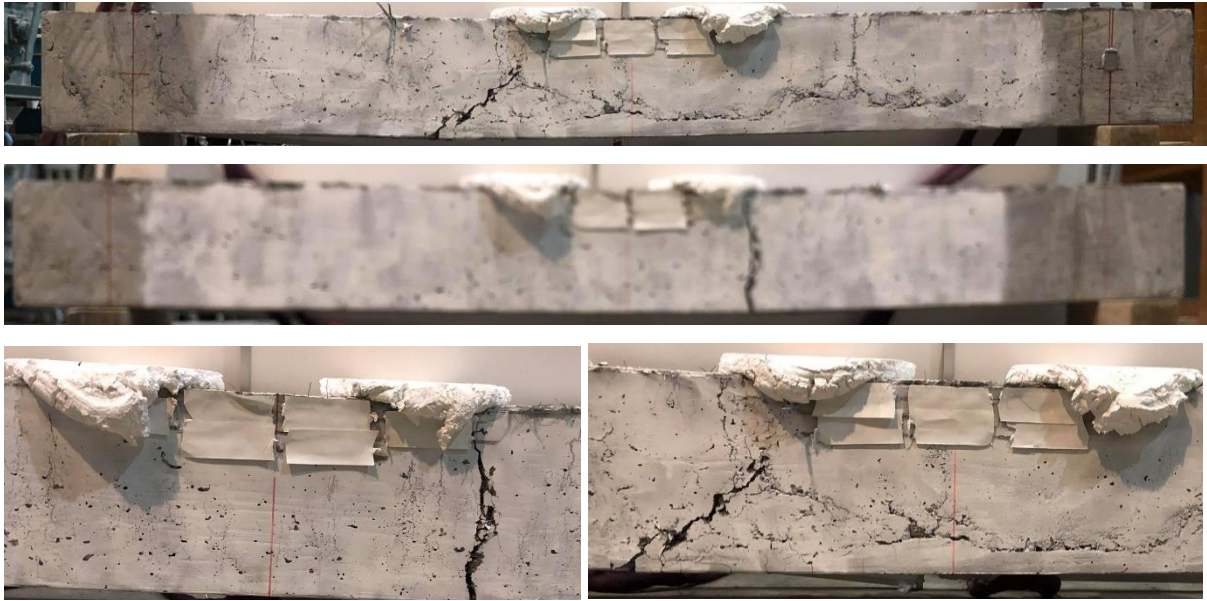


Fig. 6.5 Beam C60_FBF_30-45-55-65 over fatigue life under flexural fatigue.

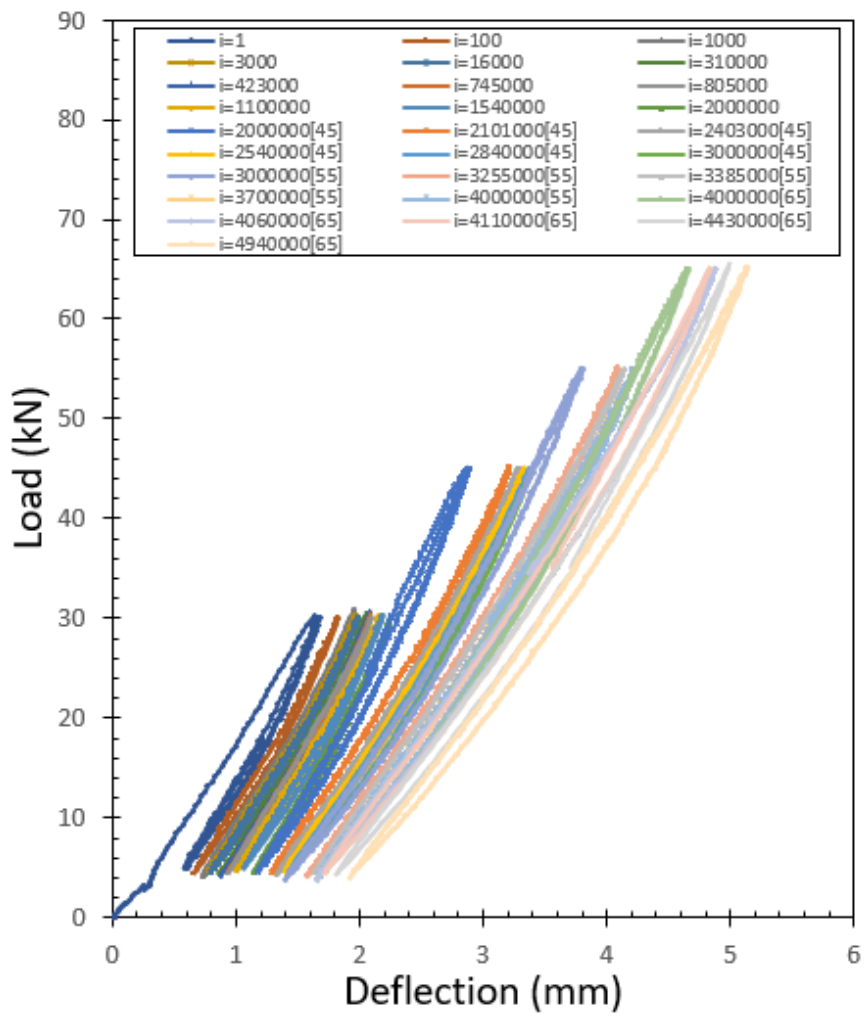


Fig. 6.6 Load versus deflection under flexural fatigue for beam C60_FBF_30-45-55-65.

Beam C60_FBF_30-45-55-65

For the increasing study case of the fatigue stress levels, one SFRC structural beam – C60_FBF_30-45-55-65 – was tested under flexural cyclic loading with 5 kN as a minimum flexural load and 30 kN, 45 kN, 55 kN, 65 kN as a maximum flexural load for two, one, one, one million cycles, respectively and sequentially, as shown in Figs. 6.3, 6.5, 6.6, and 6.8. Figure 6.6 shows the load versus mid-span deflection relationship over fatigue life under a low to a high-stress level of flexural fatigue load showing an increase in mid-span deflection as cycles progress. Figure 6.7 shows the strain distribution at midspan on the front face of the beam (L150), showing the strain evolution for both rebar and concrete throughout the application of flexural cyclic loading until the end of fatigue life. The average rebar strain within the constant moment region is plotted against the maximum and minimum flexural cyclic load for the variable fatigue stress levels during the fatigue life, starting from the first cyclic loading (N_1) and showing the evolution of average rebar strain, as shown in Fig. 6.8.

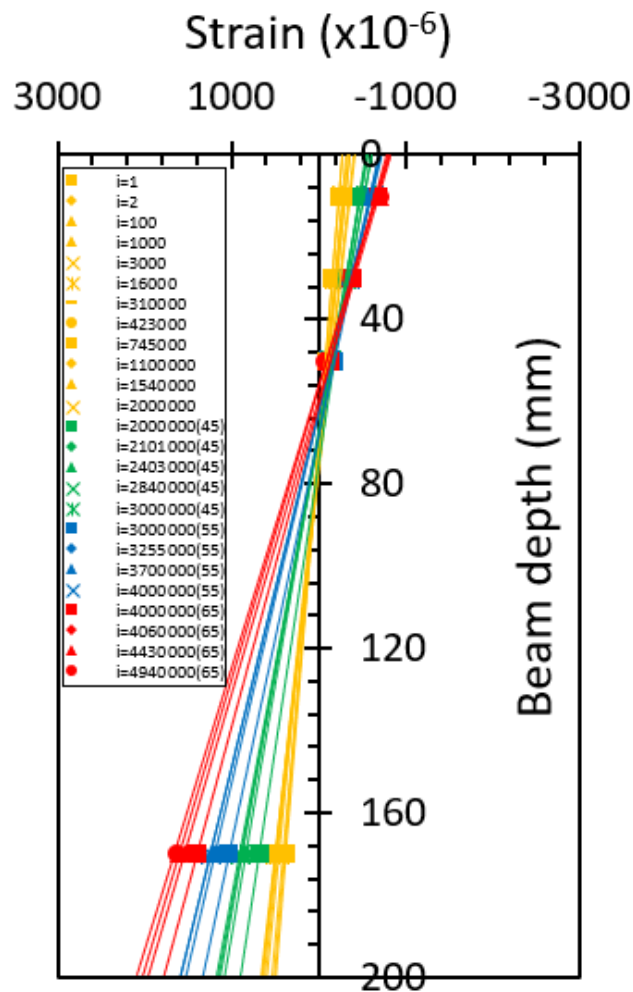


Fig. 6.7 Mid-span strain distribution under flexural fatigue for beam C60_FBF_30-45-55-65.

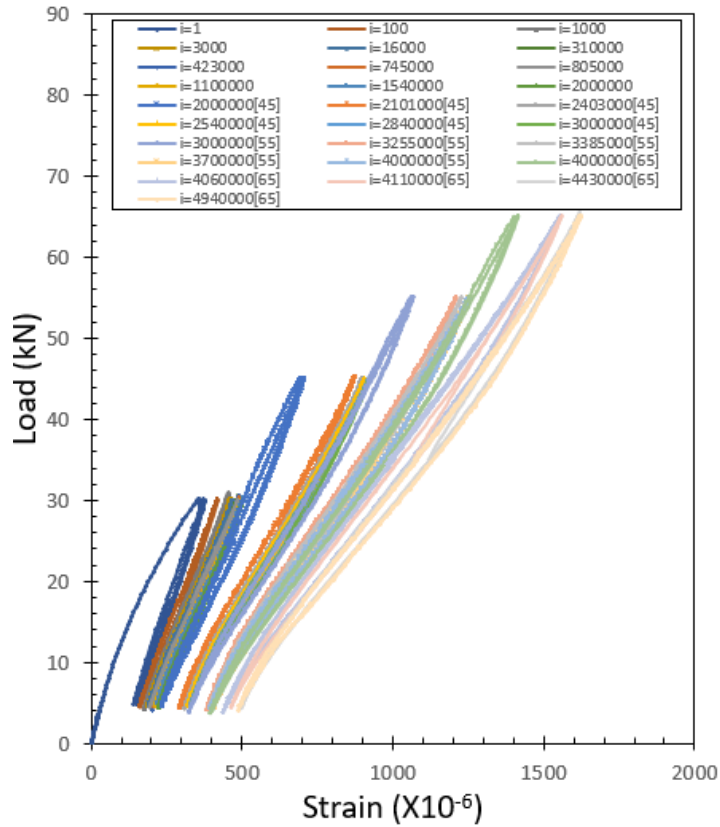


Fig. 6.8 Load versus average rebar strain under flexural fatigue for beam C60_FBF_30-45-55-65.

During the fatigue life of the tested beam – C60_FBF_30-45-55-65 – a higher flexural fatigue load level was applied by increasing the flexural load monotonically then the cyclic flexural load was applied between 5 kN as a minimum fatigue load level and the increased flexural load as a maximum fatigue load level. While the flexural applied load was increased monotonically, the mid-span deflection and the crack length and width were increased and structural stiffness was decreased as noted from the decrease of the inclination of the load-deflection curve and N.A. position, as shown in Figs. 6.6, 6.7, 6.8, and 6.12. As well, an evolution of both the rebar and concrete strain was observed for the SFRC structural beams, as shown in Figs. 6.7, 6.8, 6.10, and 6.11.

After increasing the flexural load monotonically, the cyclic flexural load was applied under the desired higher flexural fatigue load level. During that application of repeated cyclic loading, again an increase on both the rebar and concrete strain was observed for the SFRC structural beams, resulting in increasing mid-span deflection and crack length and width and decreasing structural stiffness as noted from the decrease of the inclination of the load-deflection curve and N.A. position, as shown in Figs. 6.9, 6.10, 6.11, and 6.12. finally, at a higher fatigue load

level of a 65 kN of flexural maximum load level was applying, a rupture fatigue failure took place in a manner of rebar rupture achieving 4981386 cycles of fatigue life, as summarized in Table 6.2.

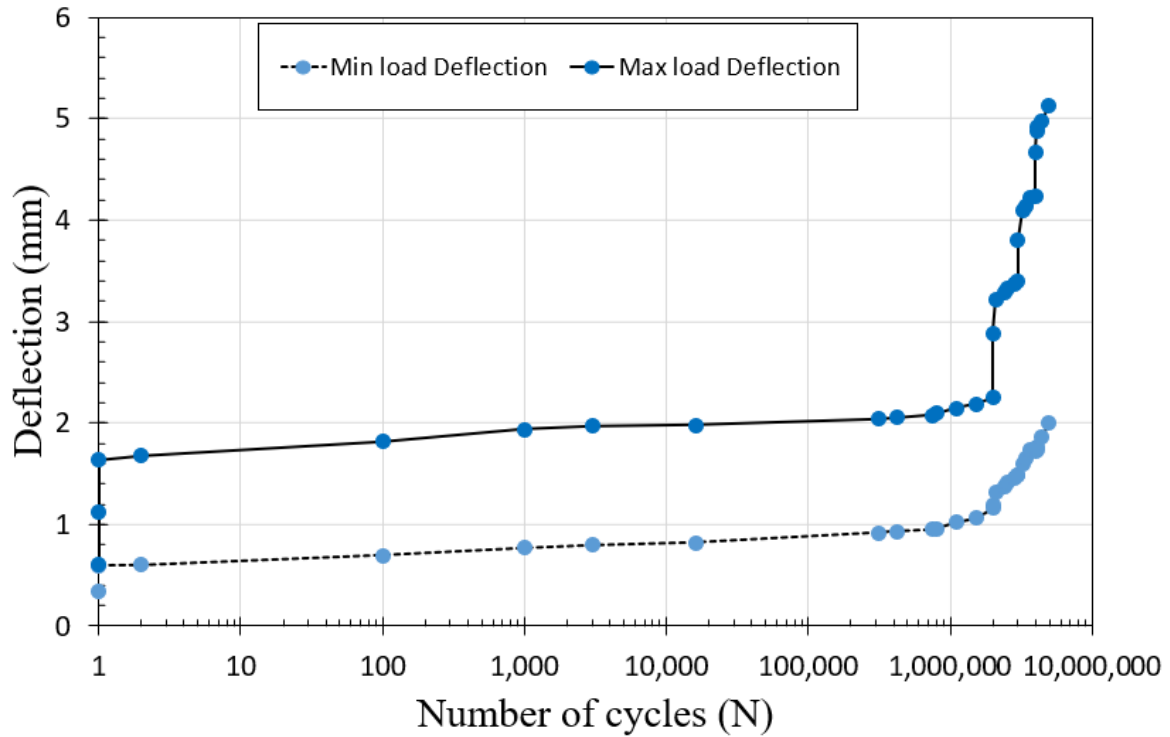


Fig. 6.9 Mid-span deflection at maximum and minimum load level under flexural fatigue for beam C60_FBF_30-45-55-65.

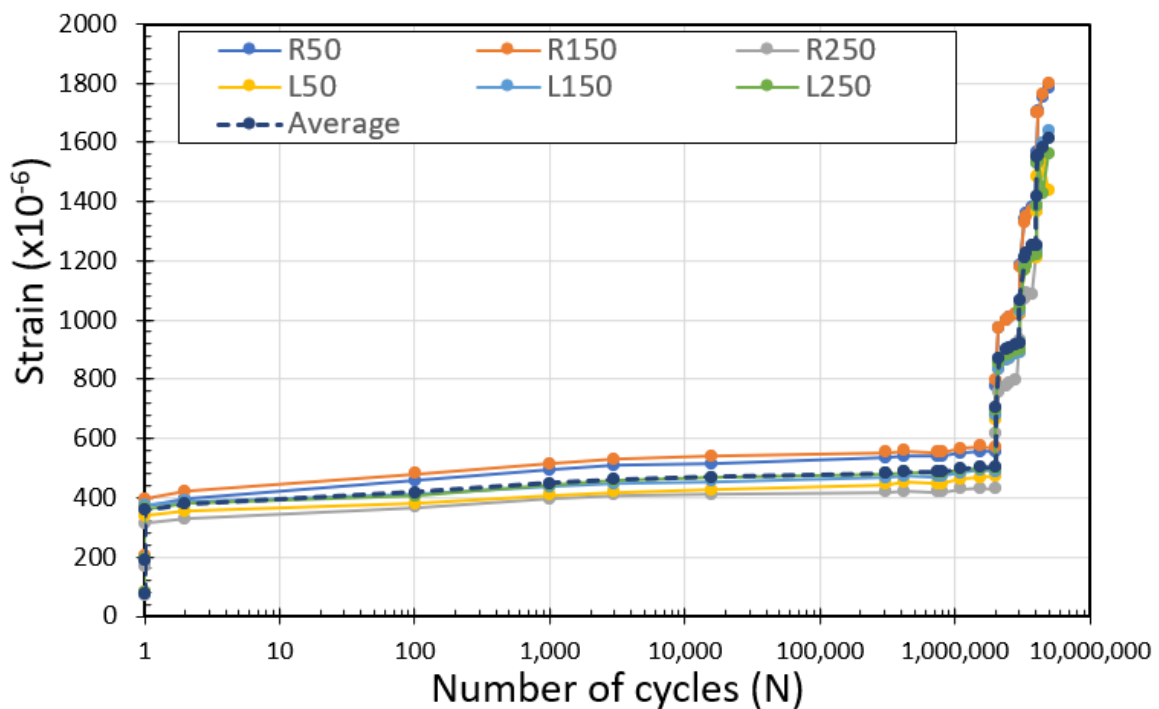


Fig. 6.10 Rebar strain evolution under flexural fatigue for beam C60_FBF_30-45-55-65.

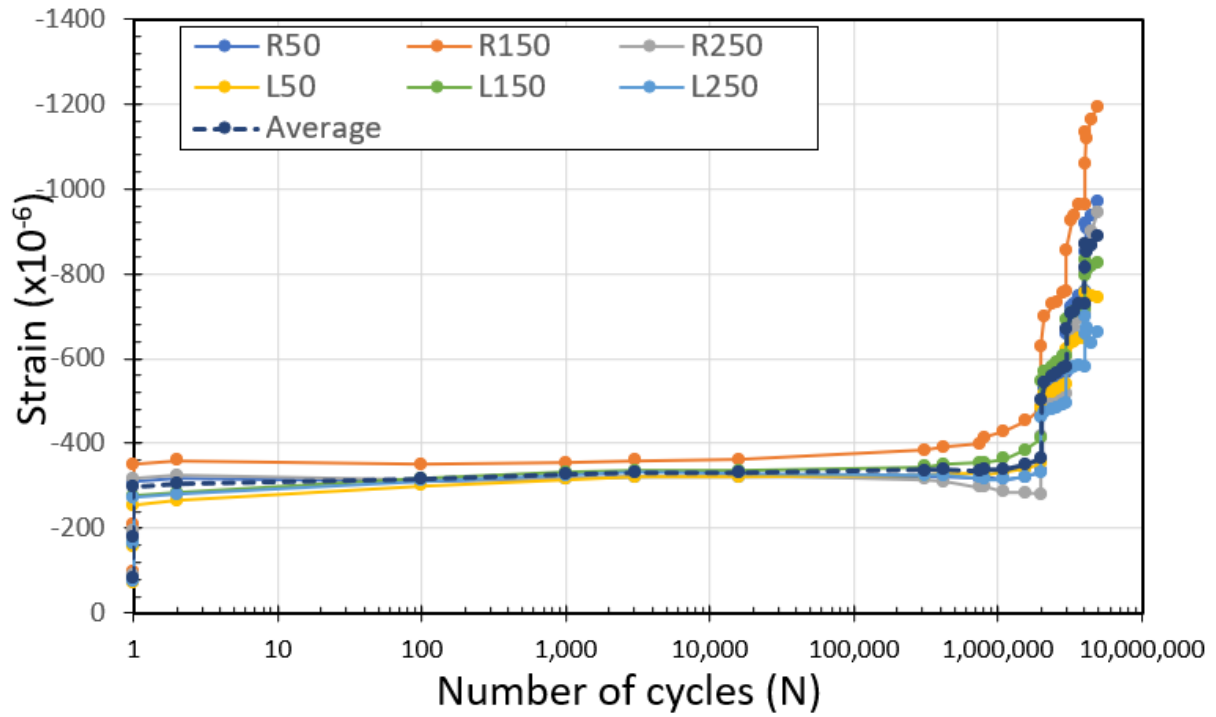


Fig. 6.11 ultimate concrete strain evolution under flexural fatigue for beam C60_FBF_30-45-55-65.

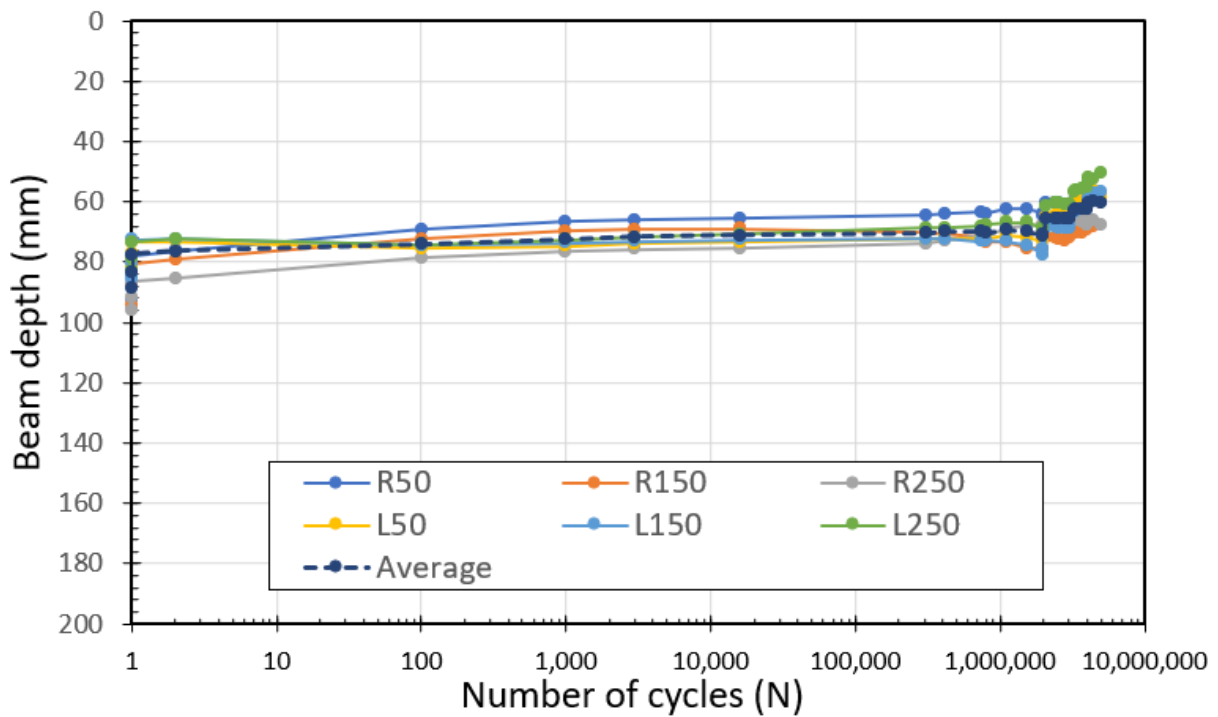


Fig. 6.12 Neutral axis position evolution under flexural fatigue for beam C60_FBF_30-45-55-65.

Beam C60_FBF_45

For the medium fatigue stress level, one SFRC structural beam – C60_FBF_45 – was tested under flexural cyclic loading with 5 kN as a minimum flexural load and 45 kN as a maximum flexural load, as shown in Figs. 6.13, 6.14, and 6.16. Figure 6.14 shows the load versus mid-span deflection relationship over fatigue life under a medium-stress level of flexural fatigue load showing an increase in mid-span deflection as cycles progress. Figure 6.15 shows the strain distribution at midspan on the front face of the beam (L150), showing the strain evolution for both rebar and concrete throughout the application of flexural cyclic loading until the end of fatigue life. The average rebar strain within the constant moment region of C60_FBF_45 is also plotted against the maximum and minimum flexural cyclic load for the medium fatigue stress levels during the fatigue life, starting from the first flexural cyclic loading (N_1) and showing the evolution of average rebar strain, as shown in Fig. 6.16. After a complete of two million cycles of flexural loading, SFRC beam C60_FBF_45 was subjected to a residual flexural static test to measure their residual capacity, as shown in Figs. 6.17 and 6.18. The result is listed in Table 6.2. Residual flexural capacity was measured achieving a 115.79 kN until a ductile flexural failure of rebar followed by concrete crushing inside the constant moment region, even after the fatigue loading emphasizing the effect of higher compressive strength.

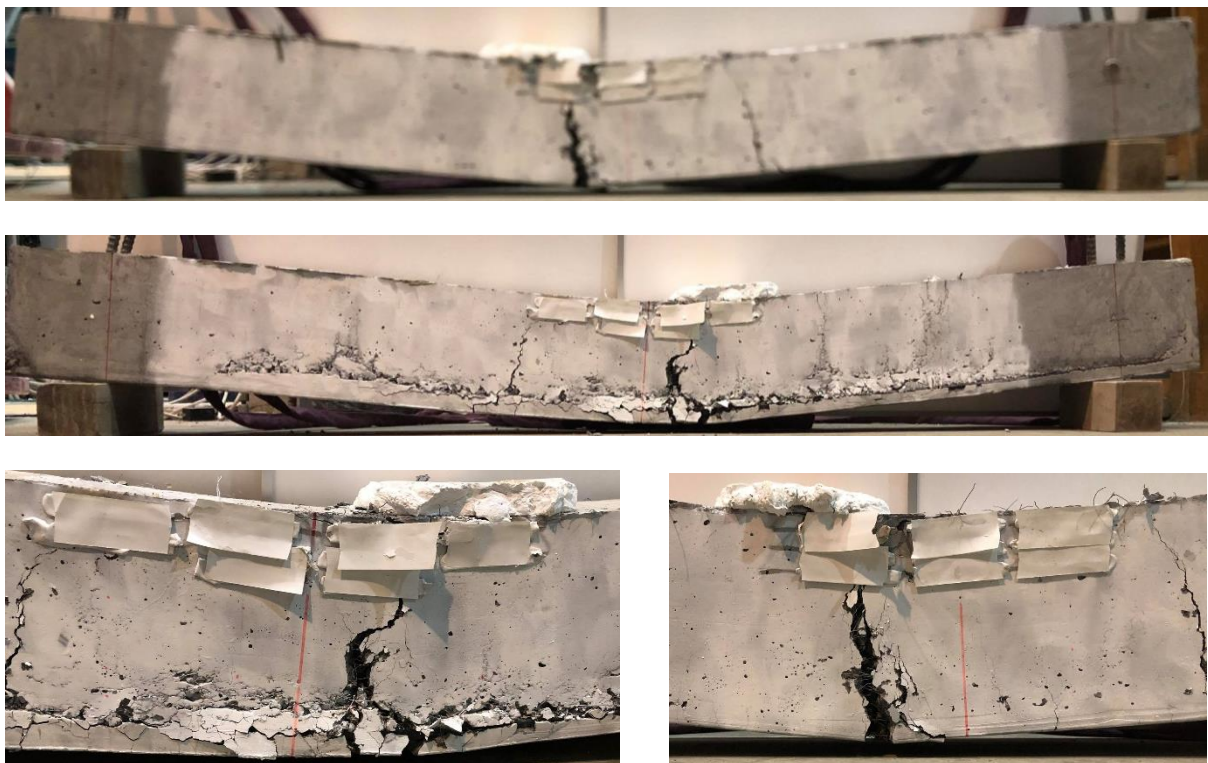


Fig. 6.13 Beam C60_FBF_45 over fatigue life under flexural fatigue.

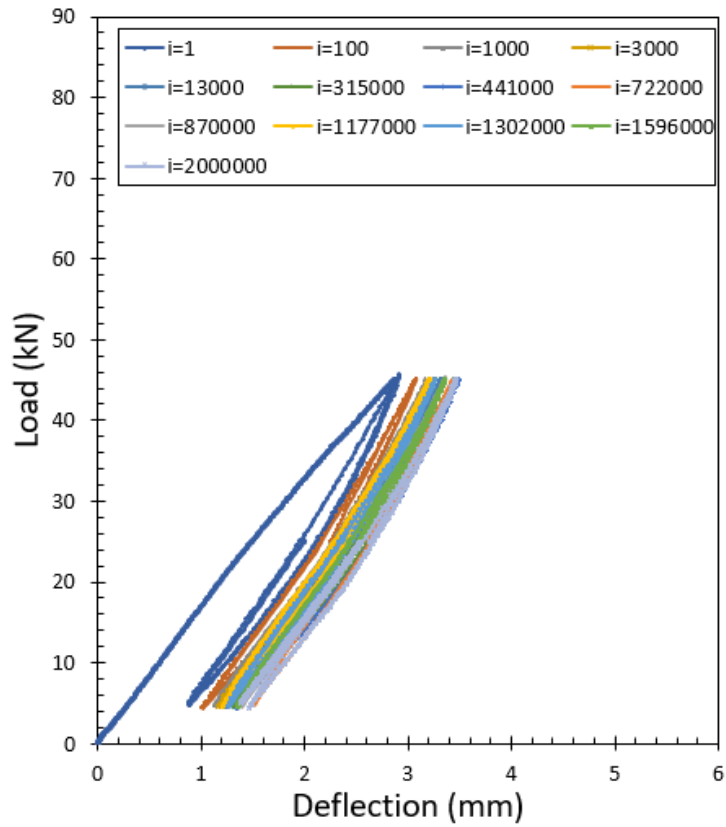


Fig. 6.14 Load versus deflection under flexural cyclic loading for beam C60_FBF_45.

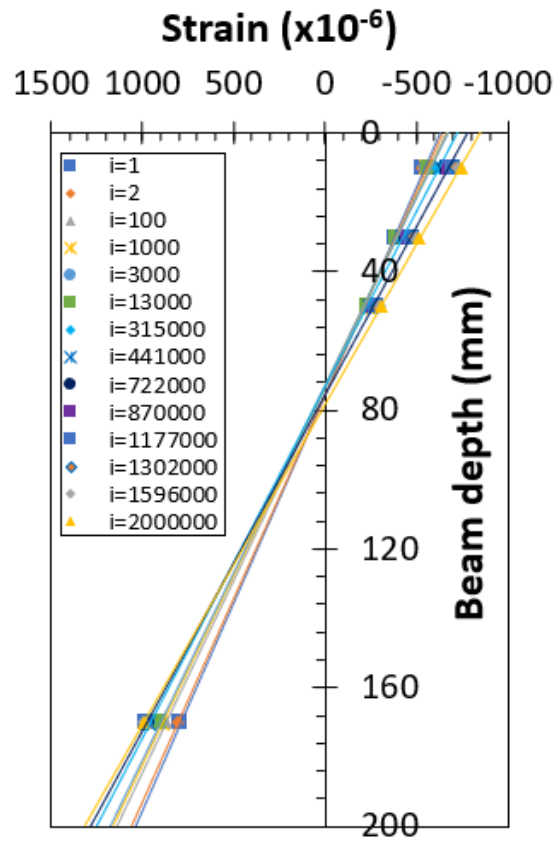


Fig. 6.15 Mid-span strain distribution under flexural cyclic loading for beam C60_FBF_45.

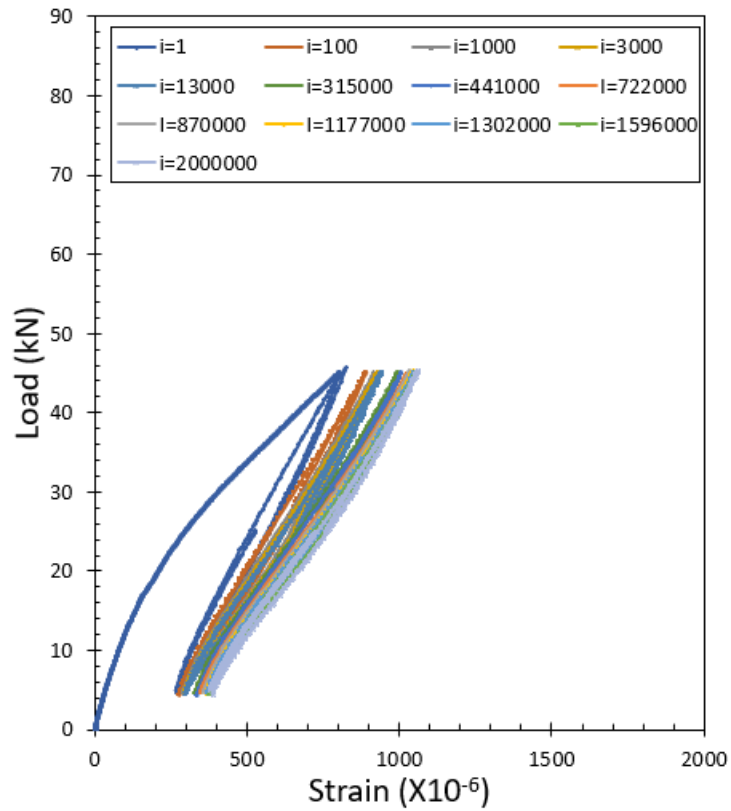


Fig. 6.16 Load versus average rebar strain under flexural cyclic loading for beam C60_FBF_45.

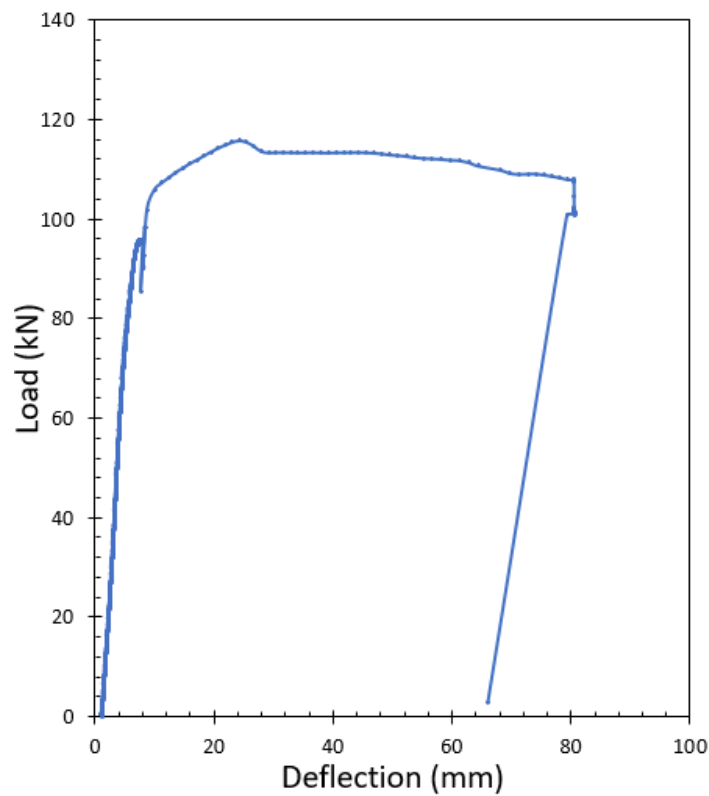


Fig. 6.17 Load versus deflection under residual flexural static loading for beam C60_FBF_45.

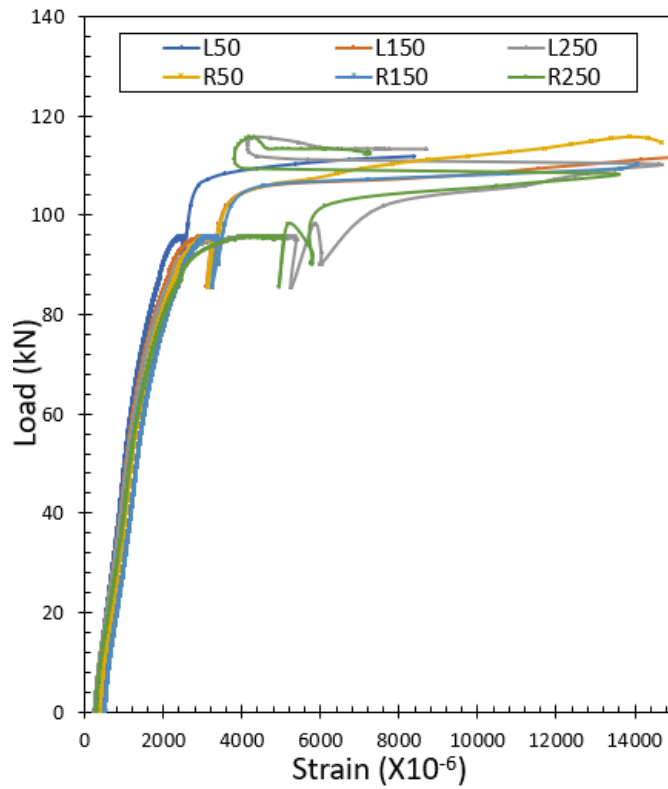


Fig. 6.18 Load versus rebar strain under residual flexural static loading for beam C60_FBF_45.

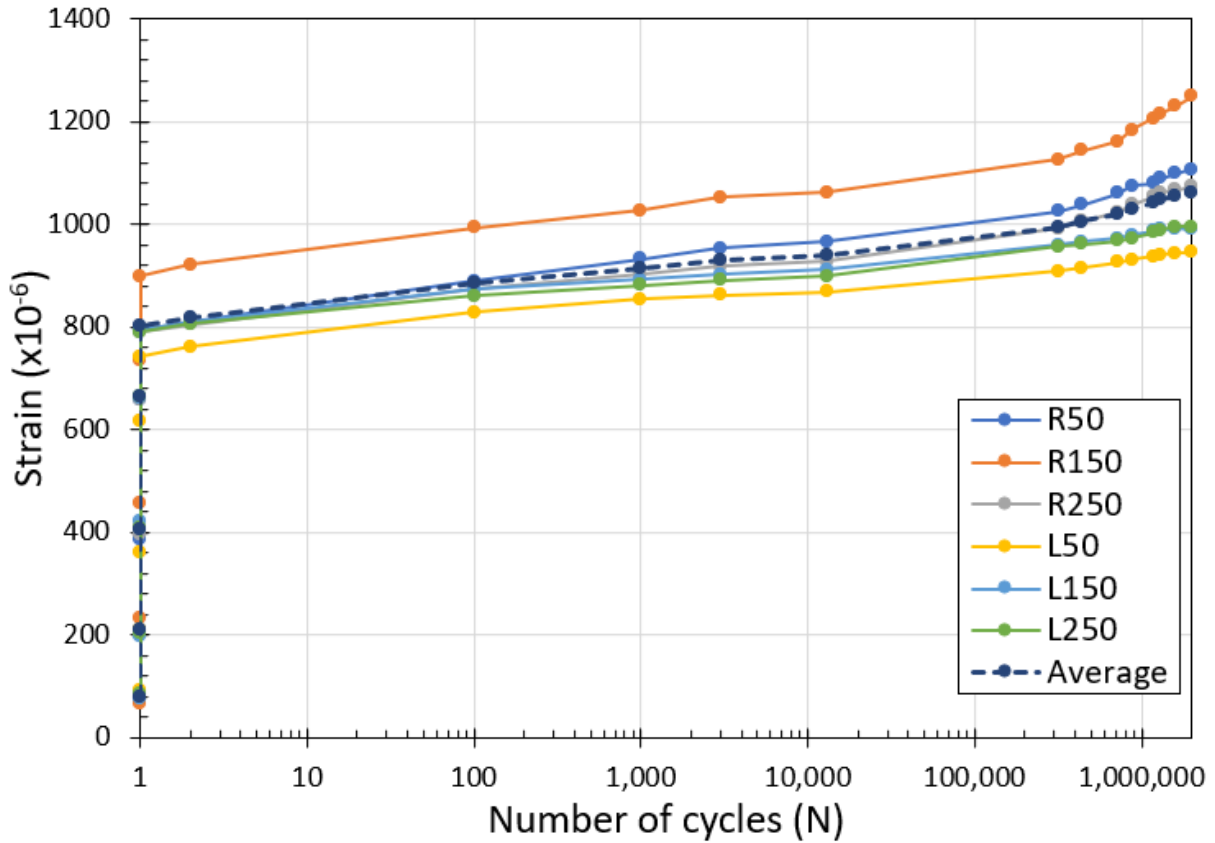


Fig. 6.19 Rebar strain evolution under flexural fatigue for beam C60_FBF_45.

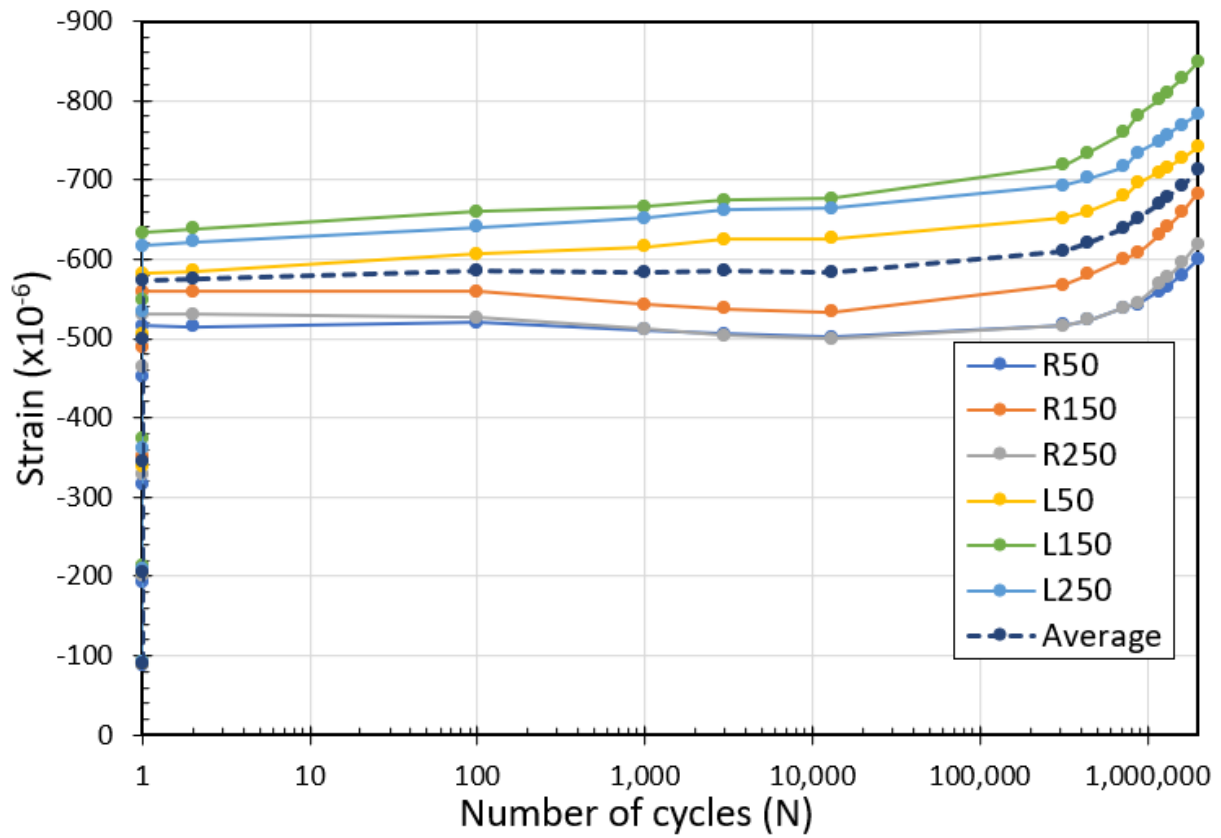


Fig. 6.20 ultimate concrete strain evolution under flexural fatigue for beam C60_FBF_45.

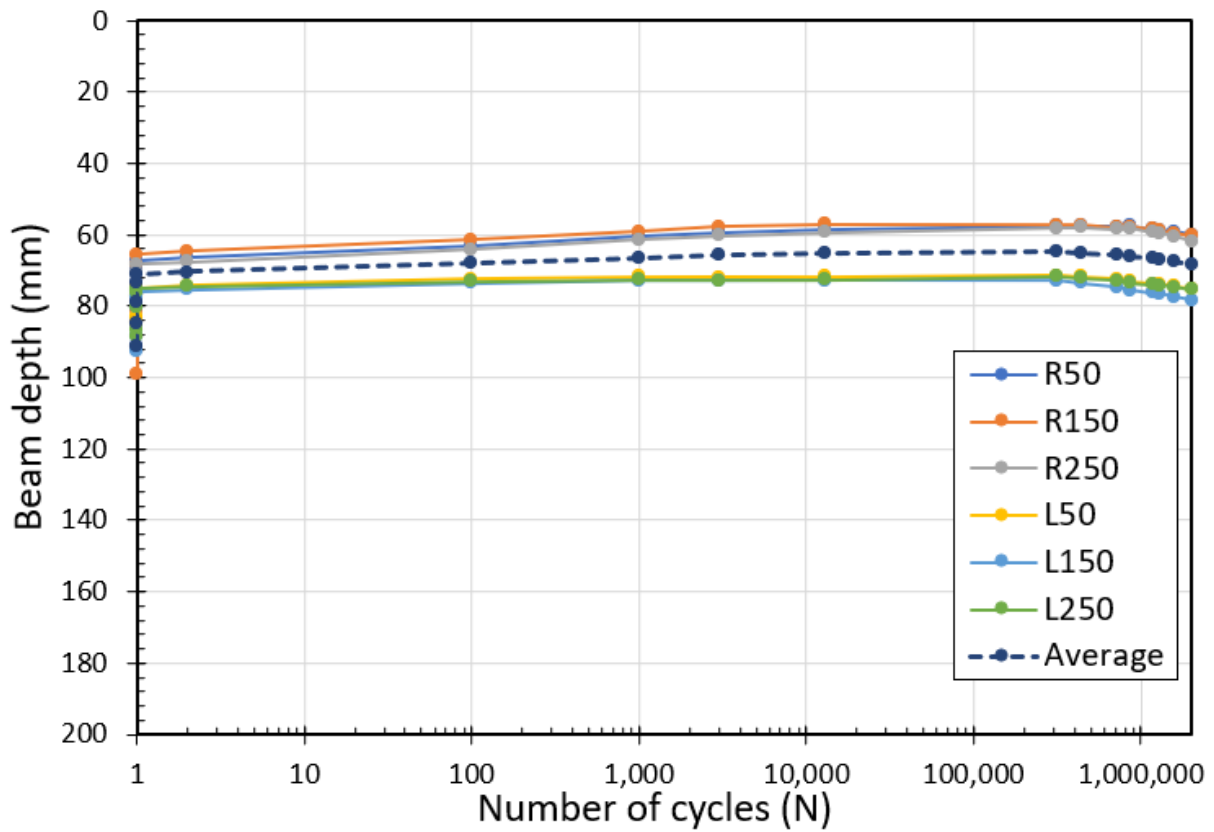


Fig. 6.21 Neutral axis position evolution under flexural fatigue for beam C60_FBF_45.

Finally, the average experimental data of the fatigue response of the SFRC structural beam – C60_FBF_45 – over the fatigue life to be used in the inverse analysis calculation method. The degradation of the crack-bridging strength would be evaluated by achieving a good fitting between the experimental and calculated fatigue response of the tested structural SFRC beams. As a result, the average experimental rebar strain, ultimate surface concrete strain, and N.A. position were monitored and plotted in Figs. 6.19, 6.20, and 6.21 respectively, from the data monitored inside the constant moment region.

Beam C60_FBF_55

For the high fatigue stress level, one SFRC structural beam – C60_FBF_55 – was tested under flexural cyclic loading with 5 kN as a minimum flexural load and 55 kN as a maximum flexural load, as shown in Figs. 6.22, 6.23, and 6.25. Figure 6.23 shows the load versus mid-span deflection relationship over fatigue life under a high-stress level of flexural fatigue load showing an increase in mid-span deflection as cycles progress. Figure 6.24 shows the strain distribution at midspan on the front face of the beam (R150), showing the strain evolution for both rebar and concrete throughout the application of flexural cyclic loading until fatigue failure. The average rebar strain within the constant moment region of C60_FBF_55 is also plotted against the maximum and minimum flexural cyclic load for the high fatigue stress levels during the fatigue life, starting from the first flexural cyclic loading (N_1) and showing the evolution of average rebar strain until rebar brittle rupture at 979605 cycles, as shown in Figs. 6.22, 6.23, and 6.25.

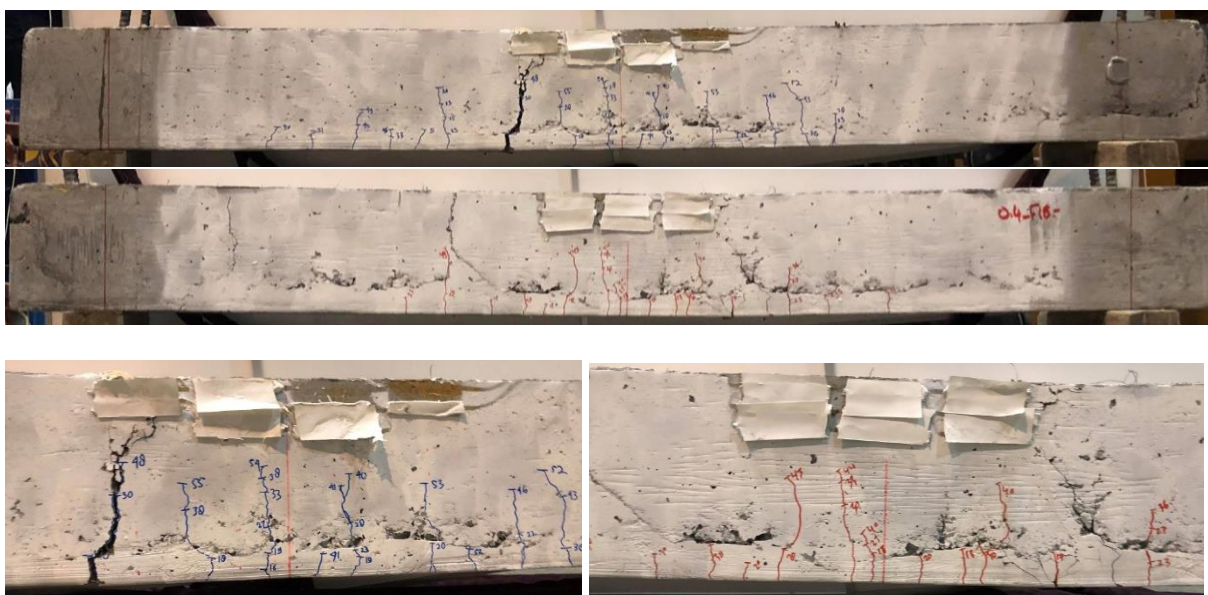


Fig. 6.22 Beam C60_FBF_55 over fatigue life under flexural cyclic loading.

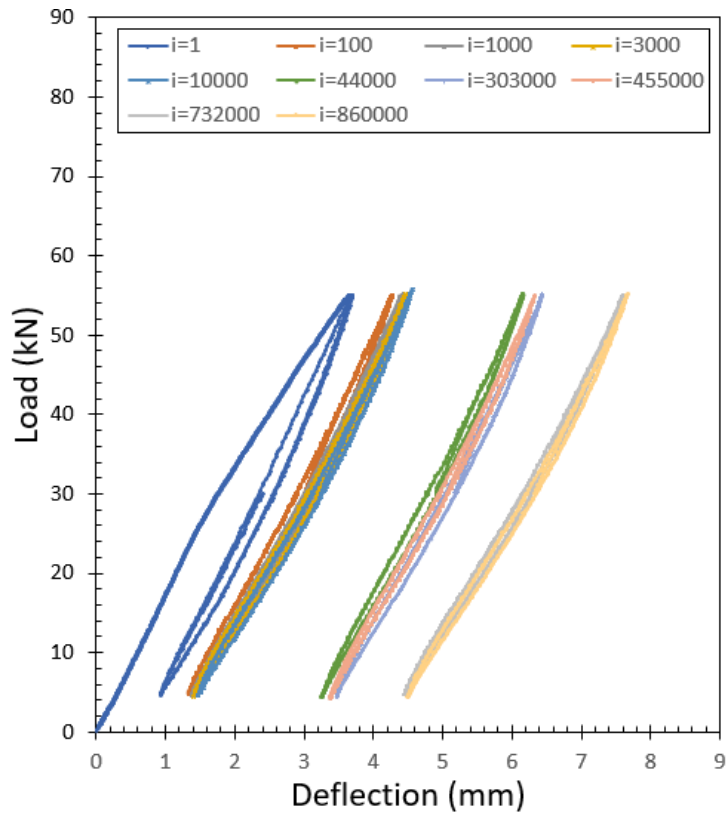


Fig. 6.23 Load versus deflection under flexural cyclic loading for beam C60_FBF_55.

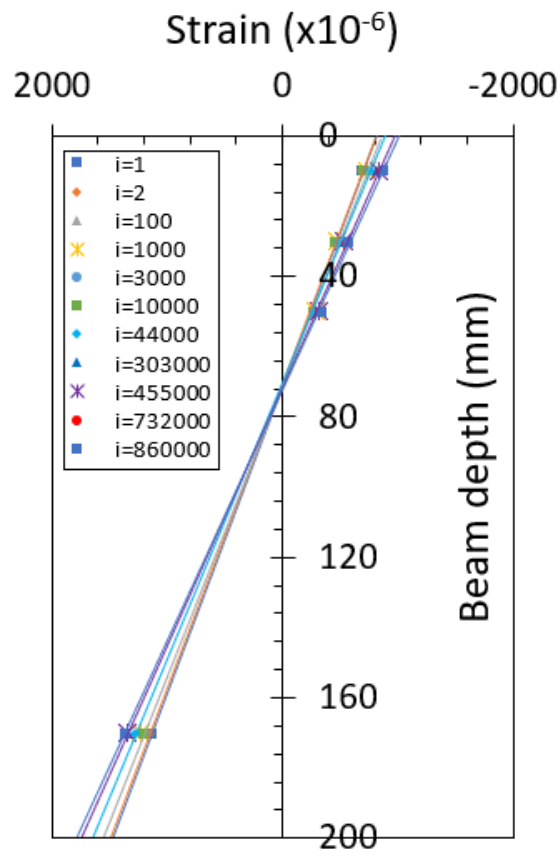


Fig. 6.24 Mid-span strain distribution under flexural cyclic loading for beam C60_FBF_55.

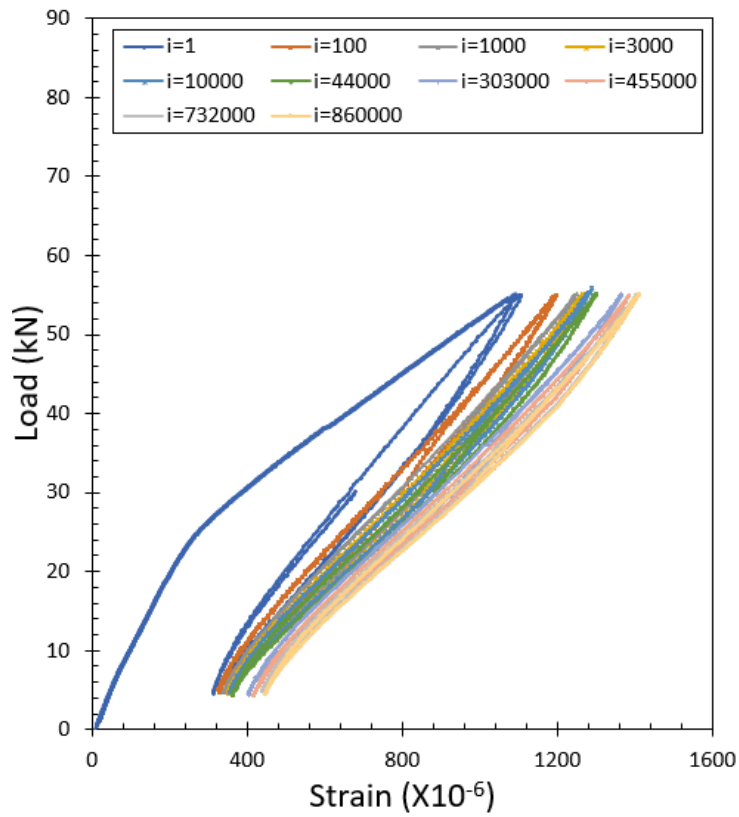


Fig. 6.25 Load versus average rebar strain under flexural cyclic loading for beam C60_FBF_55.

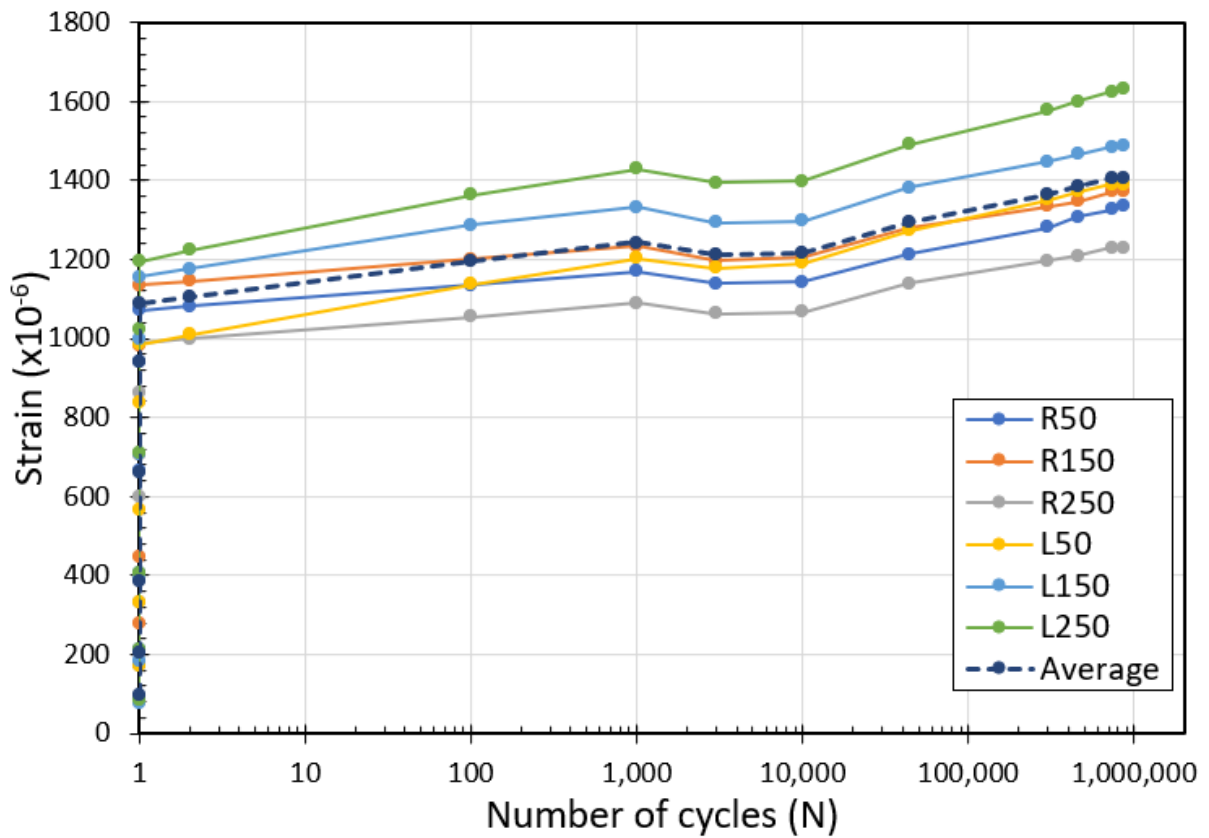


Fig. 6.26 Rebar strain evolution under flexural fatigue for beam C60_FBF_55.

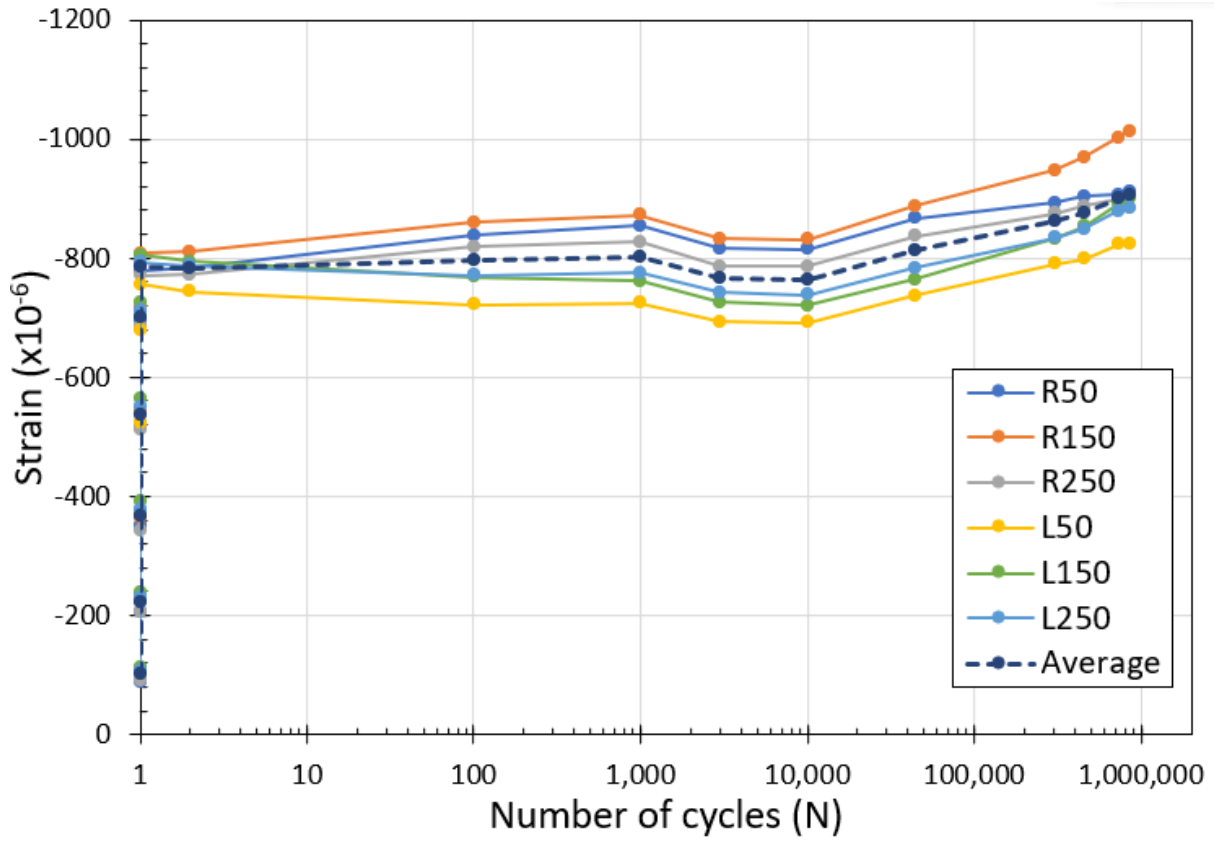


Fig. 6.27 ultimate concrete strain evolution under flexural fatigue for beam C60_FBF_55.

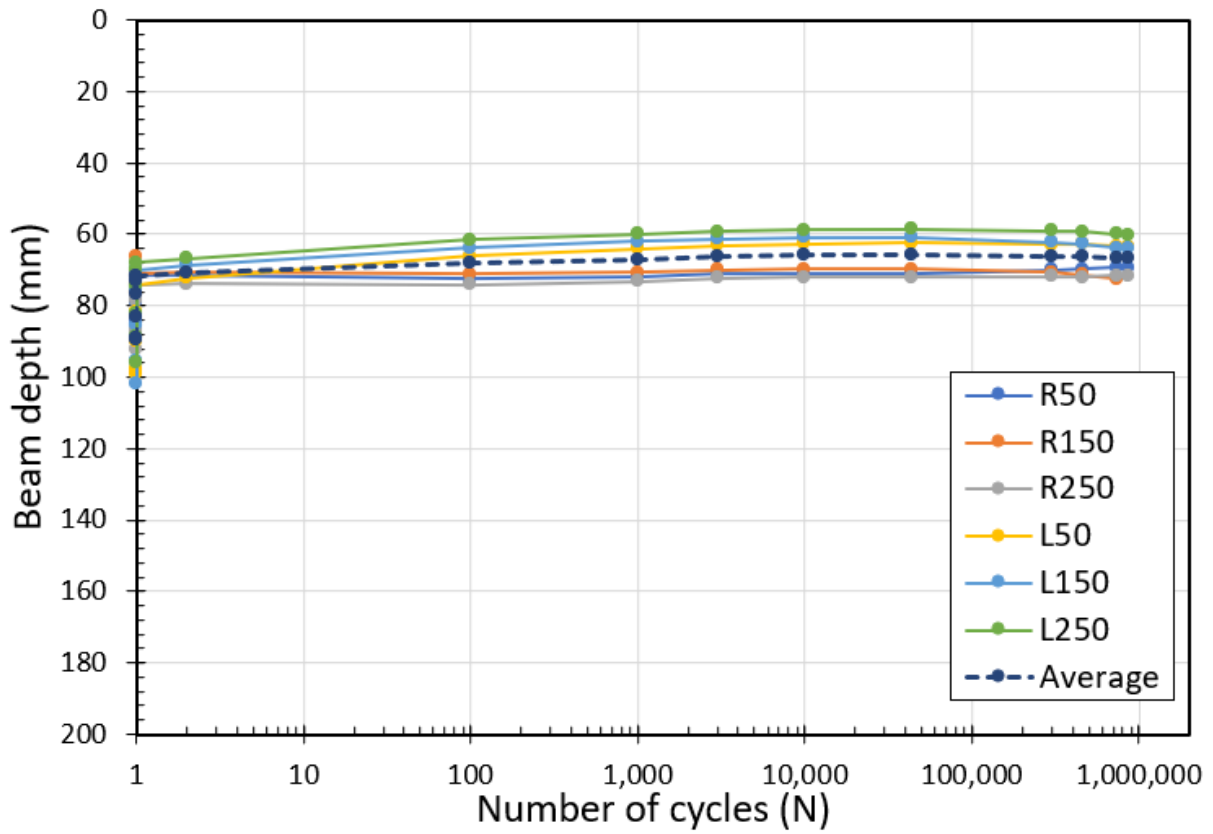


Fig. 6.28 Neutral axis position evolution under flexural fatigue for beam C60_FBF_55.

Finally, the average experimental data of the fatigue response of the SFRC structural beam – C60_FBF_55 – over the fatigue life to be used in the inverse analysis calculation method. The degradation of the crack-bridging strength would be evaluated by achieving a good fitting between the experimental and calculated fatigue response of the tested structural SFRC beams. As a result, the average experimental rebar strain, ultimate surface concrete strain, and N.A. position were monitored and plotted in [Figs. 6.26, 6.27, and 6.28](#) respectively, from the data monitored inside the constant moment region.

6.3.2.2 Reinforcement Ratio Effect

A flexural cyclic loading test was carried out on three SFRC structural beams, with lower ordinary rebar reinforcement ratio compared with the beams set in the first and second series, where the SFRC structural beams were reinforced with two rebars of 13 mm nominal diameter, aiming to capture the difference in the flexural fatigue response and the influence degree on the evaluate degradation and evolution model of crack-bridging strength over fatigue life using the inverse analysis method, as explained in section 3.4.3. Also, residual flexural capacity after completion of two million cycles was evaluated in the case of beams that survived without fatigue failure, as summarized in [Table 6.2](#). As the lower rebar reinforced ratio might change the crack width growth and the contribution of fibers in bridging the cracks, that would lead to changing in the evolution process of the rebar strain level and the rate of degradation of the crack-bridging strength over the fatigue life, which is still undiscovered area. As a result, The first SFRC structural beam – D13_FBF_25-36-40 – was tested for variable fatigue load levels starting with a low-stress level and the maximum fatigue load level increased over the fatigue life until failure in a mode of rebar rupture by 3685131 flexural fatigue cycles, as shown in [Figs. 6.29, 6.30, 6.32, and 6.33](#). The second SFRC structural beam – D13_FBF_36 – was tested under a medium fatigue load level of 36 kN as a maximum fatigue load level until the end of the fatigue life by two million cycles and then the residual flexural capacity was tested through a flexural static test, as shown in [Figs. 6.37, 6.38, 6.40, 6.41, and 6.42](#). The third SFRC structural beam – D13_FBF_40 – was tested under a high fatigue load level of 40 kN as a maximum fatigue load level until the end of the fatigue life of 714580 cycles by brittle rupture of rebar, as shown in [Figs. 6.46, 6.47, and 6.49](#). The fatigue load levels were selected to have the same rebar strain level in the first cycle at the maximum fatigue load level, aiming to have an appropriate comparison with the first and second series, as listed in [Table 6.2](#).

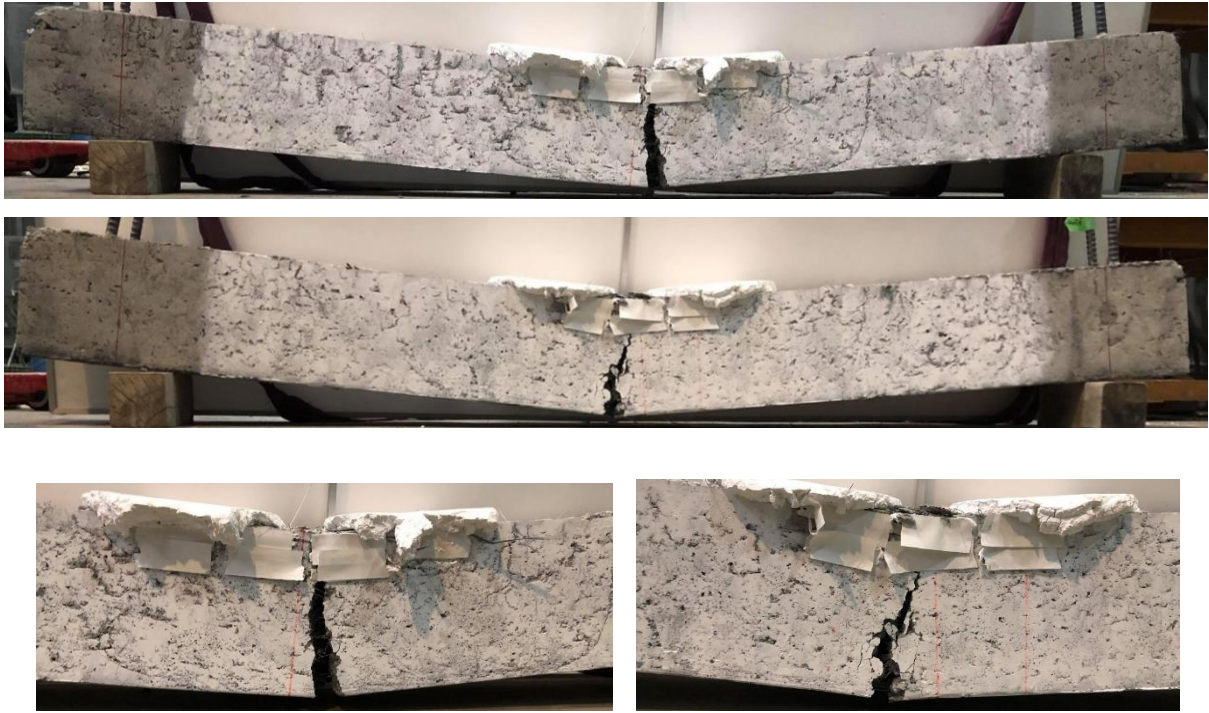


Fig. 6.29 Beam D13_FBF_25-36-40 over fatigue life under flexural fatigue.

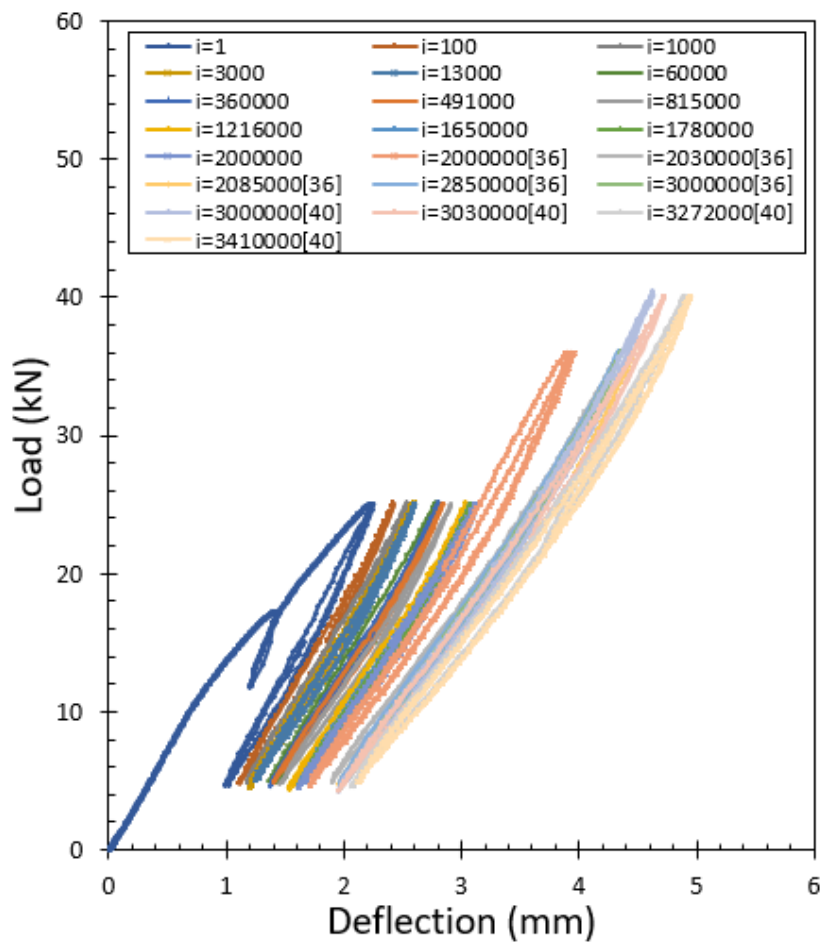


Fig. 6.30 Load versus deflection under flexural fatigue for beam D13_FBF_25-36-40.

Beam D13_FBF_25-36-40

For the increasing study case of the fatigue stress levels, one SFRC structural beam – D13_FBF_25-36-40 – was tested under flexural cyclic loading with 5 kN as a minimum flexural load and 25 kN, 36 kN, 40 kN as a maximum flexural load for two, one, one million cycles, respectively and sequentially, as shown in Figs. 6.29 6.30, 6.32, and 6.33. Figure 6.30 shows the load versus mid-span deflection relationship over fatigue life under a low to a high-stress level of flexural fatigue load showing an increase in mid-span deflection as cycles progress. Figure 6.31 shows the strain distribution at midspan on the front face of the beam (L150), showing the strain evolution for both rebar and concrete throughout the application of flexural cyclic loading until the end of fatigue life. The average rebar strain within the constant moment region is plotted against the maximum and minimum flexural cyclic load for the variable fatigue stress levels during the fatigue life, starting from the first cyclic loading (N_1) and showing the evolution of average rebar strain, as shown in Fig. 6.32.

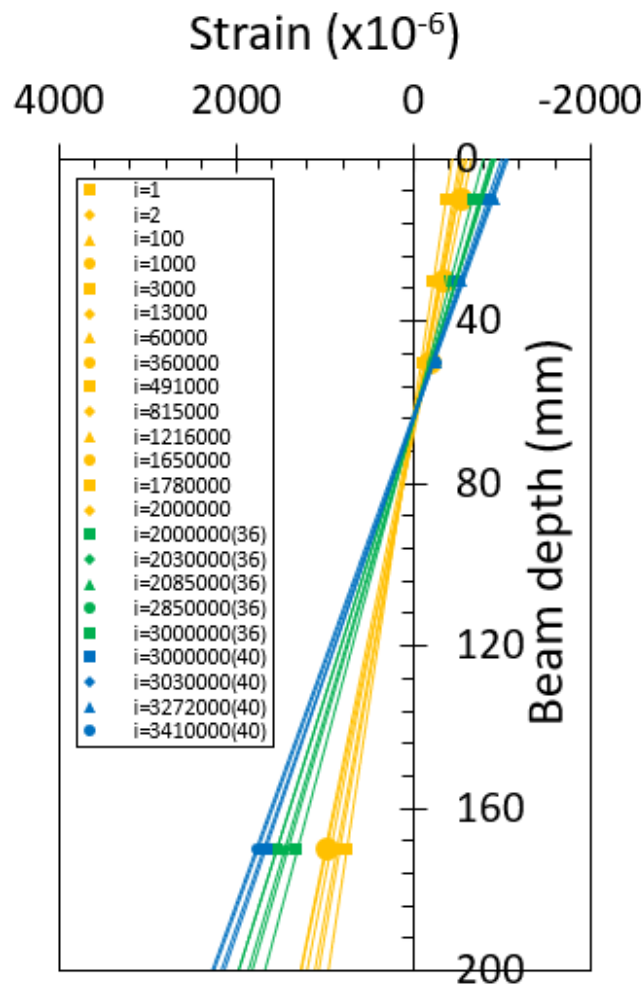


Fig. 6.31 Mid-span strain distribution under flexural fatigue for beam D13_FBF_25-36-40.

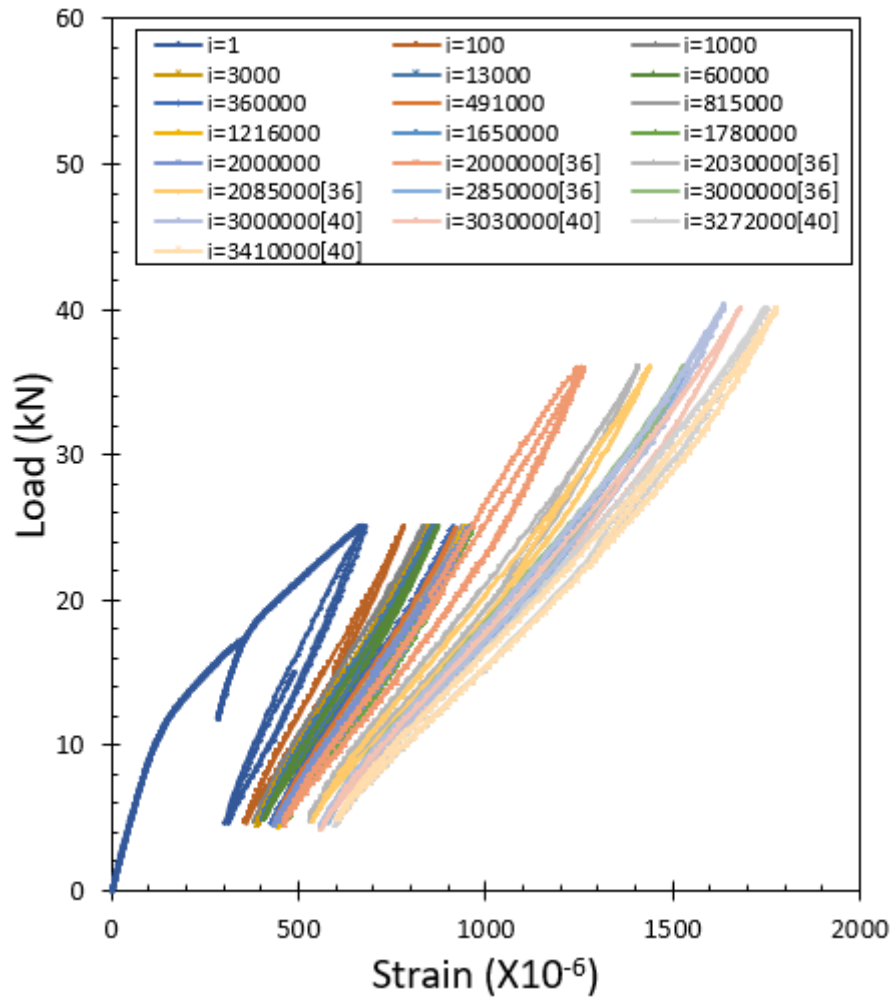


Fig. 6.32 Load versus average rebar strain under flexural fatigue
for beam D13_FBF_25-36-40.

During the fatigue life of the tested beam – D13_FBF_25-36-40 – a higher flexural fatigue load level was applied by increasing the flexural load monotonically then the cyclic flexural load was applied between 5 kN as a minimum fatigue load level and the increased flexural load as a maximum fatigue load level. While the flexural applied load was increased monotonically, the mid-span deflection and the crack length and width were increased and structural stiffness was decreased as noted from the decrease of the inclination of the load-deflection curve and N.A. position, as shown in Figs. 6.29, 6.30, 6.33, and 6.36. As well, an evolution of both the rebar and concrete strain was observed for the SFRC structural beams, as shown in Figs. 6.31, 6.32, 6.34, and 6.35.

After increasing the flexural load monotonically, the cyclic flexural load was applied under the desired higher flexural fatigue load level. During that application of repeated cyclic loading, again an increase on both the rebar and concrete strain was observed for the SFRC structural

beams, resulting in increasing mid-span deflection and crack length and width and decreasing structural stiffness as noted from the decrease of the inclination of the load-deflection curve and N.A. position, as shown in Figs. 6.33, 6.34, 6.35, and 6.36. finally, at a higher fatigue load level of a 40 kN of flexural maximum load level was applying, a rupture fatigue failure took place in a manner of rebar rupture achieving 3685131 cycles of fatigue life, as summarized in Table 6.2.

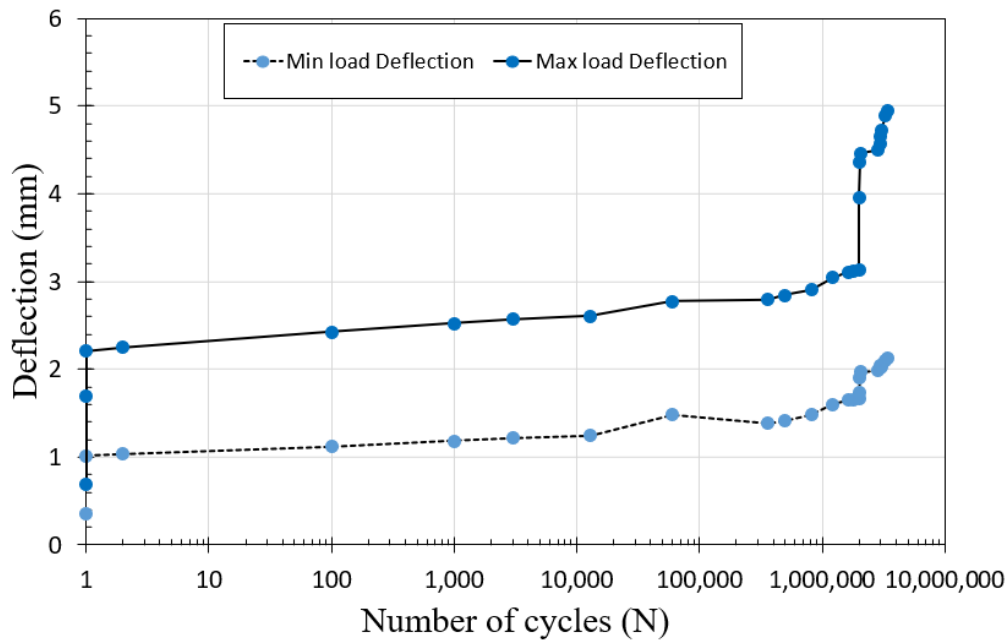


Fig. 6.33 Mid-span deflection at maximum and minimum load level under flexural fatigue for beam D13_FBF_25-36-40.

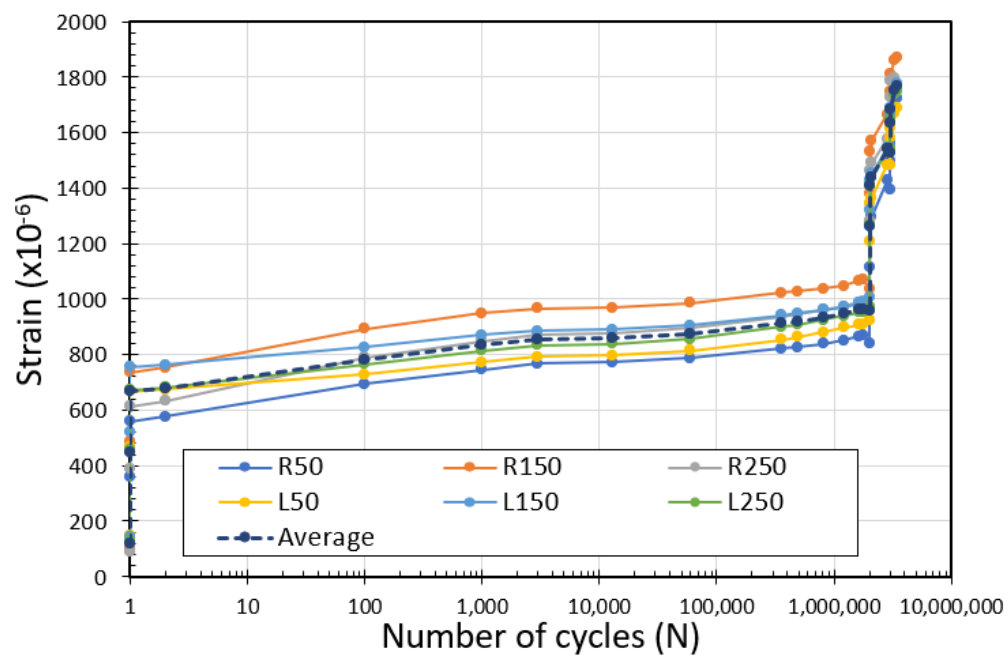


Fig. 6.34 Rebar strain evolution under flexural fatigue for beam D13_FBF_25-36-40.

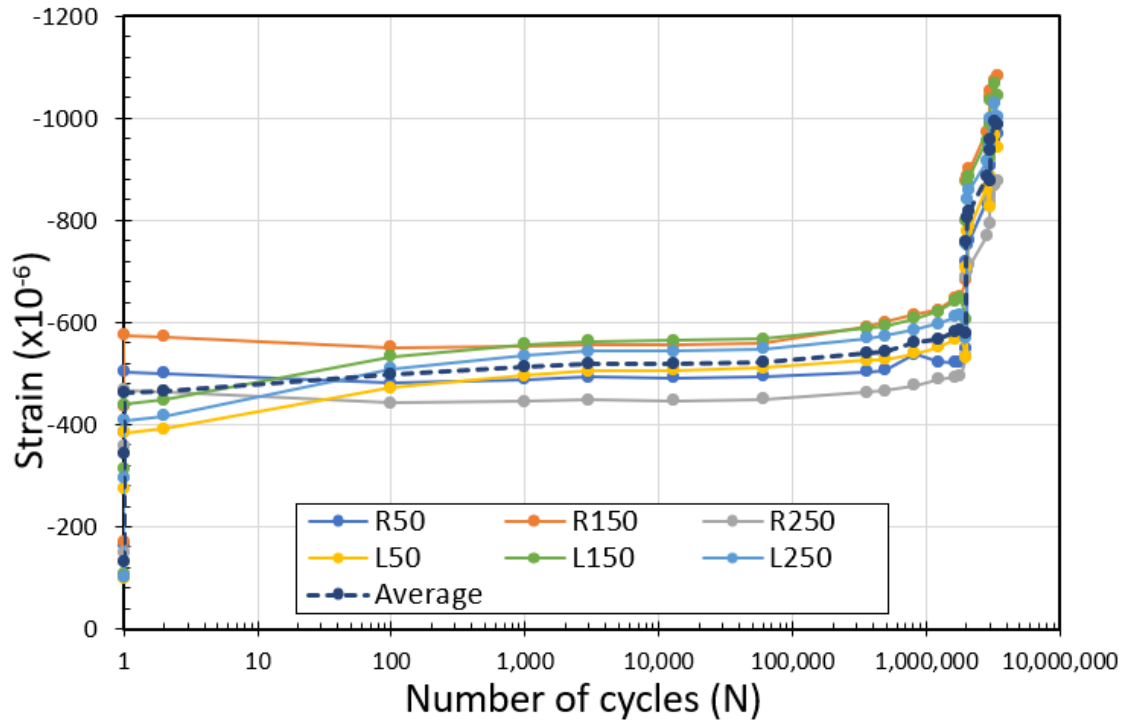


Fig. 6.35 ultimate concrete strain evolution under flexural fatigue for beam D13_FBF_25-36-40.

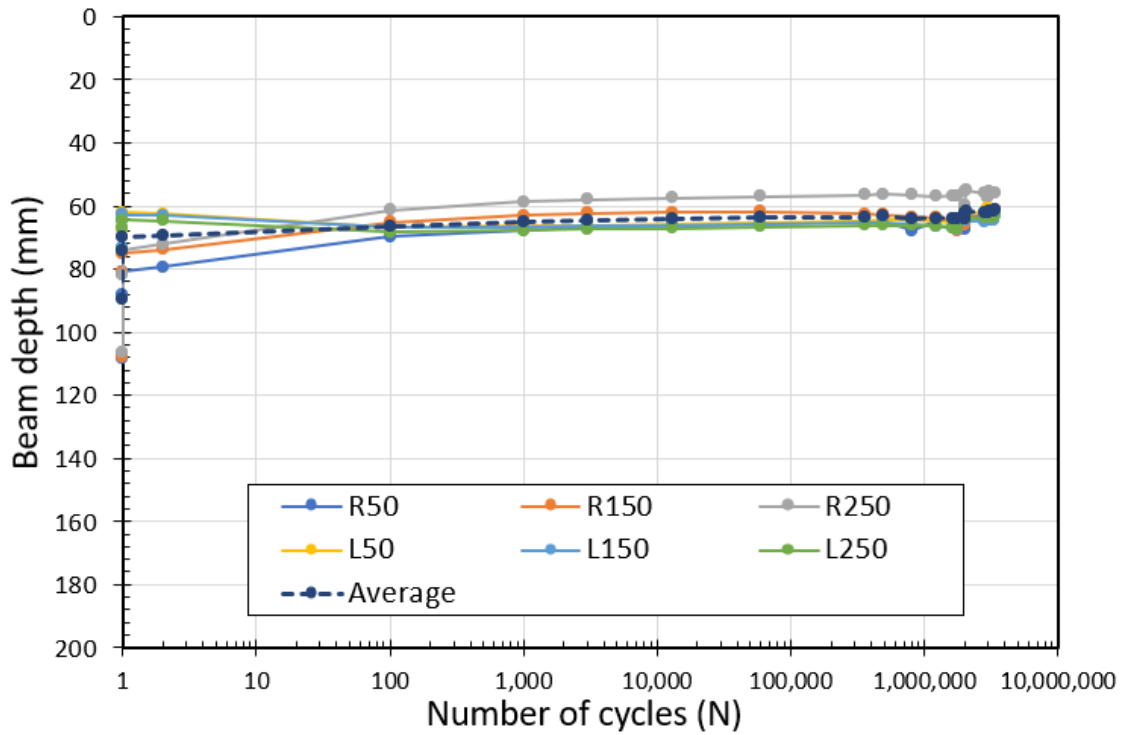


Fig. 6.36 Neutral axis position evolution under flexural fatigue for beam D13_FBF_25-36-40..

Beam D13_FBF_36

For the medium fatigue stress level, one SFRC structural beam – D13_FBF_36 – was tested under flexural cyclic loading with 5 kN as a minimum flexural load and 36 kN as a maximum flexural load, as shown in Figs. 6.37, 6.38, and 6.40. Figure 6.38 shows the load versus mid-span deflection relationship over fatigue life under a medium-stress level of flexural fatigue load showing an increase in mid-span deflection as cycles progress. Figure 6.39 shows the strain distribution at midspan on the front face of the beam (L250), showing the strain evolution for both rebar and concrete throughout the application of flexural cyclic loading until the end of fatigue life. The average rebar strain within the constant moment region of D13_FBF_36 is also plotted against the maximum and minimum flexural cyclic load for the medium fatigue stress levels during the fatigue life, starting from the first flexural cyclic loading (N_1) and showing the evolution of average rebar strain, as shown in Fig. 6.40. After a complete of two million cycles of flexural loading, SFRC beam D13_FBF_36 was subjected to a residual flexural static test to measure their residual capacity, as shown in Figs. 6.41 and 6.42. The result is listed in Table 6.2. Residual flexural capacity was measured achieving a 69.17 kN until a ductile flexural failure of rebar followed by concrete crushing inside the constant moment region, even after the fatigue loading emphasizing the effect of higher compressive strength.

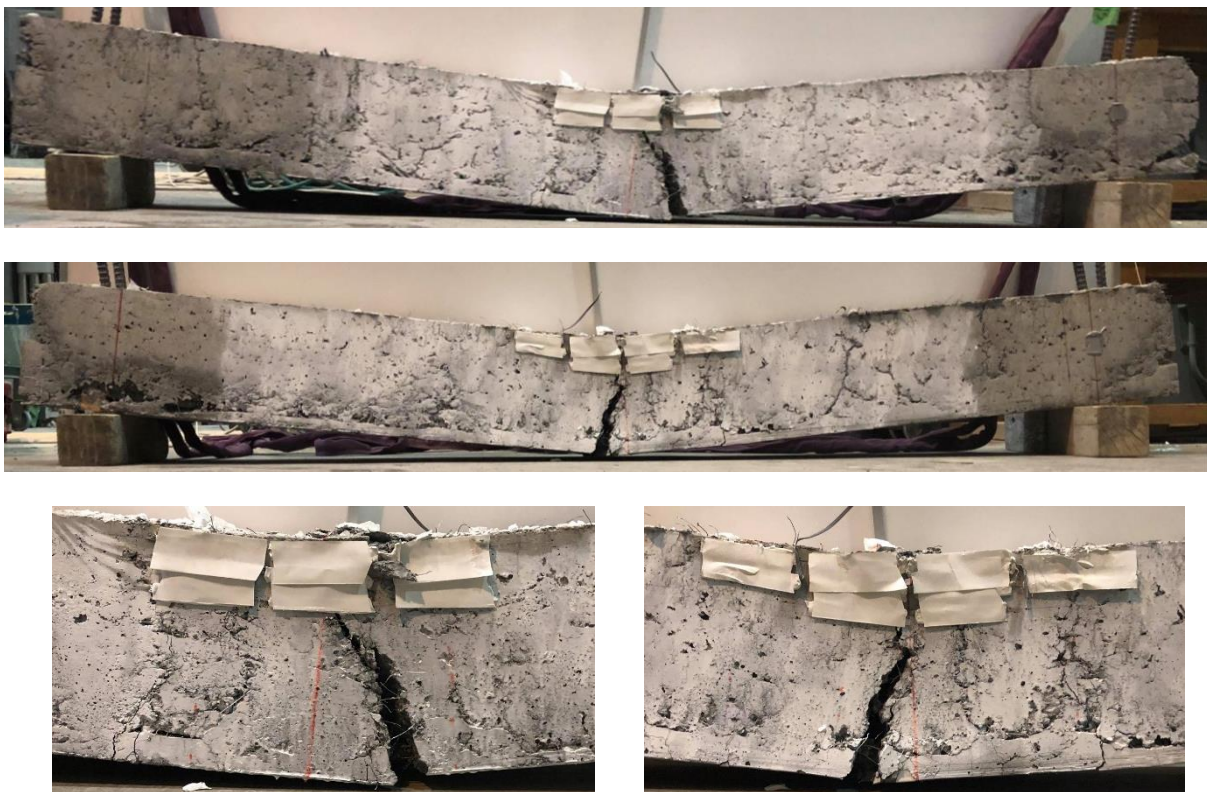


Fig. 6.37 Beam D13_FBF_36 over fatigue life under flexural fatigue.

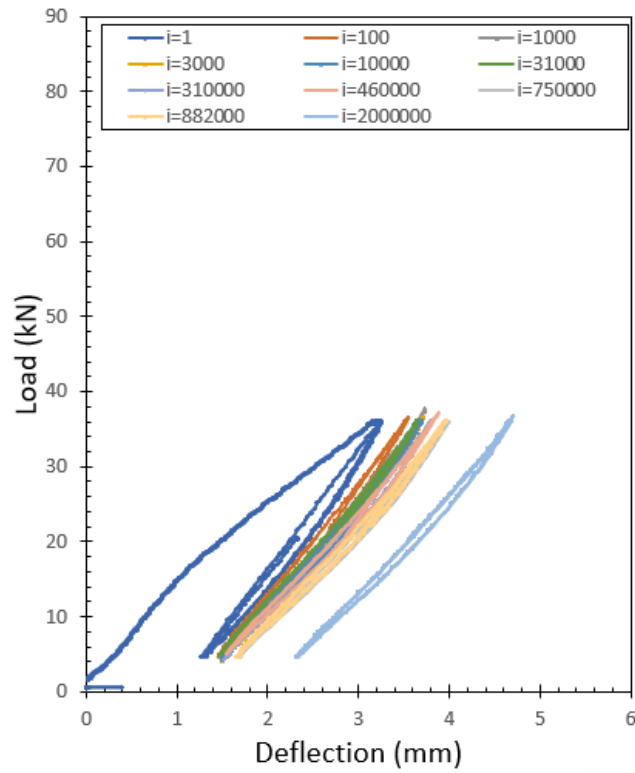


Fig. 6.38 Load versus deflection under flexural cyclic loading for beam D13_FBF_36.

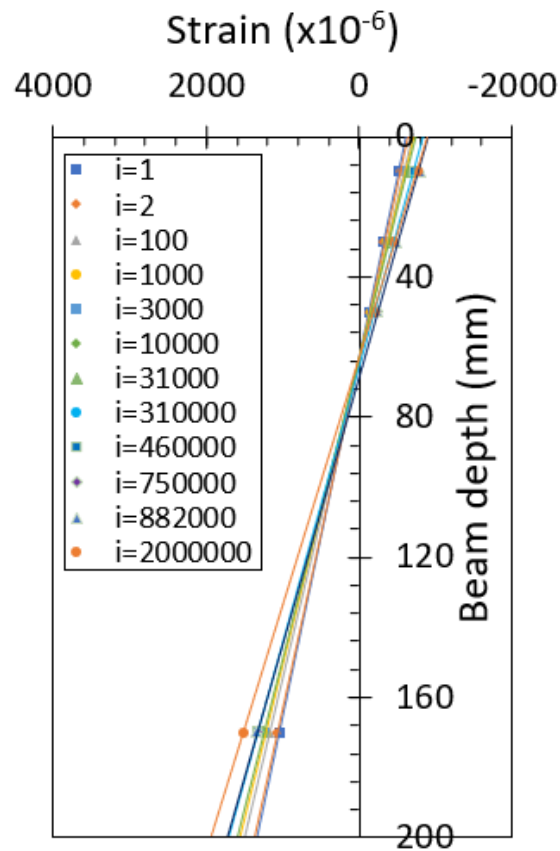


Fig. 6.39 Strain distribution under flexural cyclic loading inside constant moment region for beam D13_FBF_36.

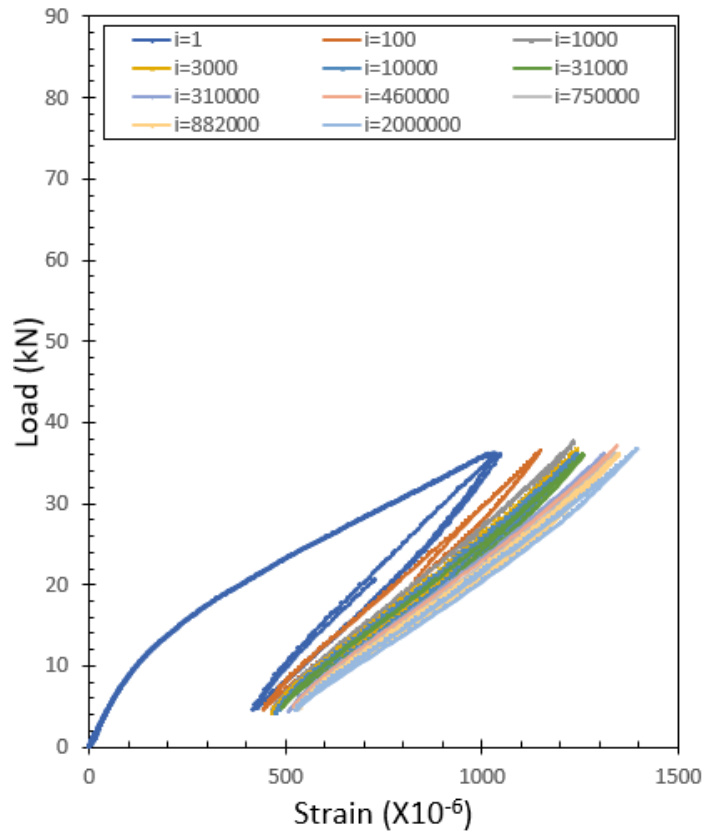


Fig. 6.40 Load versus average rebar strain under flexural cyclic loading for beam D13_FBF_36.

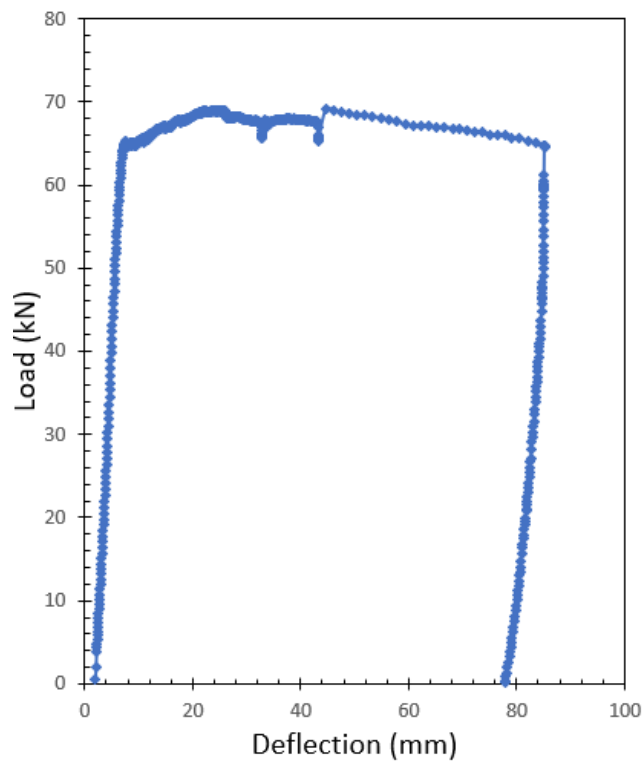


Fig. 6.41 Load versus deflection under residual flexural static loading for beam D13_FBF_36.

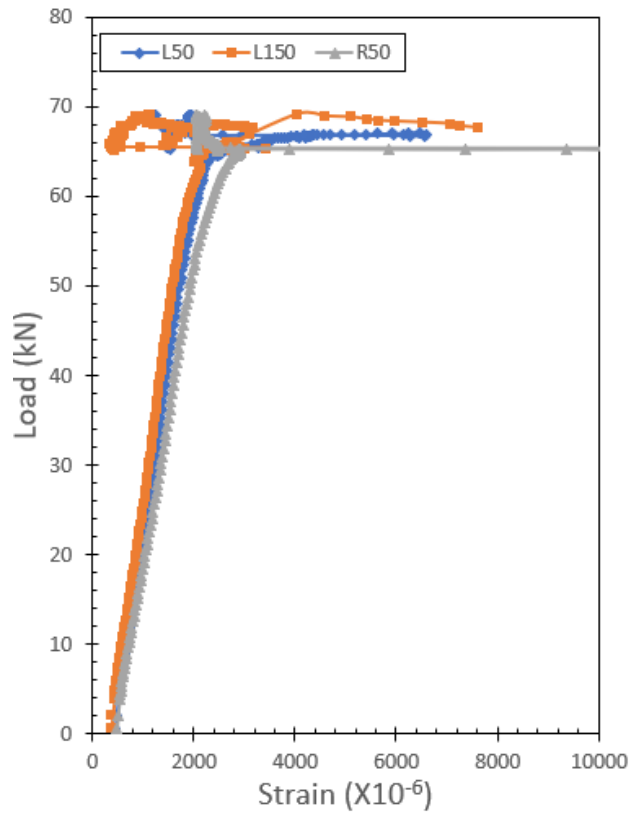


Fig. 6.42 Load versus rebar strain under residual flexural static loading for beam D13_FBF_36.

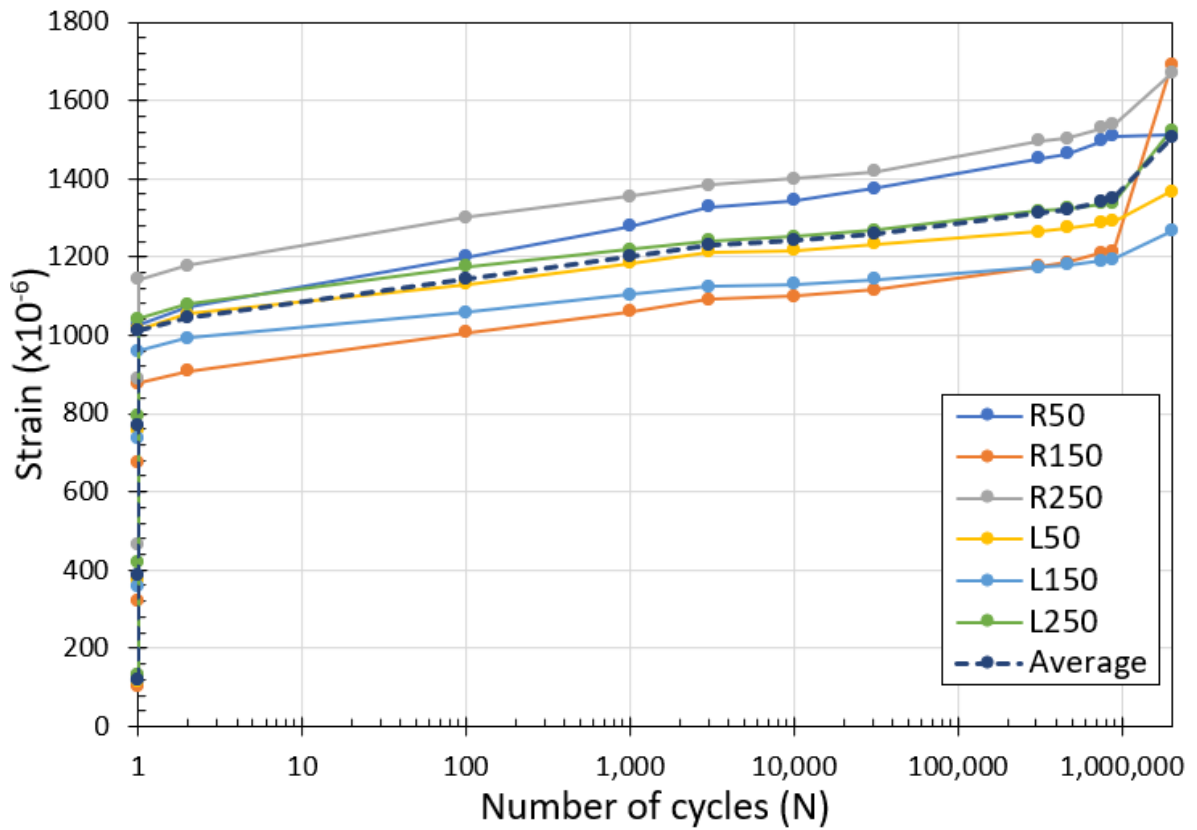


Fig. 6.43 Rebar strain evolution under flexural fatigue for beam D13_FBF_36.

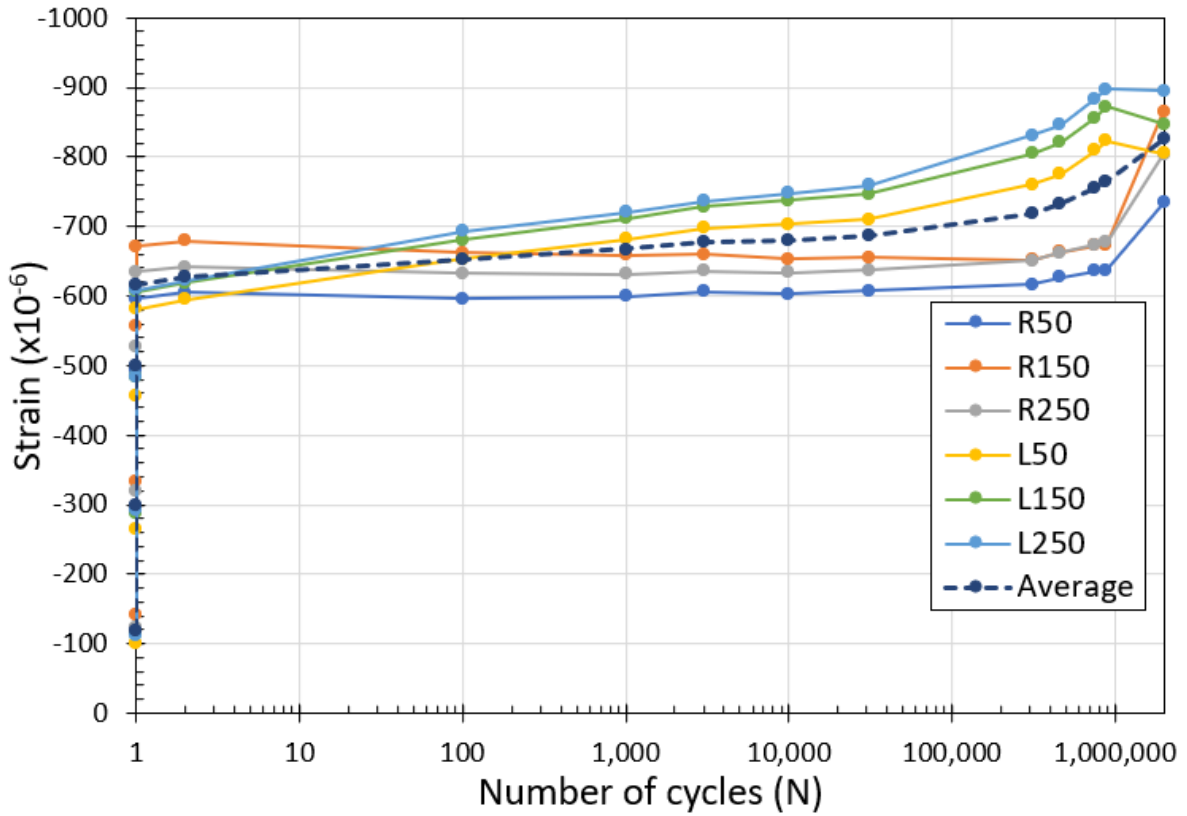


Fig. 6.44 ultimate concrete strain evolution under flexural fatigue for beam D13_FBF_36.

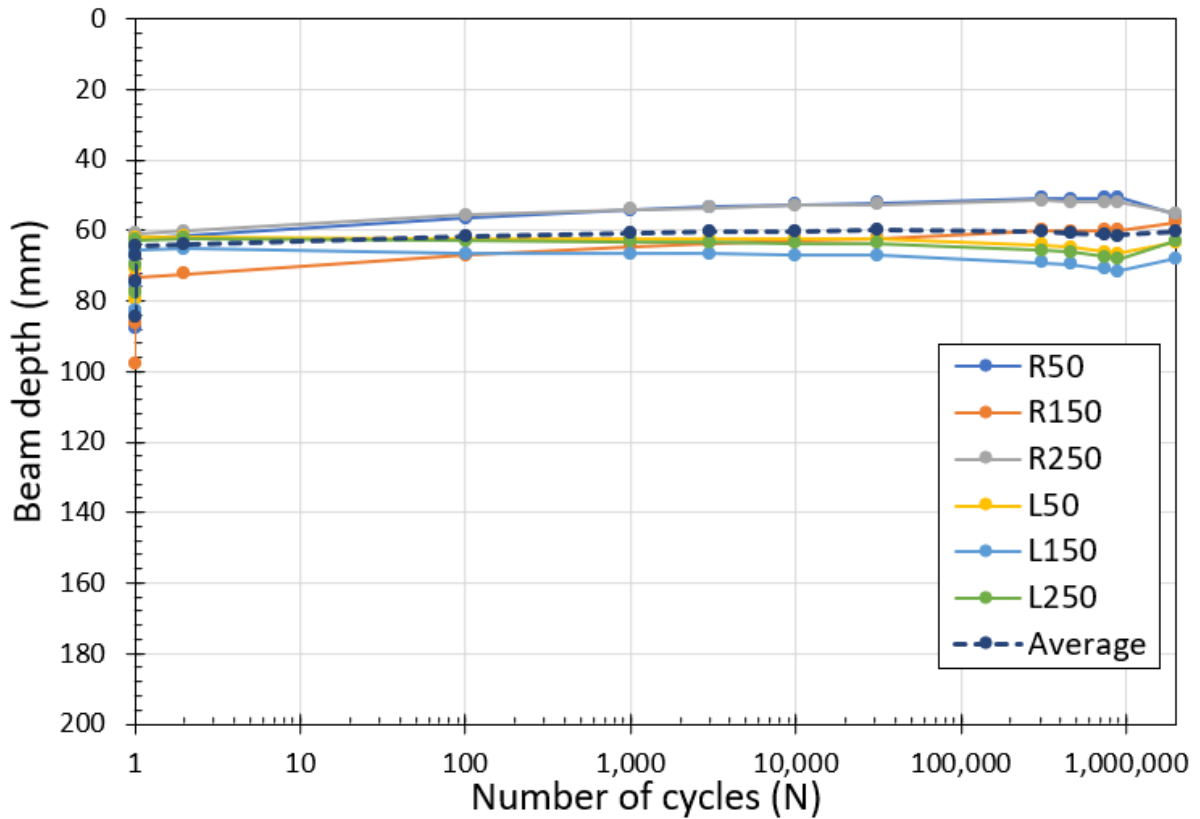


Fig. 6.45 Neutral axis position evolution under flexural fatigue for beam D13_FBF_36.

Finally, the average experimental data of the fatigue response of the SFRC structural beam – D13_FBF_36 – over the fatigue life to be used in the inverse analysis calculation method. The degradation of the crack-bridging strength would be evaluated by achieving a good fitting between the experimental and calculated fatigue response of the tested structural SFRC beams. As a result, the average experimental rebar strain, ultimate surface concrete strain, and N.A. position were monitored and plotted in Figs. 6.43, 6.44, and 6.45 respectively, from the data monitored inside the constant moment region.

Beam D13_FBF_40

For the high fatigue stress level, one SFRC structural beam – D13_FBF_40 – was tested under flexural cyclic loading with 5 kN as a minimum flexural load and 40 kN as a maximum flexural load, as shown in Figs. 6.46, 6.47, and 6.49. Figure 6.46 shows the load versus mid-span deflection relationship over fatigue life under a high-stress level of flexural fatigue load showing an increase in mid-span deflection as cycles progress. Figure 6.47 shows the strain distribution at midspan on the front face of the beam (R150), showing the strain evolution for both rebar and concrete throughout the application of flexural cyclic loading until fatigue failure. The average rebar strain within the constant moment region of D13_FBF_40 is also plotted against the maximum and minimum flexural cyclic load for the high fatigue stress levels during the fatigue life, starting from the first flexural cyclic loading (N_1) and showing the evolution of average rebar strain until rebar brittle rupture at 714580 cycles, as shown in Figs. 6.46, 6.47, and 6.49.



Fig. 6.46 Beam D13_FBF_40 over fatigue life under flexural cyclic loading.

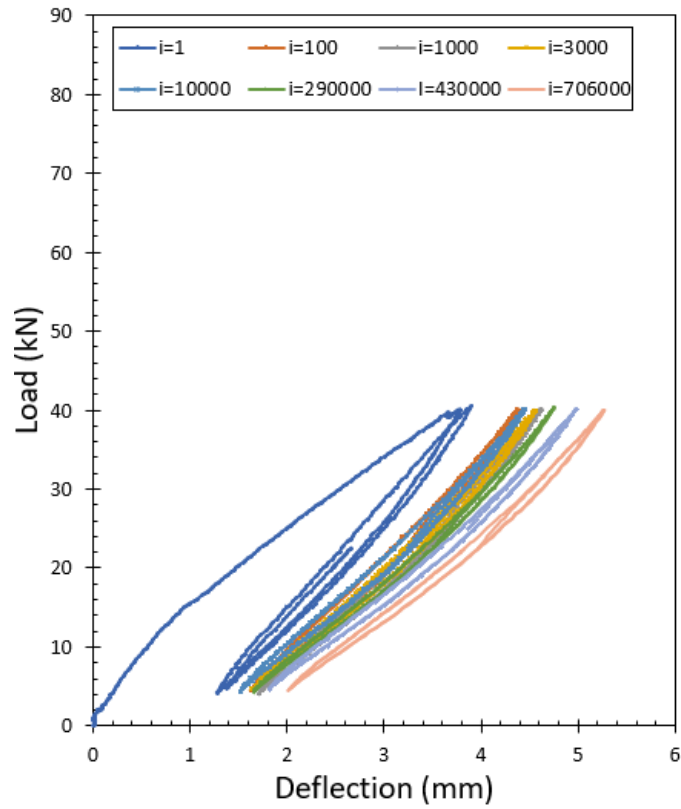


Fig. 6.47 Load versus deflection under flexural cyclic loading for beam D13_FBF_40.

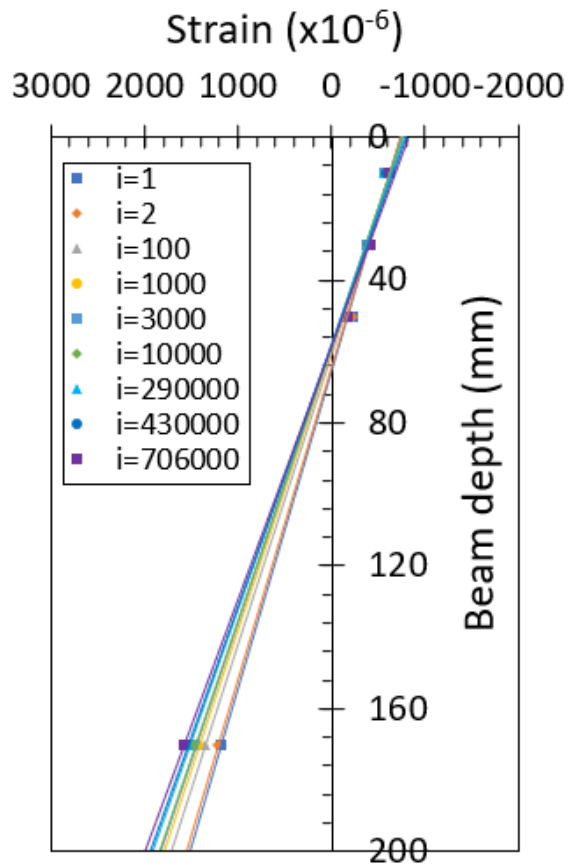


Fig. 6.48 Mid-span strain distribution under flexural cyclic loading for beam D13_FBF_40.

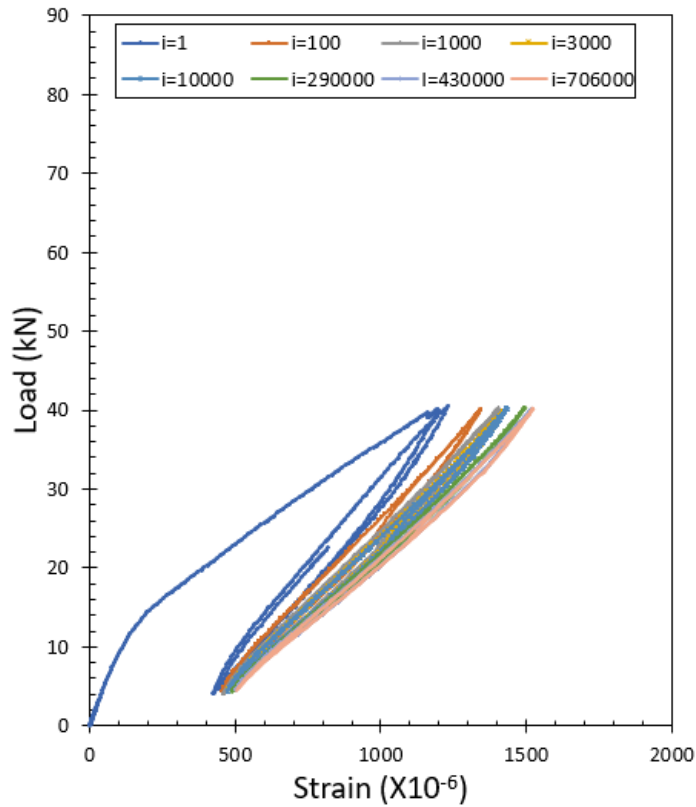


Fig. 6.49 Load versus average rebar strain under flexural cyclic loading for beam D13_FBF_40.

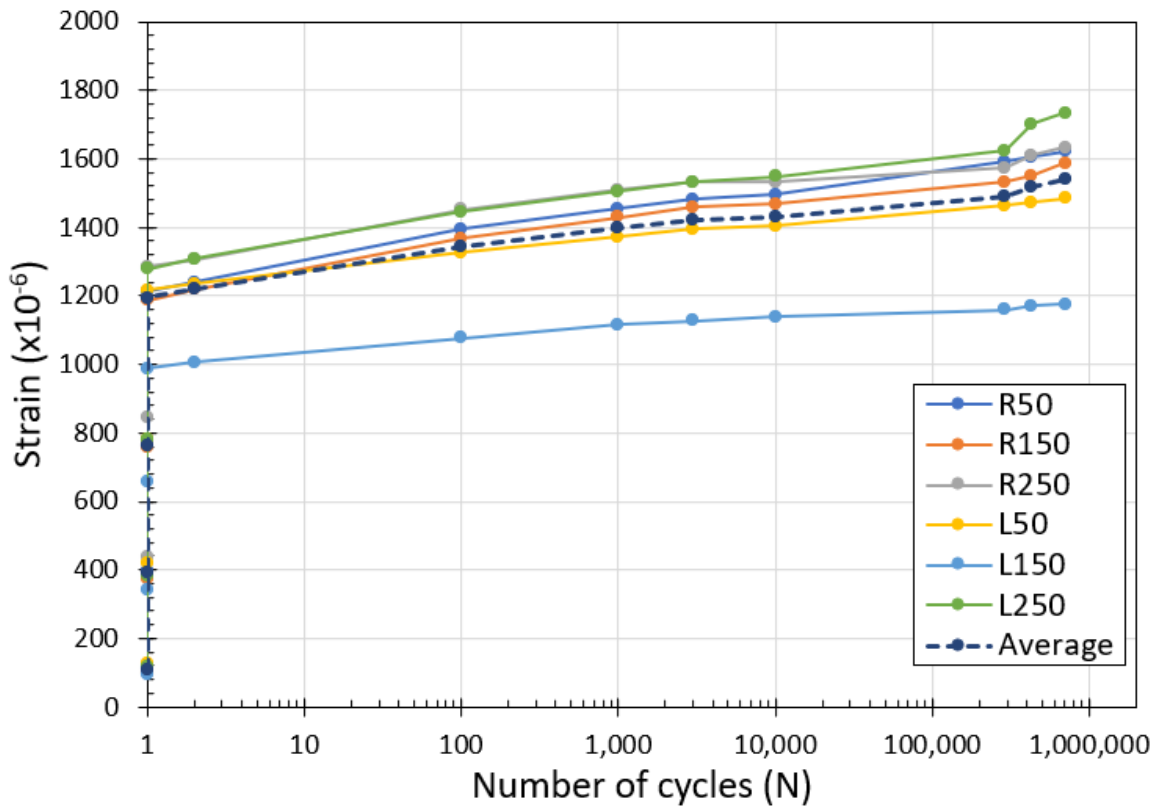


Fig. 6.50 Rebar strain evolution under flexural fatigue for beam D13_FBF_40.

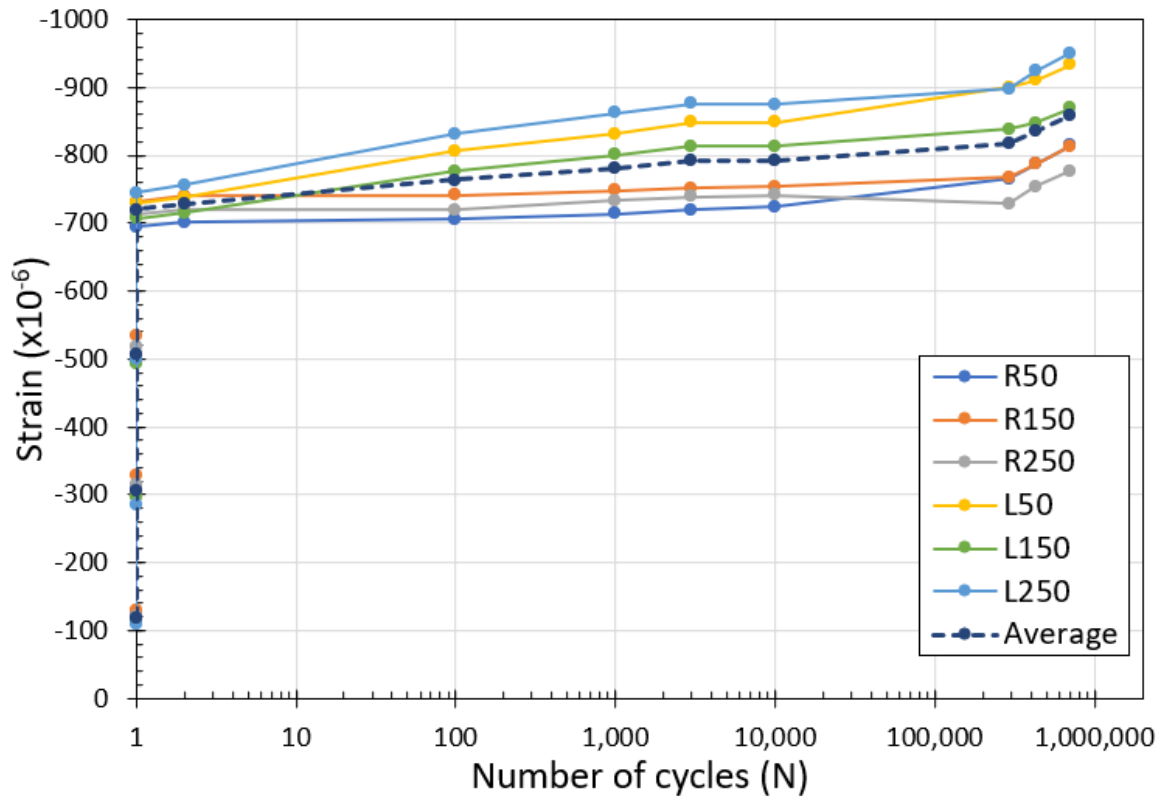


Fig. 6.51 ultimate concrete strain evolution under flexural fatigue for beam D13_FBF_40.

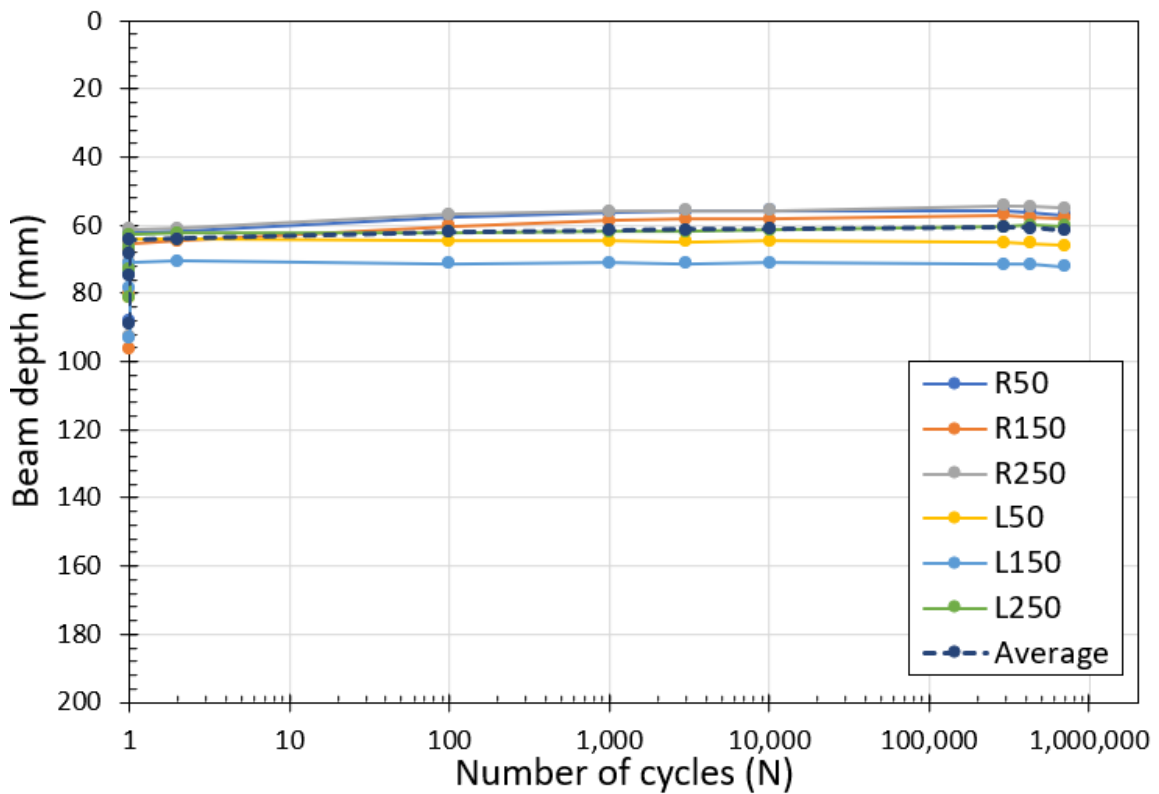


Fig. 6.52 Neutral axis position evolution under flexural fatigue for beam D13_FBF_40.

Finally, the average experimental data of the fatigue response of the SFRC structural beam – D13_FBF_40 – over the fatigue life to be used in the inverse analysis calculation method. The degradation of the crack-bridging strength would be evaluated by achieving a good fitting between the experimental **and** calculated fatigue response of the tested structural SFRC beams. As a result, the average experimental rebar strain, ultimate surface concrete strain, and N.A. position were monitored and plotted in [Figs. 6.50](#), [6.51](#), and [6.52](#) respectively, from the data monitored inside the constant moment region.

6.4 Results Discussion

In this section, the experimental flexural fatigue response and the normalized crack-bridging strength degradation and evolution model of the tested SFRC structural beams for the third series were captured as compared with the first and second series measuring the effect of higher concrete compressive strength and lower ordinary rebar reinforcement ratio. Firstly, the experimental flexural fatigue response was captured among the first, second and third series by comparing the maximum mid-span deflection, maximum rebar strain level, average rebar and ultimate surface concrete strain level, and N.A. position during the fatigue life of the tested beams under variable and single cyclic flexural load levels. Secondly, the crack-bridging strength was evaluated for the third series using the inverse analysis calculation method by achieving the best fitting between the experimental and calculated flexural fatigue response. Thirdly, the evaluated crack-bridging strength degradation and evolution model, that was proposed from the inverse analysis calculation method, was compared between the second and the third series where the effect of higher compressive strength and lower reinforcement ratio was tested on the degradation and evolution rate and mechanism of the crack-bridging strength over the fatigue life under variable and single cyclic flexural load levels.

6.4.1 Experimental Flexural Fatigue Response

The experimental flexural fatigue response was captured by measuring the maximum mid-span deflection, maximum rebar strain level, average rebar and ultimate surface concrete strain level, and N.A. position over the fatigue life of the tested SFRC structural beams under variable and single cyclic flexural load levels. The level and the evolution rate of the tested data were compared between this series and the first and second series to understand and measure the effect of higher concrete compressive strength and lower reinforcement ratio on the experimental flexural fatigue response of SFRC structural beams.

6.4.1.1 Concrete Compressive Strength Effect

A flexural cyclic loading test was carried out on three SFRC structural beams – i.e. C60_FBF_30-45-55-65, C60_FBF_45, and C60_FBF_55 – with higher compressive strength compared with the beams set in the first and second series – i.e. FBF_30-40-50-60, FBF_40, and FBF_50 –, aiming to capture the difference in the flexural fatigue response between each couple of beams having the flexural load level. As the higher concrete compressive strength would enhance the bond strength between fibers and matrix that would decelerate the degradation rate of strength, the growth rate of mid-span deflection and crack opening, and the evolution rate of both concrete and rebar strain levels over the fatigue life.

The first SFRC structural beam – C60_FBF_30-45-55-65 – was tested for variable fatigue load levels starting with a low-load level of 30 kN for two million cycles then increased to 45 kN for one million cycles after that increased to 55 kN for one million cycles and finally 65 kN over the fatigue life until failure in a mode of rebar rupture by 4981386 flexural fatigue cycles. In the first cycle, the mid-span deflection of 1.64 mm at the maximum fatigue load level of 30 kN was lower than the mid-span deflection of 2.33 mm at the first cycle of the same load level for beam FBF_30-40-50-60, as shown in Fig. 6.53. As a result, the maximum rebar strain level for C60_FBF_30-45-55-65 of 395 microstrains was lower than beam FBF_30-40-50-60 of 580 microstrains, indicating the effect of a higher compressive strength in enhancing the flexural response of the SFRC beams by providing a better bond between fibers and concrete matrix, as shown in Fig. 6.54.

By cyclic progress, the three SFRC structural beams were monitored during the application of flexural fatigue load under different load levels, by comparing beams C60_FBF_30-45-55-65, C60_FBF_45, and C60_FBF_55 with FBF_30-40-50-60, FBF_40, and FBF_50 respectively, through measuring the average response of the tested beams of rebar and concrete strain level and N.A. position and compared with the first and second series, as shown in Figs. 6.55, 6.56, and 6.57. Besides, the mid-span deflection and maximum rebar strain evolution over the fatigue life, as shown in Figs. 6.53, and 6.54. During the fatigue life, the evolution rate of the mid-span deflection was lower for higher concrete compressive strength beams under all flexural fatigue load levels because of the stronger bond mechanism between fibers and concrete matrix, as shown in Figs. 6.53. However, the evolution of the maximum rebar strain level had almost the same rate with a lower strain level at the beginning and the end of the fatigue life for higher concrete compressive strength beams, as shown in Fig. 6.54.

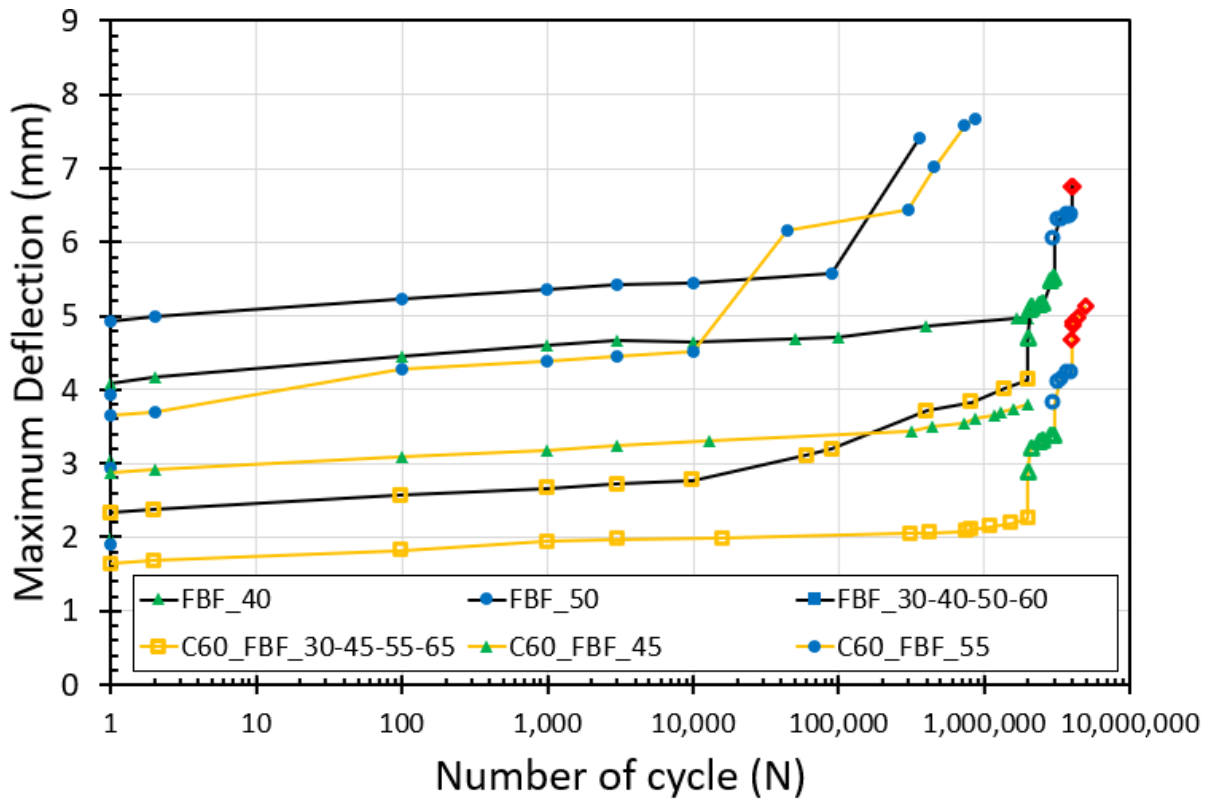


Fig. 6.53 Mid-span deflection evolution at the maximum flexural cyclic load level for the first, second, and third series over fatigue life.

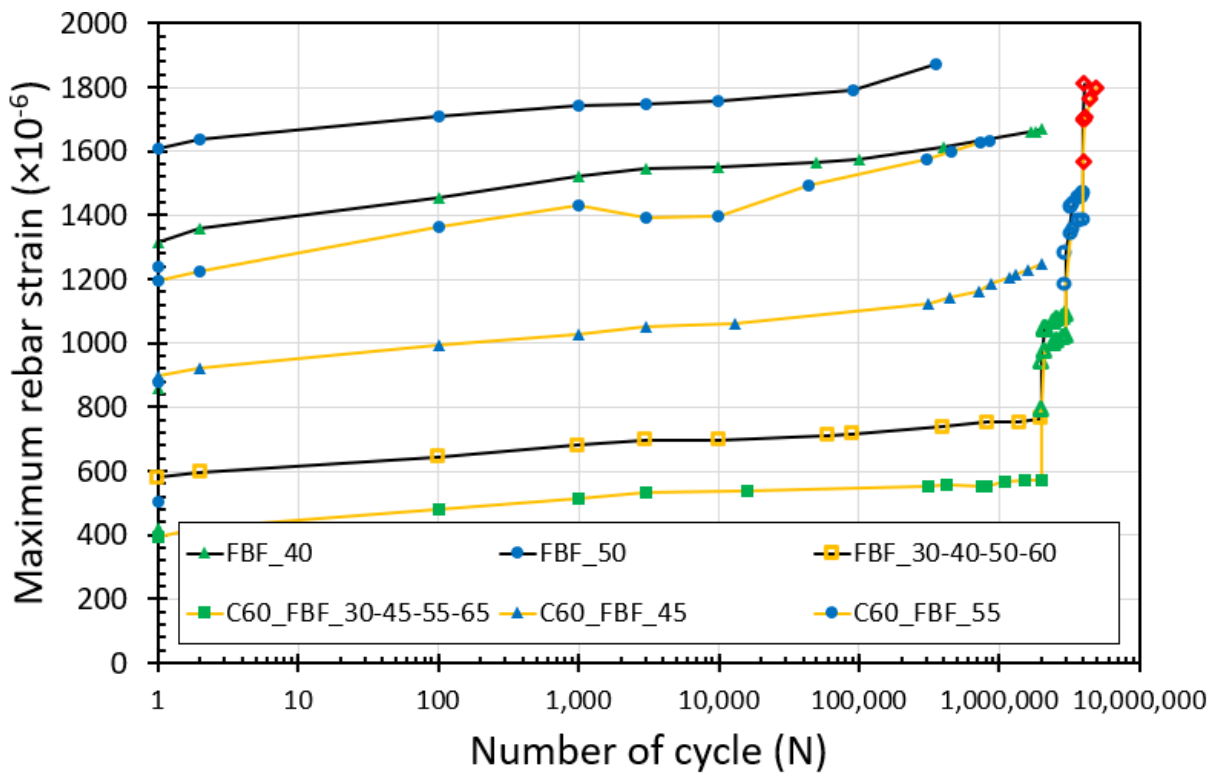


Fig. 6.54 Maximum rebar strain evolution for the first, second, and third series over fatigue life.

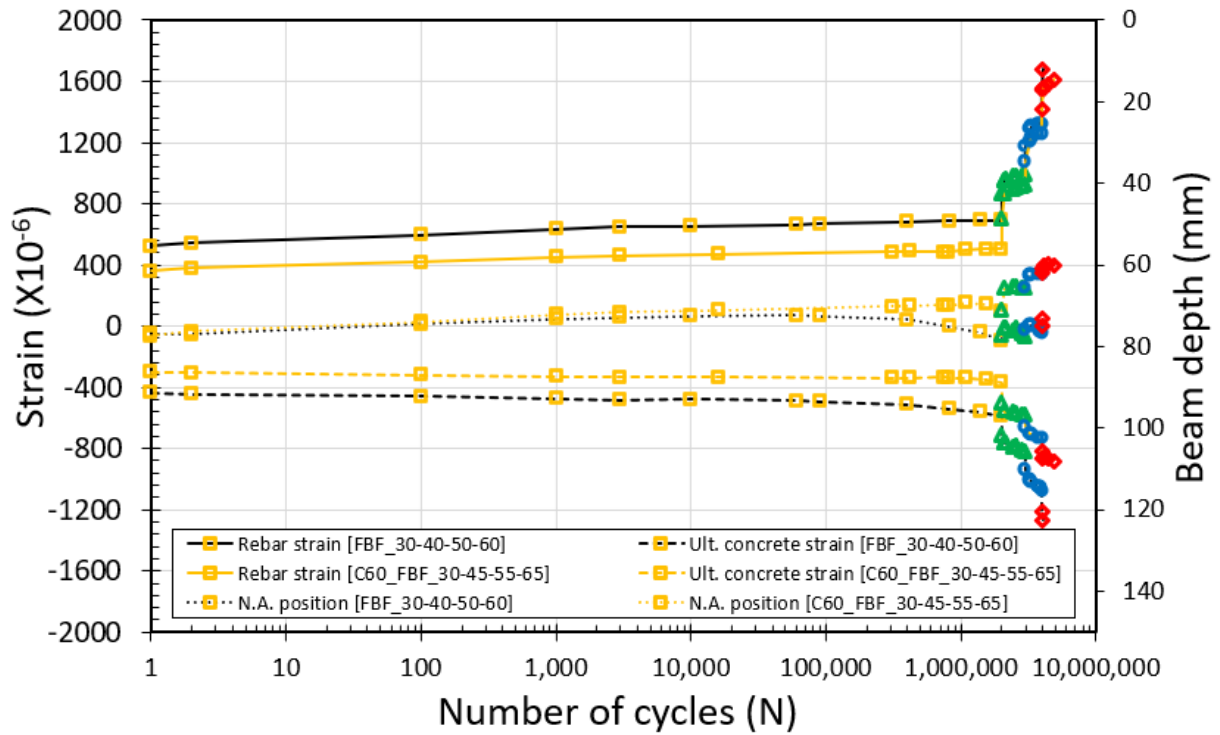


Fig. 6.55 Average experimental fatigue response of C60_FBF_30-45-55-65 versus FBF_30-40-50-60 over fatigue life.

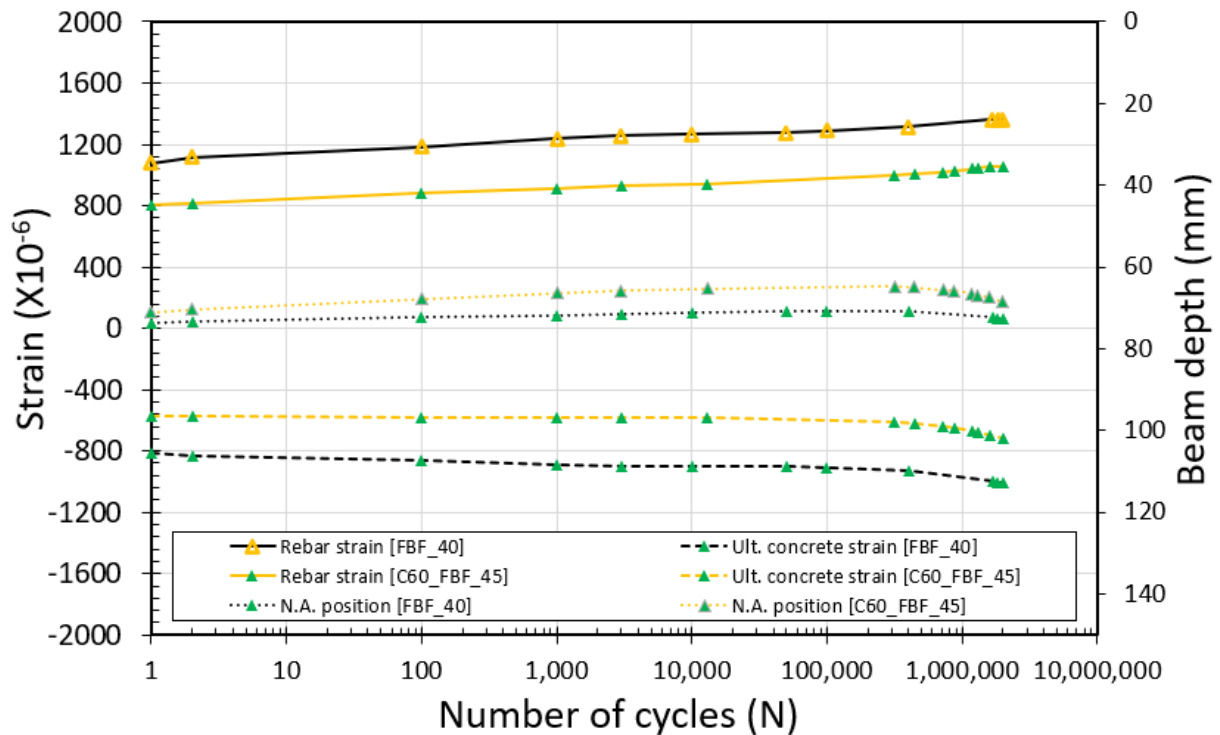


Fig. 6.56 Average experimental fatigue response of C60_FBF_45 versus FBF_40 over fatigue life.

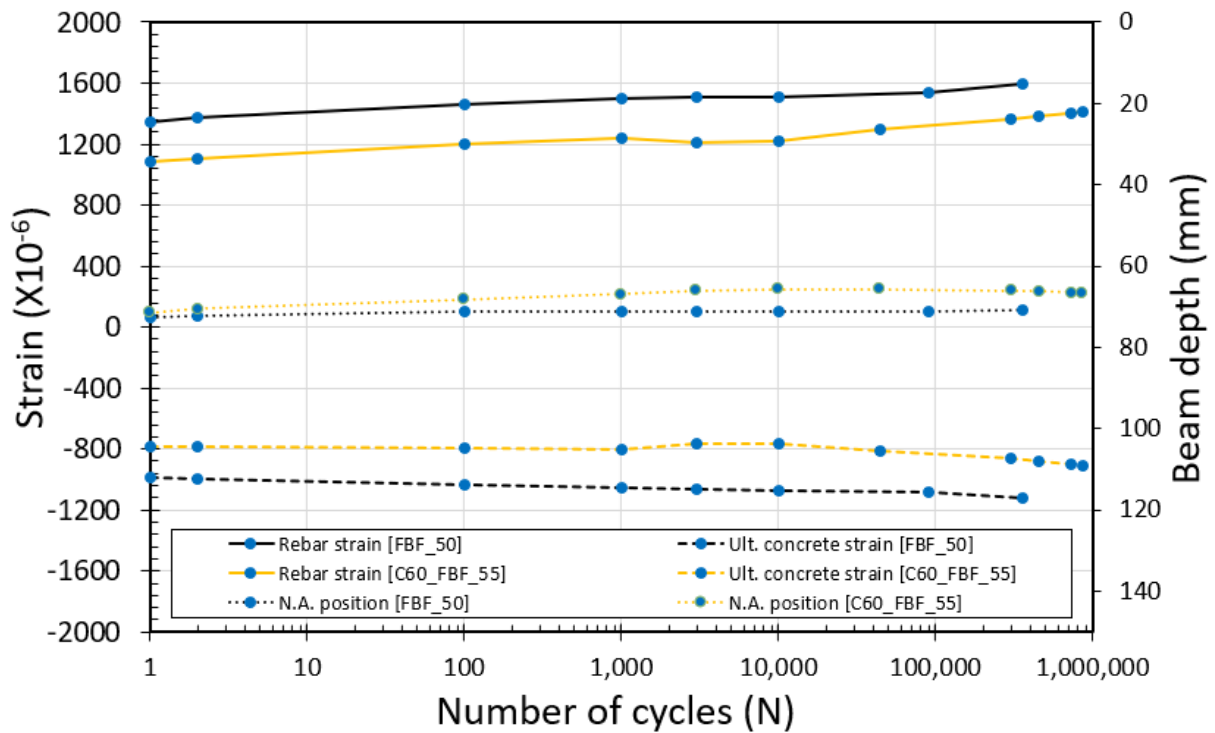


Fig. 6.57 Average experimental fatigue response of C60_FBF_55 versus FBF_50 over fatigue life.

Figures 6.55, 6.56, and 6.57 shows the comparison in the average flexural fatigue response between the beams C60_FBF_30-45-55-65, C60_FBF_45, and C60_FBF_55 with FBF_30-40-50-60, FBF_40, and FBF_50 respectively in logarithmic scale, that would have resulted in the evaluation of crack-bridging strength. The results showed that the evolution of the average experimental response had a lower rate of Beams C60_FBF_30-45-55-65, C60_FBF_45, and C60_FBF_55 with a higher compressive strength because of the stronger bond strength at fibers-matrix interface. It could be concluded that the increase of concrete compressive strength would influence decelerating the degradation rate of material strength under flexural loading and would be resulted in a lower degradation rate of crack-bridging strength.

6.4.1.2 Reinforcement Ratio Effect

A flexural cyclic loading test was carried out on three SFRC structural beams – i.e. D13_FBF_25-36-40, D13_FBF_36, and D13_FBF_40 – with lower ordinary rebar reinforcement ratio compared with the beams set in the first and second series – i.e. FBF_30-40-50-60, FBF_40, and FBF_50 –, aiming to capture the difference in the flexural fatigue response between each couple of beams having the flexural stress level. As the lower rebar reinforced ratio might change the crack width growth and the contribution of fibers in bridging

the cracks, that would lead to changes in the evolution process of the rebar strain level and the rate of degradation of the crack-bridging strength over the fatigue life.

The first SFRC structural beam – D13_FBF_25-36-40 – was tested for variable fatigue load levels starting with a low-load level of 25 kN for two million cycles then increased to 36 kN for one million cycles and finally 40 kN over the fatigue life until failure in a mode of rebar rupture by 3685131 flexural fatigue cycles. In the first cycle, the mid-span deflection of 2.21 mm at the maximum fatigue load level of 25 kN ($S=0.35$) was almost same as the mid-span deflection of 2.32 mm at the first cycle of the same stress level ($S=0.35$) with maximum fatigue load level of 30 kN for beam FBF_30-40-50-60, as shown in Fig. 6.58. As a result, the maximum rebar strain level for D13_FBF_25-36-40 of 755 microstrains was higher than beam FBF_30-40-50-60 of 580 microstrains that would be because of lower reinforcement resisting area resulting in higher rebar strain level, indicating the effect of a lower reinforcement ratio in changing the flexural response of the SFRC beams by contributed resistance of the tensile cyclic stress between rebars and steel fiber in tensile stress zone of SFRC structural beams, as shown in Figs. 6.59, and 6.60. Besides, one SFRC structural beam – D13_FBF_40 – was tested under 40 kN of maximum flexural fatigue load the same as one beam from the first series – FBF_40 – for comparison under the same load level, as shown in Figs. 6.58, 6.59, and 6.62. Under the same load level, the results show that the lower reinforcement SFRC beam – D13_FBF_40 – had a higher rebar strain level with a lower N.A. position indicating a longer crack length with a higher section damage level and lower structural stiffness comparing with the beam – FBF_40 – with a higher reinforcement ratio.

By cyclic progress, the three SFRC structural beams were monitored during the application of flexural fatigue load under different load levels, by comparing beams D13_FBF_25-36-40, D13_FBF_36, and D13_FBF_40 with FBF_30-40-50-60, FBF_40, and FBF_50, through measuring the average response of the tested beams of rebar and concrete strain level and N.A. position and compared with the first and second series, as shown in Figs. 6.60, 6.61, 6.62, and 6.63. Besides, the mid-span deflection and maximum rebar strain evolution over the fatigue life, as shown in Figs. 6.58, and 6.59. During the fatigue life, the evolution rate of the mid-span deflection was little higher for lower reinforcement ratio beams under all flexural fatigue load levels because of lower reinforcement resisting area of rebar resulting in lower structural stiffness of beams, as a comparison case between beam D13_FBF_40 and beam FBF_40 and shown in Figs. 6.58. Besides, the evolution of the maximum rebar strain level had a faster rate

with a comparison with the first and second series that would influence the crack-bridging strength degradation model with the evolution of maximum rebar strain, as shown in Fig. 6.59.

Figures 6.60, 6.61, 6.62, and 6.63 shows the comparison in the average flexural fatigue response between the beams D13_FBF_25-36-40, D13_FBF_36, and D13_FBF_40 with FBF_30-40-50-60, FBF_40, and FBF_50 in logarithmic scale, that would have resulted in the evaluation of crack-bridging strength. The results showed that the evolution of the average experimental response had a higher rate of Beams D13_FBF_25-36-40, D13_FBF_36, and D13_FBF_40 with a lower reinforcement ratio for the average rebar strain only, however, the evolution rate of concrete strain and N.A. position had the same evolution rate as the first and second series, as shown in Figs. 6.60, 6.61, 6.62, and 6.63. It could be concluded that the lower reinforcement ratio would influence accelerating the evolution rate of the rebar strain level during fatigue life that would be resulted in a lower degradation rate of crack-bridging strength.

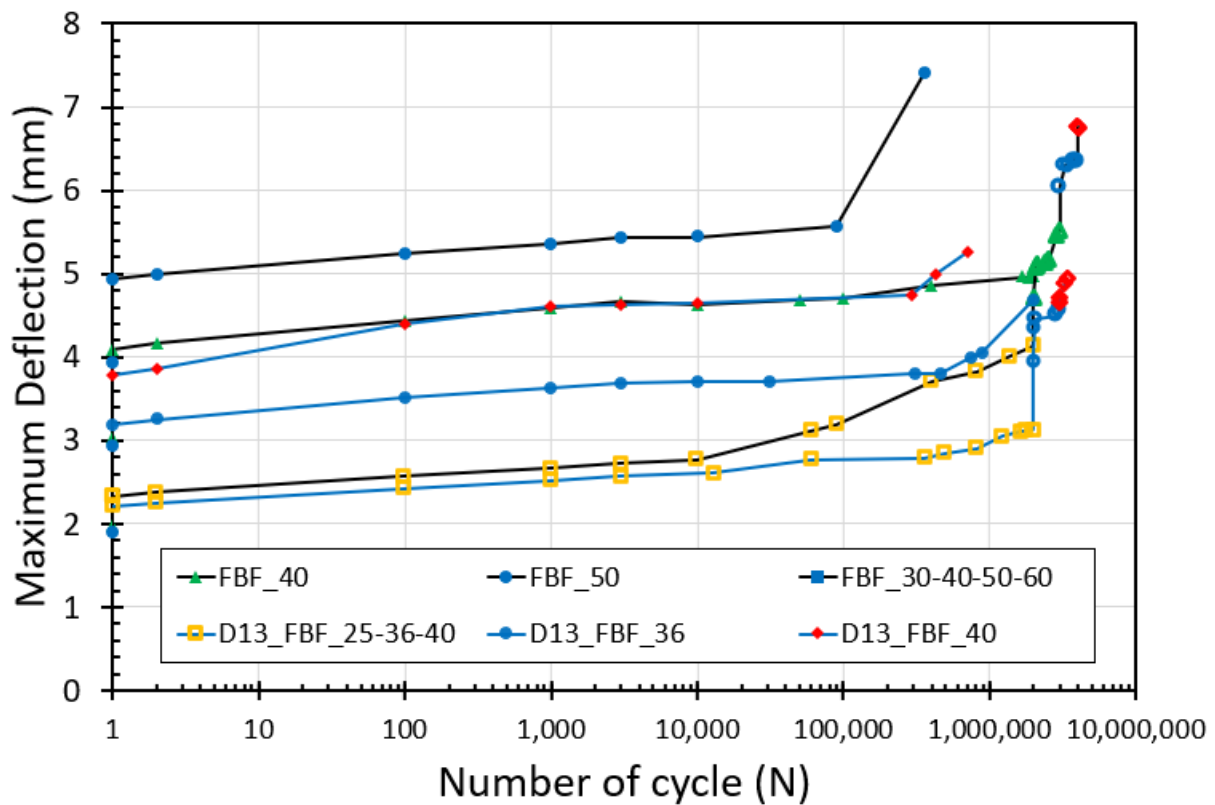


Fig. 6.58 Mid-span deflection evolution at the maximum flexural cyclic load level for the first, second, and third series over fatigue life.

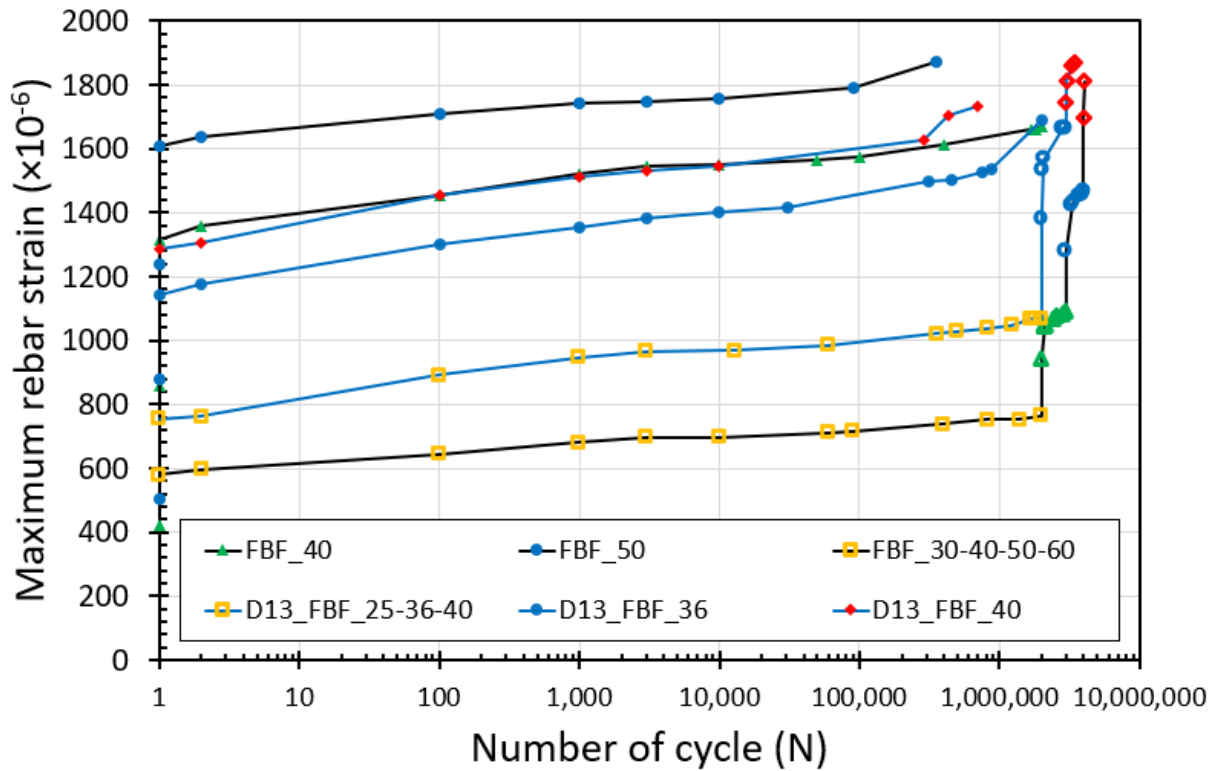


Fig. 6.59 Maximum rebar strain evolution for the first, second, and third series over fatigue life.

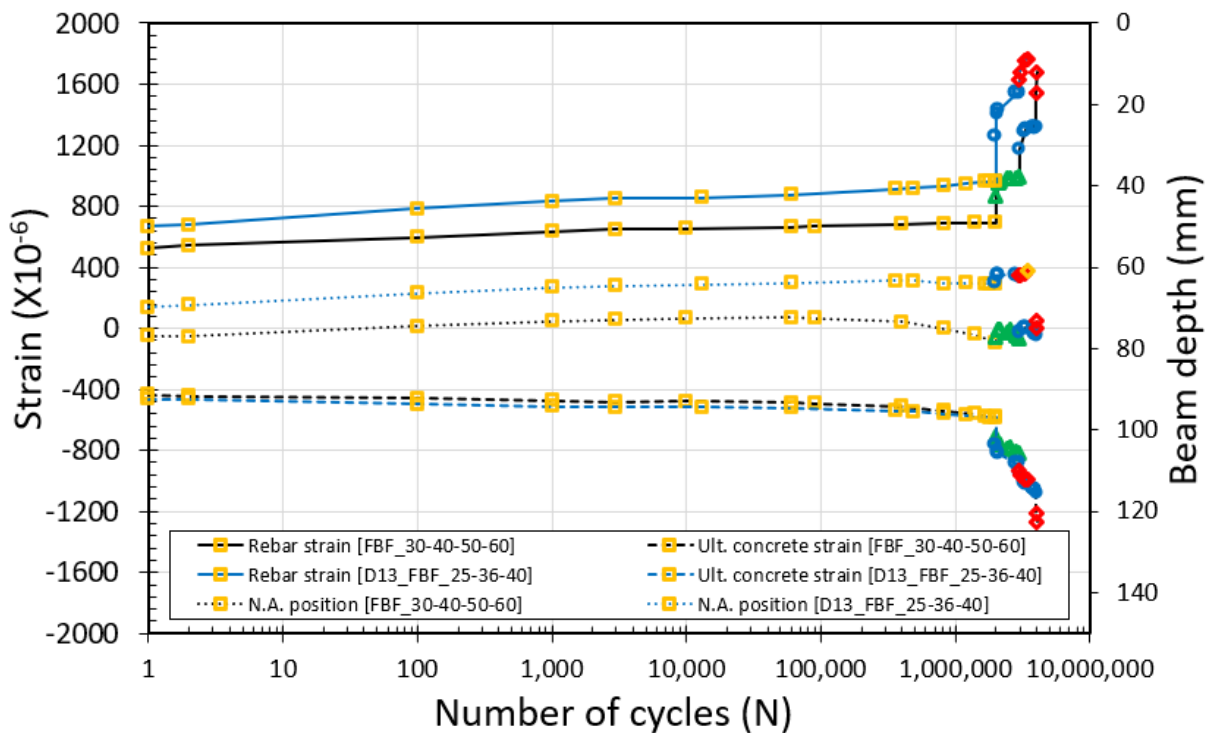


Fig. 6.60 Average experimental fatigue response of D13_FBF_25-36-40 versus FBF_30-40-50-60 over fatigue life.

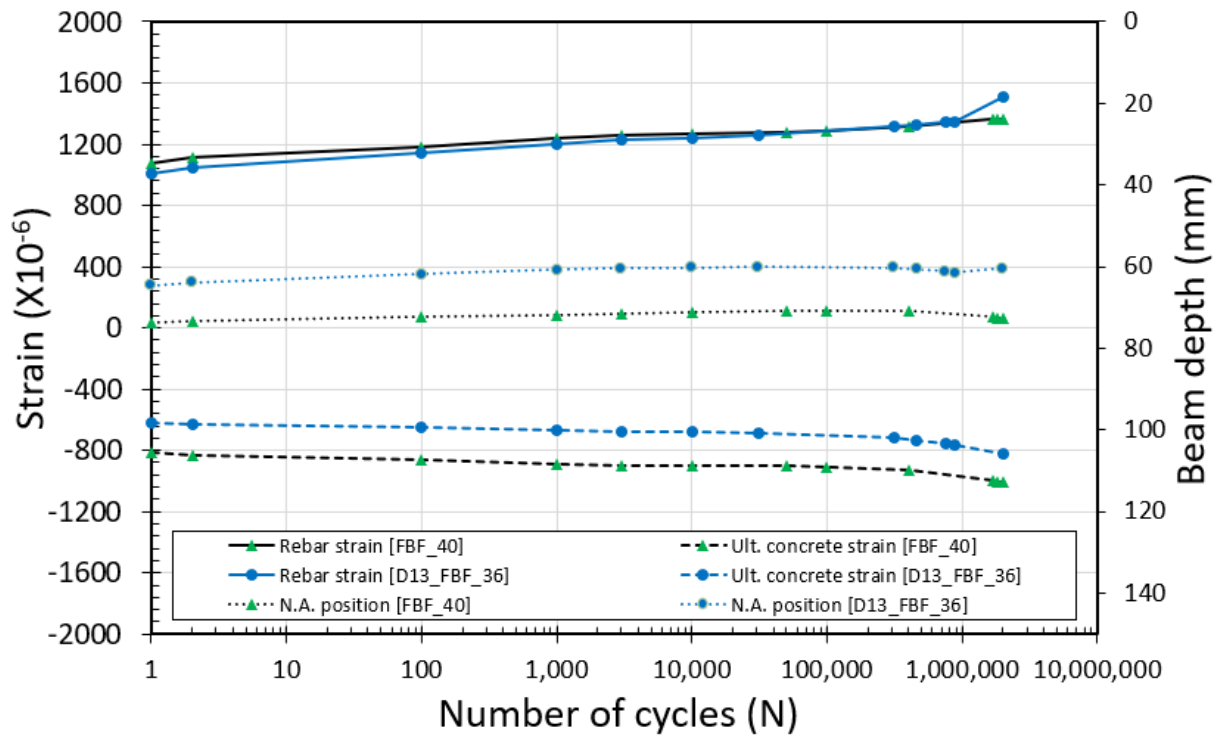


Fig. 6.61 Average experimental fatigue response of D13_FBF_36 versus FBF_40 over fatigue life.

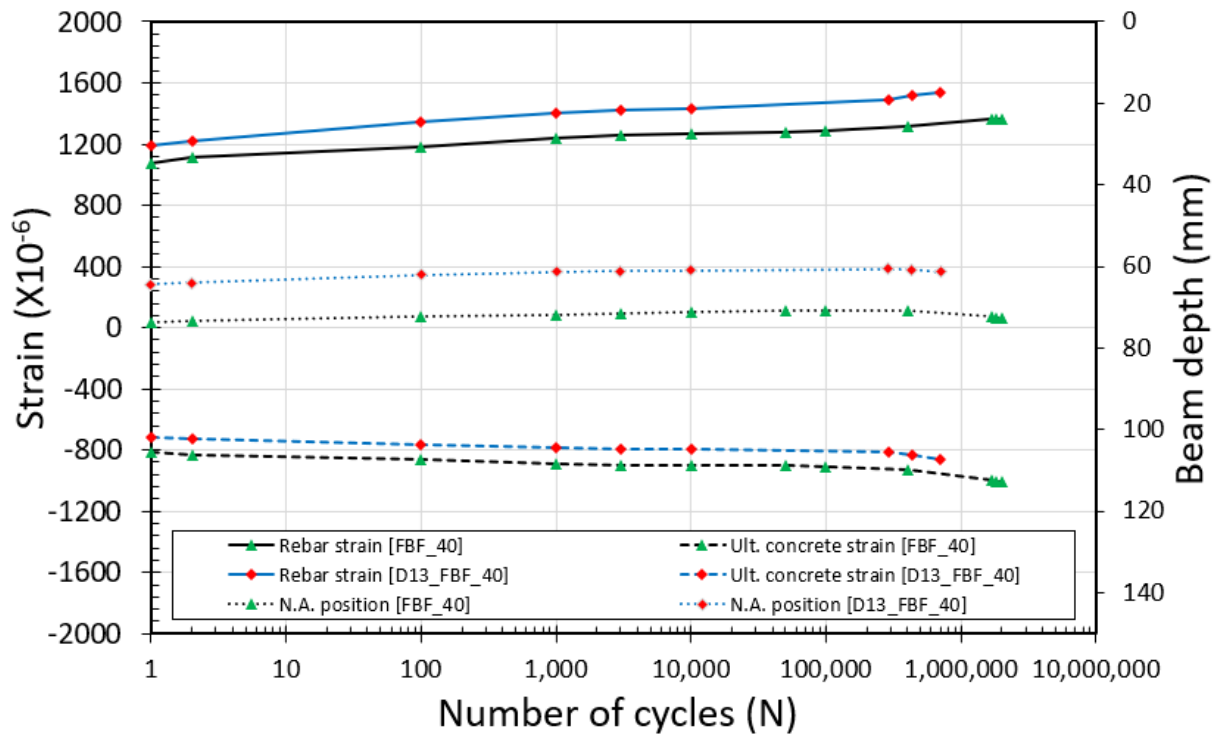


Fig. 6.62 Average experimental fatigue response of D13_FBF_40 versus FBF_40 over fatigue life.

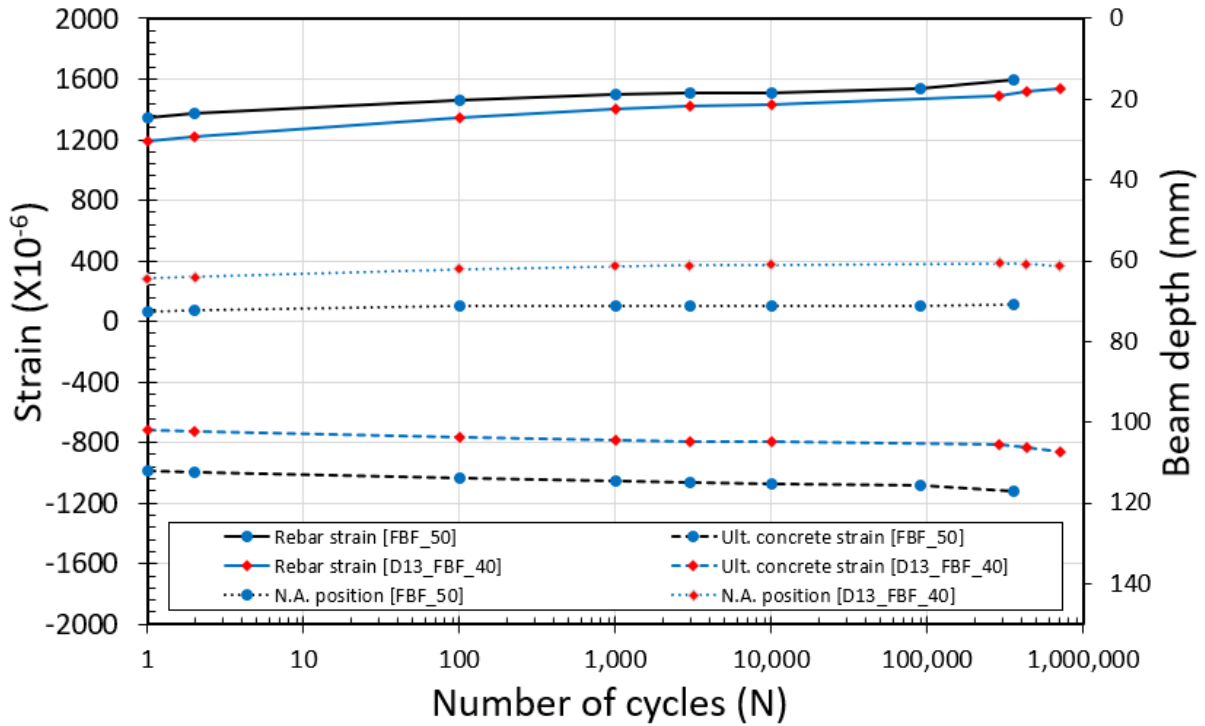


Fig. 6.63 Average experimental fatigue response of D13_FBF_40 versus FBF_50 over fatigue life.

6.4.2 Evaluated Crack-bridging Strength of The Third Series

The inverse analysis method of computation involves incremental calculations during fatigue loading as the number of cycles increases, as explained in section 3.4.3. The computations are performed iteratively for the incremental set of fatigue cycles (N_i) until fatigue rupture failure of rebar (N_f). At each increment N_i , a certain degradation or evolution level (α_i) of initial crack-bridging strength is proposed to adjust the balance between the experimentally measured results and the calculated values; if the agreement between the calculated and experimental results is not within the set threshold, the analysis is repeated using a different level of degradation or evolution until the threshold is met, as illustrated in Figs. 3.13, 6.64, 6.65, 6.66, 6.69, 6.70, and 6.71.

The normalized crack-bridging strength (β_i) is derived using Eq. (3.4) and plotted in Figs. 6.67, and 6.72, illustrating the degradation and evolution of crack-bridging strength over the fatigue life of the two sets of the SFRC structural beams, capturing the effect of higher concrete compressive strength for C60_FBF_30-45-55-65, C60_FBF_45, and C60_FBF_55 and the effect of lower rebar reinforcement ratio for D13_FBF_25-36-40, D13_FBF_36, and D13_FBF_40. Besides, the normalized crack-bridging strength at all fatigue load levels is plotted versus the evolution of the experimental maximum rebar strain, as shown in Figs. 6.68,

and 6.73. As well, The effect of increasing the maximum fatigue load level during the fatigue life had been captured on the evaluated crack-bridging strength, the maximum rebar strain evolution and crack propagation mechanics. Note, however, that the normalized crack-bridging strength at the first cycle (N_1) of fatigue loading does not necessarily start at 1.0 as discussed in section 4.4.

6.4.2.1 Concrete Compressive Strength Effect

Figures 6.64, 6.65, and 6.66 show acceptable fitting with a minimum error between the calculated and experimental flexural fatigue response in all fatigue load levels, resulting in evaluating of the crack-bridging strength degradation and evolution model over the fatigue life, as shown in Fig. 6.67. For all fatigue load levels including three SFRC beams C60_FBF_30-45-55-65, C60_FBF_45, and C60_FBF_55, there is a clear increase in average strain levels for both rebar and concrete and a decrease in the N.A. position as the number of cycles increases, as shown in Figs. 6.64, 6.65, and 6.66. The conclusion from these results is that the proposed inverse analysis method could predict the degradation and evolution of crack-bridging strength provided by fibers as flexural fatigue loading continues.

Besides, the normalized crack-bridging strength at all fatigue load levels is plotted versus the evolution of the experimental maximum rebar strain, as shown in Fig. 6.68. Figure 6.68 shows a zigzag linear relationship of the degradation and evolution of the crack-bridging strength regarding the evolution of the maximum rebar strain over the fatigue life regardless of the fatigue stress levels, that also confirmed in the first and second series and could be a useful relationship for design and assessment of SFRC structural beams under fatigue loading for a wide range of concrete compressive strength with ordinary and high strength. Besides, the degradation model of the crack-bridging strength regarding the evolution progress of maximum rebar strain has a constant linear relationship regardless of the fatigue stress levels. On the other hand, the evolution increase model of the crack-bridging strength regarding the evolution progress of maximum rebar strain through increasing the load level monotonically has a decreasing linear relationship with the increase of fatigue stress levels, as shown in Fig. 6.68.

The normalized evaluated crack-bridging strength during the fatigue life of beams C60_FBF_30-45-55-65, C60_FBF_45, and C60_FBF_55 tends to decrease with the increase of the number of loading cycles during cyclic loading, as shown in Fig. 6.67. The repeated tensile stress resulted in increasing the width of the cracks. That would lead to loss of the bond

between fibers and matrix where degradation of crack-bridging strength took place, as shown in Fig. 6.67 and illustrated in Fig. 5.26(a). Simultaneously, an increase in the level of rebar strain over the fatigue life is achieved, as shown in Fig. 6.68 for single and variable flexural fatigue load levels.

Especially, at the stage of increasing the load level monotonically to 45 kN flexural load for SFRC beam C60_FBF_30-45-55-65, the normalized crack-bridging strength increases with the increase of the load level monotonically from lower to higher fatigue load level, as shown in Fig. 6.67 as a line starts and ends by different dot shape and color. Indicating that, the mid-span deflection and the crack length and width were increased and structural stiffness was decreased, noticing a new contribution of steel fibers in bridging the cracks by transmitting tensile stress in tensile stress zone below the N.A., as shown in Fig. 5.26(b) as indicated by green color fibers. As a result, an increase in the crack-bridging strength was observed for the SFRC structural beams with the evolution of the maximum rebar strain level, as shown in Figs. 6.67, and 6.68 as a yellow line started by a square yellow dot and ended by a triangle green dot.

After increasing the flexural load monotonically, the cyclic flexural load was applied for one million cycles under the desired higher flexural fatigue load level. During that application of repeated cyclic loading, an increase in the width of the cracks took place, leading to a loss in the bond between fibers and matrix where degradation of crack-bridging strength took place again, as shown in Fig. 6.67 and illustrated in Fig. 5.26(b). Simultaneously, an increase in the level of rebar strain over the fatigue life is achieved, as shown in Fig. 6.67 as a triangle green dots.

As cycles progress, other higher fatigue load levels were tested for 55 kN and 65 kN of the maximum flexural load by increasing monotonically first, then a cyclic loading was applied for one million cycles. The same mechanism of degradation and evolution in crack-bridging strength were observed over the fatigue life and with the maximum rebar strain evolution, as shown in Figs. 6.67 and 6.68. Finally, at a higher fatigue load level where a 65 kN of flexural maximum load level was applying, a rupture fatigue failure took place in a manner of rebar rupture achieving 4981386 cycles of fatigue life, as summarized in Table 6.2 and shown in Fig. 6.5. the results achieved in the third series of higher concrete compressive strength show the same strength degradation mechanism as the first and second series as previously discussed.

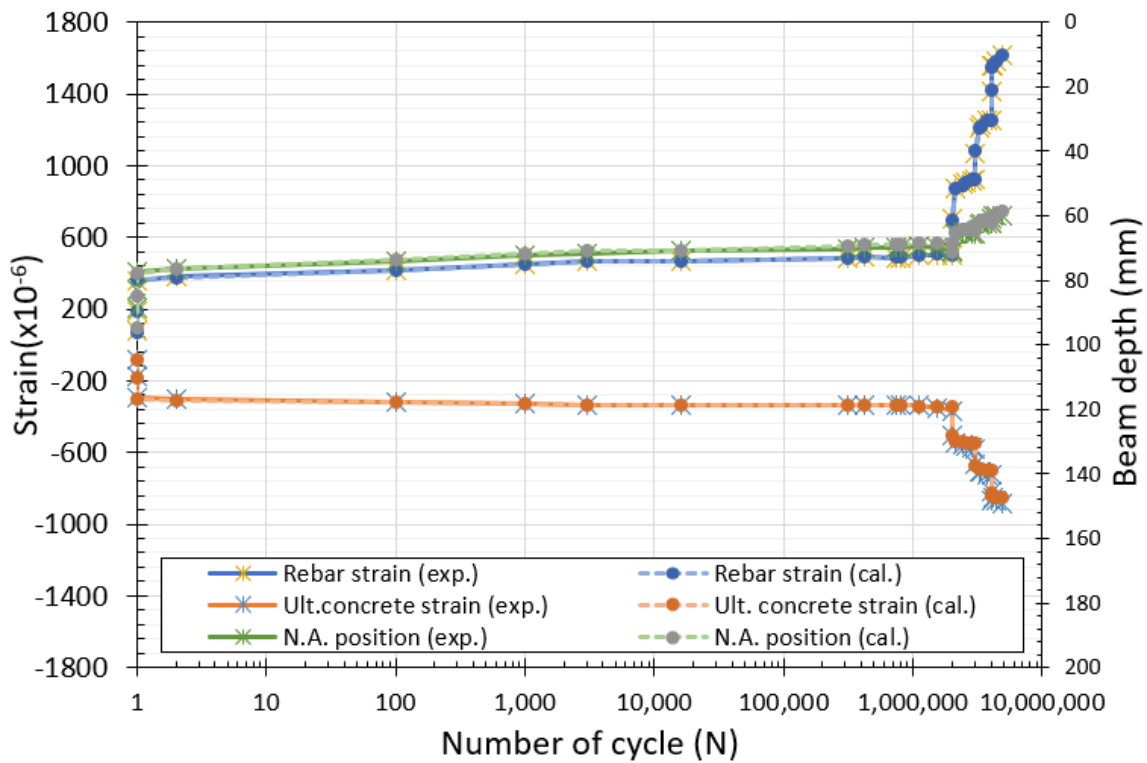


Fig. 6.64 Calculated versus experimental fatigue response of C60_FBF_30-45-55-65 over the fatigue life.

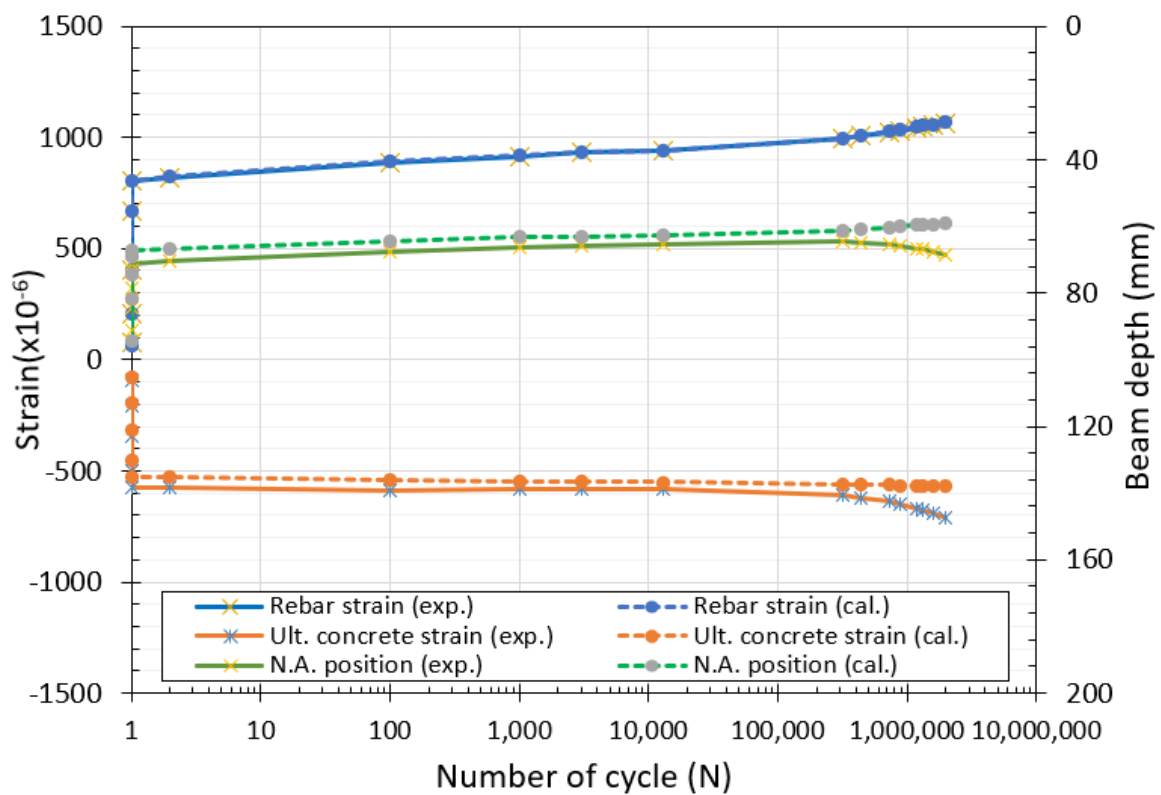


Fig. 6.65 Calculated versus experimental fatigue response of C60_FBF_45 over the fatigue life.

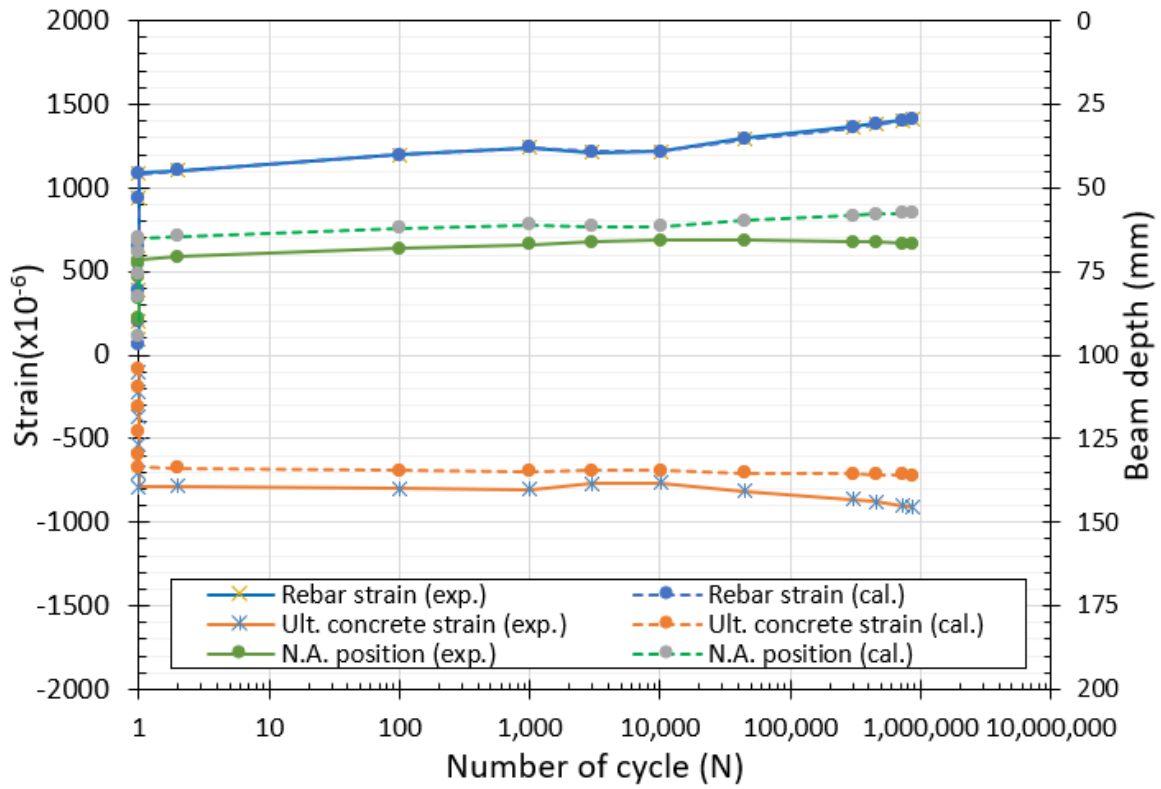
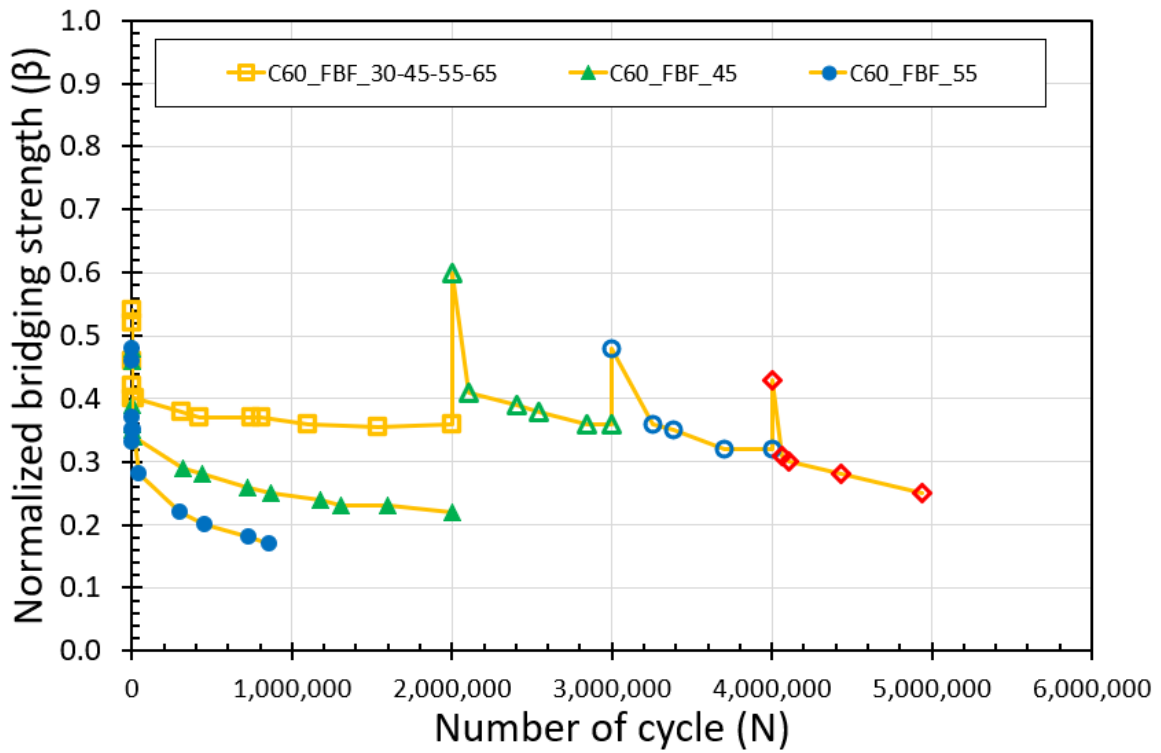


Fig. 6.66 Calculated versus experimental fatigue response of C60_FBF_55 over the fatigue life.



(a) Normal scale

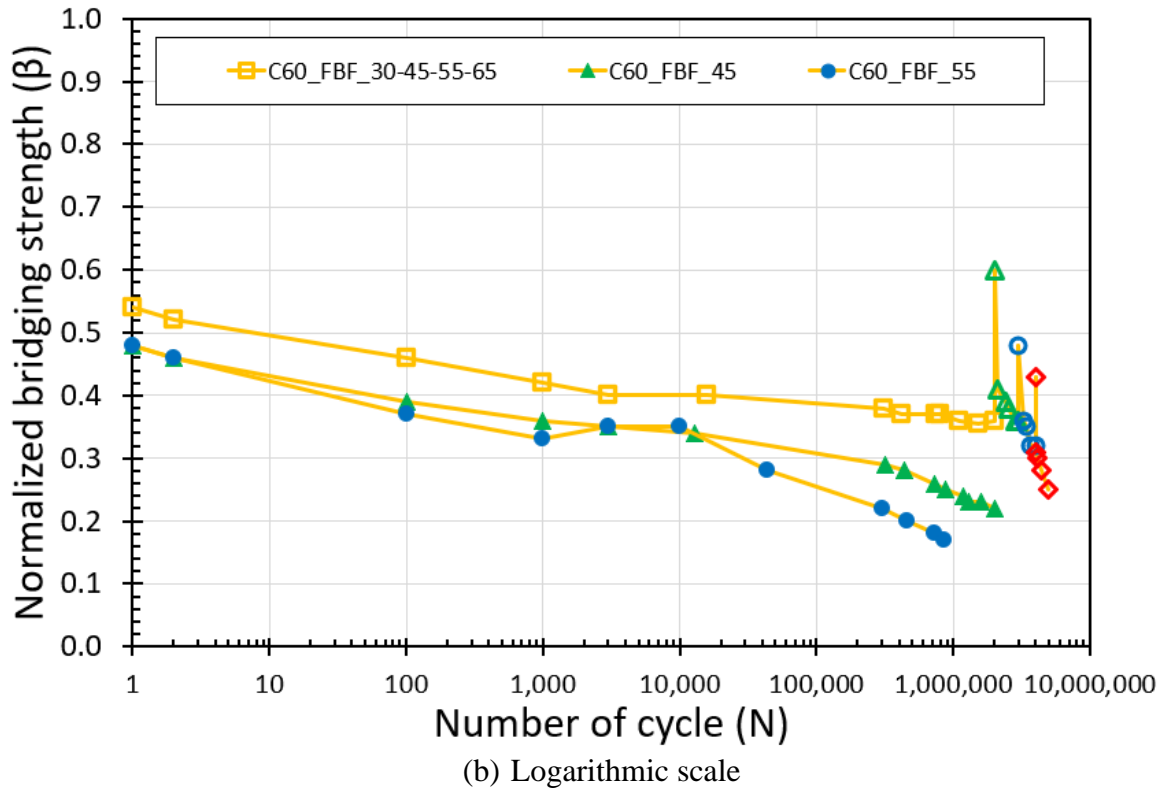


Fig. 6.67 Normalized crack-bridging strength degradation and evolution of SFRC beams with higher concrete compressive strength over flexural fatigue life.

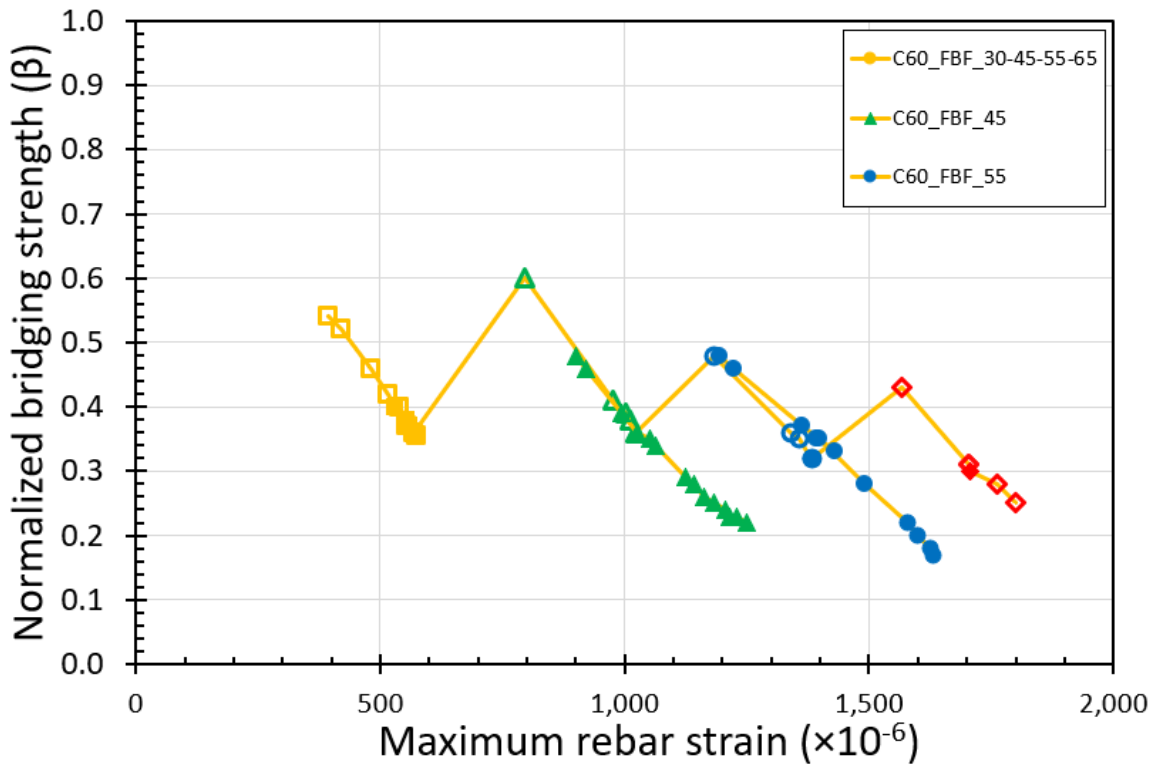


Fig. 6.68 Normalized crack-bridging strength degradation and evolution versus maximum rebar strain of SFRC beams with higher concrete compressive strength over flexural fatigue life.

6.4.2.2 Reinforcement Ratio Effect

Figures 6.69, 6.70, and 6.71 show acceptable fitting with a minimum error between the calculated and experimental flexural fatigue response in all fatigue load levels, resulting in evaluating of the crack-bridging strength degradation and evolution model over the fatigue life, as shown in Fig. 6.72. For all fatigue load levels including three SFRC beams D13_FBF_25-36-40, D13_FBF_36, and C60_FBF_40, there is a clear increase in average strain levels for both rebar and concrete and a decrease in the N.A. position as the number of cycles increases, as shown in Figs. 6.69, 6.70, and 6.71. The conclusion from these results is that the proposed inverse analysis method could predict the degradation and evolution of crack-bridging strength provided by fibers as flexural fatigue loading continues.

Besides, the normalized crack-bridging strength at all fatigue load levels is plotted versus the evolution of the experimental maximum rebar strain, as shown in Fig. 6.73. Figure 6.73 shows a zigzag linear relationship of the degradation and evolution of the crack-bridging strength regarding the evolution of the maximum rebar strain over the fatigue life regardless of the fatigue stress levels, that also confirmed in the first and second series and could be a useful relationship for design and assessment of SFRC structural beams under fatigue loading for a wide range of longitudinal rebars reinforcement ratio with lower and high reinforcement ratio. Besides, the degradation model of the crack-bridging strength regarding the evolution progress of maximum rebar strain has a constant linear relationship regardless of the fatigue stress levels. On the other hand, the evolution increase model of the crack-bridging strength regarding the evolution progress of maximum rebar strain through increasing the load level monotonically has a decreasing linear relationship with the increase of fatigue stress levels, as shown in Fig. 6.73.

The normalized evaluated crack-bridging strength during the fatigue life of beams D13_FBF_25-36-40, D13_FBF_36, and D13_FBF_40 tends to decrease with the increase of the number of loading cycles during cyclic loading, as shown in Fig. 6.72. The repeated tensile stress resulted in increasing the width of the cracks. That would lead to loss of the bond between fibers and matrix where degradation of crack-bridging strength took place, as shown in Fig. 6.72 and illustrated in Fig. 5.26(a). Simultaneously, an increase in the level of rebar strain over the fatigue life is achieved, as shown in Fig. 6.73 for single and variable flexural fatigue load levels.

Especially, at the stage of increasing the load level monotonically to 35 kN flexural load for SFRC beam D13_FBF_25-36-40, the normalized crack-bridging strength increases with the increase of the load level monotonically from lower to higher fatigue load level, as shown in Fig. 6.72 as a line starts and end by different dot shape and color. Indicating that, the mid-span deflection and the crack length and width were increased and structural stiffness was decreased, noticing a new contribution of steel fibers in bridging the cracks by transmitting tensile stress in tensile stress zone below the N.A., as shown in Fig. 5.26(b) as indicated by green color fibers. As a result, an increase in the crack-bridging strength was observed for the SFRC structural beams with the evolution of the maximum rebar strain level, as shown in Figs. 6.72, and 6.73 as a yellow line started by a square yellow dot and ended by a circle blue dot. Then, the cyclic flexural load was applied for one million cycles under the desired higher flexural fatigue load level, where an increase in the width of the cracks took place, leading to a loss in the bond between fibers and matrix where degradation of crack-bridging strength took place again, as shown in Fig. 6.72 and illustrated in Fig. 5.26(b). Simultaneously, an increase in the level of rebar strain over the fatigue life is achieved, as shown in Fig. 6.73 as a triangle green dots.

Finally, at a higher fatigue load level where a 40 kN of flexural maximum load level was applying, a rupture fatigue failure took place in a manner of rebar rupture achieving 3685131 cycles of fatigue life, as summarized in Table 6.2 and shown in Fig. 6.29. the results that achieved in the third series of lower rebar reinforcement ratio show the same strength degradation mechanism as the first and second series as previously discussed.

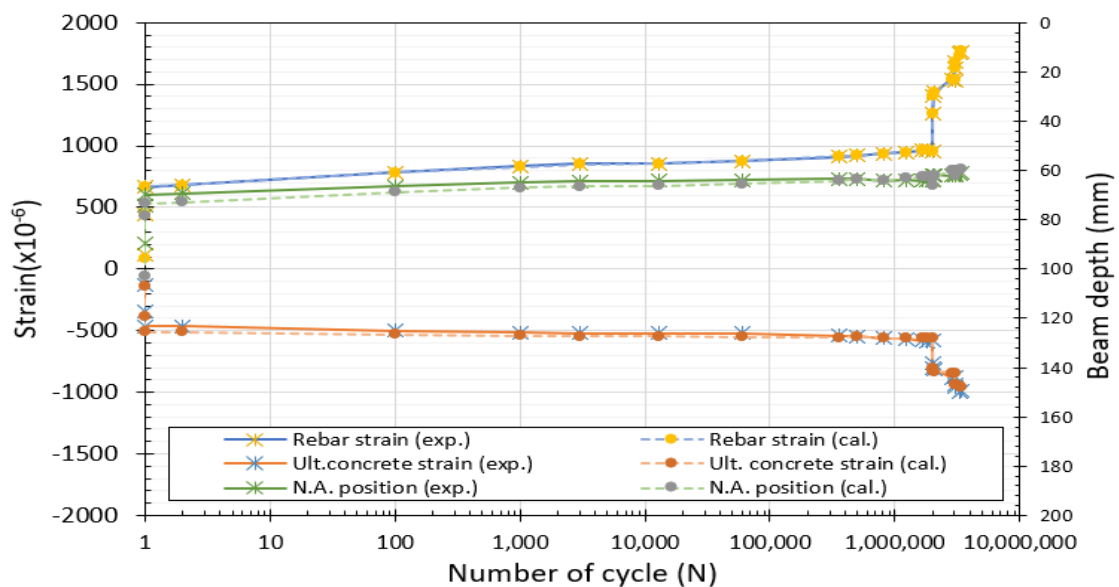


Fig. 6.69 Calculated versus experimental fatigue response of D13_FBF_25-36-40 over the fatigue life.

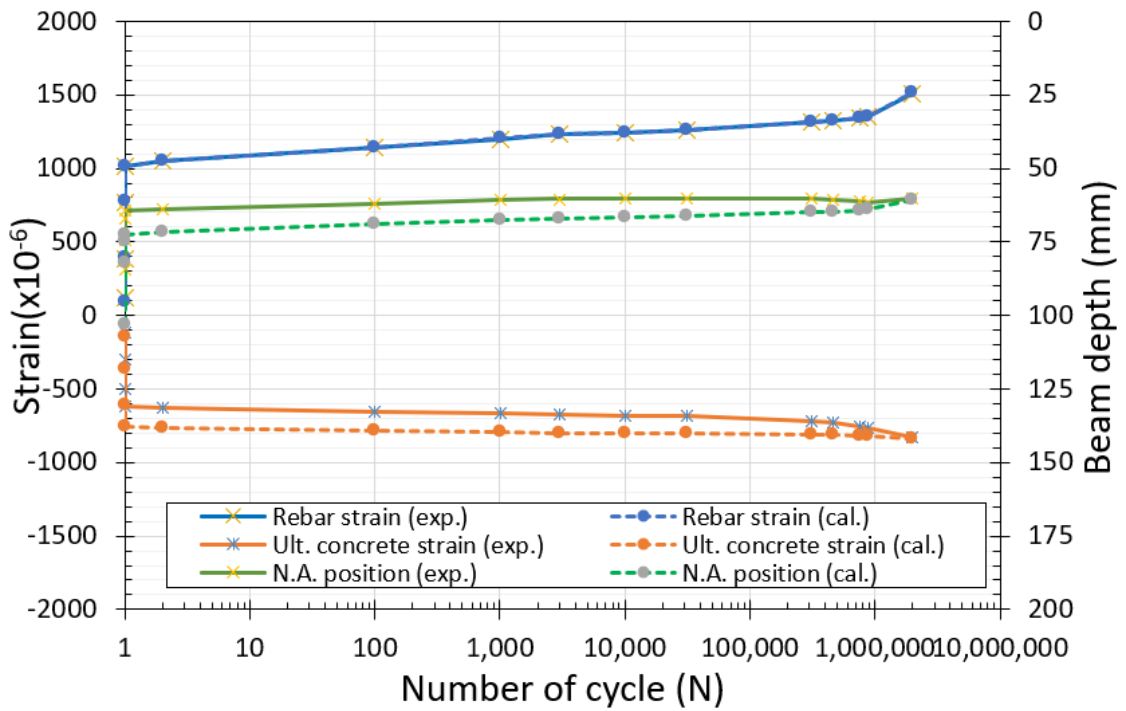


Fig. 6.70 Calculated versus experimental fatigue response of D13_FBF_36 over the fatigue life.

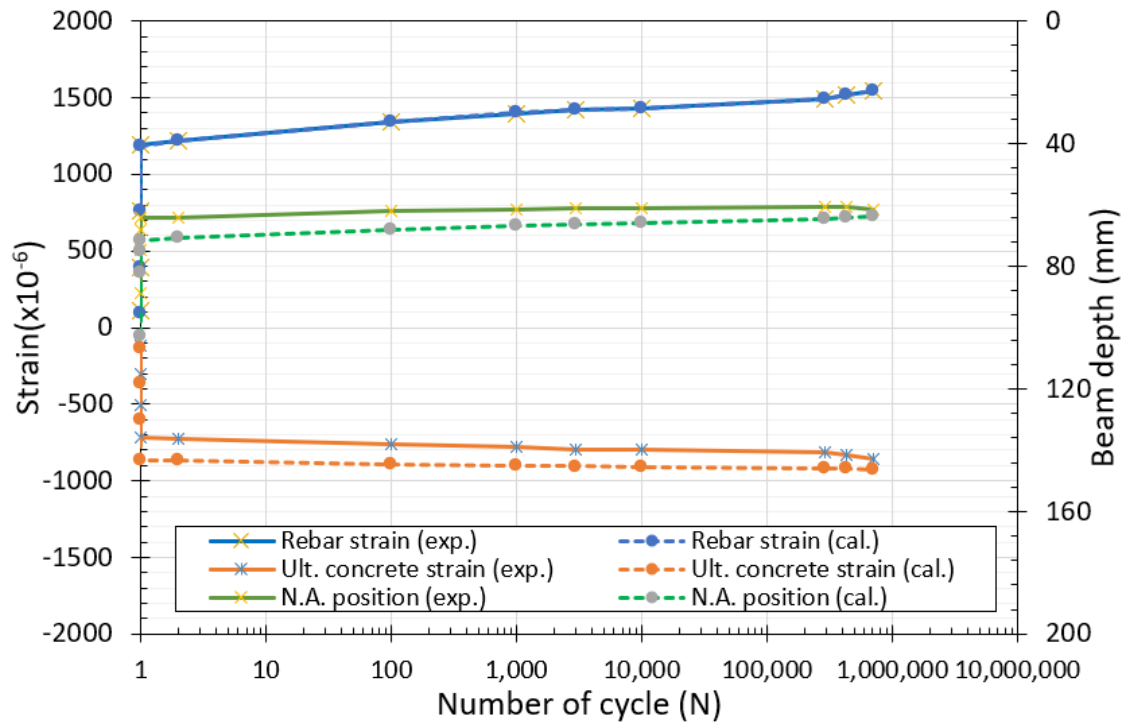
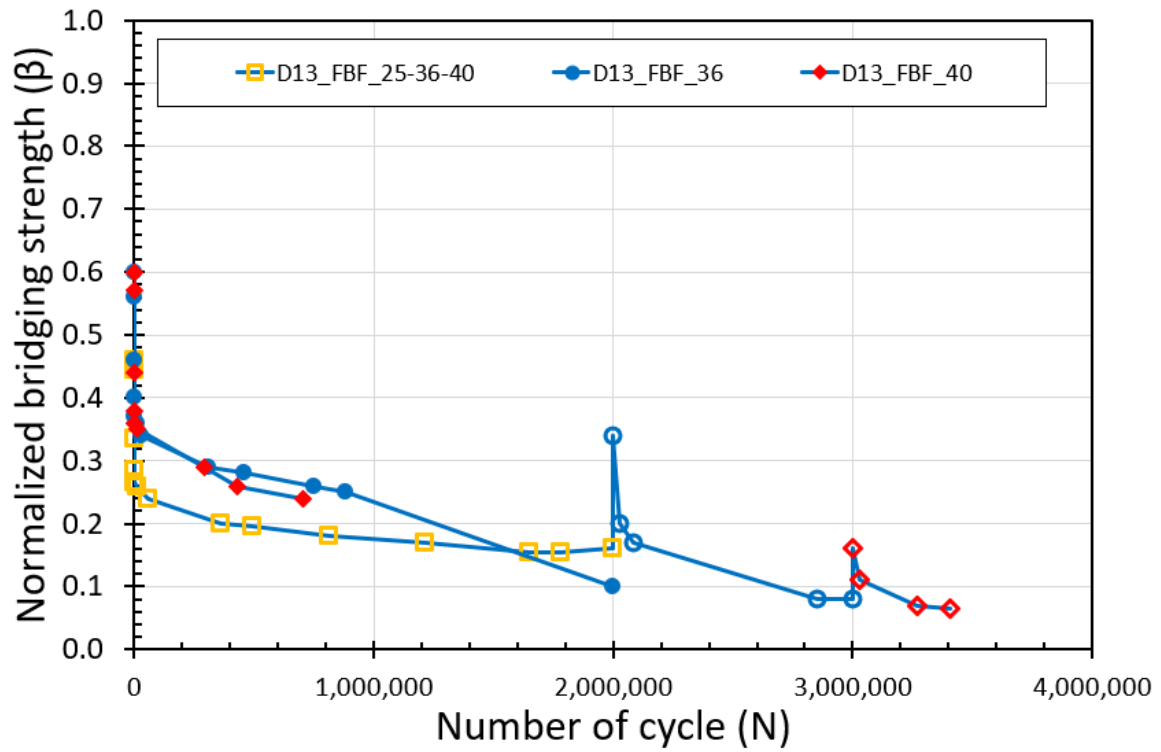
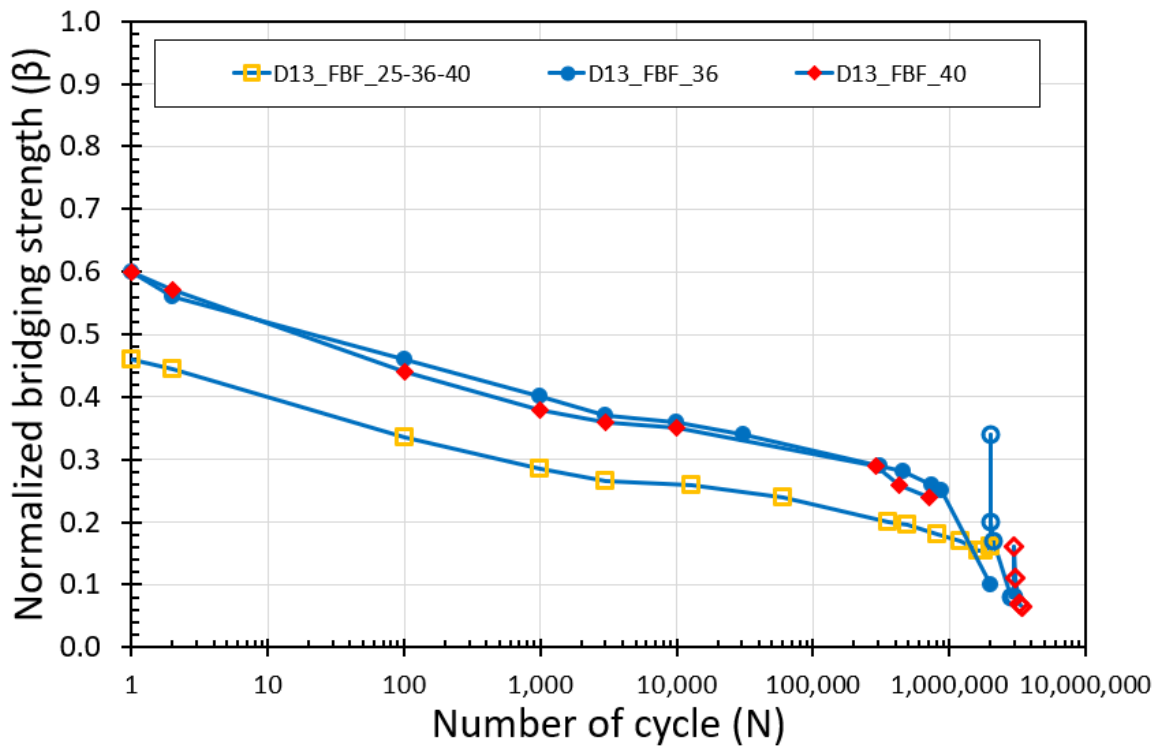


Fig. 6.71 Calculated versus experimental fatigue response of D13_FBF_40 over the fatigue life.



(a) Normal scale



(b) Logarithmic scale

Fig. 6.72 Normalized crack-bridging strength degradation and evolution of SFRC beams with lower reinforcement ratio over flexural fatigue life.

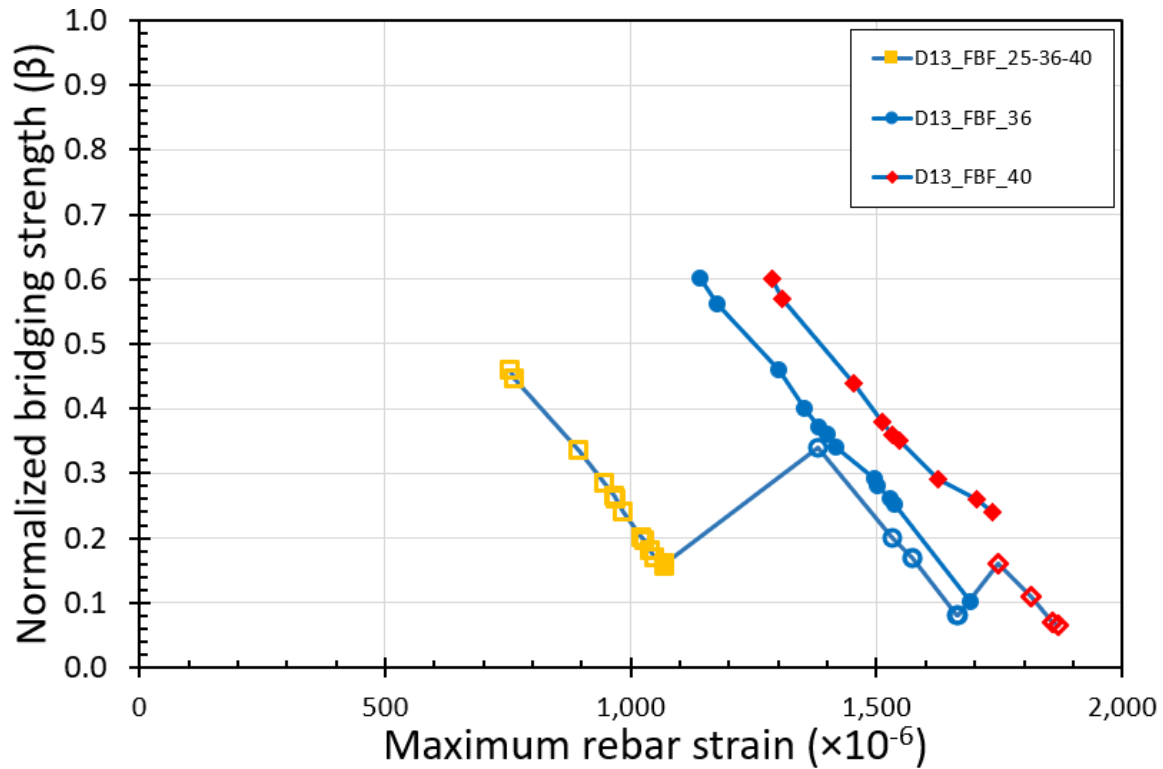


Fig. 6.73 Normalized crack-bridging strength degradation and evolution versus maximum rebar strain of SFRC beams with lower reinforcement ratio over flexural fatigue life.

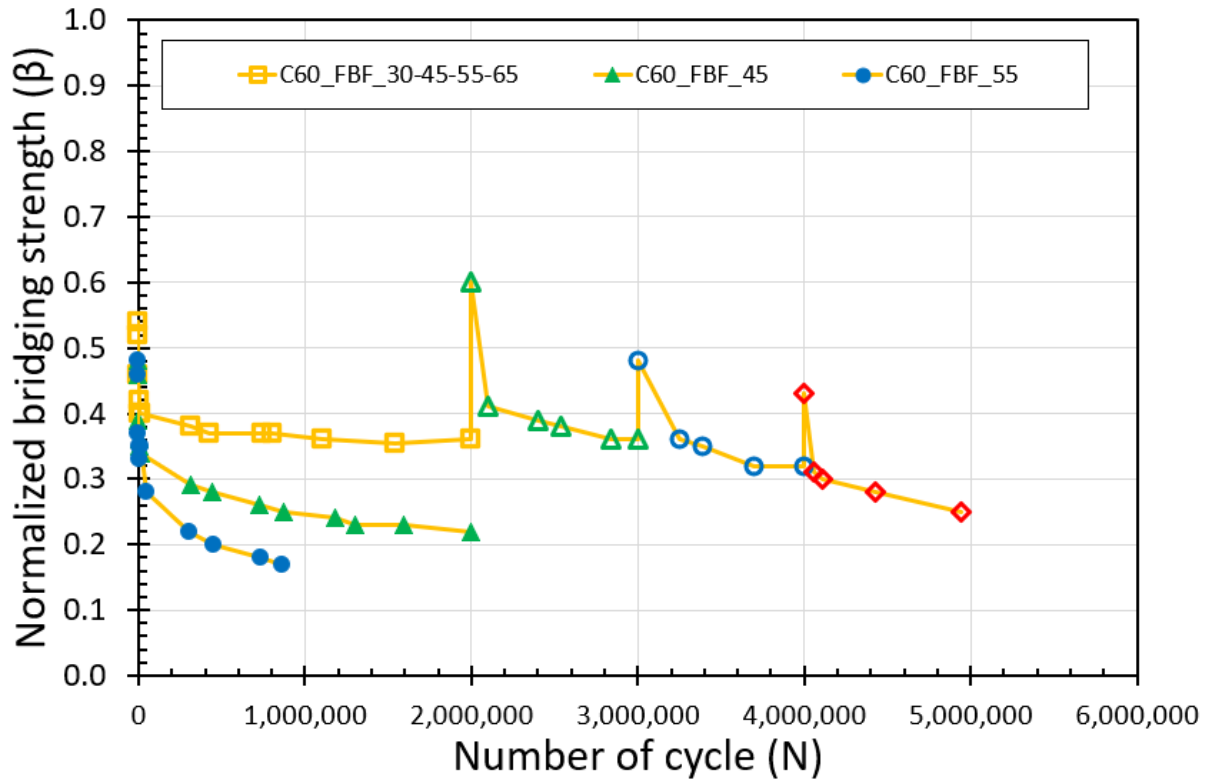
6.4.3 Crack-bridging Strength Degradation and Evolution diagram

The normalized crack-bridging strength is derived using the inverse analysis calculation method for the third series, testing the effect of higher concrete compressive strength and lower reinforcement ratio under single and variable flexural fatigue load levels and plotted in Figs. 6.74, and 6.78, illustrating the degradation of crack-bridging strength of the six SFRC structural beams – i.e. C60-FBF-30-45-55-65, C60_FBF_45, C60_FBF_55, D13_FBF_25-36-40, D13_FBF_36, and D13_FBF_40 – over the fatigue life. Besides, the evolution process of the crack-bridging strength was captured while increasing the flexural load level monotonically during the fatigue life of SFRC structural beams for the third series or after the end of the two million cycles, as shown in Figs. 6.75, and 6.79, as black solid lines. Besides, the crack-bridging strength degradation model derived from the third series was compared with the one derived from the first and second series emphasizing the effect of higher concrete compressive strength and lower reinforcement ratio, as shown in Figs. 6.76, and 6.80. Finally, two diagrams of the normalized crack-bridging strength degradation and evolution induced by hooked-end steel fibers for SFRC structural beams under flexural fatigue loading were plotted in Fig. 6.77, and 6.81. The proposed diagram of the crack-bridging strength degradation and evolution could be a useful relationship for the fatigue design and assessment of SFRC beams.

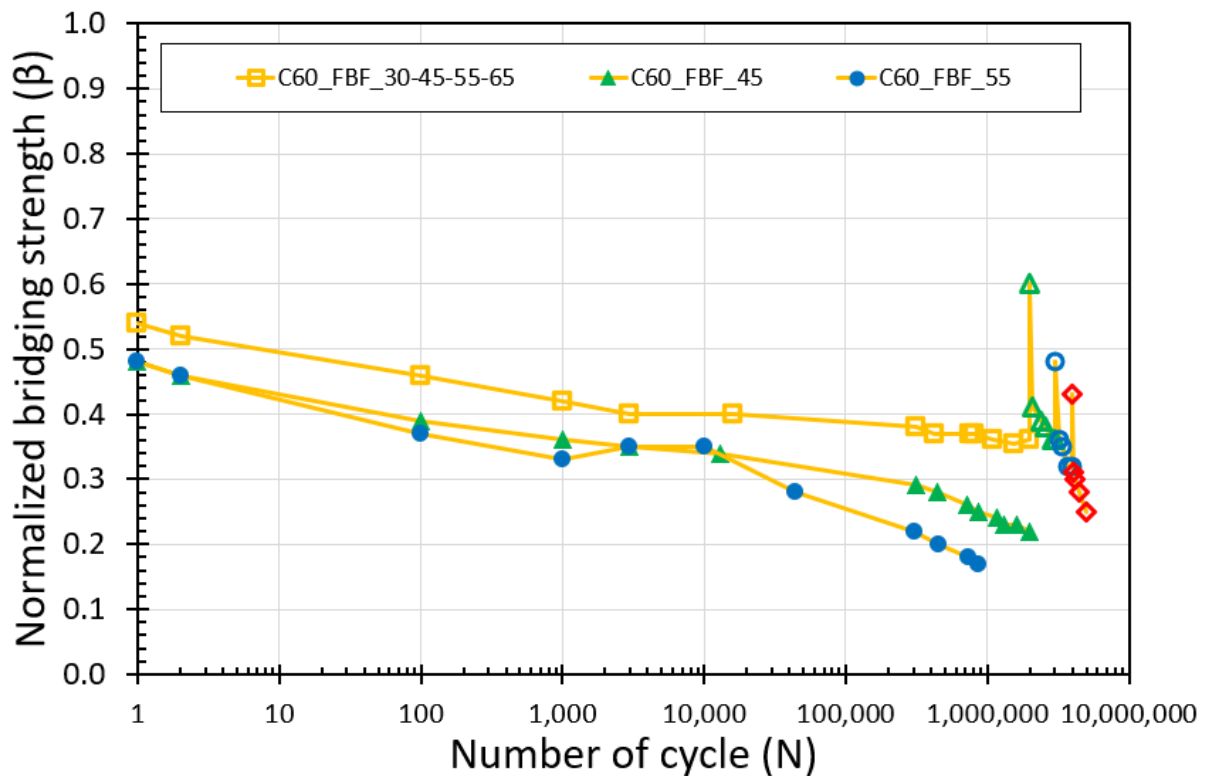
6.4.3.1 Concrete Compressive Strength Effect

The higher concrete compressive strength influenced a higher bond mechanism between fibers and the surrounding concrete matrix and decelerating the evolution rate of the strain levels over the fatigue life, as indicated in section 6.4.1.1. Using the inverse analysis method, the crack-bridging strength was evaluated for over the fatigue life under single and variable flexural load levels, capturing the degradation and evolution mechanism by applying fatigue load and monotonically increasing the load level respectively for C60_FBF_30-45-55-65, C60_FBF_45, and C60_FBF_55 SFRC structural beams, as shown in Fig. 6.74. Besides, The proposed crack-bridging strength degradation and evolution model had plotted versus the maximum rebar strain evolution, as shown in Fig. 6.75. The results showed that the degradation mechanism has a constant linear relationship over a wide range of fatigue load level regarding the maximum rebar strain level evolution for the higher concrete compressive strength as well as normal concrete compressive strength, as shown in Fig. 6.75. As cycles progress, the repeated cyclic loading leads to crack growth that would lead to loss of bond between the matrix and the fibers, as well as increasing in rebar strain level, simultaneously. Besides, the evolution mechanism of the crack-bridging strength has a linear relationship over fatigue life with a decreased slope for a higher fatigue load level regarding the maximum rebar strain level evolution depending on the damaged level, as shown in Fig. 6.75 as inclined solid black lines. As increasing the fatigue load level monotonically, new fibers would contribute to bridging the growth of the cracks with the old fibers that had a certain damaged level at the fiber-matrix interface, leading to an increase in the crack-bridging strength.

A comparison process was carried out between the first, second, and third series regarding the evaluated crack-bridging strength degradation and evolution model, aiming to capture the effect of the higher concrete compressive strength effect, as shown in Fig. 6.76. It is obvious from Figure 6.76 that, the degradation rate of the evaluated crack-bridging strength is lower for the higher concrete compressive strength structural beams than the beams of the first and second series because of the enhanced bond strength at the fibers-matrix interface. However, the evolution rate of the evaluated crack-bridging strength is almost as same as the second series, as it only depends on the damaged level at the fiber-matrix interface, as shown in Fig. 6.76. As a result, a new diagram of degradation and evolution of crack-bridging strength was proposed regarding the evolution of the maximum rebar strain for the higher concrete compressive strength, as shown in Fig. 6.77. The proposed diagram in Figure 6.77 has the same bridging evolution as circle curved lines and lower bridging degradation as yellow parallel inclined lines.



(a) Normal scale



(b) Logarithmic scale

Fig. 6.74 Normalized crack-bridging strength degradation over the fatigue life under various flexural fatigue load level.

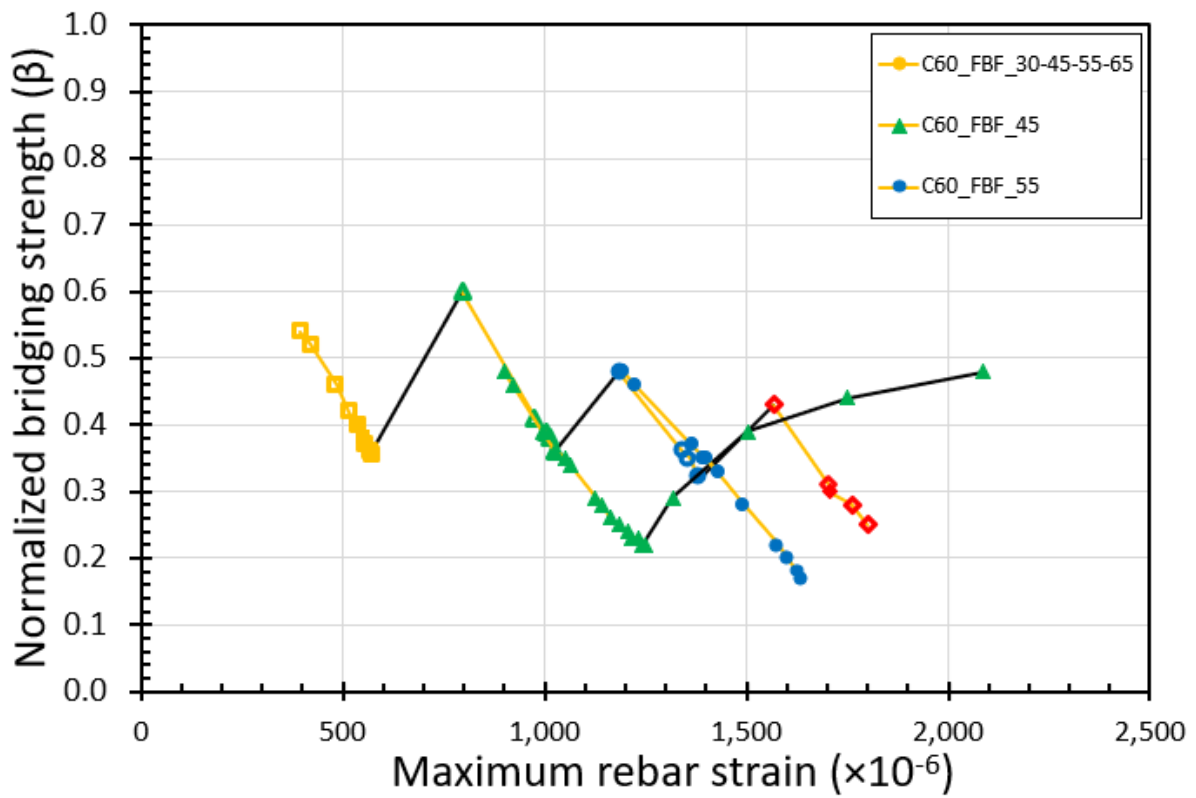
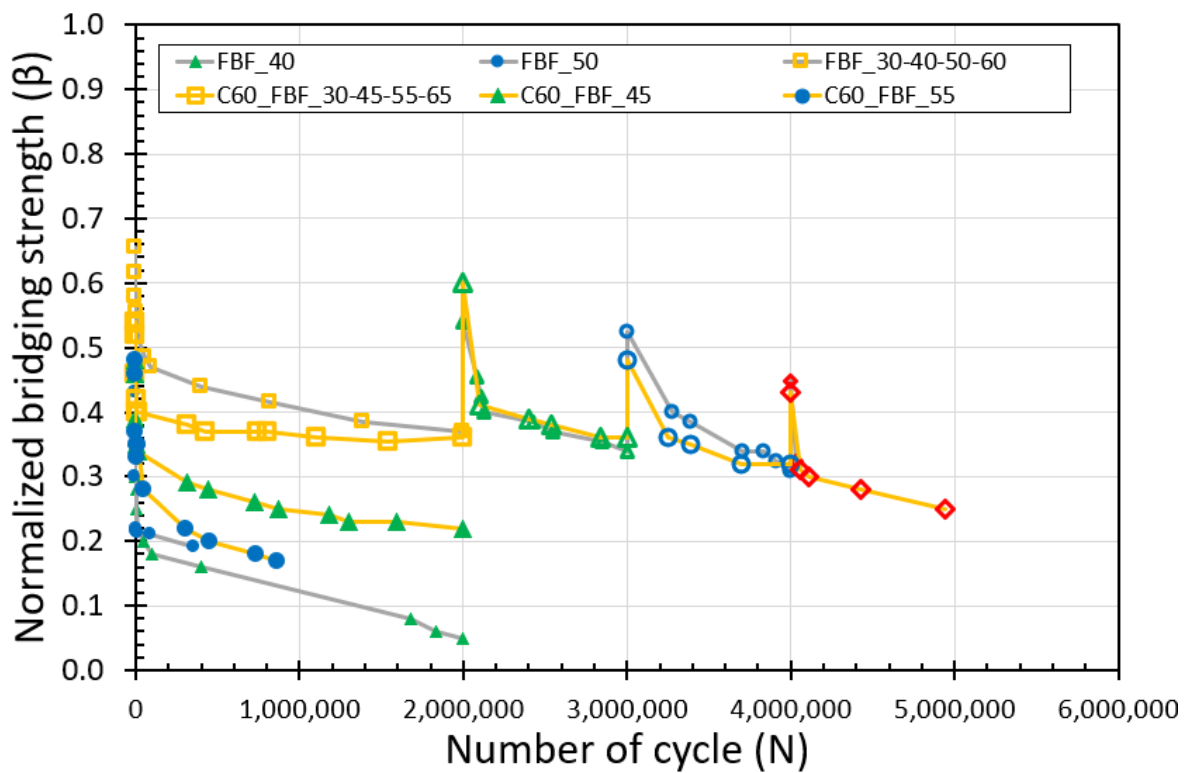
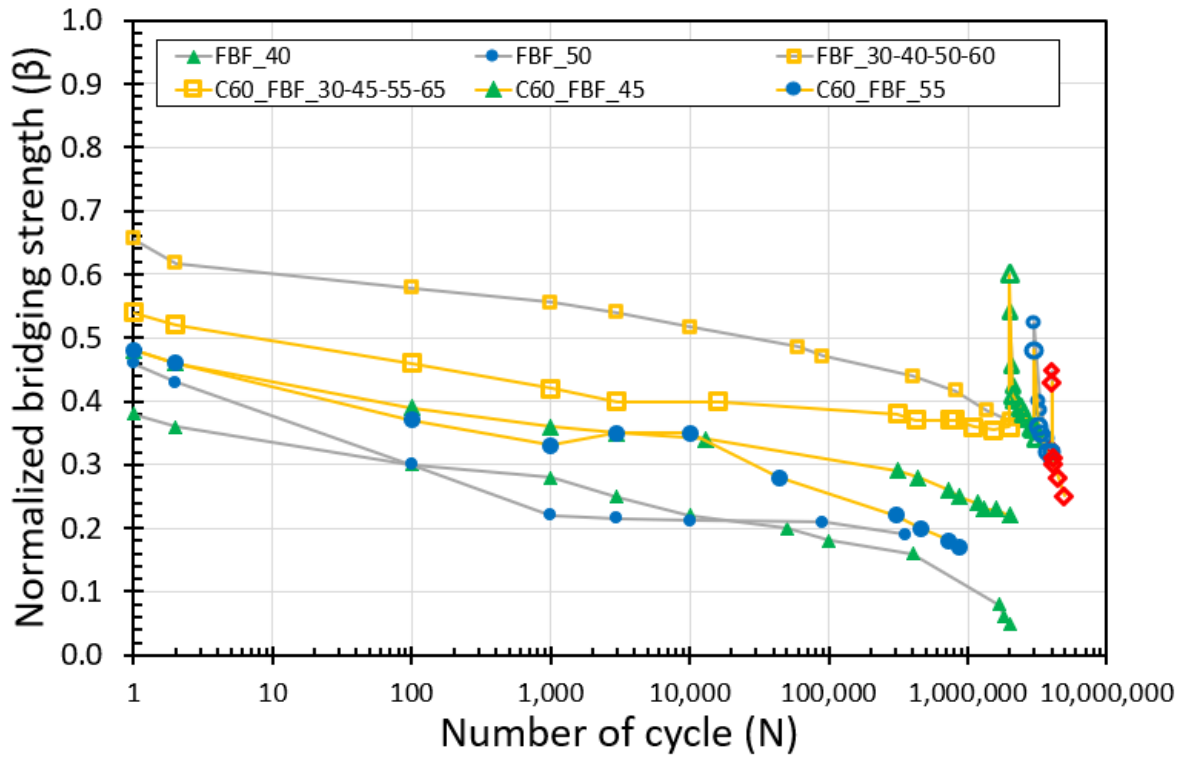


Fig. 6.75 Normalized crack-bridging strength degradation versus maximum rebar strain under various flexural fatigue load level.



(a) Normal scale



(b) Logarithmic scale

Fig. 6.76 Normalized crack-bridging strength degradation over the fatigue life under various flexural fatigue load level for higher concrete strength effect.

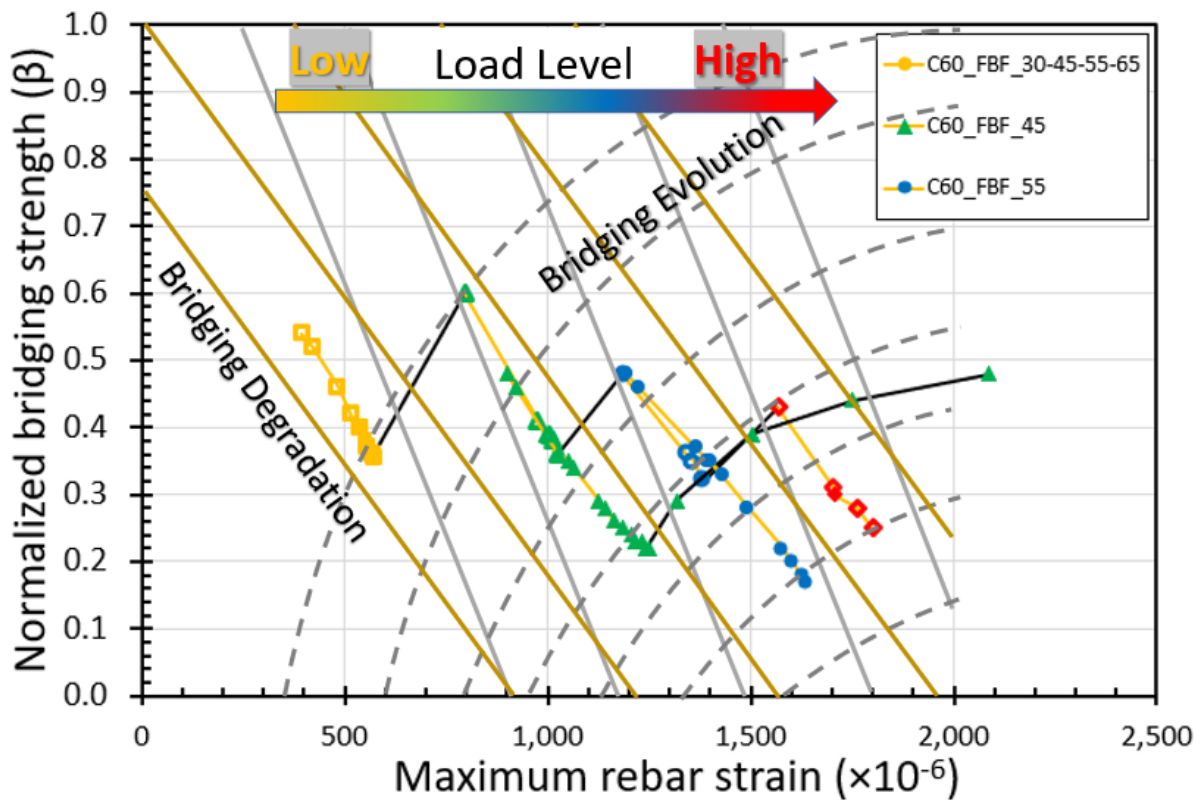
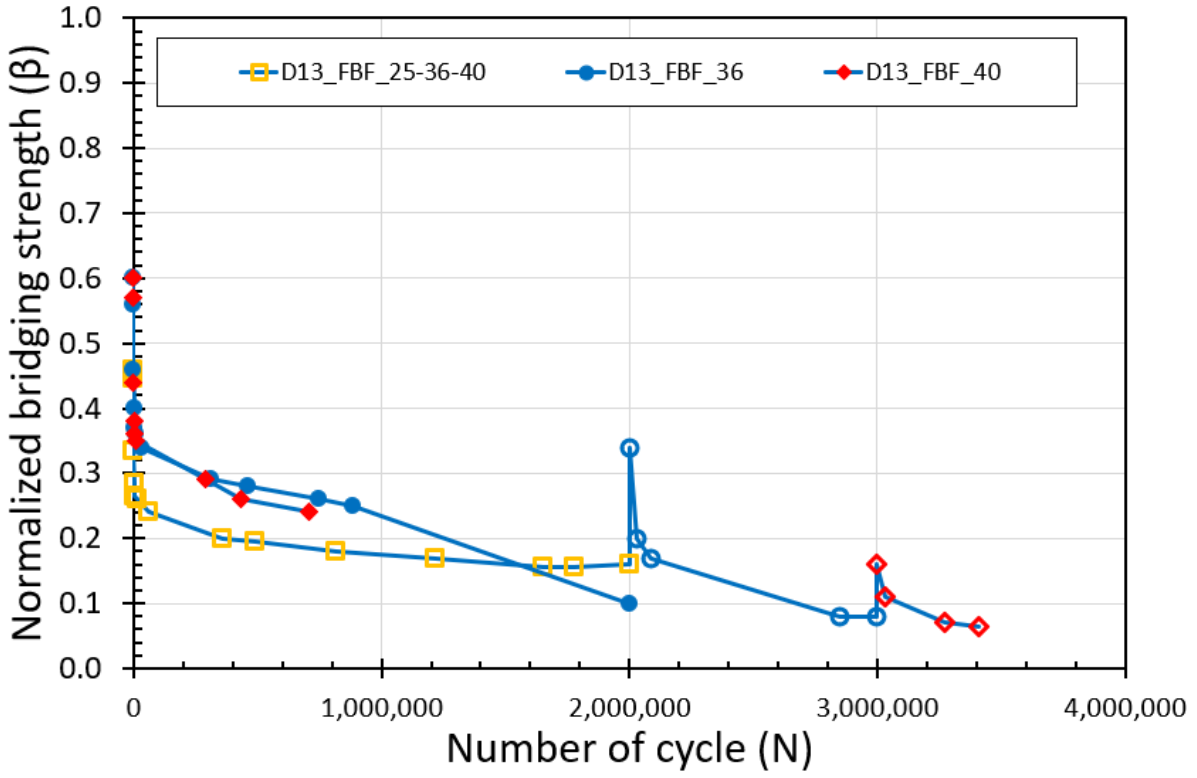


Fig. 6.77 Normalized crack-bridging strength degradation and evolution diagram versus maximum rebar strain under various flexural fatigue load level.

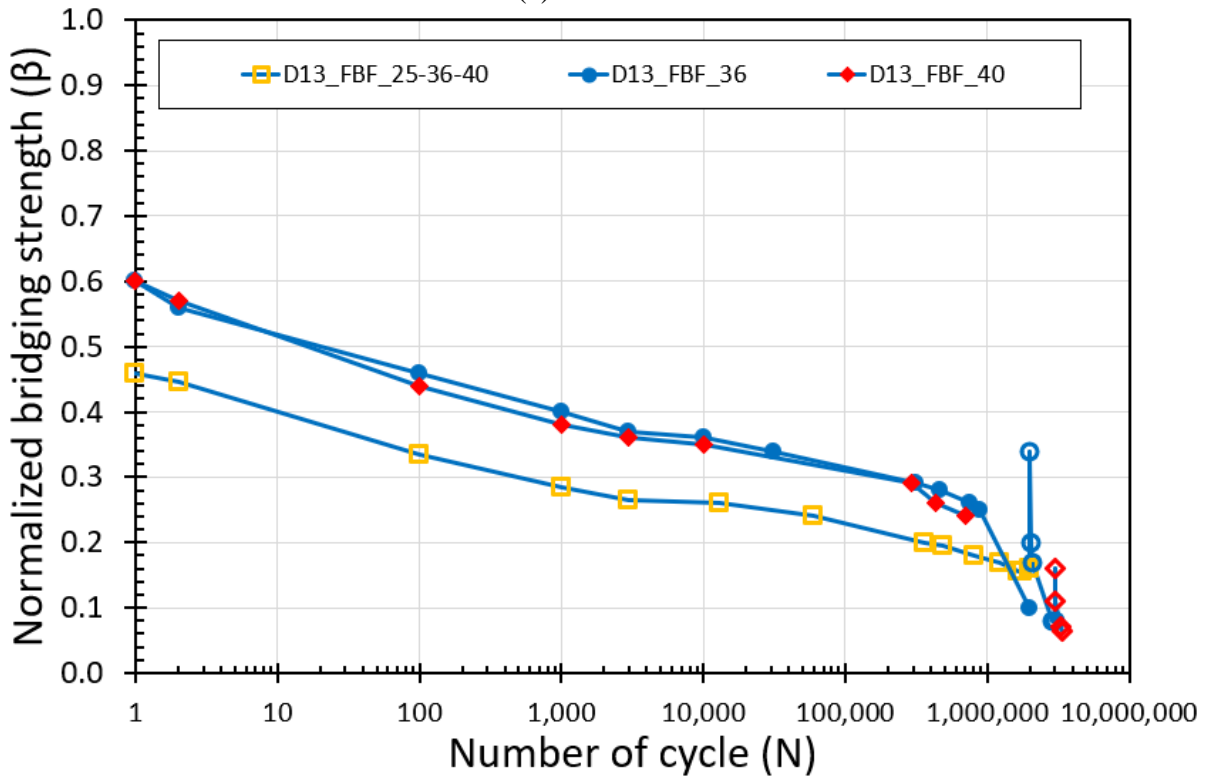
6.4.3.2 Reinforcement Ratio Effect

The ordinary rebar lower reinforcement ratio influenced a lower structural stiffness of the tested beams with longer crack length across the section of beams and accelerating the evolution rate of the rebar strain levels over the fatigue life, as indicated in section 6.4.1.2. Using the inverse analysis method, the crack-bridging strength was evaluated for over the fatigue life under single and variable flexural load levels, capturing the degradation and evolution mechanism by applying fatigue load and monotonically increasing the load level respectively for D13_FBF_25-36-40, D13_FBF_36, and D13_FBF_40 SFRC structural beams, as shown in Fig. 6.78. Besides, The proposed crack-bridging strength degradation and evolution model had plotted versus the maximum rebar strain evolution, as shown in Fig. 6.79. The results showed that the degradation mechanism has a constant linear relationship over a wide range of fatigue load levels regarding the maximum rebar strain level evolution for the lower reinforcement ratio as well as the normal reinforcement ratio from the first and second series, as shown in Fig. 6.79. As cycles progress, the repeated cyclic loading leads to crack growth that would lead to loss of bond between the matrix and the fibers, as well as increasing in rebar strain level, simultaneously. Besides, the evolution mechanism of the crack-bridging strength has a linear relationship over fatigue life with a decreased slope for a higher fatigue load level regarding the maximum rebar strain level evolution depending on the damaged level, as shown in Fig. 6.79 as inclined solid black lines. As increasing the fatigue load level monotonically, new fibers would contribute to bridging the growth of the cracks with the old fibers that had a certain damaged level at the fiber-matrix interface, leading to an increase in the crack-bridging strength.

A comparison process was carried out between the first, second, and third series regarding the evaluated crack-bridging strength degradation and evolution model, aiming to capture the effect of the lower reinforcement ratio effect, as shown in Fig. 6.80. It is obvious from Figure 6.80 that, the degradation rate of the evaluated crack-bridging strength is almost as same as for the normal reinforcement ratio structural beams of the first and second series because of no enhancement on bond strength at the fibers-matrix interface. Also, the evolution rate of the evaluated crack-bridging strength is almost as same as the second series, as it only depends on the damaged level at the fiber-matrix interface. As a result, a new diagram of degradation and evolution of crack-bridging strength was proposed regarding the evolution of the maximum rebar strain for the lower reinforcement ratio, as shown in Fig. 6.81. The proposed diagram in Figure 6.81 has the same bridging evolution as circle curved lines and lower bridging degradation as blue parallel inclined lines because of a higher evolution rate of rebar strain level.



(a) Normal scale



(b) Logarithmic scale

Fig. 6.78 Normalized crack-bridging strength degradation over the fatigue life under various flexural fatigue load level.

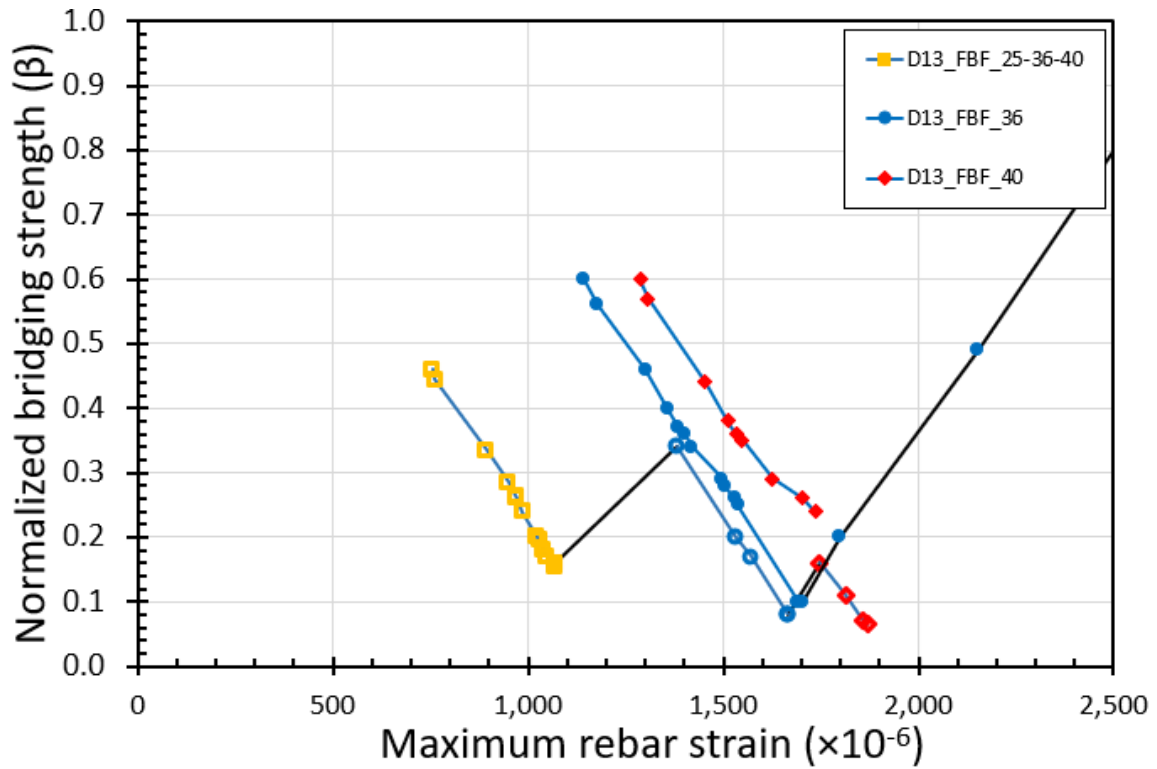
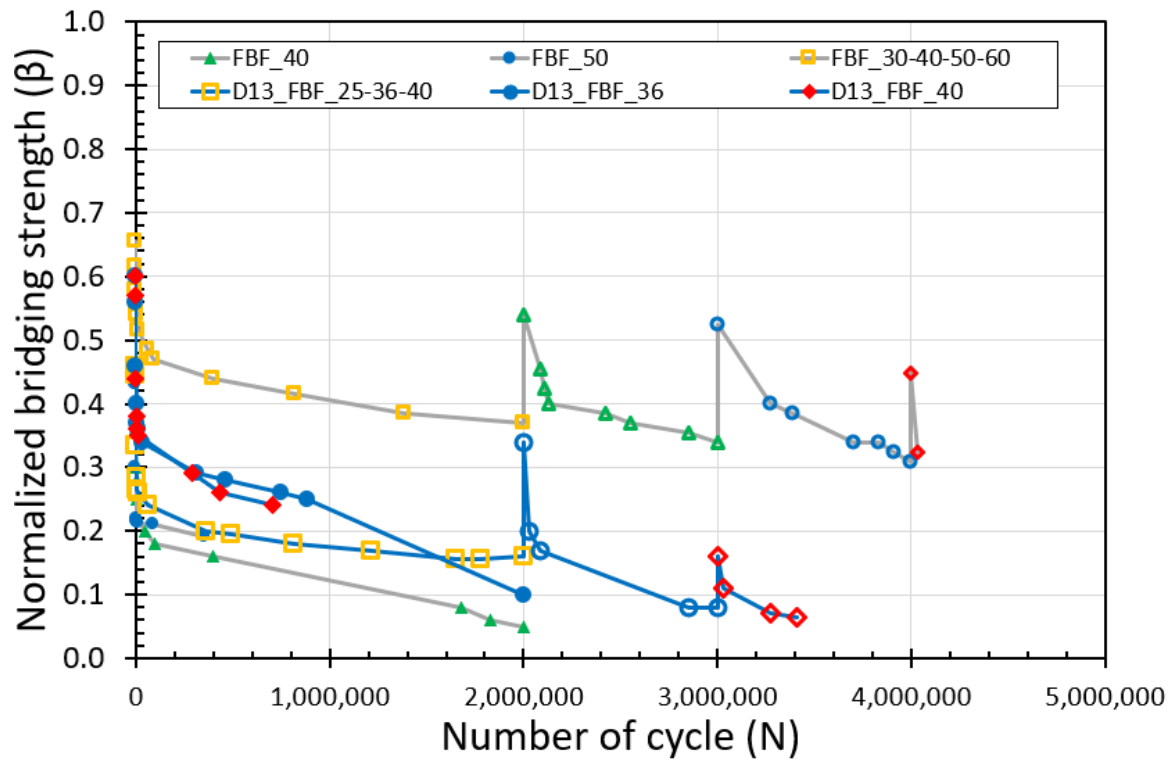
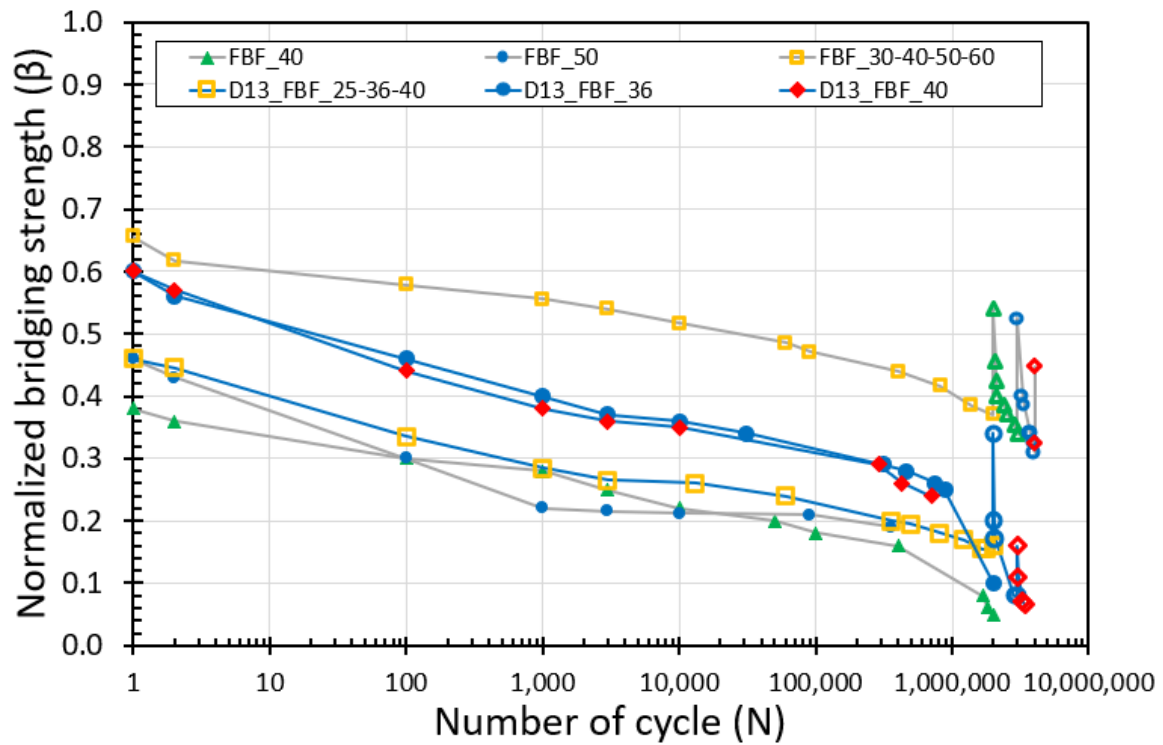


Fig. 6.79 Normalized crack-bridging strength evolution versus maximum rebar strain under various flexural fatigue load level.



(a) Normal scale



(b) Logarithmic scale

Fig. 6.80 Normalized crack-bridging strength degradation over the fatigue life under various flexural fatigue load level for lower reinforcement ratio effect.

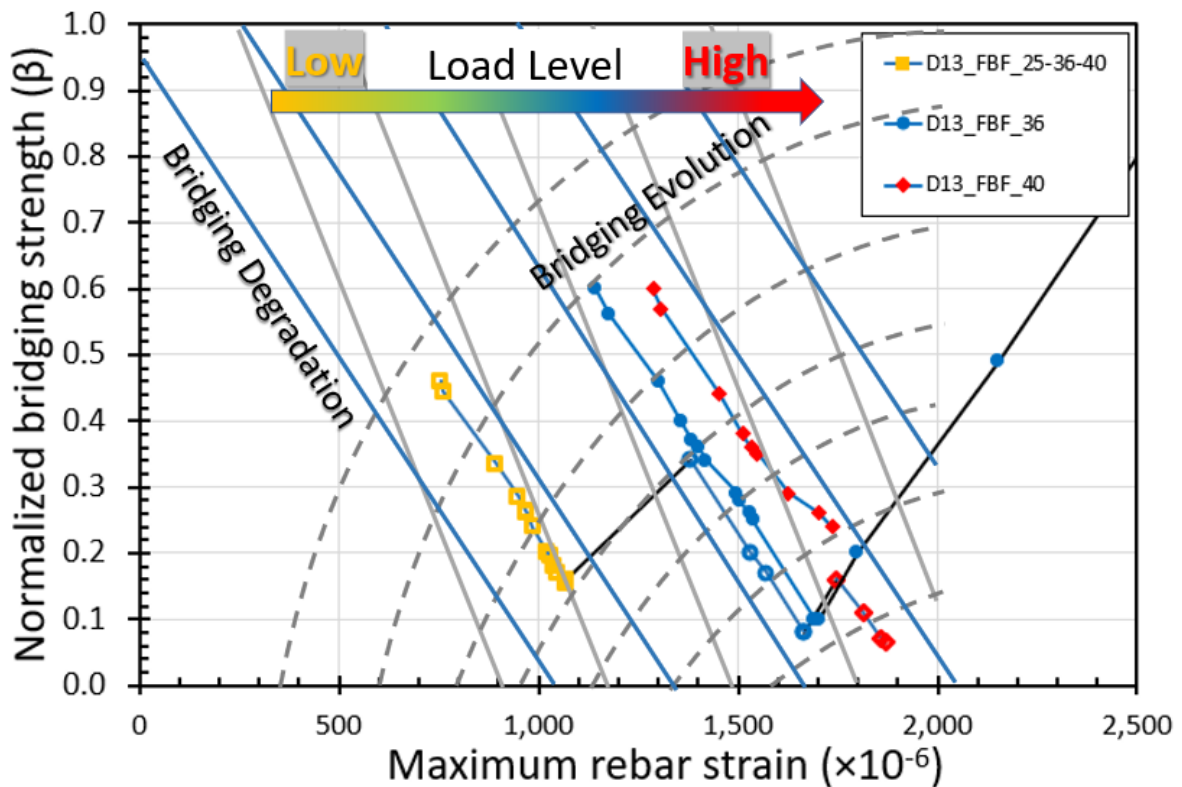


Fig. 6.81 Normalized crack-bridging strength degradation and evolution diagram versus maximum rebar strain under various flexural fatigue load level.

6.5 Conclusion

The research work of the third series presented in this chapter aimed at capturing the effect of higher concrete compressive strength and lower ordinary reinforcement ratio on the evaluated degradation and evolution crack-bridging strength model provided by hooked-end steel fibers over the whole fatigue life of structural beams under cyclic loading with a variable flexural load until a rupture fatigue failure. An inverse analysis method is used to derive a degradation and evolution model for crack-bridging strength from the experimental fatigue response of SFRC structural beams. The degradation and evolution model was captured for a wide range of fatigue load levels and the main conclusions that can be drawn from this work are as follow:

1. The good fit obtained with the proposed degradation and evolution model for the crack-bridging strength provided by steel fibers confirms the applicability of inverse analysis assuming a plane strain distribution since no strain redistributions in the compressive stress zone was observed.
2. The normalized crack-bridging strength was proposed for each different level of flexural fatigue stress of each SFRC structural beam during fatigue life, which monotonically changes by increasing or decreasing regarding the changing in the fatigue load level over the fatigue life and regarding the evolution of rebar strain level.
3. The normalized crack-bridging strength tends to monotonically degrade under flexural fatigue loading over the fatigue life and regarding the evolution of rebar strain level for all fatigue stress levels because of loss of bond strength at fiber-matrix interface.
4. The normalized evaluated crack-bridging strength increased by increasing the flexural load level monotonically with the contribution of the new fibers in bridging the cracks inside the tensile stress zone and the contribution of the old fibers with the desired damage level, with almost the decreased inclination regarding the fatigue stress level and the bond damage level at the fiber-matrix interface.
5. Increasing the concrete compressive strength enhanced the bond strength at fibers-matrix interface with lower mid-span deflection and rebar and concrete strain levels of SFRC structural beams under flexural cyclic loading over the fatigue life for a variable fatigue load levels.

6. The increased concrete compressive strength resulted in a lower degradation rate of the evaluated crack-bridging strength regarding the evolution of maximum rebar strain. However, the evolution rate of the crack-bridging strength did not influence the increased concrete compressive strength.
7. decreasing the ordinary bars reinforcement ratio degraded the structural stiffness of the tested beams with higher crack length at the cracked section and accelerated rate of rebar strain evolution of SFRC structural beams under flexural cyclic loading over the fatigue life for a variable fatigue load levels.
8. The decreased reinforcement ratio resulted in a lower degradation rate of the evaluated crack-bridging strength regarding the evolution of maximum rebar strain. However, the evolution rate of the crack-bridging strength did not influence the decreased reinforcement ratio.
9. Using the proposed degradation and evolution diagram of crack-bridging strength with the material constitutive laws based on direct sectional analysis calculations over of fatigue loading cycles, an accurate full design and assessment procedure for the whole fatigue life of SFRC beams under flexural fatigue loading is expected to be accomplished.

Chapter 7

7 Fiber's Volume and Shape Effect on The Crack-bridging Strength Degradation of SFRC Structural Beams under Flexural Fatigue

7.1 Introduction

This chapter examines the influence of double hooked-end steel fibers on the flexural static and fatigue experimental response, and evaluate the crack-bridging strength induced by double hooked-end steel fibers with a lower volume fraction of 1.0 % and higher concrete compressive strength on the reinforced concrete structural beams subjected to flexural static and cyclic loading under various fatigue stress levels. Furthermore, by the end of this chapter, a diagram of the crack-bridging strength degradation and evolution over the fatigue life of SFRC structural beams under flexural cyclic loading regarding fatigue stress levels would be proposed based on inverse analysis calculation methods and to be compared with the one proposed for the second and third series in chapter five and six. As well, this chapter aims to understand the mechanism of crack-bridging strength evaluated from the inverse analysis calculation method based on changing the fiber's shape and volume fraction under various fatigue load levels. The experimental program for the fourth series of SFRC beams on the structural scale under static and fatigue loading conditions is presented. Firstly, the experimental static and fatigue response data of structural beams are captured to be compared with the first, second, third series, and to be used in the execution of the inverse analysis calculation method under various flexural fatigue load level. Finally, the crack-bridging strength is evaluated for the fourth series for the changed double hooked-end steel fibers with 1.0 % volume fraction and higher concrete compressive strength of SFRC structural beams under various flexural fatigue load level over their fatigue life varying from a low, medium, to

high fatigue stress level and compared with the proposed crack-bridging strength degradation and evolution diagram of the second and third in the last two chapters.

7.2 Experimental Program

The experimental program of the fourth series consisted of SFRC specimens that are tested on both material and structural scale, with a higher compressive strength of 0.40 water to cement ratio with double hooked-end steel fibers and volume fraction of 1.0 % as compared with the previous series as described in chapter five and six.

Material level tests were carried out to evaluate the material properties such as concrete compressive strength (f_{cm}), concrete first cracking tensile strength (f_{ct}), concrete modulus of elasticity (E_c). As well, the steel fiber reinforced concrete's tension softening curve and fracture energy (G_f) were evaluated using dog-bone specimens under direct tensile test, as listed in [Table 7.1](#). The results of the tests are presented and evaluated with particular emphasis on the effects of steel fibers on the fatigue response of the beams.

Besides, structural scale tests consist of six structural scales SFRC beams with 1.0% double hooked-end steel fibers (Dramix 5D 65/60 BG), having the same cross-section area of 150 mm x 200 mm and a span length (l) of 1700 mm with 300 mm of constant moment loading span (s) and effective depth (d) of 170 mm, each had two conventional rebars with a nominal diameter (D) of 16 mm and using a higher concrete compressive strength of 82.68 MPa for the effective use of the double hooked-end fiber that has higher tensile strength, as listed in [Table 7.2](#). two SFRC structural beams had been tested under flexural static test for measuring the flexural capacity of the SFRC structural beams, but the other four SFRC structural beams had been tested under flexural cyclic loading with various load levels ranging from low to high fatigue stress level, as listed in [Table 7.2](#). The experimental program was set to capture the flexural static and fatigue response of SFRC structural beams reinforced with double hooked-end steel fibers. The beams were instrumented to measure the rebar strains, surface concrete strains, and mid-span deflections having testing configurations as shown in [Fig. 4.1](#). The structural beams are labeled as follows: 5D_FB δ _ Ω , in which, 5D reflects that the fiber type, F reflects that the material of the beam is SFRC, δ reflects whether the flexural test is under static or fatigue loading, and Ω reflects the maximum fatigue load in kN for fatigue loading test and the beam's number for static loading test.

Table 7.1: Test program of material scale specimens.

| Specimen | Description | SFRC |
|------------------------------------|-----------------------------------|-------|
| Cylinder (D =100 mm & L=200 mm) | Number of specimens | 9 |
| | Compressive strength (MPa) | 82.68 |
| | Young's modulus (GPa) | 33.33 |
| Cylinder (D =150 mm & L=150 mm) | Number of specimens | 7 |
| | Tensile strength (MPa) | 4.35 |
| Dog-bone specimen | Number of specimens | 3 |
| | Equivalent tensile strength (MPa) | 4.17 |
| | Fracture energy (N/mm) | 20.7 |

Table 7.2: Test program of structural scale beams.

| Beam ID | Test type | Fiber volume (%) | Flexural capacity (kN) | Min. fatigue load (kN) | Max. fatigue load (kN) | Fatigue life | Residual flexural capacity (kN) |
|-----------|-----------|------------------|------------------------|------------------------|------------------------|--------------|---------------------------------|
| 5D_FBS_1 | Static | 1.0 | 106.8 | – | – | – | – |
| 5D_FBS_2 | Static | 1.0 | 105.4 | – | – | – | – |
| 5D_FBF_30 | Fatigue | 1.0 | – | 5.0 | 30.0 | 2,000,000 ↑ | 116.6 |
| 5D_FBF_45 | Fatigue | 1.0 | – | 5.0 | 45.5 | 2,000,000 ↑ | 119.4 |
| 5D_FBF_56 | Fatigue | 1.0 | – | 5.0 | 56.0 | 602,201 | – |
| 5D_FBF_67 | Fatigue | 1.0 | – | 5.0 | 67.0 | 234,067 | – |

Note: The structural beams were tested under a four-point bending static and fatigue test. The vertical arrow in fatigue life cells indicates the end of the fatigue test without fatigue failure.

7.2.1 Material and Mix Proportion

The concrete used in the fourth series for SFRC was a high-grade concrete with a target mean strength (f_{cm}) of 80 MPa. The following materials were used in the fourth series in mixing and production of concrete: cement, coarse aggregate, fine aggregate, steel fibers, water, and superplasticizer. Table 7.3 shows the mix proportions of SFRC. Ordinary portland cement meeting the Japanese industrial standards (JIS) was used as the binding material, with a specific

gravity of 3.15. Crushed coarse and fine aggregates were used with maximum aggregate sizes of 13.0 mm and 4.75 mm and specific gravities of 2.66 and 2.65, respectively. The steel fibers were gradually sprinkled into the mix by hand to a 1.0% volume fraction of the full SFRC volume, and care was taken to obtain a homogenous and workable mixture. Furthermore, a high-performance air-entraining water-reducing agent (Types: SP8SV and SBsX3) were used in SFRC in a range of 0.75% per each to the weight of the cement for each concrete mix as a superplasticizer to obtain an average 120 mm slump value. The water to cement ratio was 40% for SFRC. Finally, the SFRC batches were introduced into their molds and compacted, then the specimens were removed from the molds after 3 days and cured for 28 days.

The steel fibers, that were used in the fourth series, were Dramix 3D 65/60 BG with an aspect ratio of 65, a length of 60 mm, having a rounded cross-section with a smooth surface, and a double hooked-end shape as shown in Fig. 7.1. The properties of steel fibers are given in Table 7.4 and with an ultimate tensile strength of 2300 MPa as reported by the manufacturer.

Table 7.3: Mix proportion of the first series for NC and SFRC.

| Ingredient | Amount (kg/m ³) |
|--------------------------------|-----------------------------|
| Portland cement | 463 |
| Water | 185 |
| Fine aggregate | 999 |
| Coarse aggregate | 669 |
| Double hooked-end steel fibers | 78.5 |
| Superplasticizer | 5.05 |

Table 7.4: Hooked-end steel fibers properties.


| Description | Value |
|------------------------------|--|
| Length (mm) | 60 |
| Diameter (mm) | 0.9 |
| Density (kg/m ³) | 7850 |
| Tensile strength (MPa) | 2300 |
| Aspect ratio | 65 |
| Fiber shape |  |



Fig. 7.1 Double hooked-end steel fibers.

The structural beams were reinforced with tensile reinforcement consisted of two 16 mm nominal diameter bars, resulting in a tensile reinforcement ratio of 1.34 percent for the fourth series. The longitudinal reinforcing bars were hot rolled deformed steel bars, all from the same batch with a nominal yield strength of 382.5 MPa and Young's modulus of 200 GPa. The structural beams were designed to be failed under flexural loading conditions, using an appropriate concrete cross-section of structural beams to resist the shear stress during loading without any need for shear reinforcement and compression reinforcement.

7.2.2 Specimens

The test program consisted of several SFRC specimens that were tested on both material and structural scales for the fourth series test set. The fourth series aims to capture the flexural static and fatigue response of SFRC over the fatigue life under variable fatigue load levels using 1.0% volume fraction of double hooked-end steel fibers with a high concrete compressive strength as compared with the first, second, and third series. Besides, as same as the previous series the execution of the inverse analysis calculations method requires detailed information about the material properties of SFRC, as a result, material level tests were carried out to identify the materials constitutive laws, targeting finally in the evaluation of the degradation and evolution in the crack-bridging strength over the fatigue life of SFRC structural beams.

Six structural scale beams reinforced with two ordinary steel reinforcing bars and made of steel fiber reinforced concrete were tested under 4-points bending test monotonically and under cyclic loading with as same testing set up as the first series. The details of the tested structural beams of the fourth series are discussed in [Table 7.2](#). All structural beams have a rectangular cross-section with a dimension of 150 x 200 mm and a length of 2000 mm. The structural beams were tested under flexural loading test with a span length (l) of 1700 mm, with 300 mm of constant moment loading span (s), and an effective depth (d) of 170 mm as shown in [Fig.](#)

4.1. All structural beams were reinforced with two ordinary steel reinforcing bars with a diameter (D) of 16 mm with a tensile longitudinal reinforcement ratio of 1.34 percent to be failed inside the constant moment region in a flexural failure mode as shown in Fig. 4.6.

The concrete material properties were determined for the fourth series by testing several specimens at a material scale as shown in Fig. 7.1. Test configurations of the fourth series for measuring concrete compressive strength (f_{cm}), concrete modulus of elasticity (E_c), and concrete first cracking tensile strength (f_{ct}) was as same as the first series, as shown in Figs. 4.8, and 4.9. Measuring the steel fiber reinforced concrete's tension softening curve and fracture energy (G_f) of the double hooked-end steel fibers were carried out by testing the dog-bone specimens under the uniaxial tensile test, as listed in Table 7.1 and shown in Fig. 7.4. Finally, three SFRC specimens with an hourglass-shaped – dog-bone – geometry, as shown in Fig. 7.2, having dimensions with length of 500 mm and thickness of 150 mm with a decreased width from 230 mm to 150 mm were tested under uniaxial tensile test to measure the steel fiber reinforced concrete's post-cracking behavior and fracture energy (G_f) (Ali 2018), as shown in Fig. 7.3. The tensile stresses presented in the analysis are in terms of equivalent tensile stress, which is the resultant of the applied tensile load divided by the cross-sectional area at the most narrow cross-section with a dimension of 150 x 150 mm, as listed in Table 7.1.



Fig. 7.2 Formwork of the dog-bone SFRC specimen.

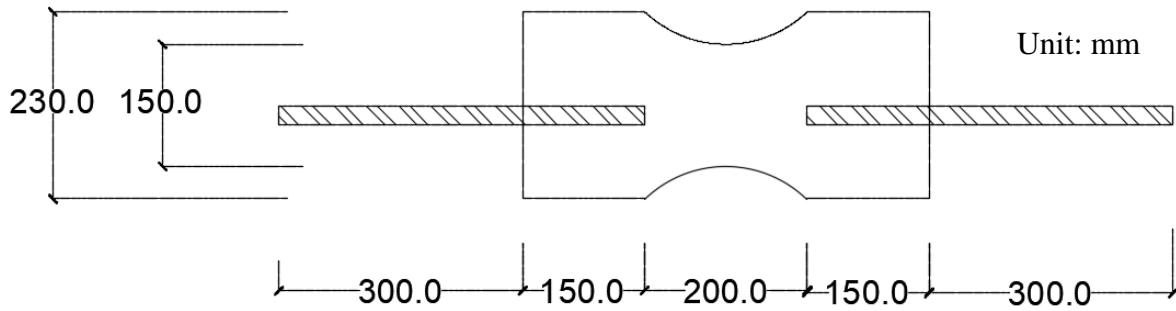


Fig. 7.3 Geometry of the dog-bone SFRC specimens.

Before casting, one 19 mm 8.8 grade steel bar was placed 150 mm within each end of the formwork. The level and alignment of the threaded rods were checked from the inside of the form and then locked in place using a nut on the outside of the wall of the formwork, as shown in Figs. 7.2 and 7.3.

The specimens were cast horizontally in wooden molds using the procedure outlined in (EN14651 2007). That is, the center portion of the mold was filled to approximately 90% of the height of the specimen, which was then followed by pouring of the ends. The molds were externally compacted using a steel rod manually. The use of internal vibration units on SFRC should be avoided to ensure uniform distribution of the fibers through the cross-section of the sample. Before testing, the dogbone specimens were lightly painted white to facilitate the crack detection process.

7.2.3 Testing Setup and Instrumentations

The dogbone specimens were tested in an Instron servo-hydraulic universal testing machine (UTM). The steel bars protruding from the specimens were connected to the UTM by nuts. There is significant conjecture within the literature on whether the ends of uniaxial tension test specimens should be fixed (non-rotating) at each end, pinned at each end such that the sample can freely rotate about a center point, or fixed at one end and pinned at the other (Rots and de Borst 1989, van Mier 1997). Ideally, the specimen should be fixed at each end; however, in laboratory experiments, the heterogeneity of the material, the specimen manufacturing, and the gripping and alignment of the specimen in the loading frame are not easily controlled and may result in inducing secondary bending moments within the specimen. To avoid this, in this study one end was fixed while the other was fitted with a universal joint to eliminate any residual tension that may develop during the gripping process.

To measure the COD, linear variable displacement transducers (LVDTs) were attached to the North, South, East, and West faces of the specimen to monitor the average vertical deformation during loading until rupture. The gauges were centered on the specimen and had gauge lengths of 200 mm, as shown in Fig. 7.4. Loading was applied using displacement control, initially at a rate of 0.06 mm/min until the formation of the dominant crack. After cracking, the rate was increased to 0.6 mm/min with additional rate increases introduced as the test progressed until a complete separation of the tested specimen, as shown in Fig. 7.5.



Fig. 7.4 The dog-bone SFRC specimens with the attached transducers.

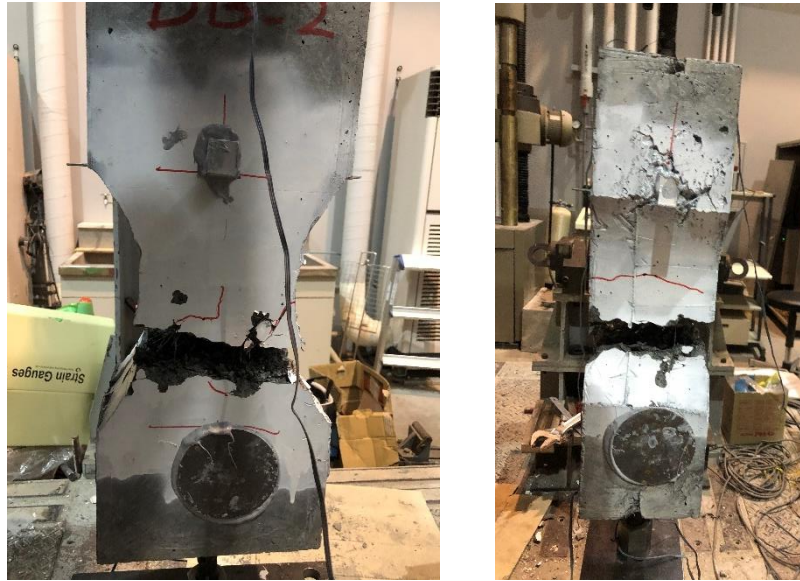


Fig. 7.5 The dog-bone SFRC specimens tensile rupture.

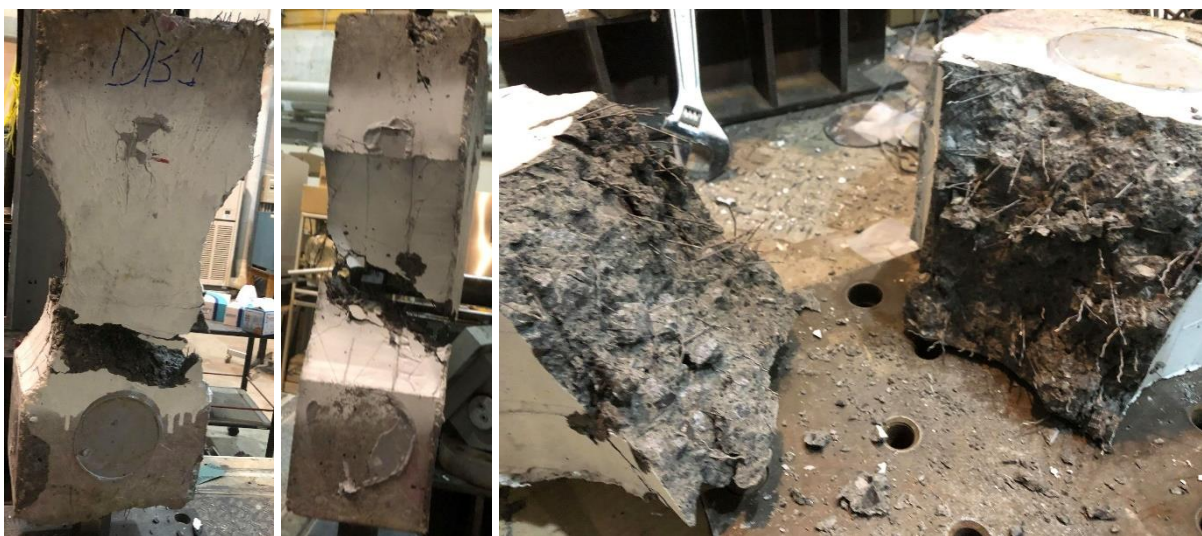
7.3 Experimental Results

In the fourth series, several specimens were tested under the material and structural level to capture and analyze the static and fatigue response of SFRC beams reinforced with 1.0 % volume fraction of double hooked-end steel fibers and high strength concrete under flexural loads and to evaluate the crack-bridging strength degradation and evolution over the fatigue life under variable fatigue load levels. Firstly, a direct uniaxial tensile test was carried out on dog-bone SFRC specimens to calculate the initial crack-bridging strength – tension softening curve – to be used in sectional analysis calculations. Secondly, two SFRC structural beams were tested under static loading to determine the ultimate flexural load capacity and confirm a constant crack-bridging strength during the monotonical application of load without any degradation through the utilization of the inverse analysis calculation method. As well, the static flexural experimental response was captured in terms of mid-span deflection, rebar, and concrete strain levels, and flexural capacity to be compared with the first series to emphasize the difference in crack-bridging between the single and double hooked-end steel fibers. Finally, four structural beams were tested under flexural fatigue loading under different stress levels ranging from low to high-stress levels. The following sections discuss the test results of the individual beams. As a result, the results of inverse analysis calculations are presented in the following section in a model of degradation of the crack-bridging strength induced by double hooked-end steel fibers over the fatigue life of different flexural fatigue stress levels.

7.3.1 Dog-bone SFRC Specimens under Uniaxial Tensile Loading

The crack-bridging strength – or the tension softening curve – is a fracture mechanics parameter that describes post-cracking behavior, represents the fracture energy (G_f) of SFRC in the tensile stress zone, and is used in the sectional analysis calculations to understand the response of structural beams to loading. It is obtained from the material scale uniaxial tensile test results obtained in the direct tensile test of dog bone SFRC specimens until complete rupture as shown in Figs. 7.4 and 7.5 (Ali 2018). In this section, the results and test observations of the uniaxial tension test specimens are reported. For the fourth series, three dogbone specimens were cast and tested with a given label “DB_specimen number”. The specimen dimensions and test arrangements are shown in Figure 7.3, and 7.4 and listed in Table 7.1.

To determine the crack opening displacement, the average of the four transducers is taken; no further manipulation of the data is required as all cracking, for all tested specimens, occurred within the gauged length. The tensile stresses presented in the analysis are in terms of equivalent tensile stress, which is the resultant of the applied tensile load divided by the cross-sectional area at the most narrow cross-section. It is worthy of note that the response of SFRC structural elements is typically concerned with the behavior of members with small crack widths of less than 2 mm, however, the response at significantly large crack widths of larger than 2 mm is mainly of academic interest. The relationship of equivalent tensile stress versus the crack opening displacement for the three dog-bone specimens until a complete separation of the two pairs of the dog-bone specimens is shown in Figures 7.6 and 7.7.



(a) The rupture of specimen DB_01.



(b) The rupture of specimen DB_02.



(c) The rupture of specimen DB_03.

Fig. 7.6 The dog-bone SFRC specimens tensile rupture.

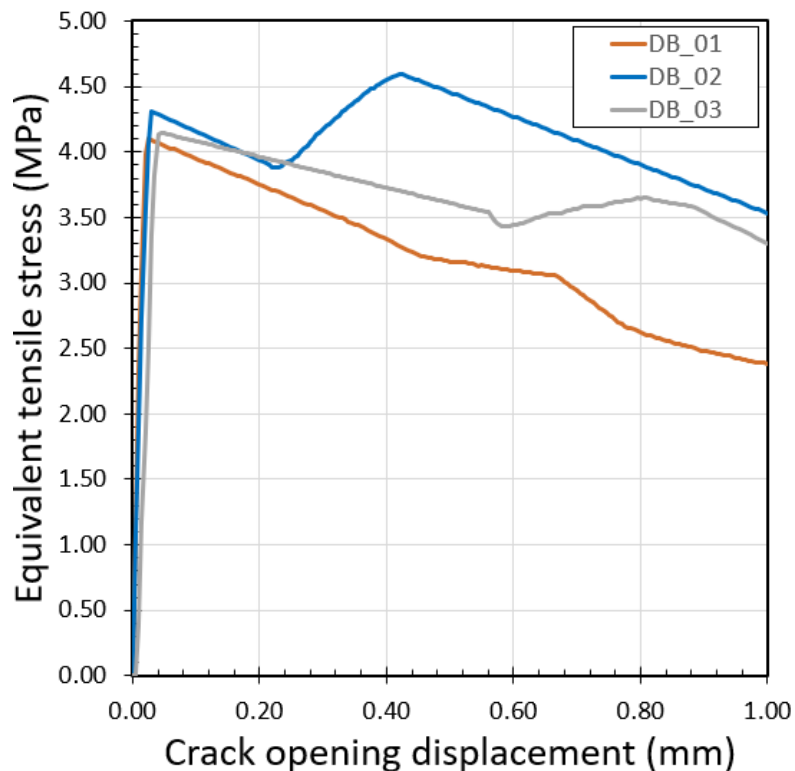
Initially, upon loading, the specimens behaved approximately linear elastically and it was assumed that the deformation was uniformly distributed over the gauge length. Close to the peak stress, the overall response became softer due to micro-cracking, as shown in Fig. 7.7(a). The fracture processes of all specimens consisted of three key stages. The first stage involved the formation of a hairline crack of less than 0.05 mm in width. This corresponded to the end of the linear elastic range of the tensile stress-strain response and a significant reduction in stiffness was observed. Once initiated, the dominant crack propagated along the weakest cross-section along a surface, as shown in Fig. 7.6. At this stage, the peak stress had been achieved. This was shortly followed by a sharp reduction in load, coinciding with a significant opening

of the crack, as the elastic strain energy stored in the specimen and testing rig was recovered. After the crack had stabilized, the load again increased as the fibers became, as shown in Fig. 7.7(b). In some circumstances, such as DB_02, secondary cracks propagated out of a primary crack as the crack opening displacement increased, as shown in Fig. 7.6(b). Interestingly in dog bone specimen DB_02, the stress-induced within the engaged fibers exceeded the previously attained peak matrix strength, and multiple cracking was observed, as shown in Fig. 7.6(b).

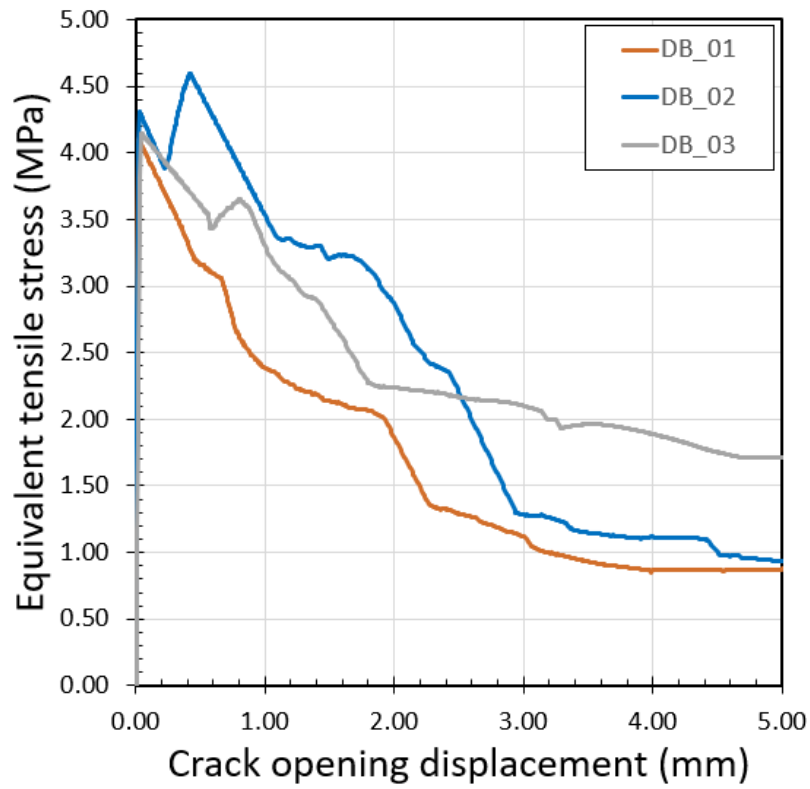
Soon after cracking had stabilized, it was clear that the concrete provided no direct contribution to the tensile strength of the dogbone specimens and that the strength was due to the fibers alone. That is, no tensile stresses were transmitted through the crack via aggregate interlock or friction. It should be noted that the concrete tensile strength continues to function in the load-carrying capacity of the specimen through the bond and development of interfacial shear strength between the fibers and surrounding concrete matrix. The long tail of the curves reflects the progressively crack-bridging strength of the SFRC specimens, which was averaged for the three dog bone SFRC specimens and summarized in Eq. (7.1), as shown in Fig. 7.8.

$$\sigma = f_{st} \quad (MPa) \quad \text{for } \omega = 0.0$$

$$\sigma = 4.1244 \exp(-0.291 * COD) \quad (MPa) \quad \text{for } 0 < \omega \leq 5 \text{ mm} \quad (7.1)$$



(a) The initial part of equivalent tensile stress versus average crack opening displacement.



(b) The equivalent tensile stress versus average crack opening displacement.

Fig. 7.7 The dog-bone SFRC specimens crack-bridging strength.

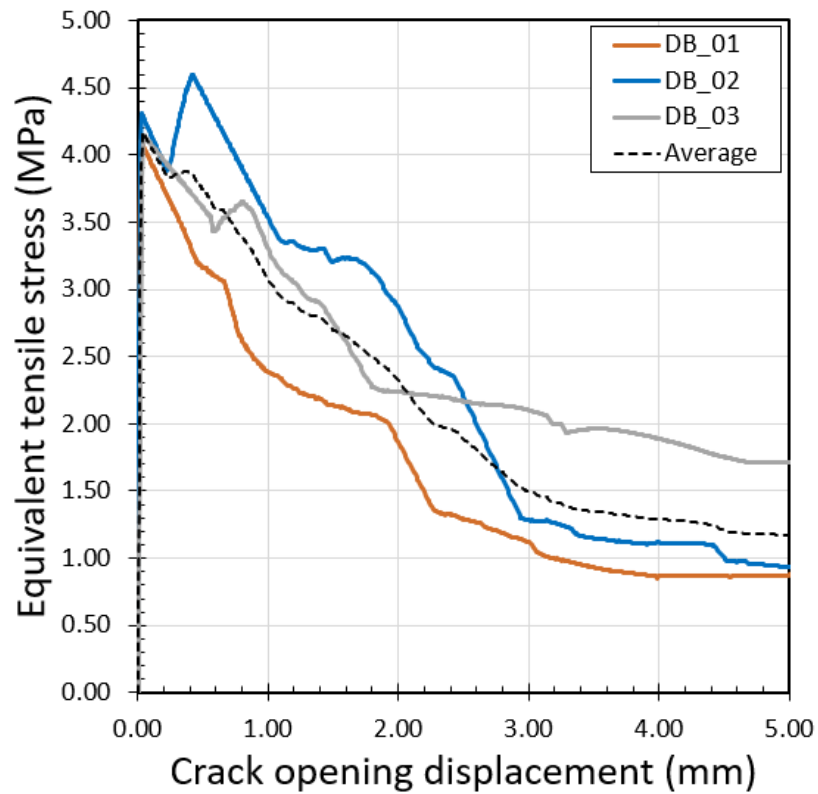


Fig. 7.8 Average crack-bridging strength of dog bone specimens.

7.3.2 Static Flexural Loading of SFRC Structural Beam

The static flexural test was carried out on two SFRC structural beams reinforced with double hooked-end steel fibers and high strength concrete, aiming to estimate the flexural capacity of SFRC structural beams, identify the yielding load, confirm the experimental structural response of SFRC beams against the calculated response obtained by direct sectional analysis calculations using the initial crack-bridging strength over the whole loading process, and capturing the effect of fiber's hook level on the flexural static response by comparing that series with the first series. The SFRC structural beams of 5D_FBS_01 and 5D_FBS_02 exhibited a flexural capacity of 106.8 kN and 105.4 kN respectively and the flexural load corresponding to yielding of the rebar in the constant moment region was 82.0 kN and 83.6 kN respectively, as shown in Figs. 7.9, 7.10, 7.14, and 7.15, with an average crack spacing – or reference length (L_R) – of 40 mm, as shown in Figs. 7.9, and 7.14.

As explained in section 4.3.4, the surface concrete strain was measured at several sections on both faces of the SFRC structural beams within the constant moment region. Further, rebar strains were measured at three points on the two rebars and the load versus rebar strain curves for the specified locations inside the constant moment region are given in Figures 7.11, and 7.16 for beams 5D_FBS_01 and 5D_FBS_02 respectively. After testing, the experimental strain distributions were plotted for these three sections of the SFRC structural beam to estimate the ultimate compressive concrete strain at the extreme compression fiber and the N.A. position. Figures 7.12, and 7.17 show the strain distribution at midspan on the front face of the beam (R150), showing the strain evolution for both rebar and concrete throughout the application of flexural monotonic loading until tensile ductile failure of the steel rebars followed by concrete crushing in the compression zone, as shown in Figs. 7.9, and 7.14 achieving a flexural capacity of 106.8 kN and 105.4 kN for beams 5D_FBS_01 and 5D_FBS_02 respectively.

All experimental measurements within the constant moment region of the three sections, in which rebar strain gauges were attached, between the front and back faces, were averaged and plotted versus flexural load (shown as solid lines) to reflect the average experimental response of structural beams for beams 5D_FBS_01 and 5D_FBS_02 respectively, as shown in Figs. 7.13, and 7.18. The applied load was divided into increments and the computation was performed incrementally. During load application, the rebar strain, the ultimate compressive concrete strain, and the N.A. position are calculated from the direct sectional analysis calculations using the initial crack-bridging strength that was derived from the direct uniaxial

tensile test of dog bone SFRC specimens obtained in the previous section on the material scale over the whole loading process, as explained in Section 3.3. Finally, the calculated results using the method of sectional analysis for the region before the rebar yielding point are also plotted in [Figures 7.13, and 7.18](#) and shown as dotted lines. The calculated flexural response of SFRC structural beam from the sectional analysis calculation method achieves a good fit with the experiment flexural response for both SFRC structural beams 5D_FBS_01 and 5D_FBS_02 respectively, as shown in [Figs. 7.13, and 7.18](#). The initial crack-bridging strength – that was obtained from the material scale tests of the uniaxial tensile test – was obtained in the sectional analysis calculations with a constant amount of fracture energy without and degradation during the whole load increments application of the static test, having a good fitting between the resulted calculated flexural response and the experimental flexural response, as shown in [Figs. 7.13, and 7.18](#).



Fig. 7.9 Beam 5D_FBS_01 after failure under static loading.

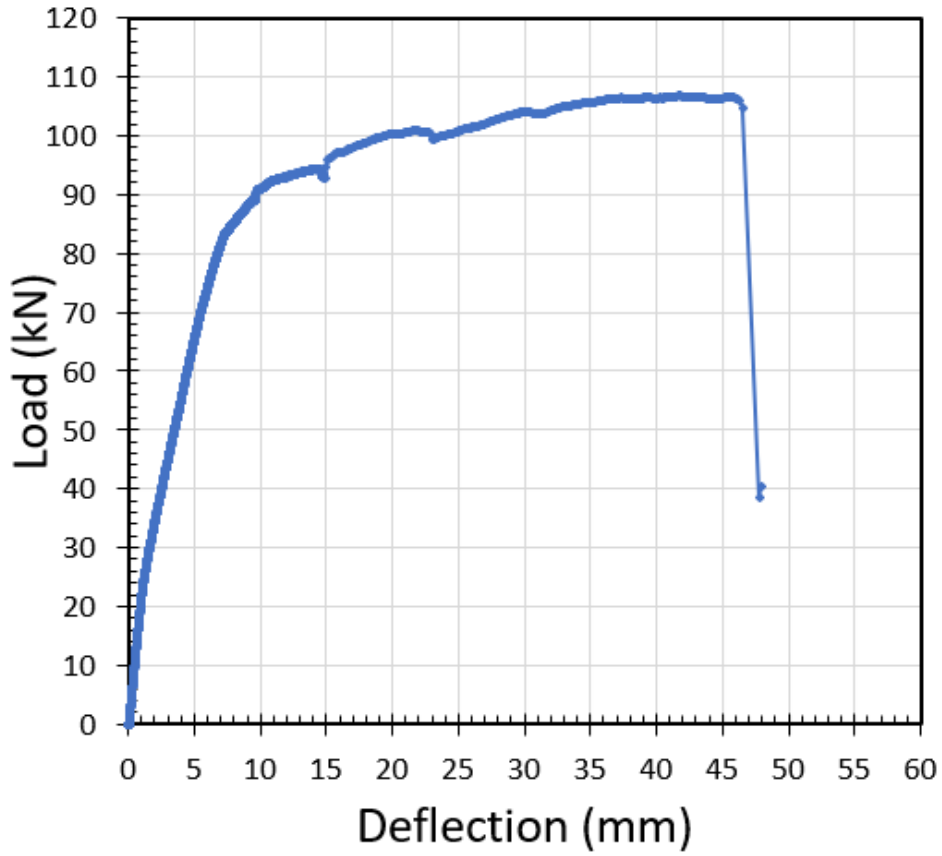


Fig. 7.10 Load versus deflection under static loading for beam 5D_FBS_01.

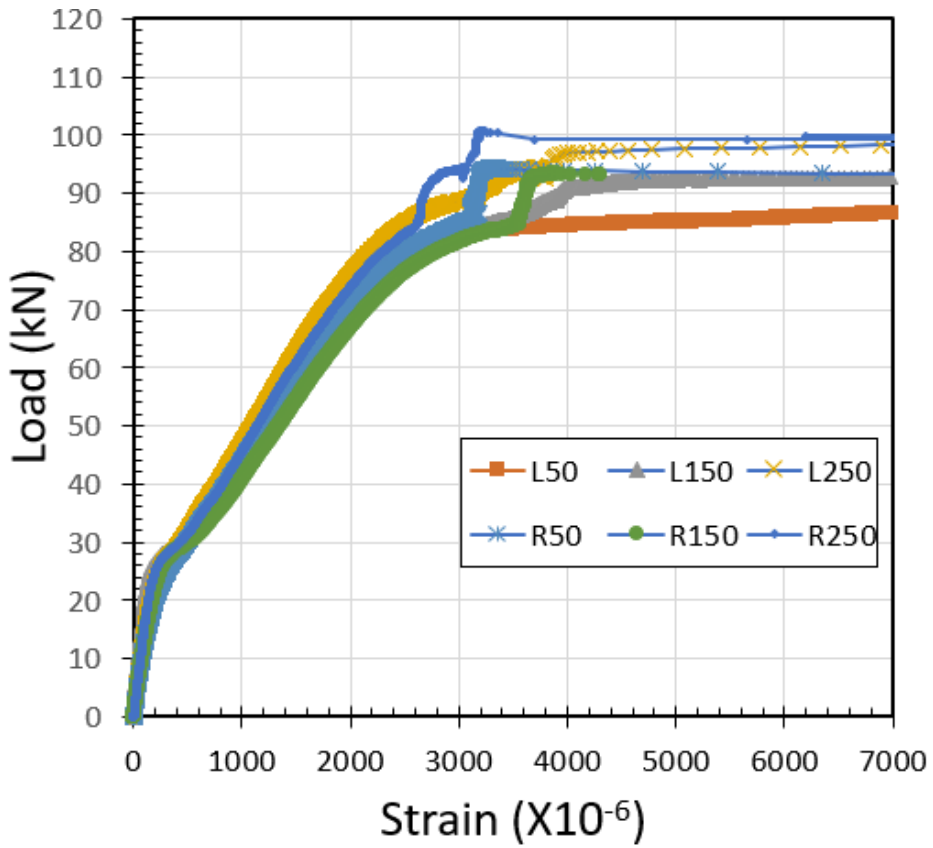


Fig. 7.11 Load versus rebar strain under static loading for beam 5D_FBS_01.

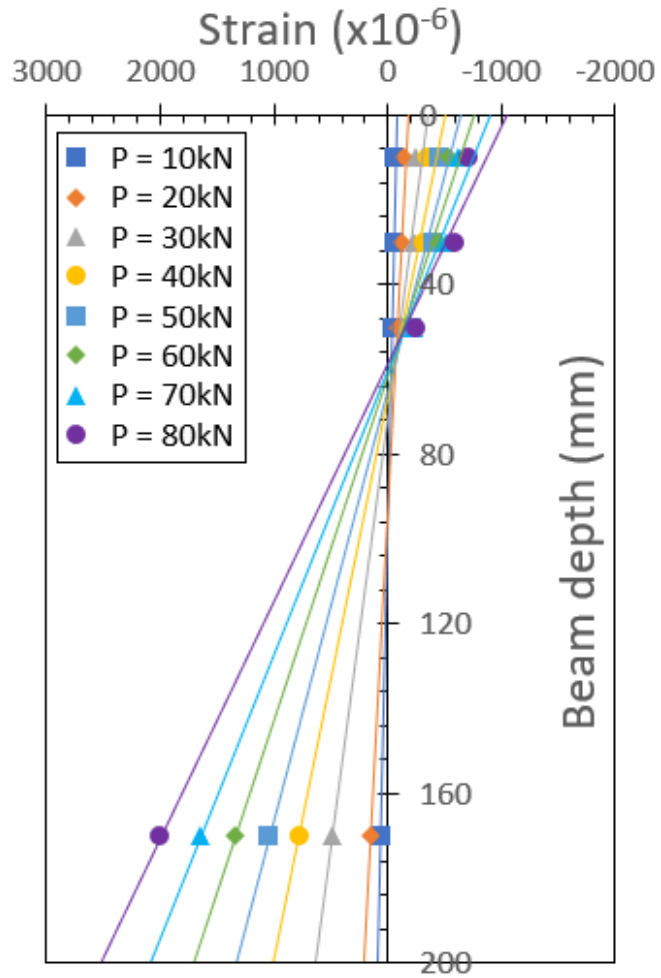


Fig. 7.12 Strain distribution of the mid-span section for beam 5D_FBS_01.

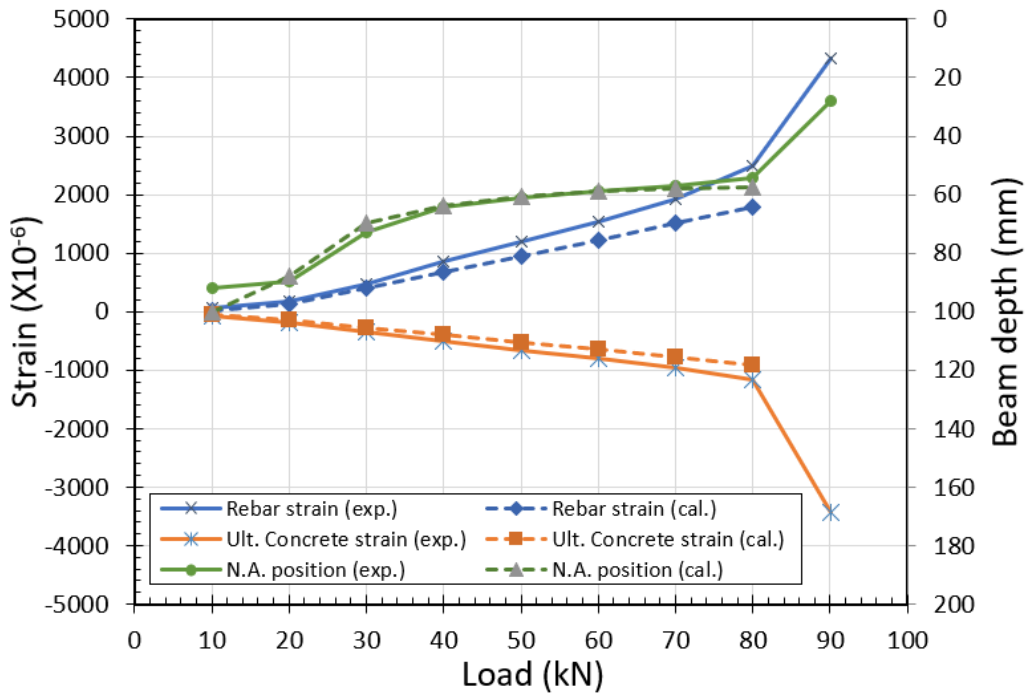


Fig. 7.13 Experimental versus calculated response under static loading for beam 5D_FBS_01.



Fig. 7.14 Beam 5D_FBS_02 after failure under static loading.

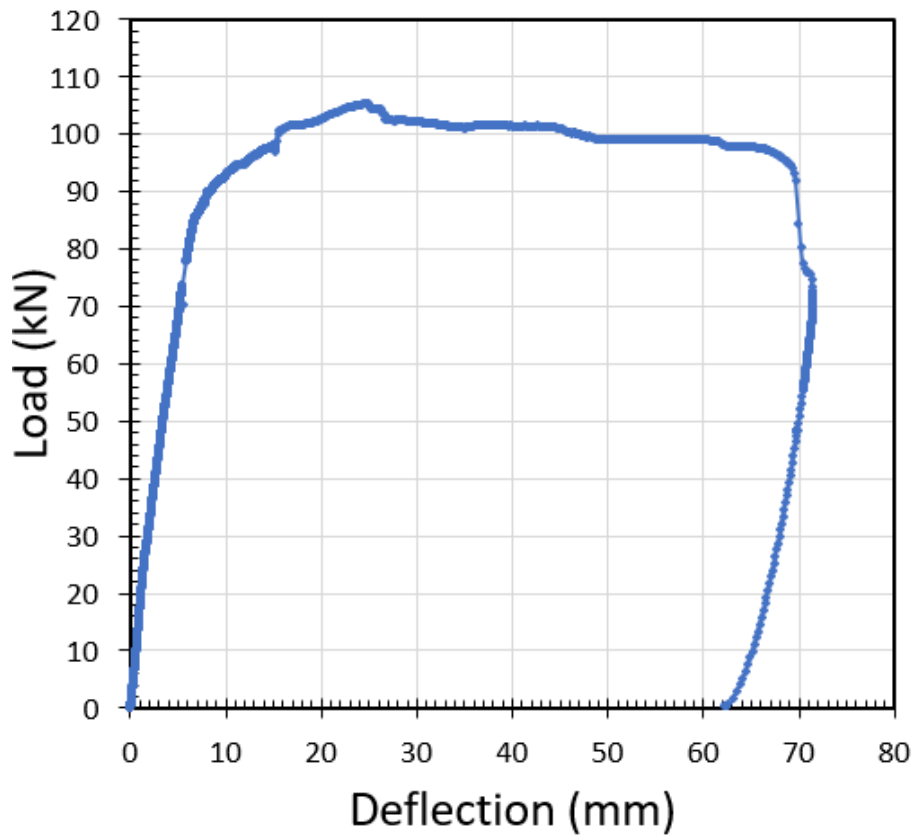


Fig. 7.15 Load versus deflection under static loading for beam 5D_FBS_02.

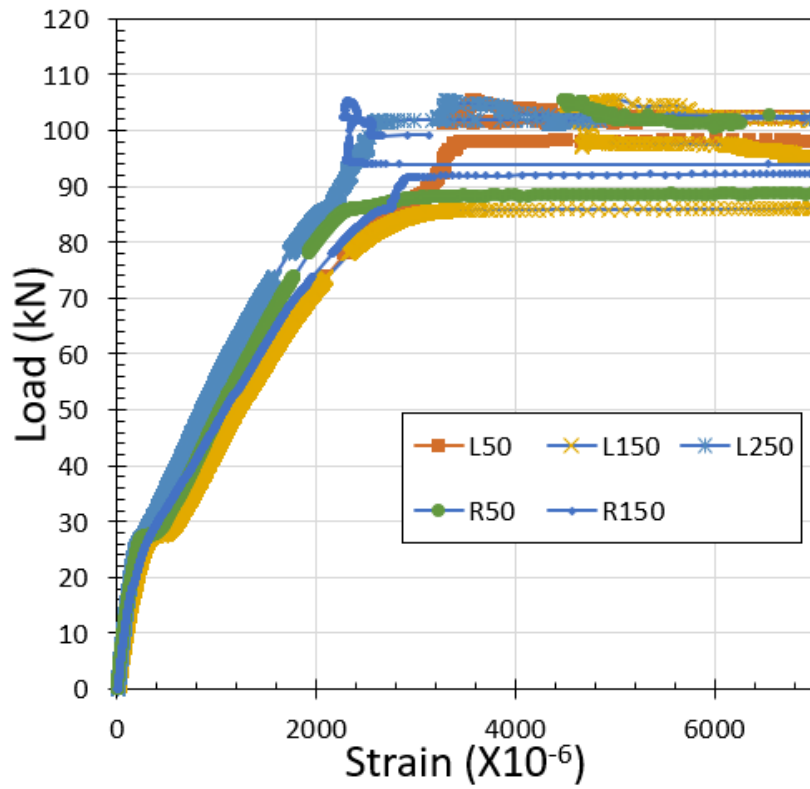


Fig. 7.16 Load versus rebar strain under static loading for beam 5D_FBS_02.

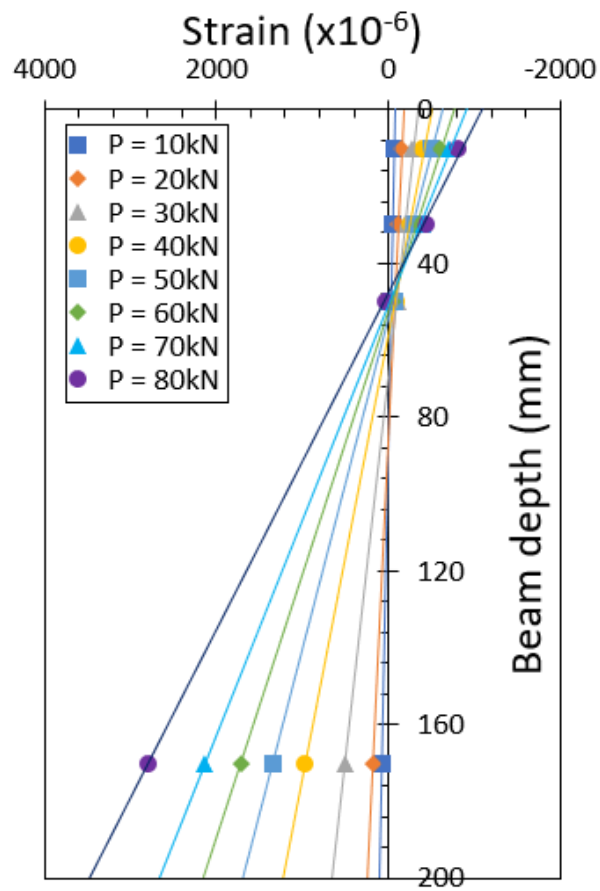


Fig. 7.17 Strain distribution of the mid-span section for beam 5D_FBS_02.

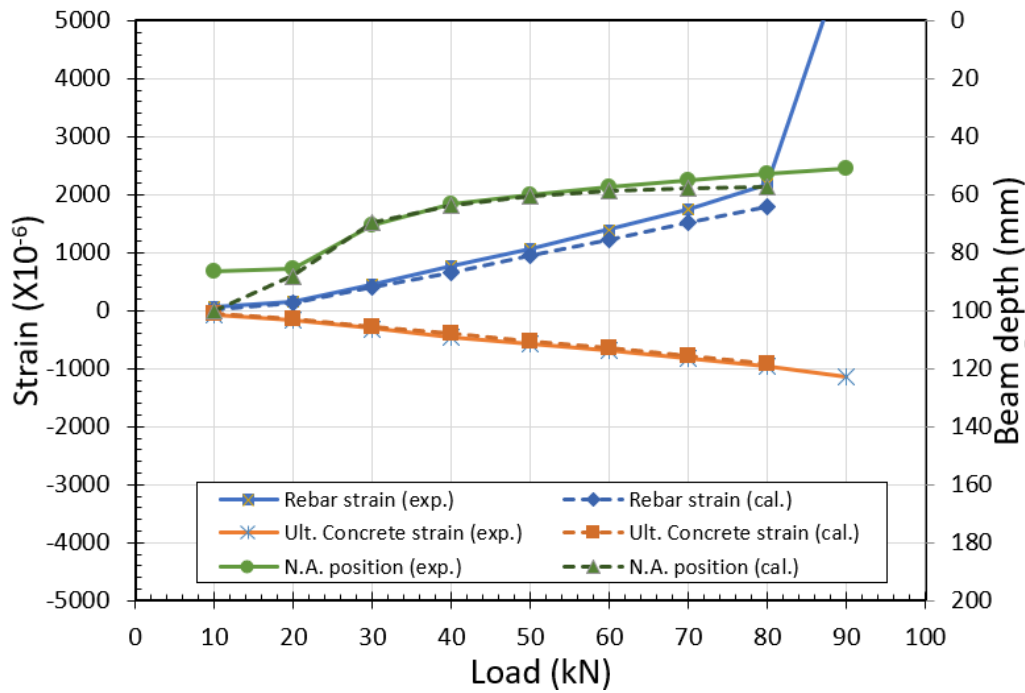


Fig. 7.18 Experimental versus calculated response under static loading for beam 5D_FBS_02.

7.3.3 Fatigue Flexural Loading of SFRC Structural Beams

A flexural cyclic loading test was carried out on four SFRC structural beams for measuring the flexural fatigue response to evaluate the degradation and evolution of crack-bridging strength over fatigue life using the inverse analysis method, as explained in section 3.4.3. Also, residual flexural capacity after completion of two million cycles was evaluated in the case of beams that survived without fatigue failure, as summarized in Table 7.2. During fatigue loading, as the number of loading cycles increases, an evolution of both the rebar and concrete strain was observed for the SFRC structural beams, resulting in increasing mid-span deflection and crack length and width and decreasing structural stiffness as noted from the decrease of the inclination of the load-deflection curve and N.A. position, as illustrated in the following paragraphs, with an average crack spacing – or reference length (L_R) – of 40 mm, as shown in Figs. 7.19, 7.25, 7.31, and 7.35.

Beam 5D_FBF_30

For the low fatigue stress level ($S = 0.283$), one SFRC structural beam – 5D_FBF_30 – was tested under flexural cyclic loading with 5 kN as a minimum flexural load and 30 kN as a maximum flexural load, with the same maximum fatigue load level as one beam of the first series FBF_30 and one beam of the third series C60_FBF_30 where the fatigue response would be compared to capture the effect of the hooked level and the volume fraction of the fibers, as

shown in Fig. 7.19. Figure 7.20 shows the load versus mid-span deflection relationship over fatigue life under a low-stress level of flexural fatigue load showing an increase in mid-span deflection as cycles progress. Figure 7.21 shows the strain distribution at midspan on the front face of the beam (L150), showing the strain evolution for both rebar and concrete throughout the application of flexural cyclic loading until the end of fatigue life without any strain distribution in the compression stress zone. The average rebar strain within the constant moment region of 5D_FBF_30 is also plotted against the maximum and minimum flexural cyclic load for the three fatigue stress levels during the fatigue life, starting from the first flexural cyclic loading (N_1) and showing the evolution of average rebar strain, as shown in Fig. 7.22. After a complete of two million cycles of flexural loading, SFRC beam 5D_FBF_30 was subjected to residual flexural static tests to measure their residual capacity, as shown in Figs. 7.23 and 7.24. The result is listed in Table 7.2. Residual flexural capacity is a little different from the original capacity of the beams under static loading, even after the fatigue loading.

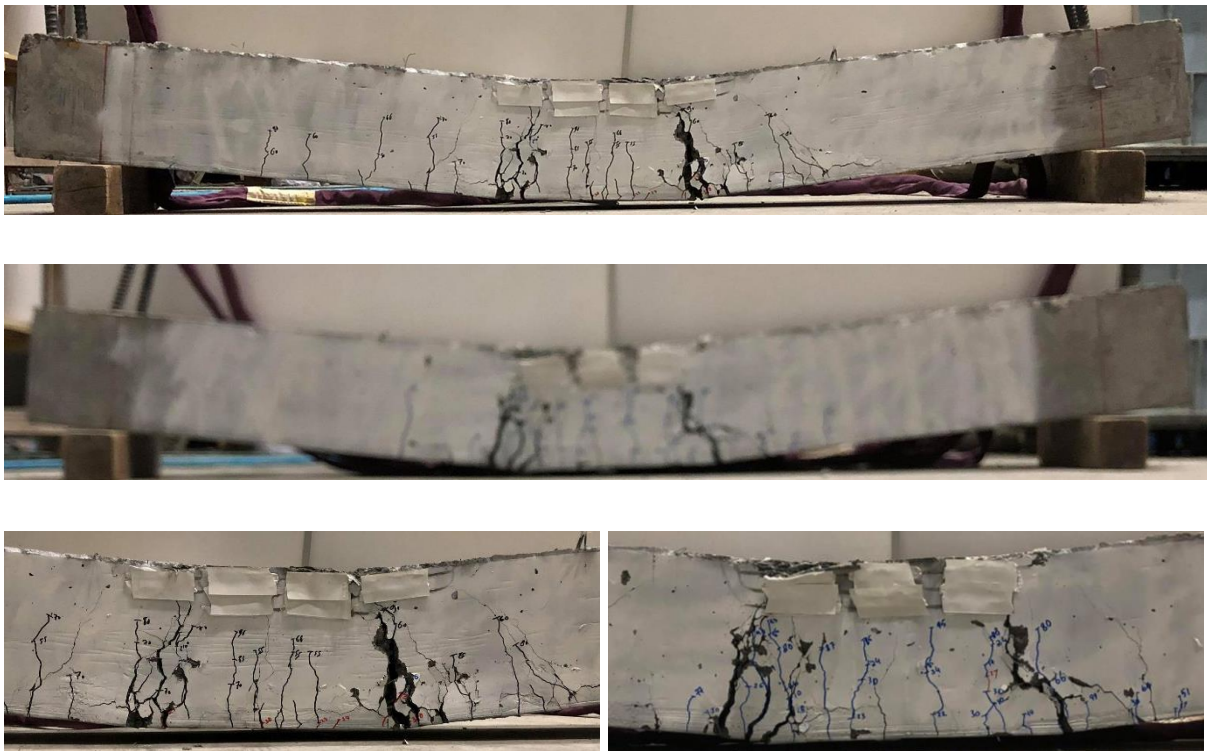


Fig. 7.19 Beam 5D_FBF_30 over fatigue life under flexural cyclic loading.

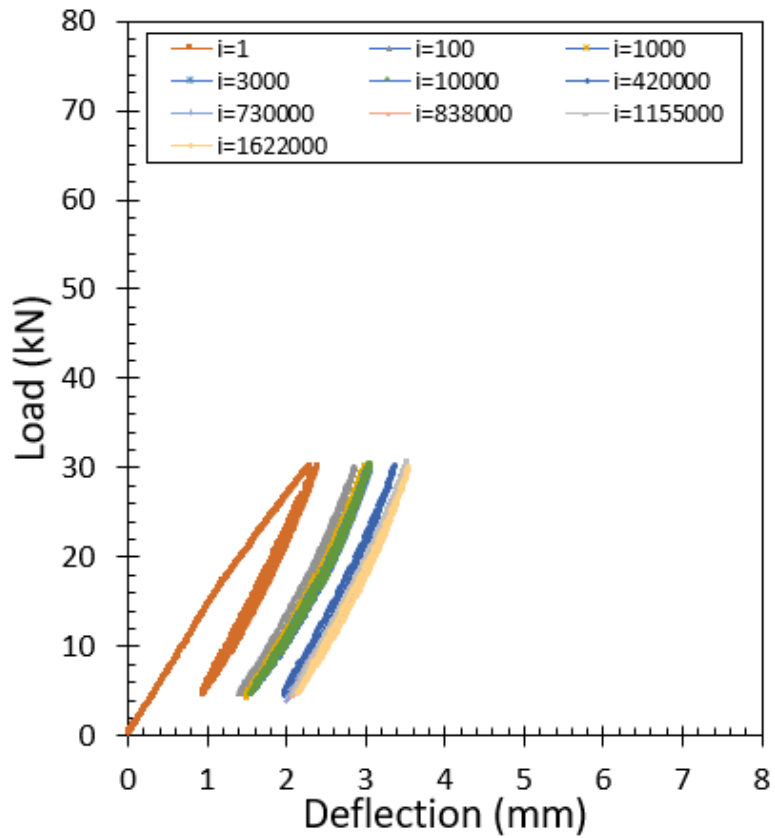


Fig. 7.20 Load versus deflection under flexural cyclic loading for beam 5D_FBF_30.

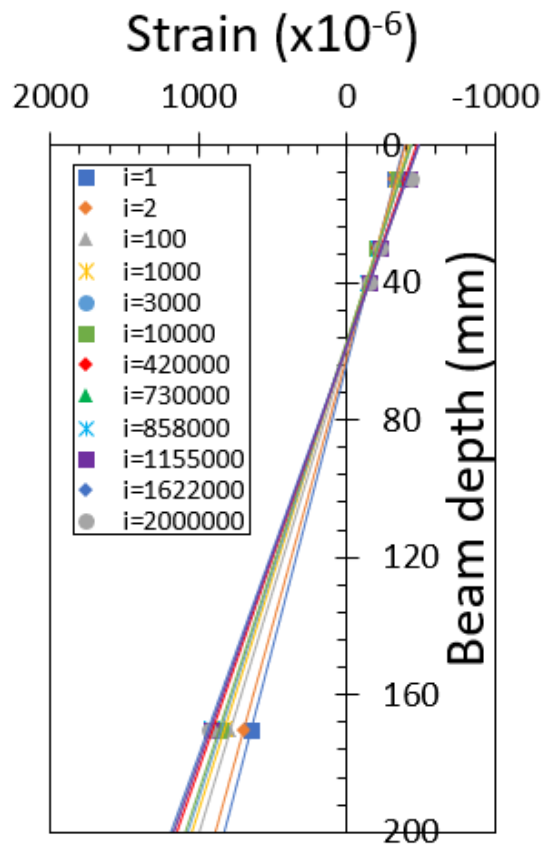


Fig. 7.21 Mid-span strain distribution under flexural cyclic loading for beam 5D_FBF_30.

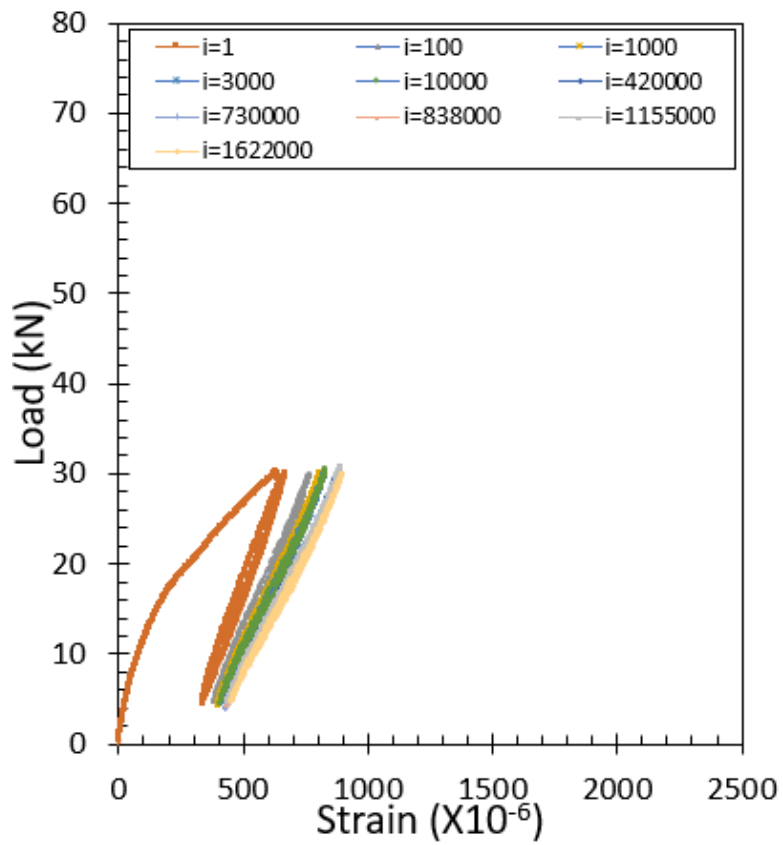


Fig. 7.22 Load versus average rebar strain under flexural cyclic loading for beam 5D_FBF_30.

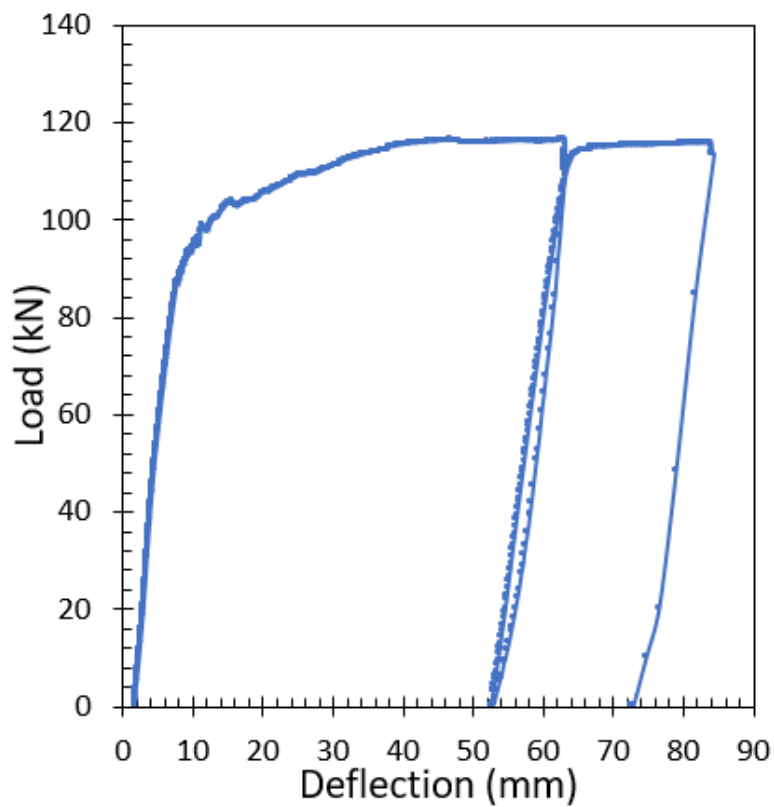


Fig. 7.23 Load versus deflection under residual flexural static loading for beam 5D_FBF_30.

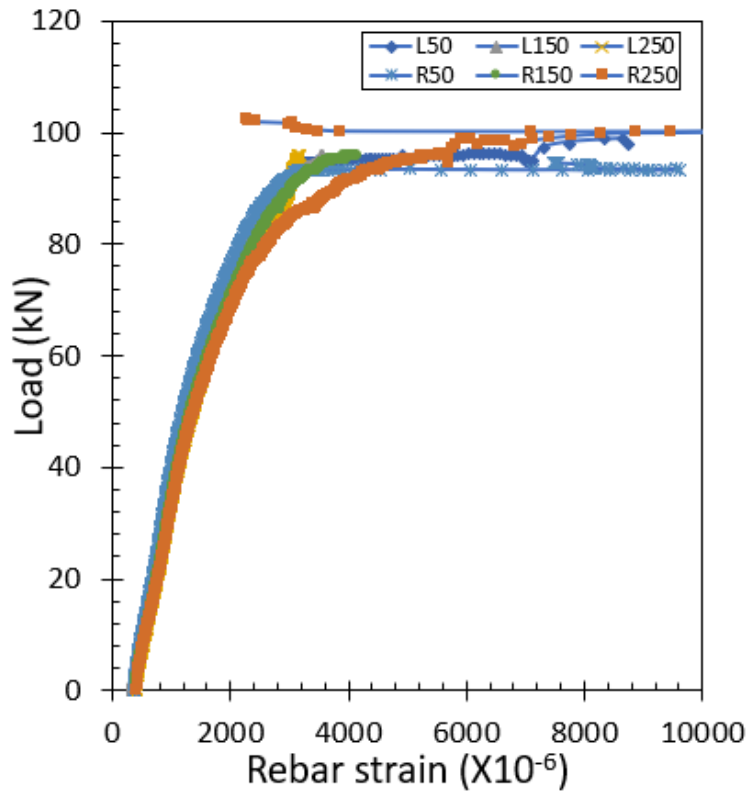


Fig. 7.24 Load versus rebar strain under residual flexural static loading for beam 5D_FBF_30.

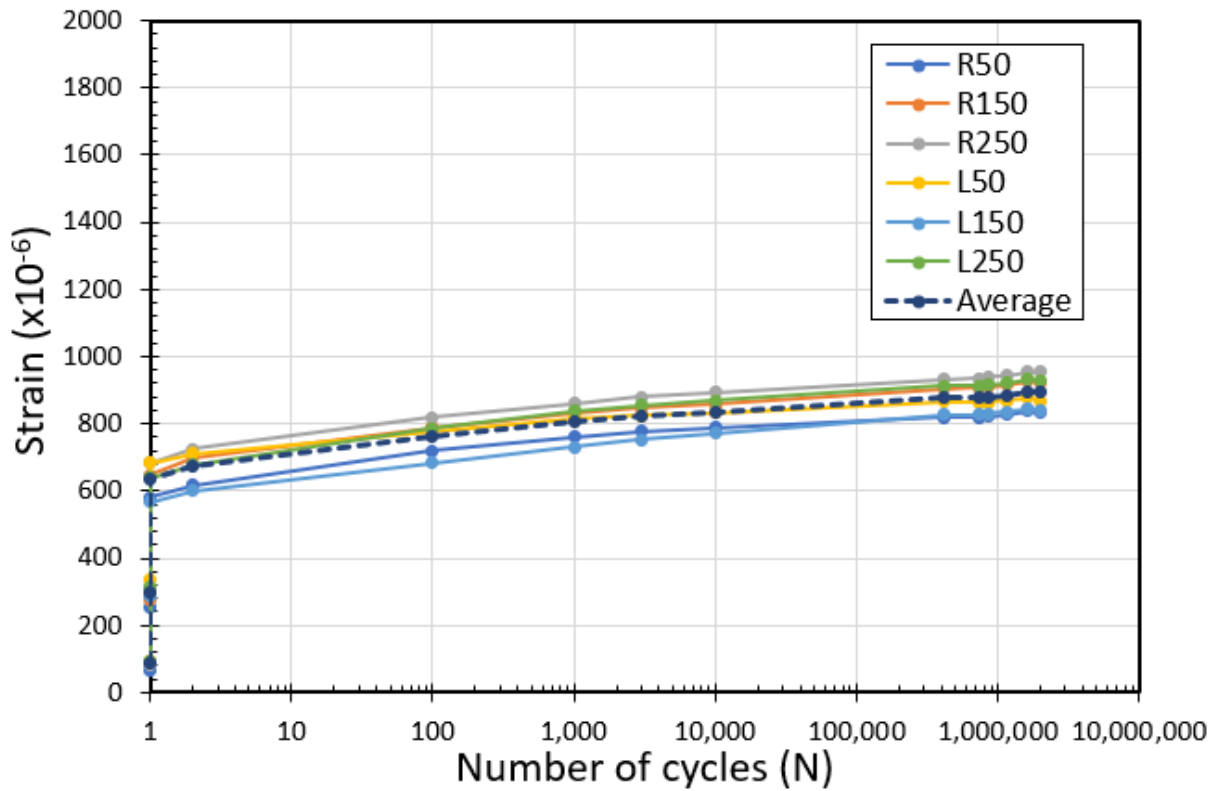


Fig. 7.25 Rebar strain evolution under flexural fatigue for beam 5D_FBF_30.

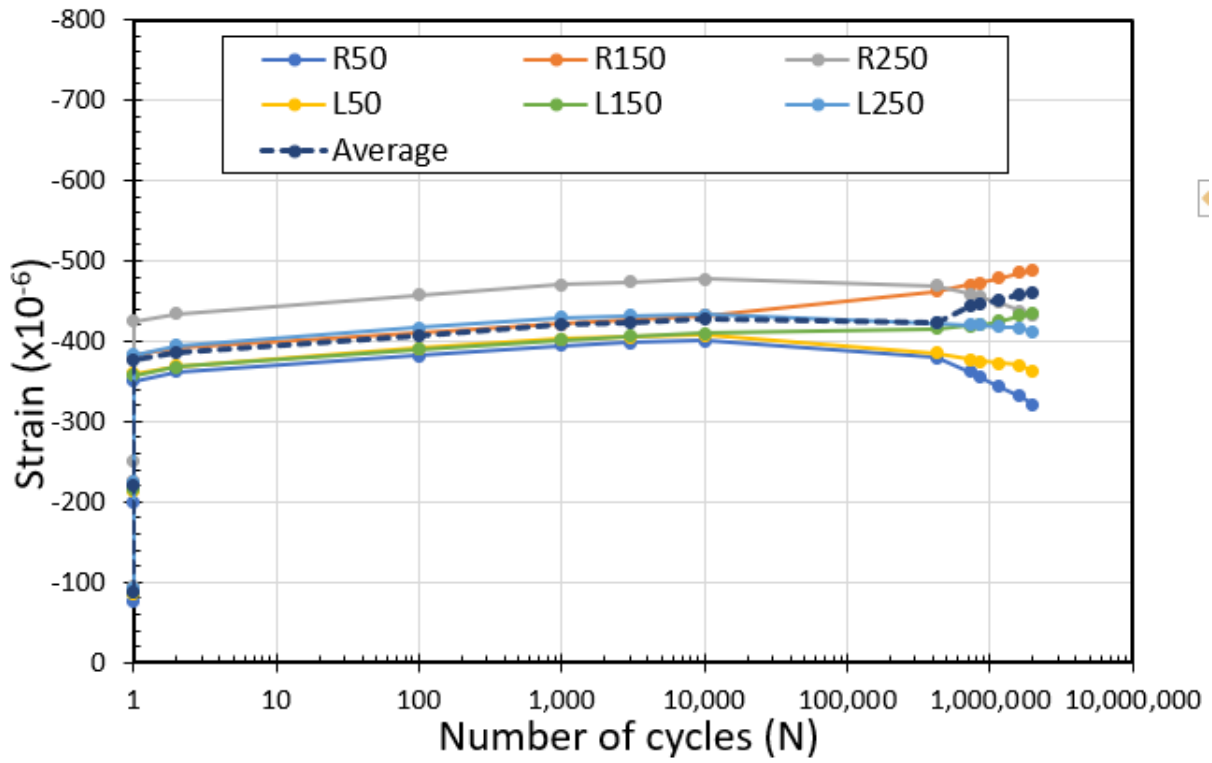


Fig. 7.26 ultimate concrete strain evolution under flexural fatigue for beam 5D_FBF_30.

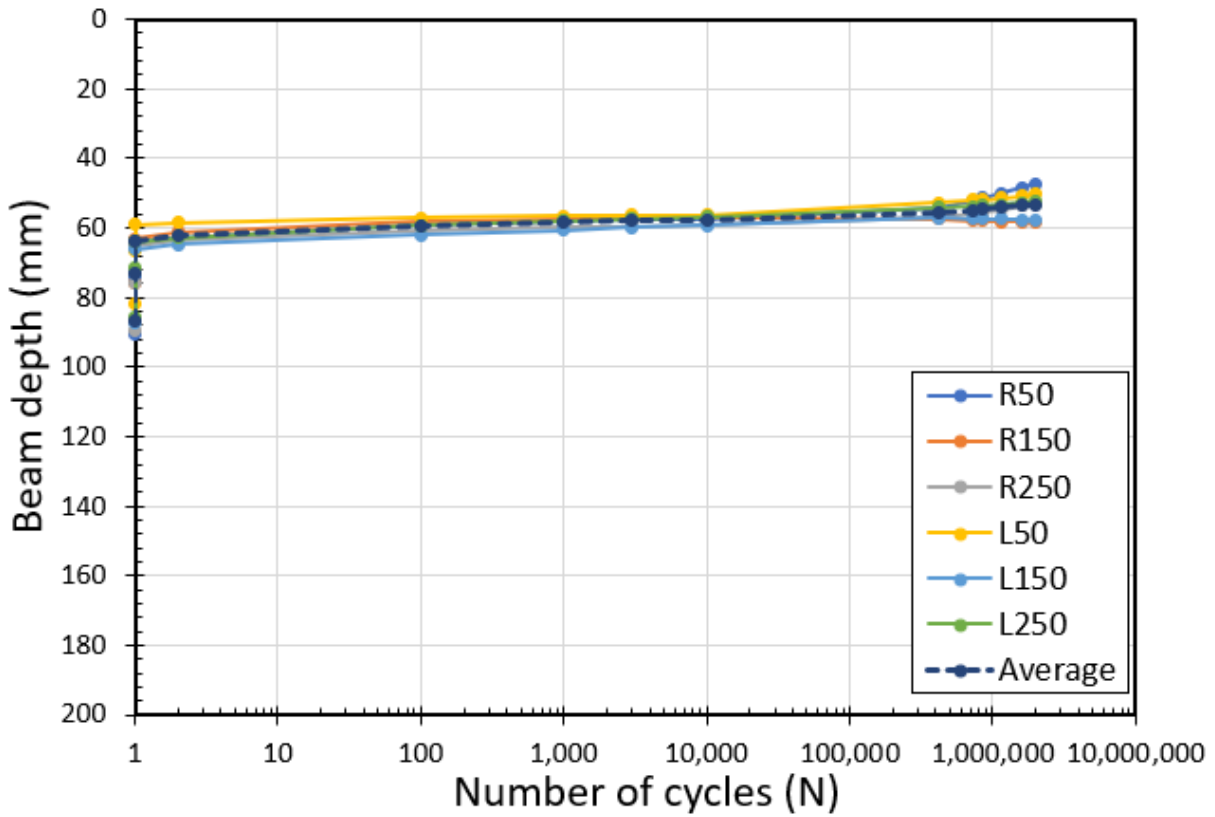


Fig. 7.27 Neutral axis position evolution under flexural fatigue for beam 5D_FBF_30.

Finally, the average experimental data of the fatigue response of the SFRC structural beam – 5D_FBF_30 – over the fatigue life to be used in the inverse analysis calculation method. The degradation of the crack-bridging strength would be evaluated by achieving a good fitting between the experimental and calculated fatigue response of the tested structural SFRC beams. As a result, the average experimental rebar strain, ultimate surface concrete strain, and N.A. position were monitored and plotted in [Figs. 7.25](#), [7.26](#), and [7.27](#) respectively, from the data monitored inside the constant moment region.

Beam 5D_FBF_45

For the medium fatigue stress level ($S = 0.43$), one SFRC structural beam – 5D_FBF_45 – was tested under flexural cyclic loading with 5 kN as a minimum flexural load and 45.5 kN as a maximum flexural load, with the same maximum fatigue stress level as one beam of the first series FBF_40 and same maximum fatigue load level as one beam of the third series C60_FBF_45 where the fatigue response would be compared to capture the effect of the hooked level and the volume fraction of the fibers, as shown in [Fig. 7.28](#). [Figure 7.29](#) shows the load versus mid-span deflection relationship over fatigue life under a medium-stress level of flexural fatigue load showing an increase in mid-span deflection as cycles progress and compared to 5D_FBF_45. [Figure 7.30](#) shows the strain distribution at midspan on the front face of the beam (R150), showing the strain evolution for both rebar and concrete throughout the application of flexural cyclic loading until the end of fatigue life by two million cycles. The average rebar strain within the constant moment region of 5D_FBF_45 is also plotted against the maximum and minimum flexural cyclic load for the medium fatigue stress levels during the fatigue life, starting from the first flexural cyclic loading (N_1) and showing the evolution of average rebar strain, as shown in [Fig. 7.31](#). After a complete of two million cycles of flexural loading, SFRC beam 5D_FBF_45 was subjected to residual flexural static tests to measure their residual capacity, as shown in [Figs. 7.32](#) and [7.33](#). The result is listed in [Table 7.2](#). Residual flexural capacity is a little different from the original capacity of the beams under static loading, even after the fatigue loading.

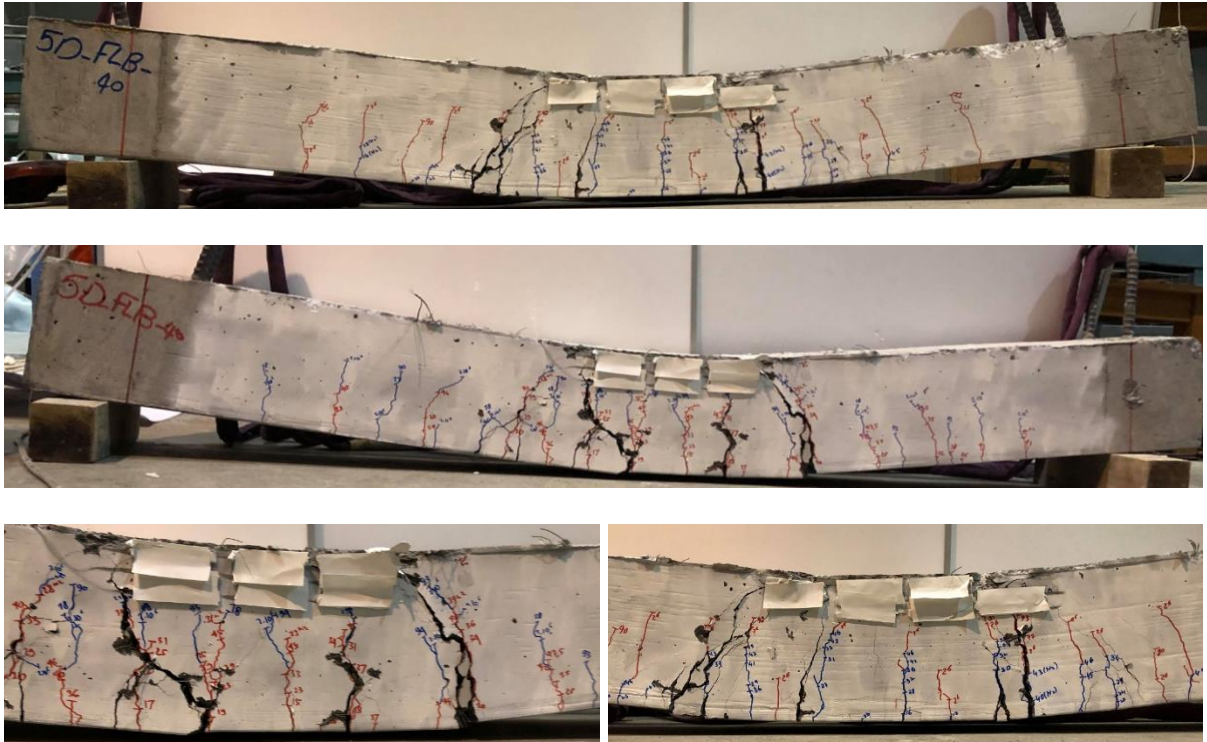


Fig. 7.28 Beam 5D_FLB_45 over fatigue life under flexural cyclic loading.

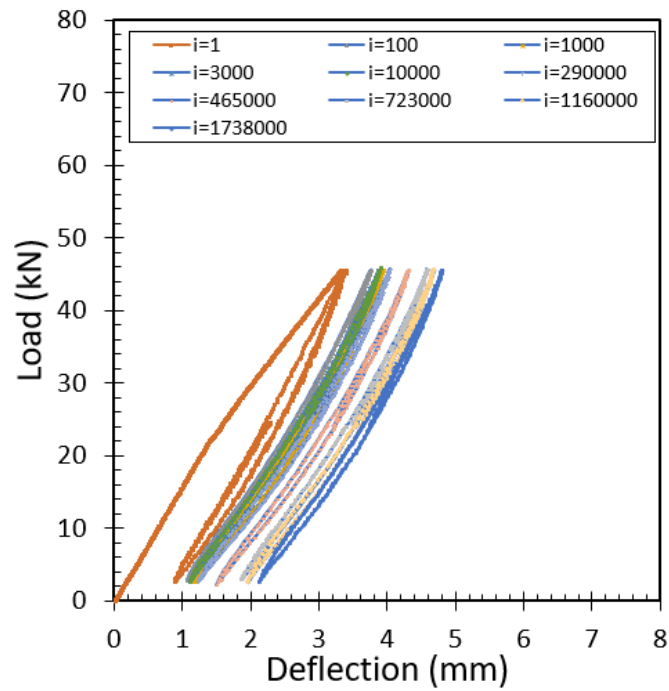


Fig. 7.29 Load versus deflection under flexural cyclic loading for beam 5D_FLB_45.

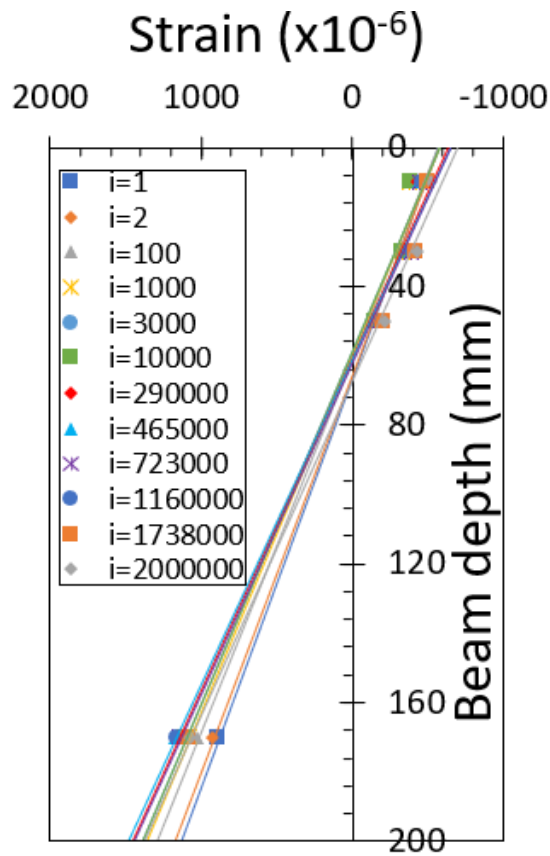


Fig. 7.30 Mid-span strain distribution under flexural cyclic loading for beam 5D_FBF_45.

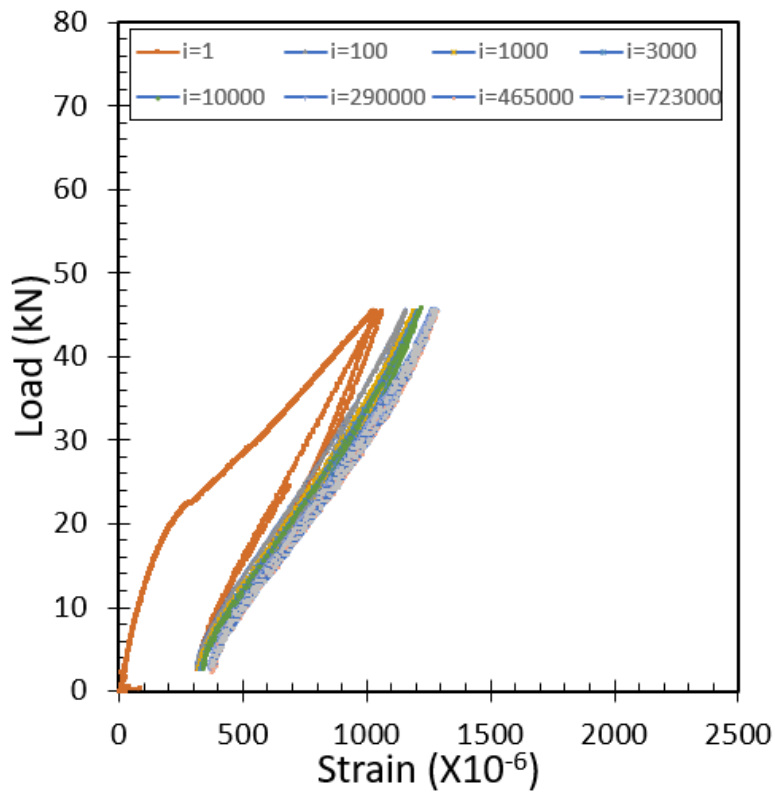


Fig. 7.31 Load versus average rebar strain under flexural cyclic loading for beam 5D_FBF_45.

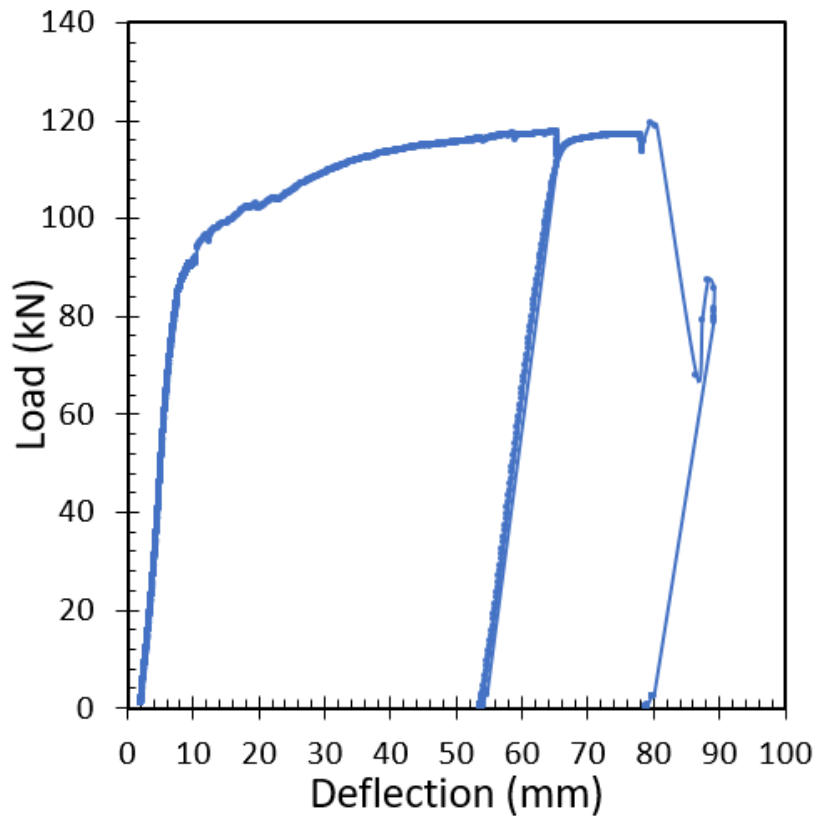


Fig. 7.32 Load versus deflection under residual flexural static loading for beam 5D_FBF_45.

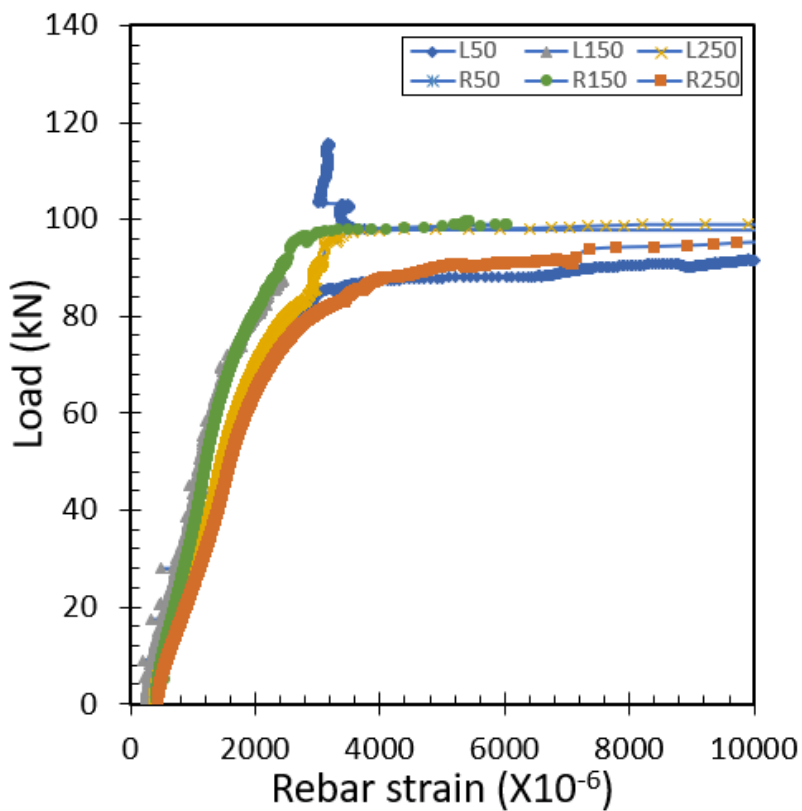


Fig. 7.33 Load versus rebar strain under residual flexural static loading for beam 5D_FBF_45.

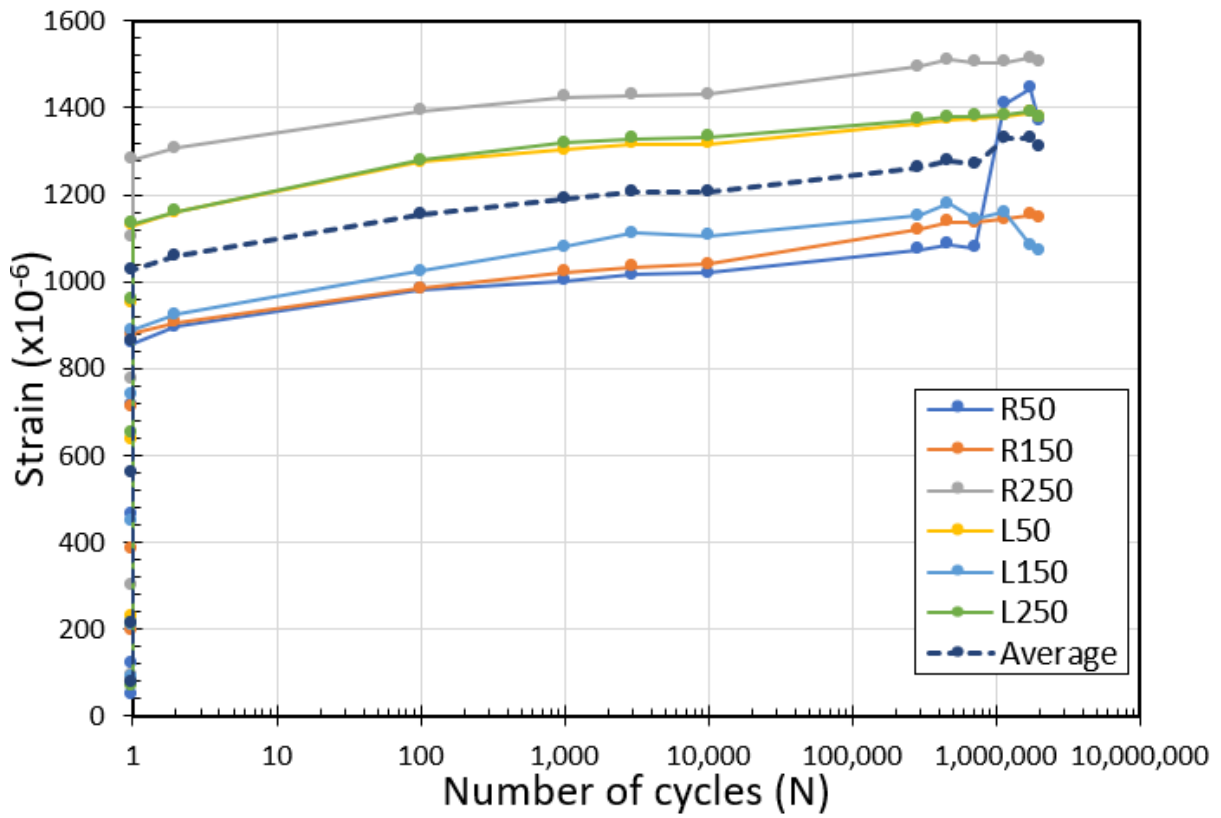


Fig. 7.34 Rebar strain evolution under flexural fatigue for beam 5D_FBF_45.

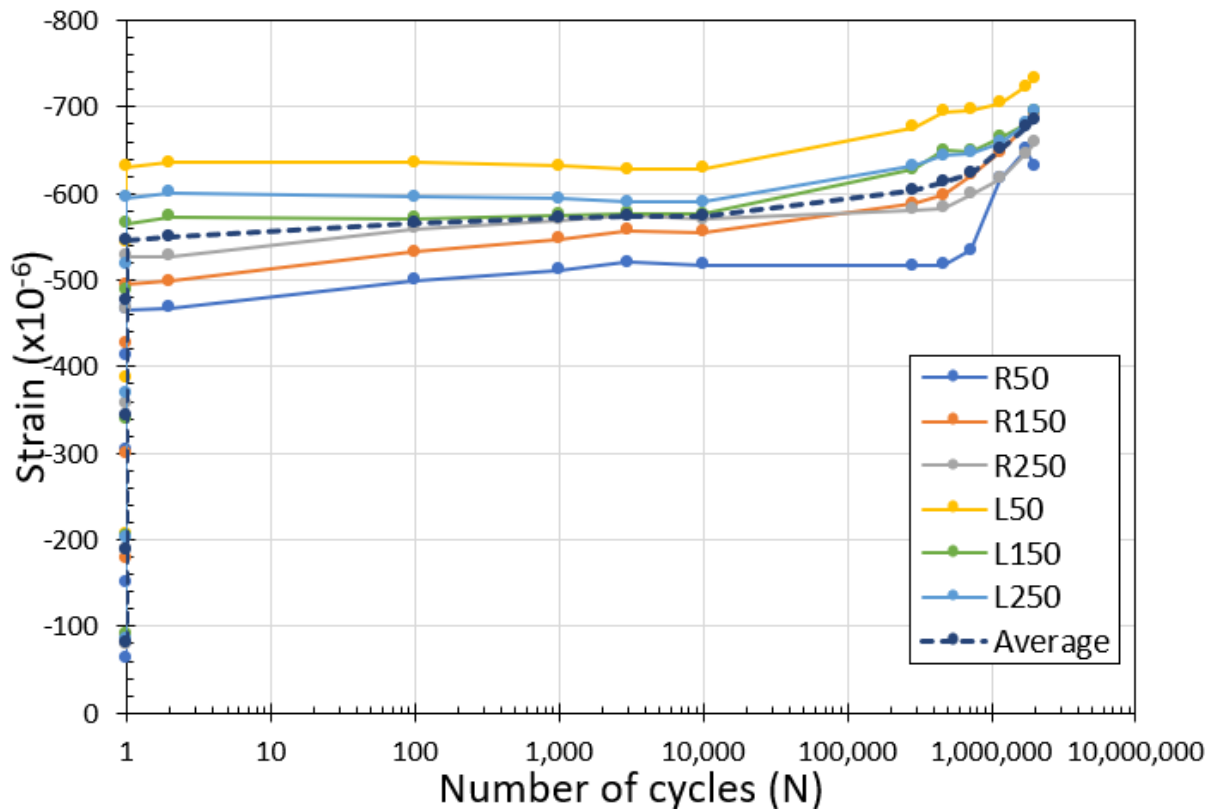


Fig. 7.35 ultimate concrete strain evolution under flexural fatigue for beam 5D_FBF_45.

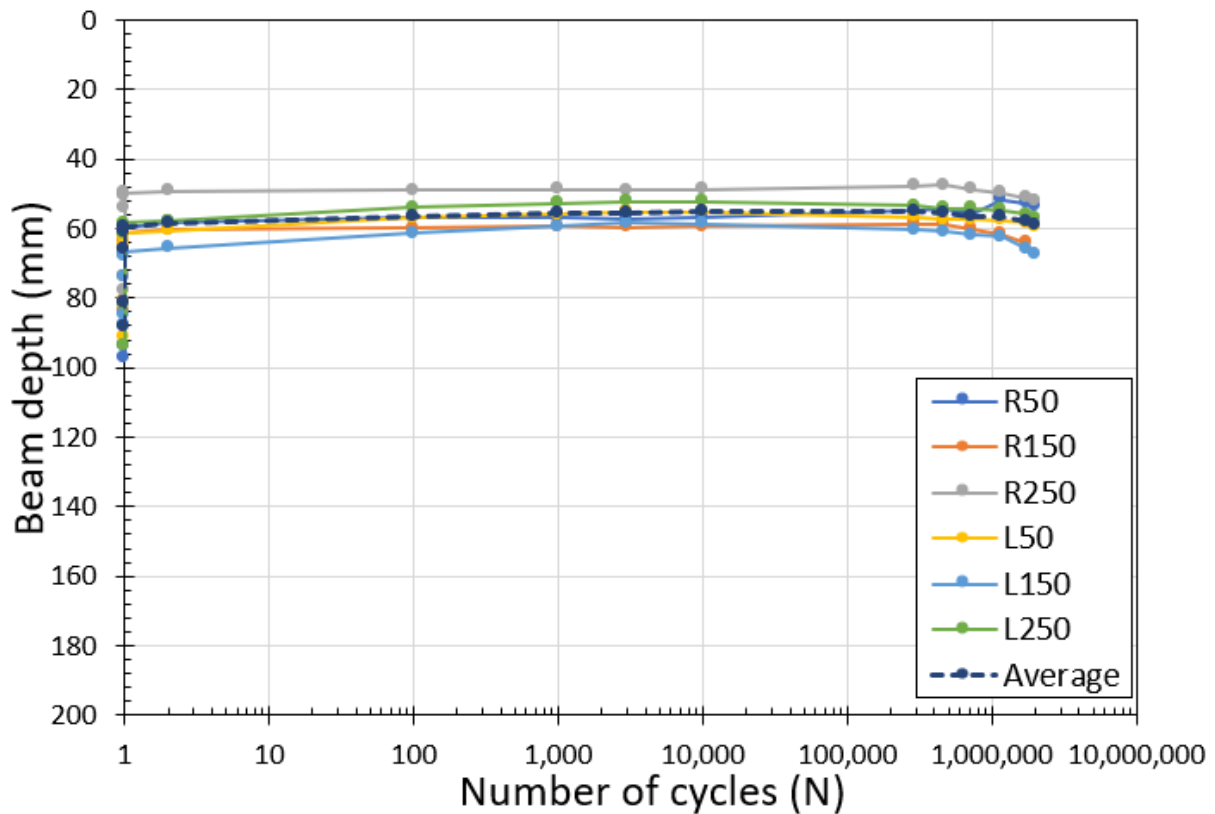


Fig. 7.36 Neutral axis position evolution under flexural fatigue for beam 5D_FBF_45.

Finally, the average experimental data of the fatigue response of the SFRC structural beam – 5D_FBF_45 – over the fatigue life to be used in the inverse analysis calculation method. The degradation of the crack-bridging strength would be evaluated by achieving a good fitting between the experimental and calculated fatigue response of the tested structural SFRC beams. As a result, the average experimental rebar strain, ultimate surface concrete strain, and N.A. position were monitored and plotted in Figs. 7.34, 7.35, and 7.36 respectively, from the data monitored inside the constant moment region.

Beam 5D_FBF_56

For the high fatigue stress level ($S = 0.528$), one SFRC structural beam – 5D_FBF_56 – was tested under flexural cyclic loading with 5 kN as a minimum flexural load and 56 kN as a maximum flexural load, with the same maximum fatigue stress level as one beam of the first series FBF_50 and same maximum fatigue load level as one beam of the third series C60_FBF_55 where the fatigue response would be compared to capture the effect of the hooked level and the volume fraction of the fibers, as shown in Fig. 7.37. Figure 7.38 shows the load versus mid-span deflection relationship over fatigue life under a high-stress level of flexural fatigue load showing an increase in mid-span deflection as cycles progress and

compared to 5D_FBF_30 and 5D_FBF_45. [Figure 7.39](#) shows the strain distribution at midspan on the front face of the beam (L150), showing the strain evolution for both rebar and concrete throughout the application of flexural cyclic loading until fatigue failure. The average rebar strain within the constant moment region of 5D_FBF_56 is also plotted against the maximum and minimum flexural cyclic load for the high fatigue stress levels during the fatigue life, starting from the first flexural cyclic loading (N_1) and showing the evolution of average rebar strain until rebar brittle rupture at 602201 cycles, as shown in [Figs. 7.40](#) and [7.37](#).

Finally, the average experimental data of the fatigue response of the SFRC structural beam – 5D_FBF_56 – over the fatigue life to be used in the inverse analysis calculation method. The degradation of the crack-bridging strength would be evaluated by achieving a good fitting between the experimental and calculated fatigue response of the tested structural SFRC beams. As a result, the average experimental rebar strain, ultimate surface concrete strain, and N.A. position were monitored and plotted in [Figs. 7.41](#), [7.42](#), and [7.43](#) respectively, from the data monitored inside the constant moment region.

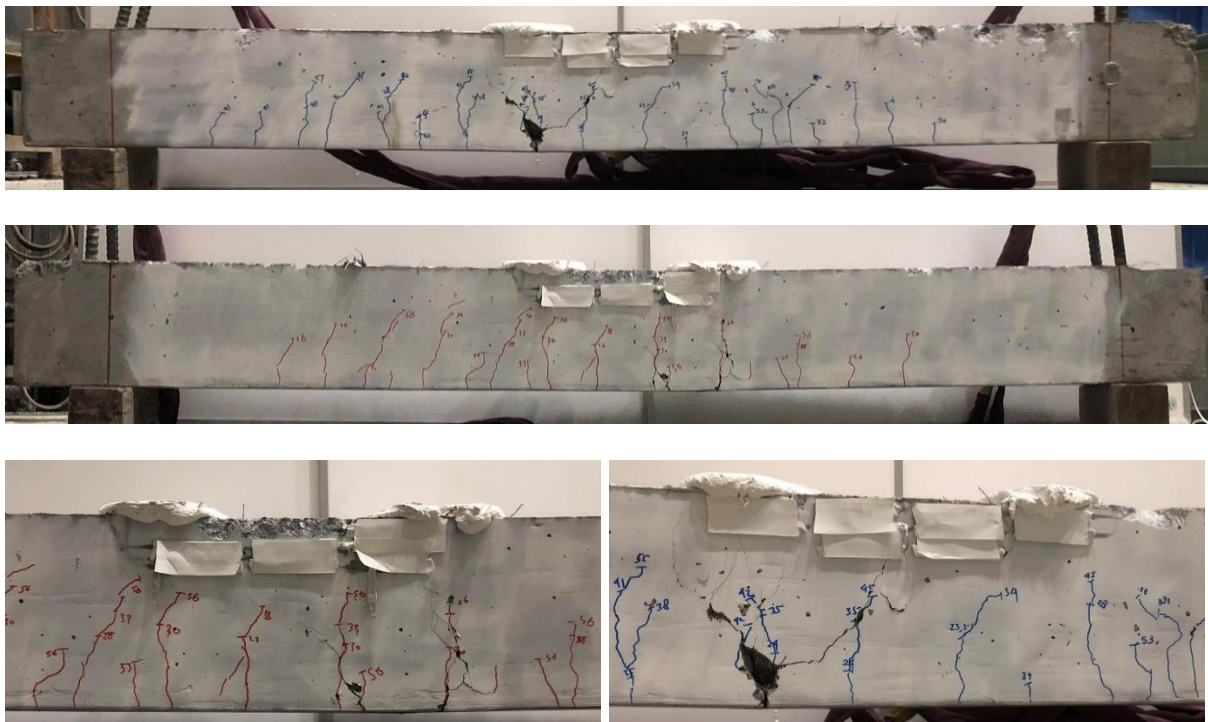


Fig. 7.37 Beam 5D_FBF_56 over fatigue life under flexural cyclic loading.

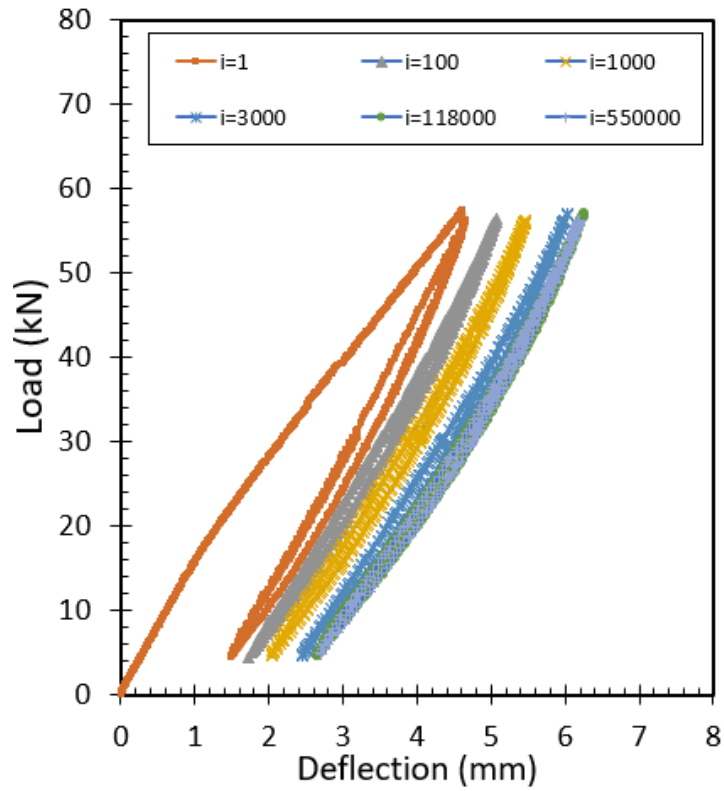


Fig. 7.38 Load versus deflection under flexural cyclic loading for beam 5D_FBF_56.

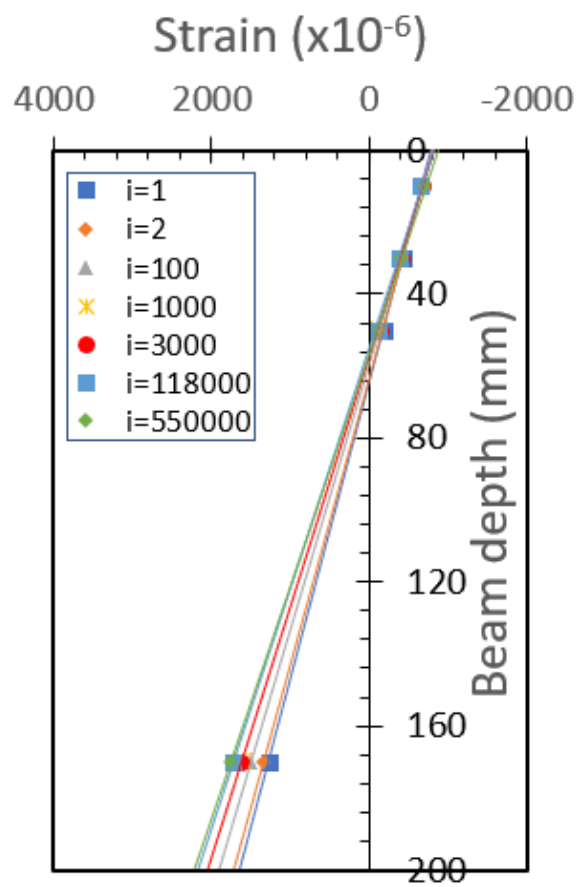


Fig. 7.39 Mid-span strain distribution under flexural cyclic loading for beam 5D_FBF_56.

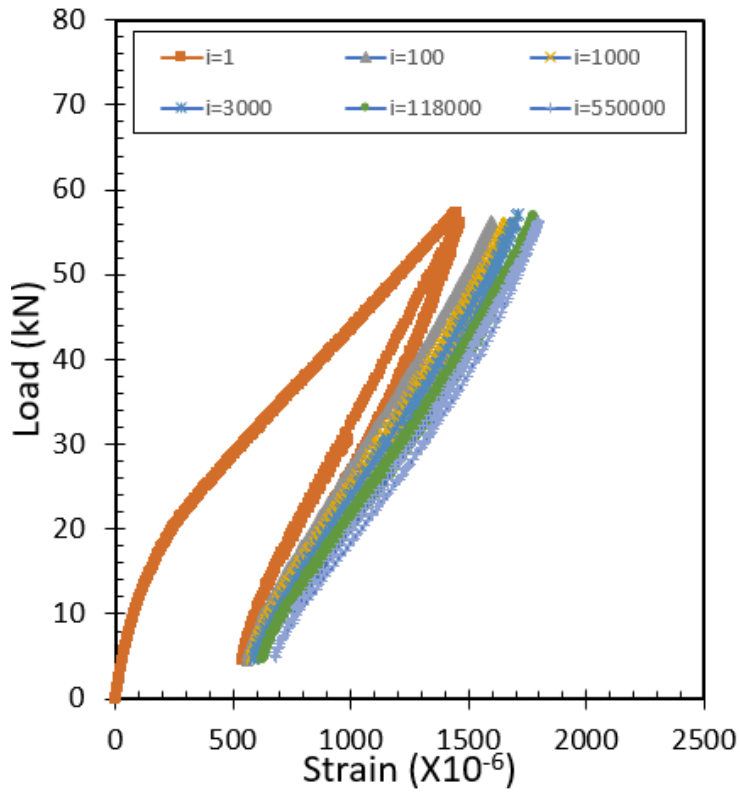


Fig. 7.40 Load versus average rebar strain under flexural cyclic loading for beam 5D_FBF_56.

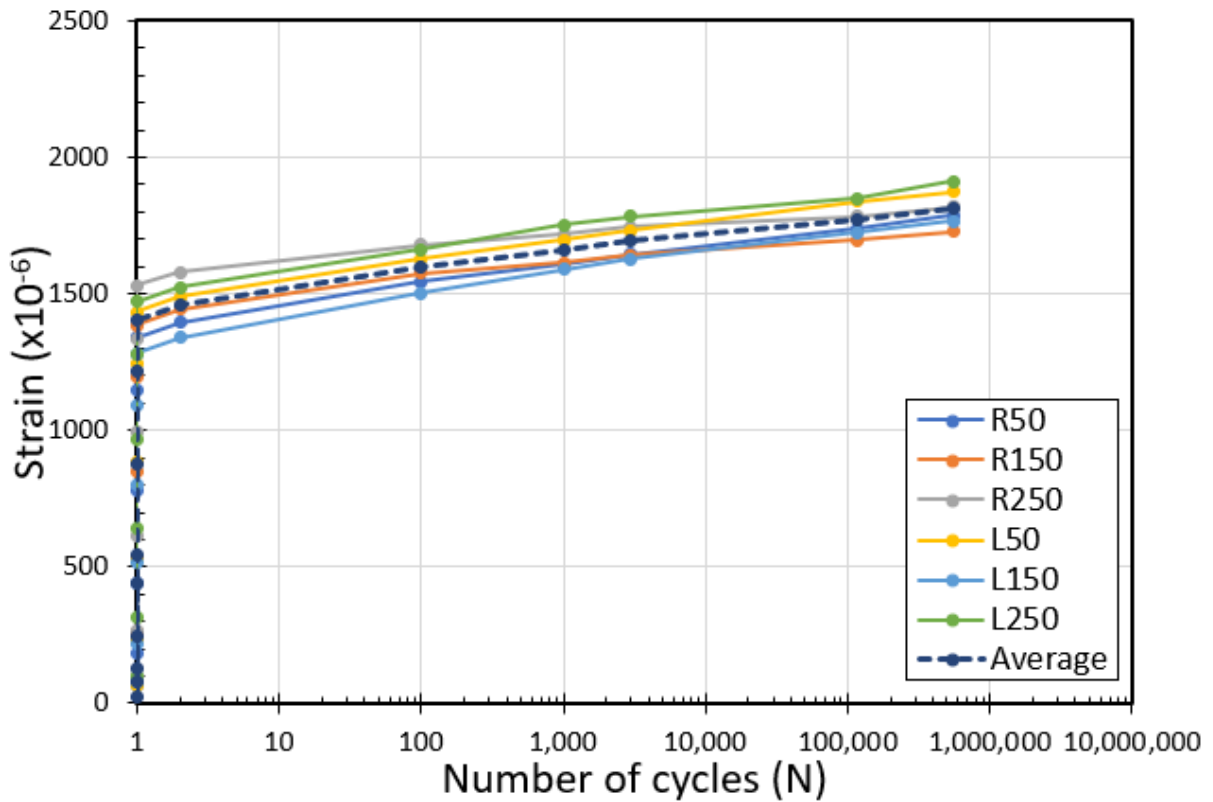


Fig. 7.41 Rebar strain evolution under flexural fatigue for beam 5D_FBF_56.

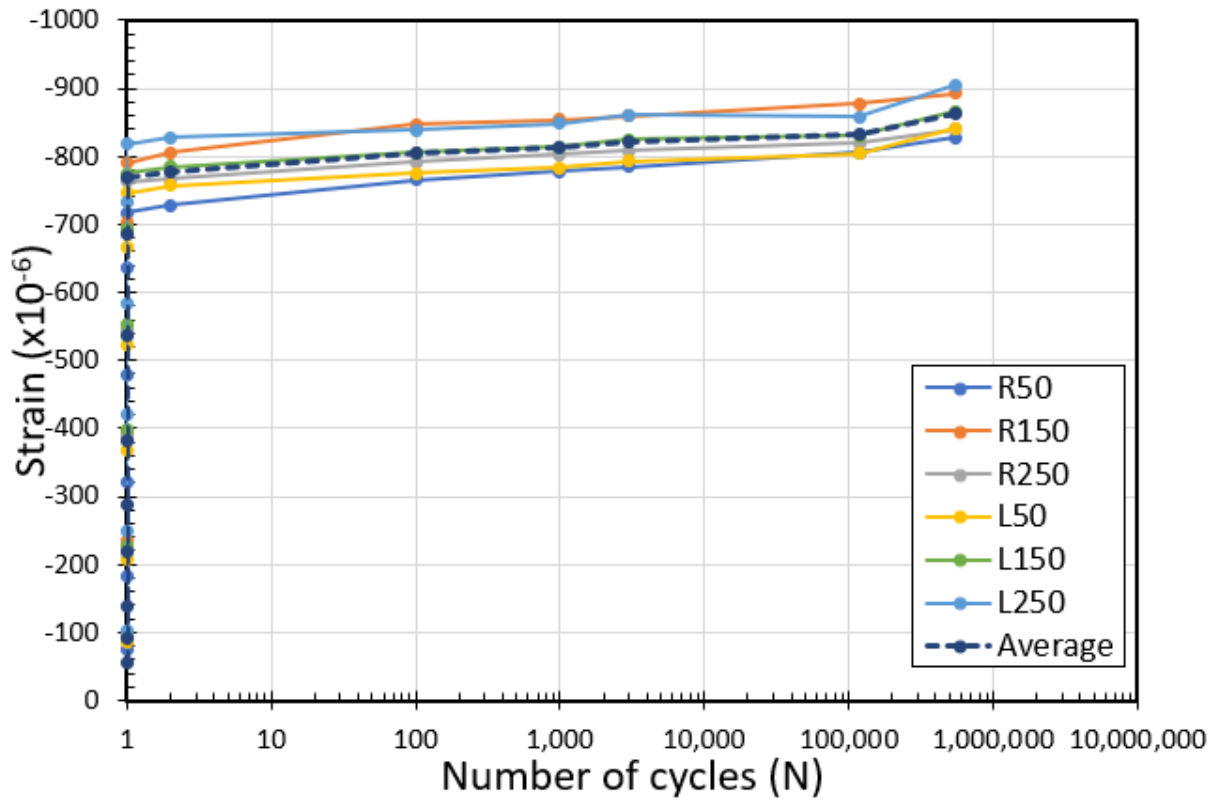


Fig. 7.42 ultimate concrete strain evolution under flexural fatigue for beam 5D_FBF_56.

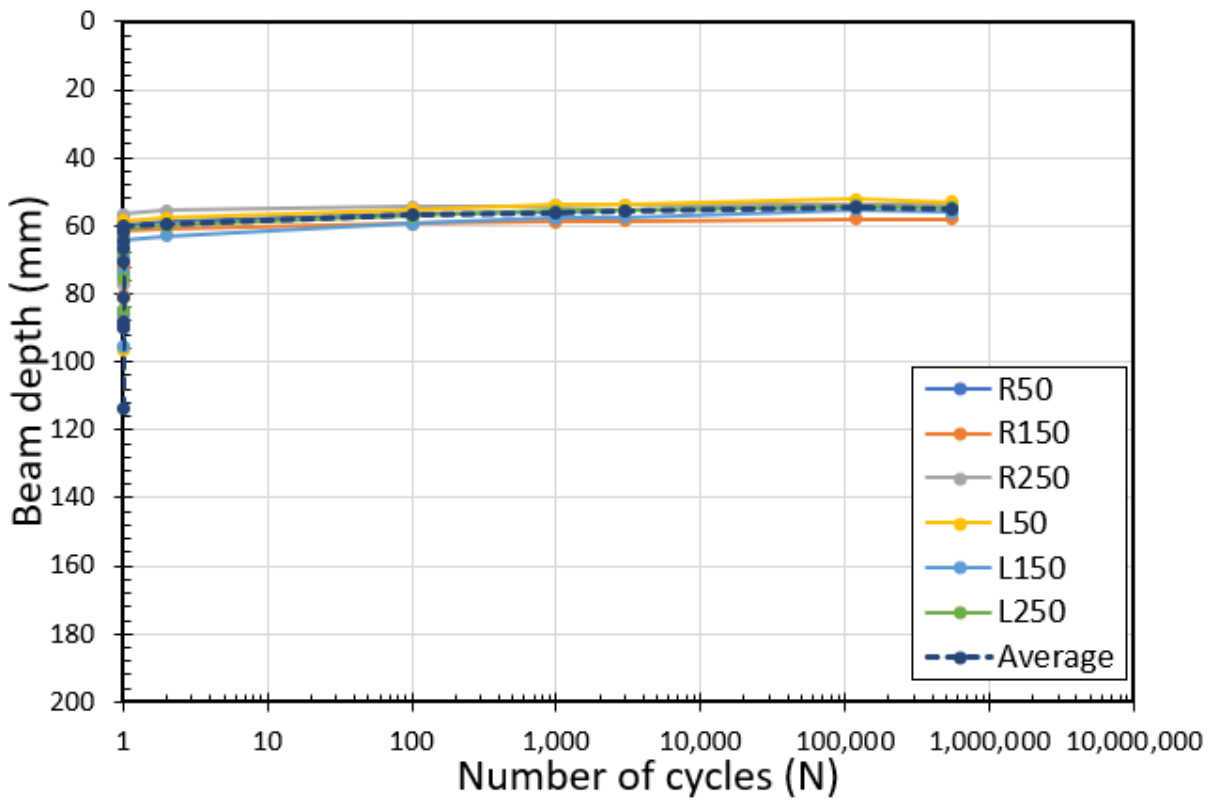


Fig. 7.43 Neutral axis position evolution under flexural fatigue for beam 5D_FBF_56.

Beam 5D_FBF_67

For the high fatigue stress level ($S = 0.632$), one SFRC structural beam – 5D_FBF_67 – was tested under flexural cyclic loading with 5 kN as a minimum flexural load and 67 kN as a maximum flexural load, as shown in Fig. 7.44. Figure 7.45 shows the load versus mid-span deflection relationship over fatigue life under a high-stress level of flexural fatigue load showing an increase in mid-span deflection as cycles progress and compared to 5D_FBF_30, 5D_FBF_45, and 5D_FBF_56. Figure 7.46 shows the strain distribution at midspan on the front face of the beam (L150), showing the strain evolution for both rebar and concrete throughout the application of flexural cyclic loading until fatigue failure. The average rebar strain within the constant moment region of 5D_FBF_67 is also plotted against the maximum and minimum flexural cyclic load for the high fatigue stress levels during the fatigue life, starting from the first flexural cyclic loading (N_1) and showing the evolution of average rebar strain until rebar brittle rupture at 234067 cycles, as shown in Figs. 7.47 and 7.44.

Finally, the average experimental data of the fatigue response of the SFRC structural beam – 5D_FBF_67 – over the fatigue life to be used in the inverse analysis calculation method. The degradation of the crack-bridging strength would be evaluated by achieving a good fitting between the experimental and calculated fatigue response of the tested structural SFRC beams. As a result, the average experimental rebar strain, ultimate surface concrete strain, and N.A. position were monitored and plotted in Figs. 7.48, 7.49, and 7.50 respectively, from the data monitored inside the constant moment region.

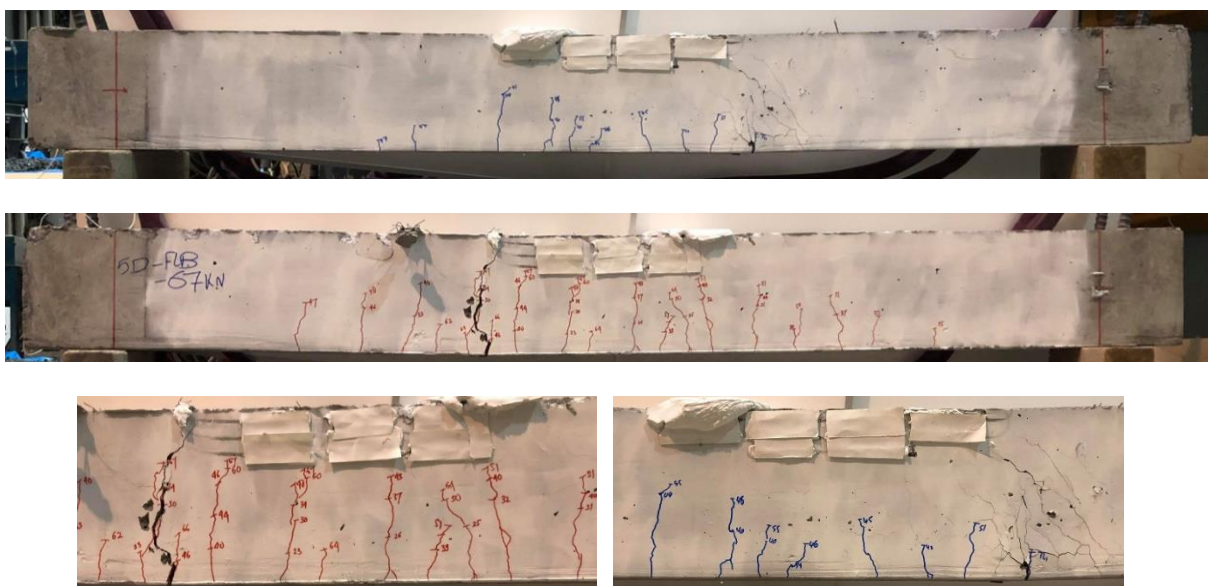


Fig. 7.44 Beam 5D_FBF_67 over fatigue life under flexural cyclic loading.

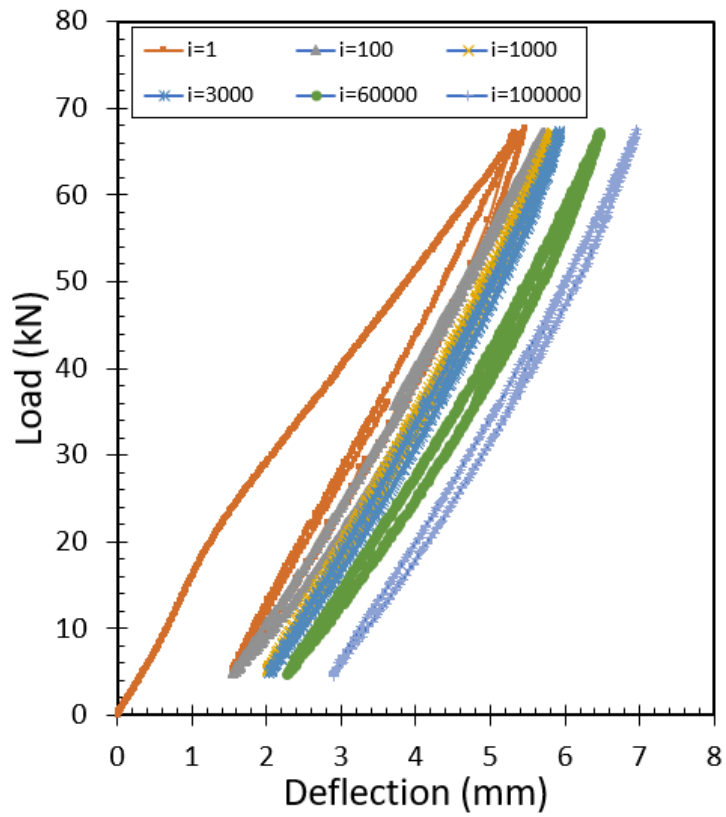


Fig. 7.45 Load versus deflection under flexural cyclic loading for beam 5D_FBF_67.

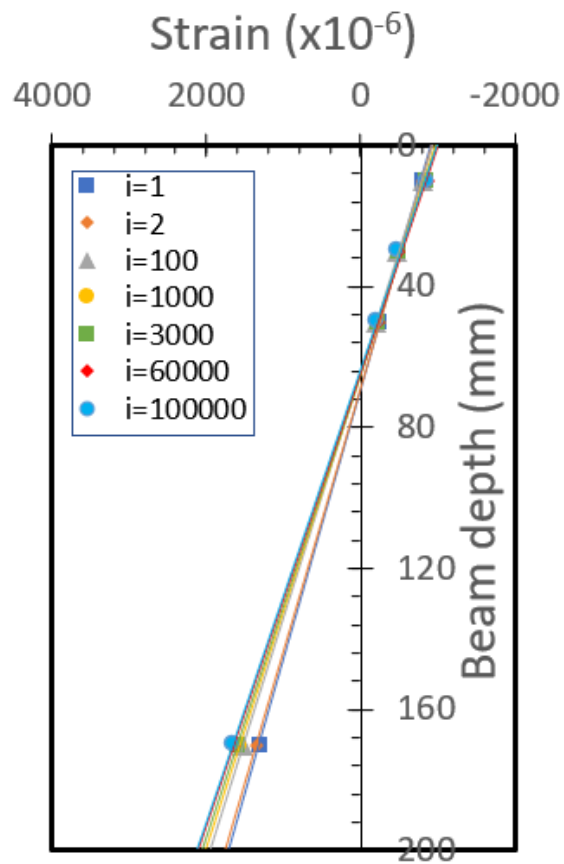


Fig. 7.46 Mid-span strain distribution under flexural cyclic loading for beam 5D_FBF_67.

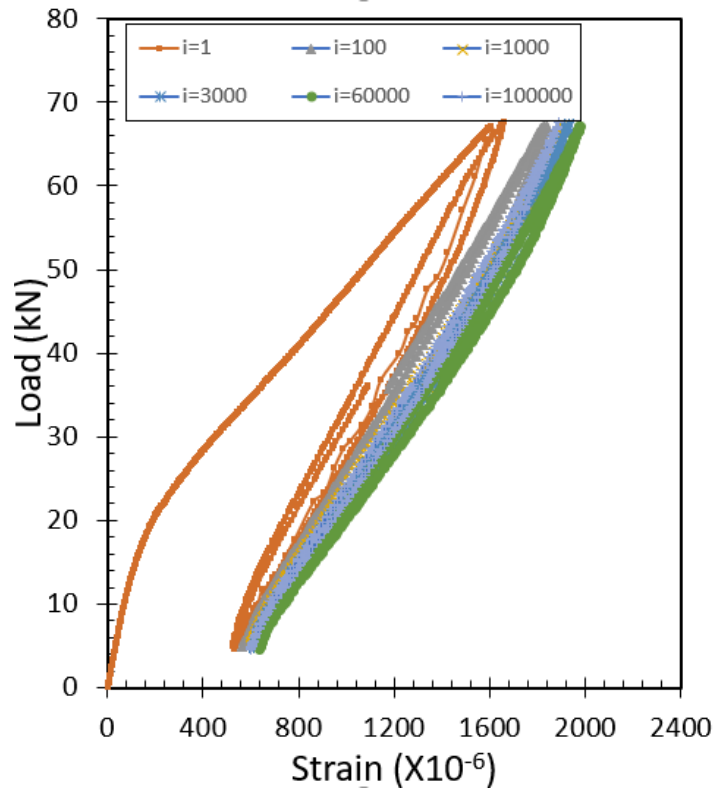


Fig. 7.47 Load versus average rebar strain under flexural cyclic loading for beam 5D_FBF_67.

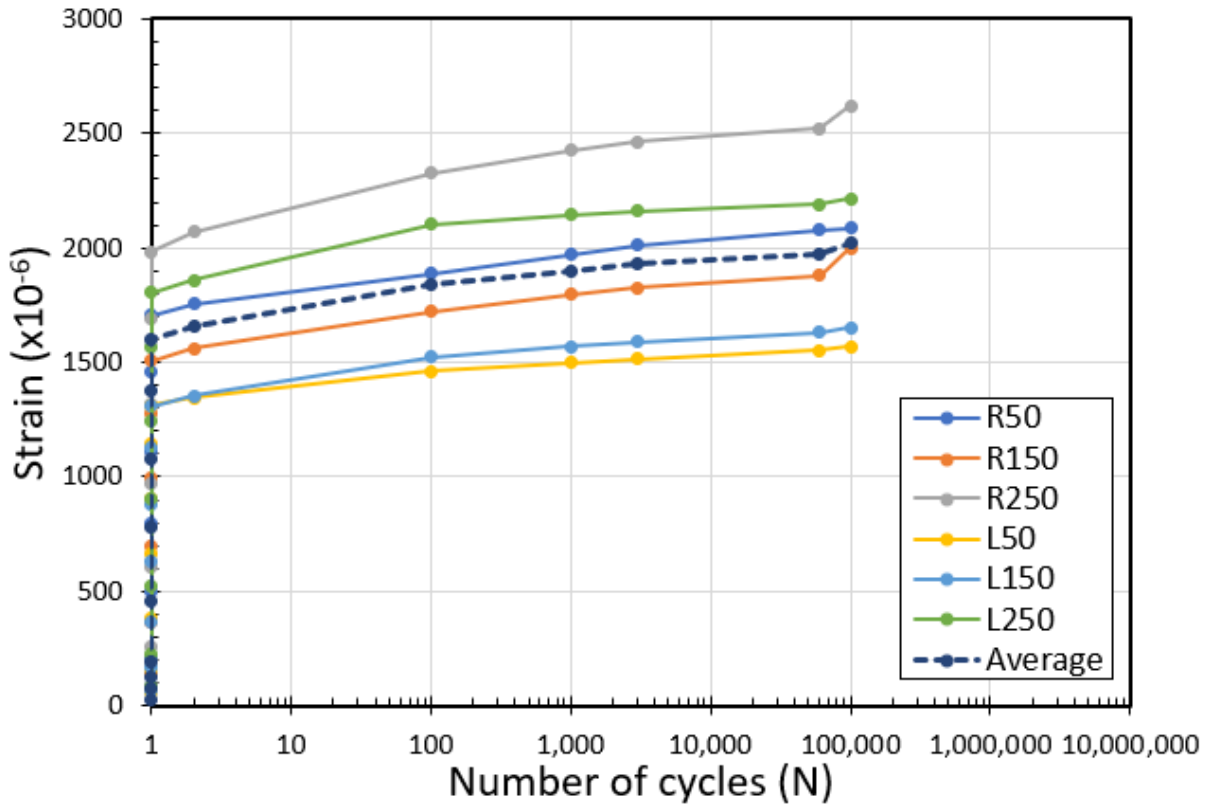


Fig. 7.48 Rebar strain evolution under flexural fatigue for beam 5D_FBF_67.

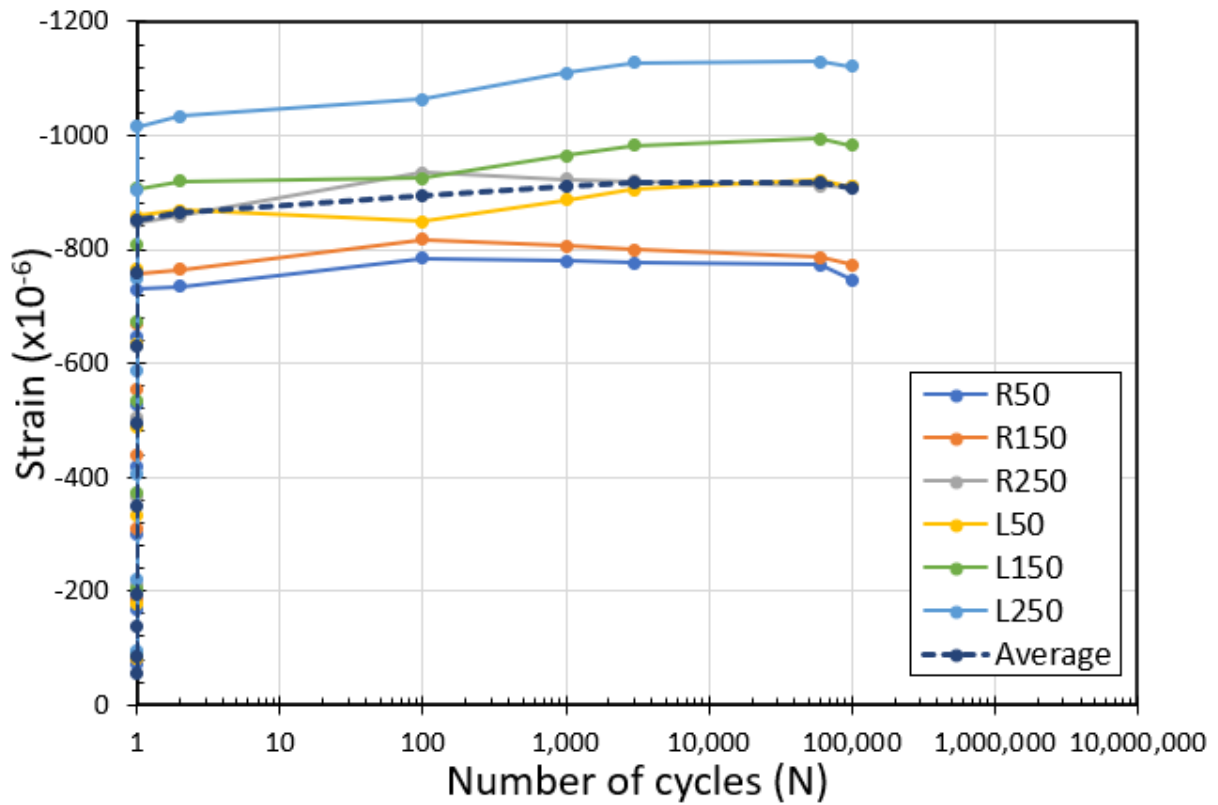


Fig. 7.49 ultimate concrete strain evolution under flexural fatigue for beam 5D_FBF_67.

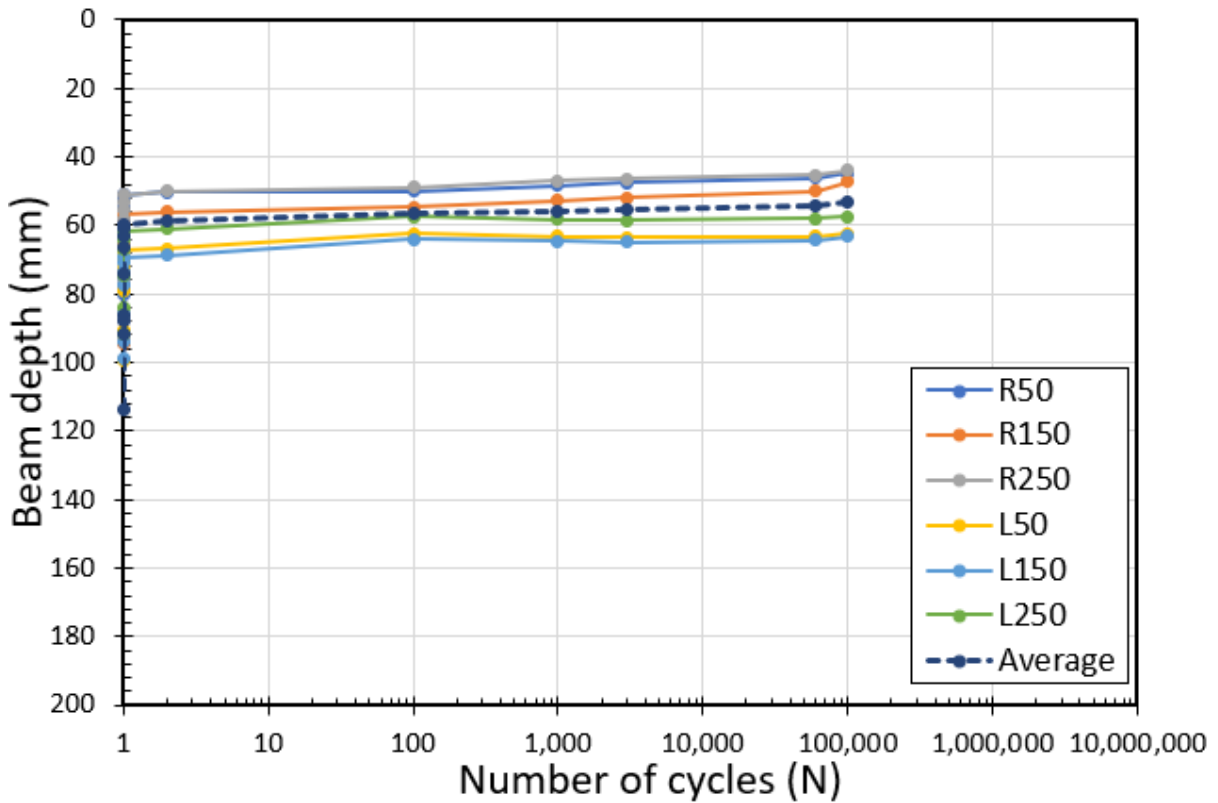


Fig. 7.50 Neutral axis position evolution under flexural fatigue for beam 5D_FBF_67.

7.4 Results Discussion

In this section, the experimental flexural static and fatigue response and the normalized crack-bridging strength degradation and evolution model of the tested SFRC structural beams for the fourth series were captured as compared with the first, second, and third series measuring the effect of hooked levels and volume fraction of the steel fibers inside the tensile stress zone. Firstly, the experimental flexural static response was measured and compared with the first series in a manner of the flexural capacity, deflection, rebar and concrete strain levels, and stiffness to capture the effect of using double hooked-end steel fibers with high concrete compressive strength. Secondly, the experimental flexural fatigue response was captured among the first and third series by comparing the maximum mid-span deflection, maximum rebar strain level, average rebar and ultimate surface concrete strain level, and N.A. position during the fatigue life of the tested beams under cyclic flexural load levels. Thirdly, the crack-bridging strength was evaluated for the fourth series using the inverse analysis calculation method by achieving the best fitting between the experimental and calculated flexural fatigue response. Finally, the evaluated crack-bridging strength degradation and evolution model, that was proposed from the inverse analysis calculation method, was compared between the first, second, and the third series where the effect of hooks level and volume fractions of steel fibers were tested on the degradation and evolution rate and mechanism of the crack-bridging strength over the fatigue life under cyclic flexural load levels.

7.4.1 Experimental Flexural static Response

The experimental flexural static response was captured by measuring the mid-span deflection, maximum rebar strain level, average rebar and ultimate surface concrete strain levels, and N.A. position over the incremental application of monotonic loading of the tested SFRC structural beams. The flexural static response of SFRC structural beams 5D_FBS_01 and 5D_FBS_02 were compared firstly with the third series beams C60_FBF_45 and C60_FBF_55 during the first cycle of the monotonical load application until the maximum fatigue load, that both had a higher concrete compressive strength, to capture the effect of double hooked-end steel fibers with 1.0% volume fraction. Secondly, the beams of the fourth series beams were compared with beam FBS_01 until the ductile tensile failure to capture the effect of higher concrete strength with double hooked-end fibers. Finally, the beams of the fourth series were compared with beams NFB_40 and NFB_50 to capture the difference in response with the normal concrete structural beams. The level and the evolution rate of the tested data were compared

between this series and the first and third series to understand and measure the effect of hooked levels and volume fraction of the steel fibers of SFRC structural beams.

From the experimental results, comparing with the third series beams – i.e. C60_FBF_45, and C60_FBF_55, it is evident that the double hooked-end steel fibers with 1% volume fraction and higher fiber's tensile strength have the same ability of contribution to taking some of the tensile and transferred the stresses to the adjacent uncracked matrix as the single hooked-end fibers with 1.5% volume fraction and lower fiber's tensile strength, resulting in a more ductile behavior and a greater load-bearing capacity, hence, lowering the mid-span deflection and stresses in the reinforcing bar and concrete, as shown in [Figs. 7.51, 7.52, 7.53, 7.54, and 7.56](#). The almost same flexural static response as the third series of SFRC beams was achieved with lower fiber's volume fraction and higher fiber's tensile strength, indicating the effect of the double hooked-end fibers with a higher fiber's tensile strength in bridging cracks. However, because of the lower volume fraction of the steel fibers, the fourth series has a higher maximum rebar strain level than the third series, as shown in [Fig. 7.53](#).

On the other hand, comparing with the first series beams – i.e. FBS_01, NFB_40, and NFB_50, it is evident that the double hooked-end steel fibers, with lower volume fraction and higher tensile strength, have a higher ability of contribution to taking some of the tensile stresses to the adjacent uncracked matrix than the single hooked-end fibers, resulting in a closer crack spacing with a smaller crack-width and lower deflections, as shown in [Figs. 7.51, and 7.52](#). This results in a more ductile behavior and a greater load-bearing capacity, hence, lowering the stresses in the reinforcing bar and concrete, as shown in [Figs. 7.53, 7.54, and 7.55](#). The better flexural static response than the first series of SFRC beams was achieved with a higher concrete compressive strength, lower fiber's volume fraction, and higher fiber's tensile strength, indicating the effect of the higher concrete strength with double hooked-end fibers and a higher fiber's tensile strength in bridging cracks.

It is noted that the effectiveness of incorporating the double hooked-end steel fibers, that have a higher tensile strength, in reinforced concrete are dominated with using a higher compressive concrete strength. It is concluded that the improvement in the static flexural response of SFRC structural beams is strongly affected by concrete compressive strength resulting in lower deflection and rebar and concrete stress levels by providing a better bond between fibers and concrete matrix. As a result, a lower fiber's volume fraction of double hooked-end steel fibers has the same achieved enhancement in the static flexural response of SFRC structural beams

as a higher volume fraction of single hooked-end steel fibers, that have same aspect ratio and lower tensile strength, using a higher concrete compressive strength.

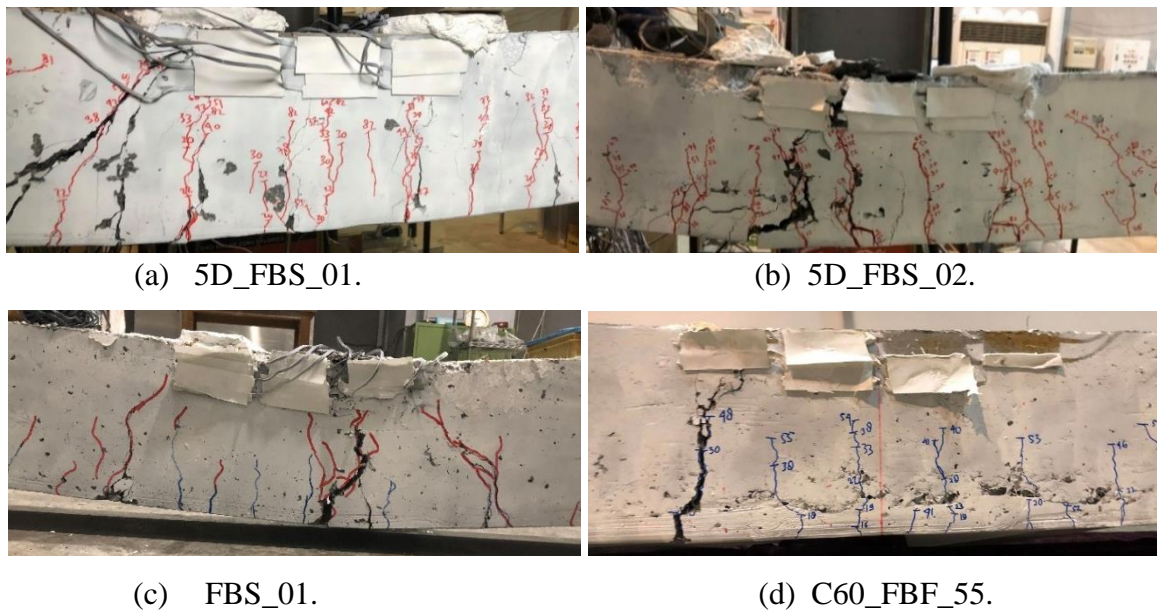


Fig. 7.51 Cracking pattern under static flexural loading of SFRC beams.

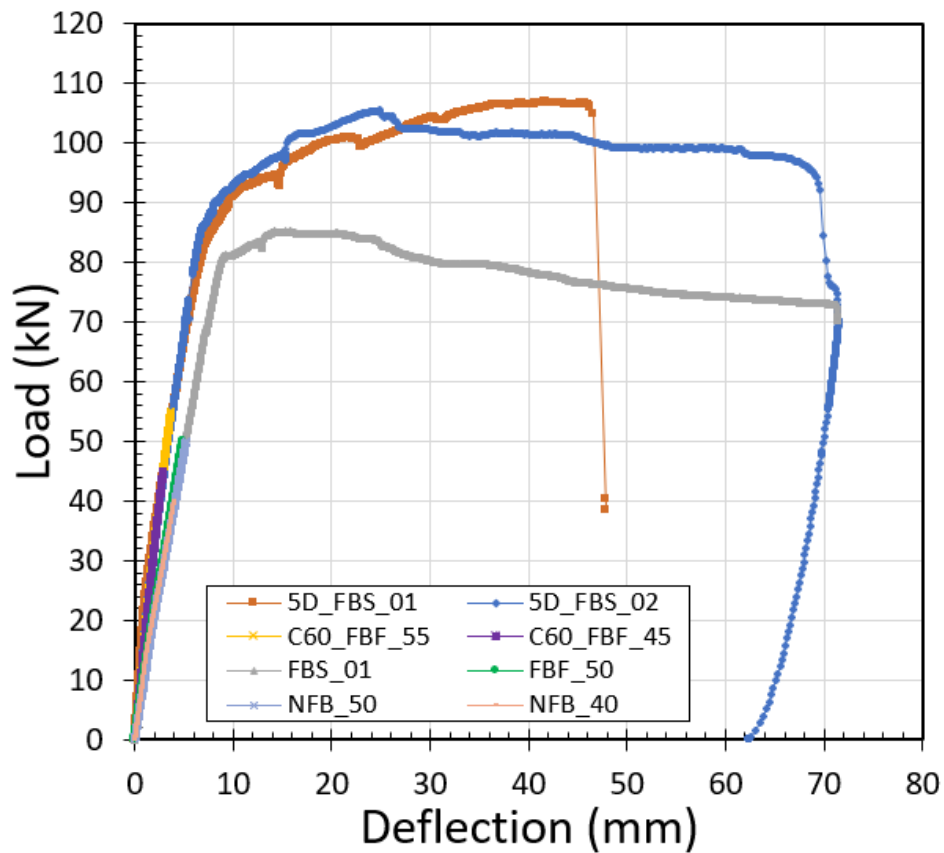


Fig. 7.52 Load versus mid-span deflection under static flexural loading of SFRC beams.

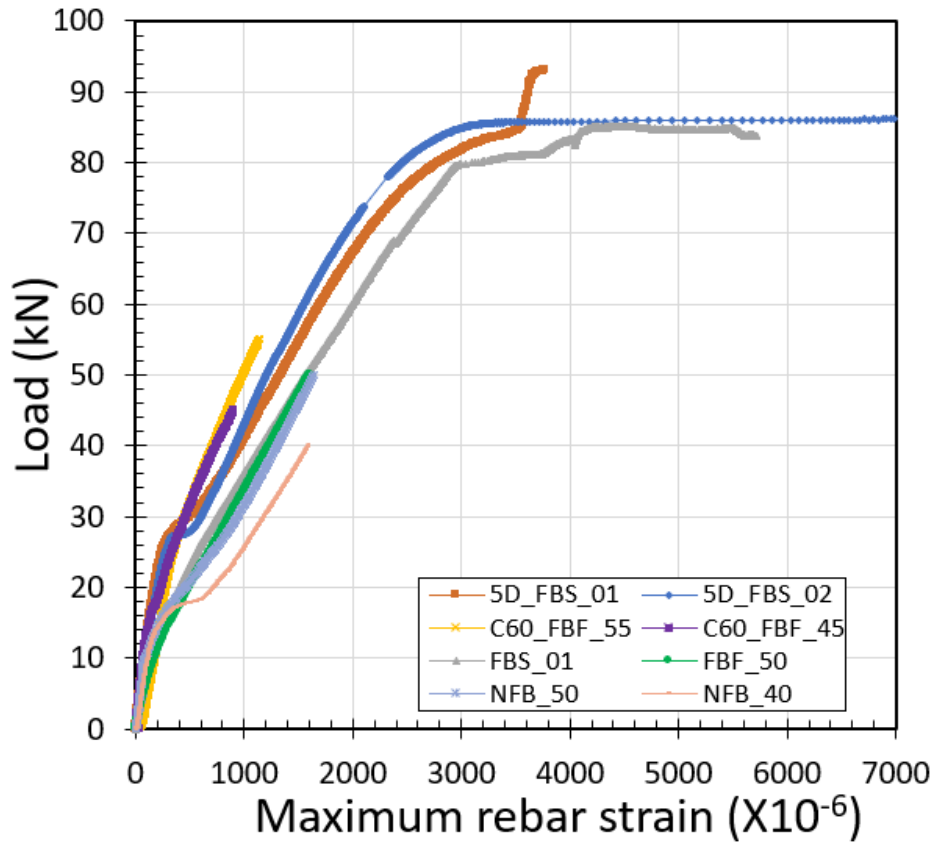


Fig. 7.53 Load versus maximum rebar strain under static flexural loading of SFRC beams.

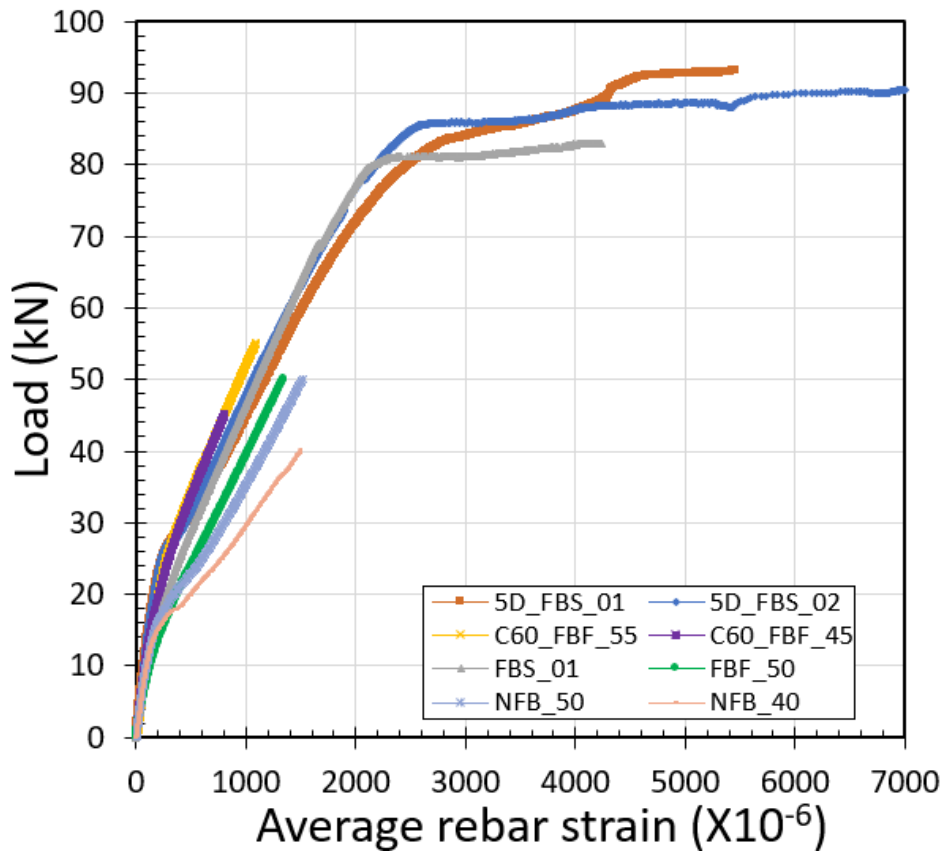


Fig. 7.54 Load versus average rebar strain under static flexural loading of SFRC beams.

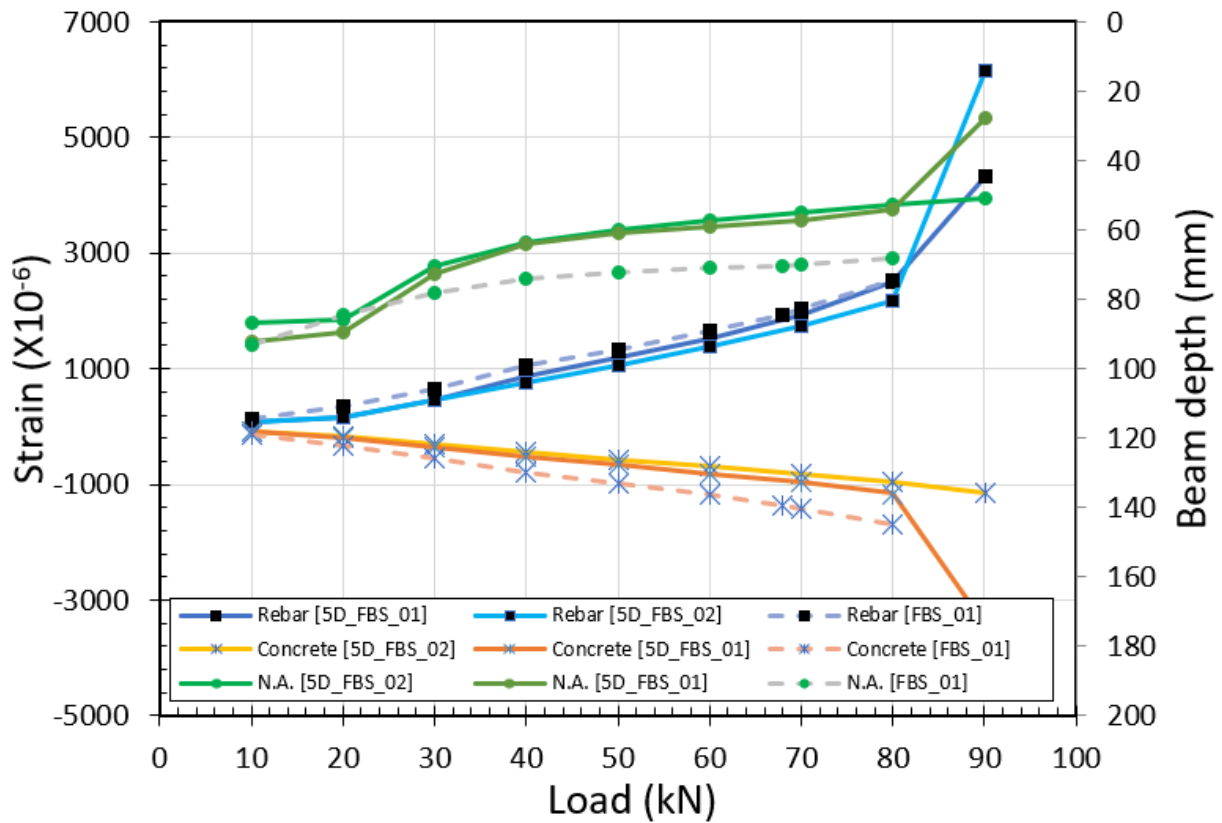


Fig. 7.55 Average static flexural response of SFRC beams for the first and fourth series.

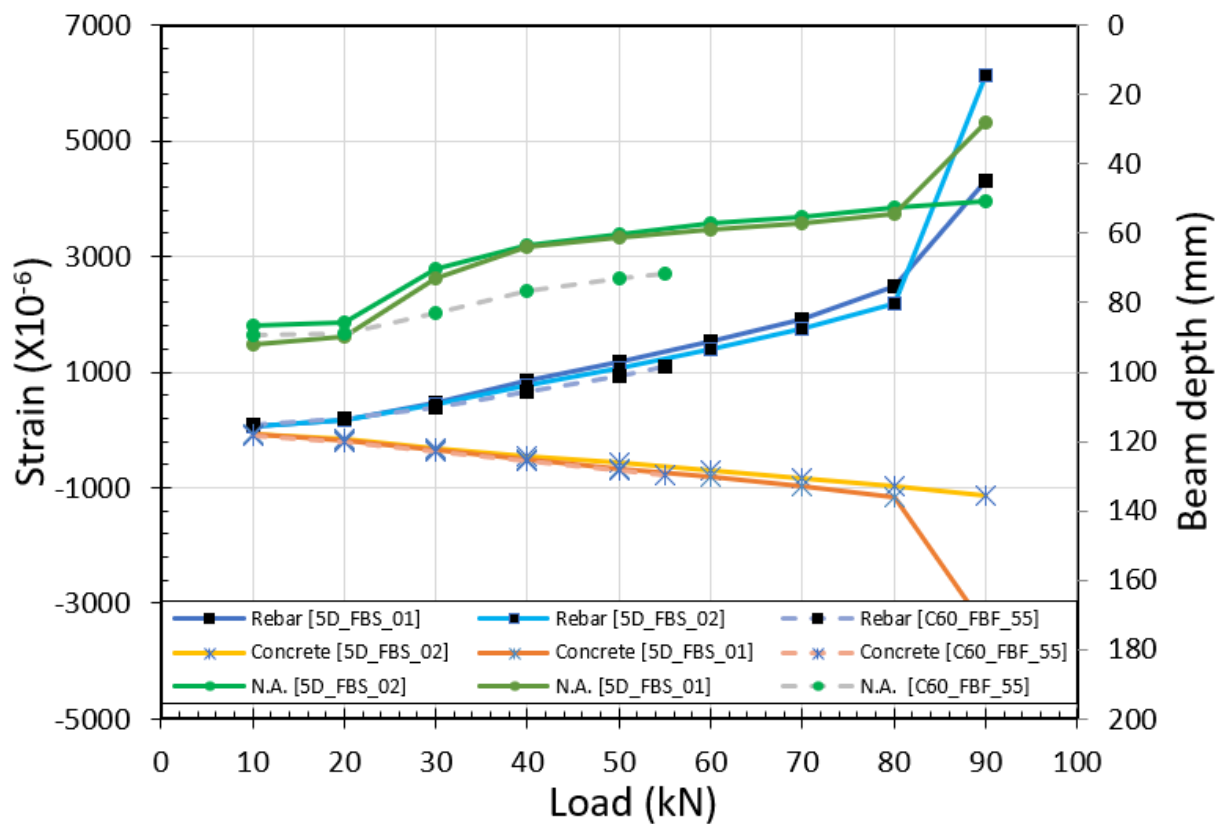


Fig. 7.56 Average static flexural response of SFRC beams for the third and fourth series.

7.4.2 Experimental Flexural Fatigue Response

The inverse analysis method of computation involves incremental calculations during fatigue loading as the number of cycles increases, as explained in section 3.4.3. The computations are performed iteratively for the incremental set of fatigue cycles (N_i) until fatigue ruptures or the completion of two million cycles (N_f). At each increment N_i , a certain degradation level (α_i) of initial crack-bridging strength is proposed to adjust the balance between the experimentally measured results and the calculated values; if the agreement between the calculated and experimental results is not within the set threshold, the analysis is repeated using a different level of degradation until the threshold is met, as illustrated in Figs. 3.13, 7.57, 7.58, 7.59, and 7.60. The normalized crack-bridging strength (β_i) is derived using Eq. (3.4) and plotted in Fig. 7.61, illustrating the degradation of crack-bridging strength over the fatigue life of the four SFRC structural beams under different fatigue load levels ranging from low to high.

Figures 7.57, 7.58, 7.59, and 7.60 show acceptable fitting with a minimum error between the calculated and experimental flexural fatigue response in all fatigue load levels, resulting in evaluating of the crack-bridging strength degradation and evolution model over the fatigue life, as shown in Fig. 7.61. For all fatigue load levels including four SFRC beams 5D_FBF_30, 5D_FBF_45, 5D_FBF_56, and 5D_FBF_67, there is a clear increase in average strain levels for both rebar and concrete and a decrease in the N.A. position as the number of cycles increases, besides the evolution of the crack-bridging strength was captured after the end of the two million cycles for beams 5D_FBF_30 and 5D_FBF_45. The conclusion from these results is that the proposed inverse analysis method could predict the degradation and evolution of crack-bridging strength provided by fibers as flexural fatigue loading continues.

Finally, the normalized crack-bridging strength at all fatigue stress levels is plotted versus the evolution of the experimental maximum rebar strain, as shown in Fig. 7.62. By cyclic progress of flexural fatigue loading, the repeated tensile stress resulted in increasing the width of the cracks. That would lead to loss of the bond between fibers and matrix where degradation of crack-bridging strength took place. Simultaneously, an increase in the level of rebar strain over the fatigue life is achieved. Figure 7.62 shows an interesting linear constant relationship between the degradation of the crack-bridging strength and the evolution of the maximum rebar strain over the fatigue life regardless of the fatigue stress level, that it would be a helpful tool for design and assessment of SFRC structural beams under fatigue loading by controlling the rebar strain level through avoiding the brittle rupture of steel reinforcing bars.

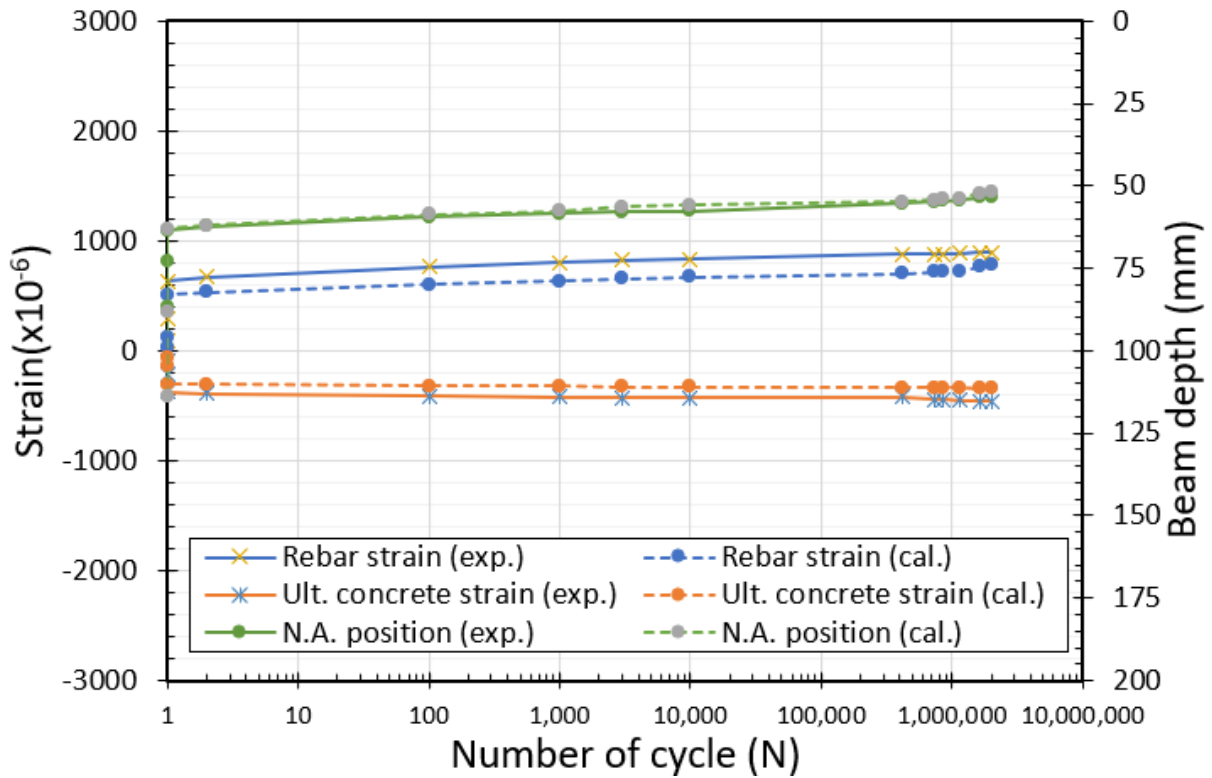


Fig. 7.57 Calculated versus experimental fatigue response of 5D_FBF_30 over the fatigue life.

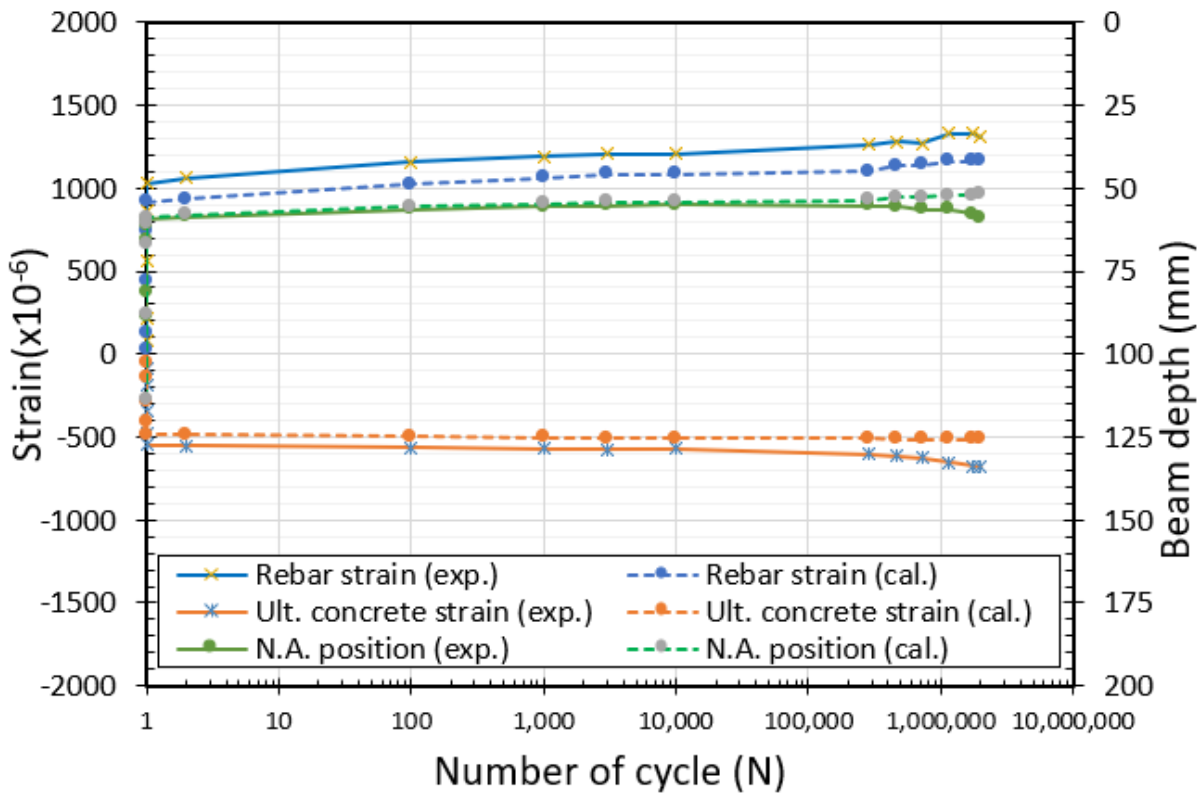


Fig. 7.58 Calculated versus experimental fatigue response of 5D_FBF_45 over the fatigue life.

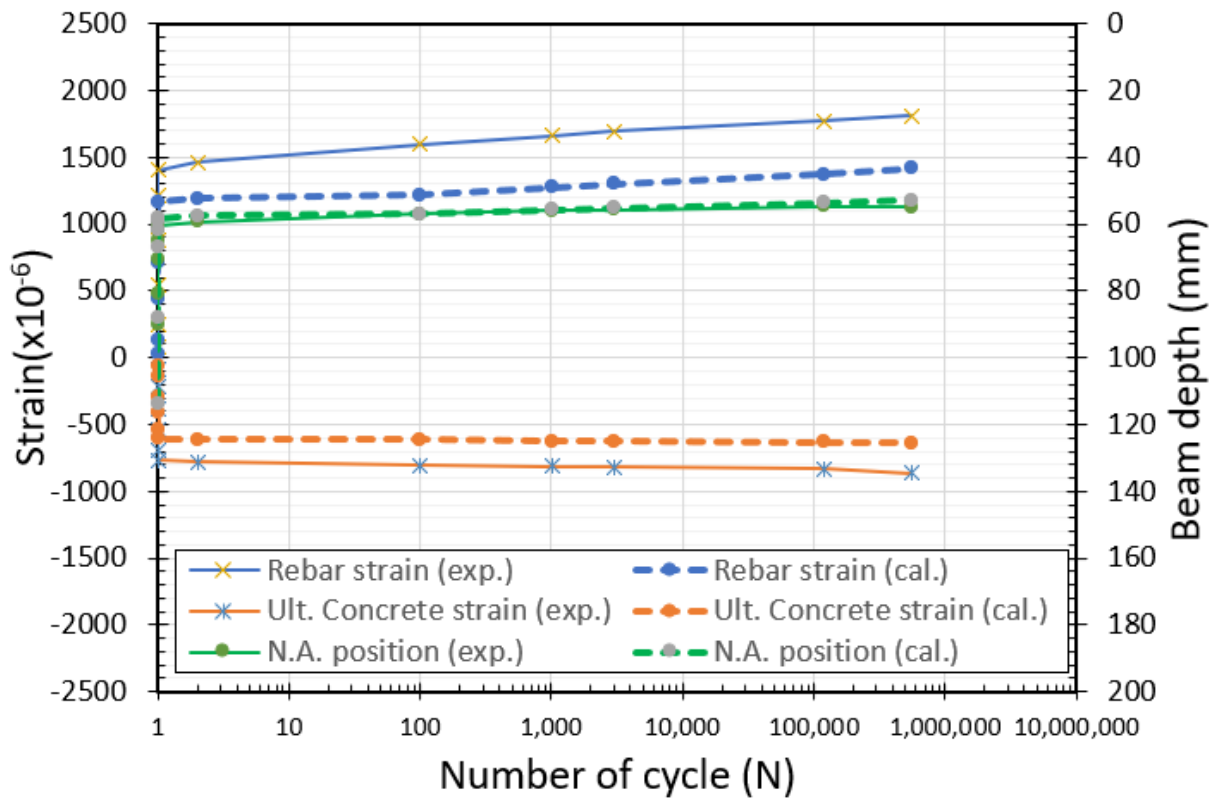


Fig. 7.59 Calculated versus experimental fatigue response of 5D_FBF_56 over the fatigue life.

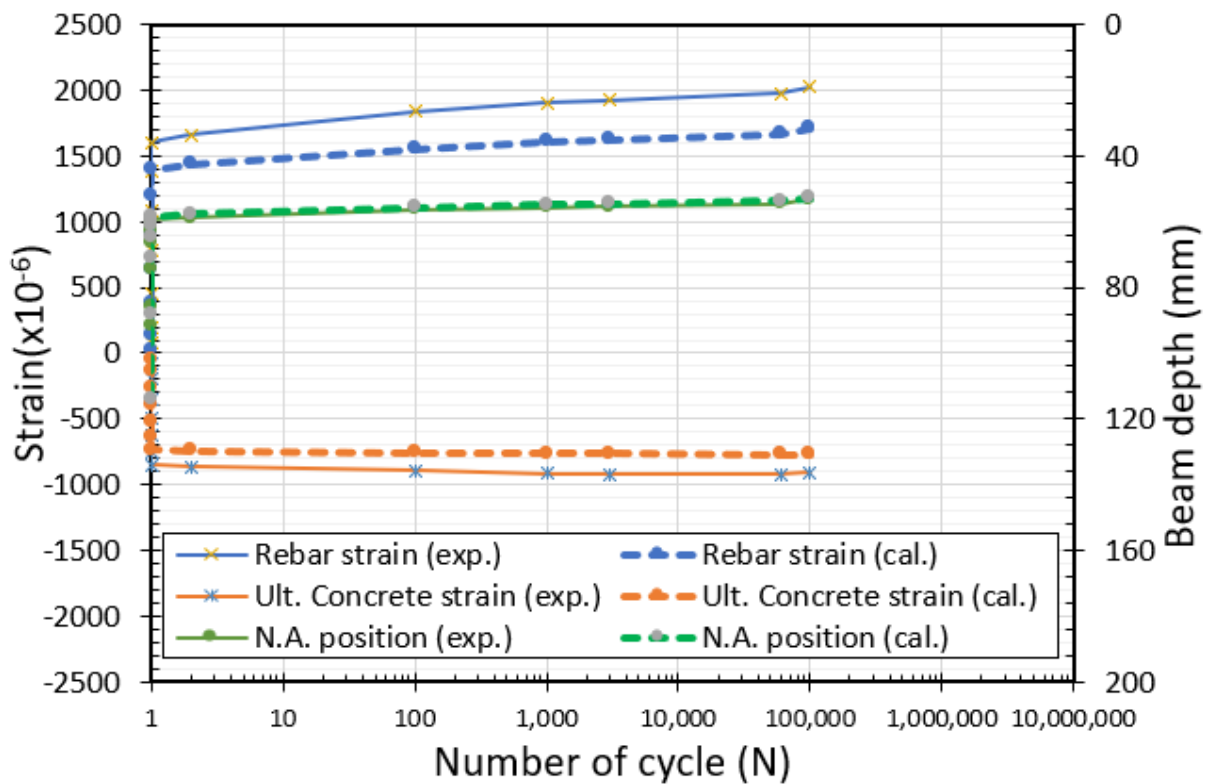


Fig. 7.60 Calculated versus experimental fatigue response of 5D_FBF_67 over the fatigue life.

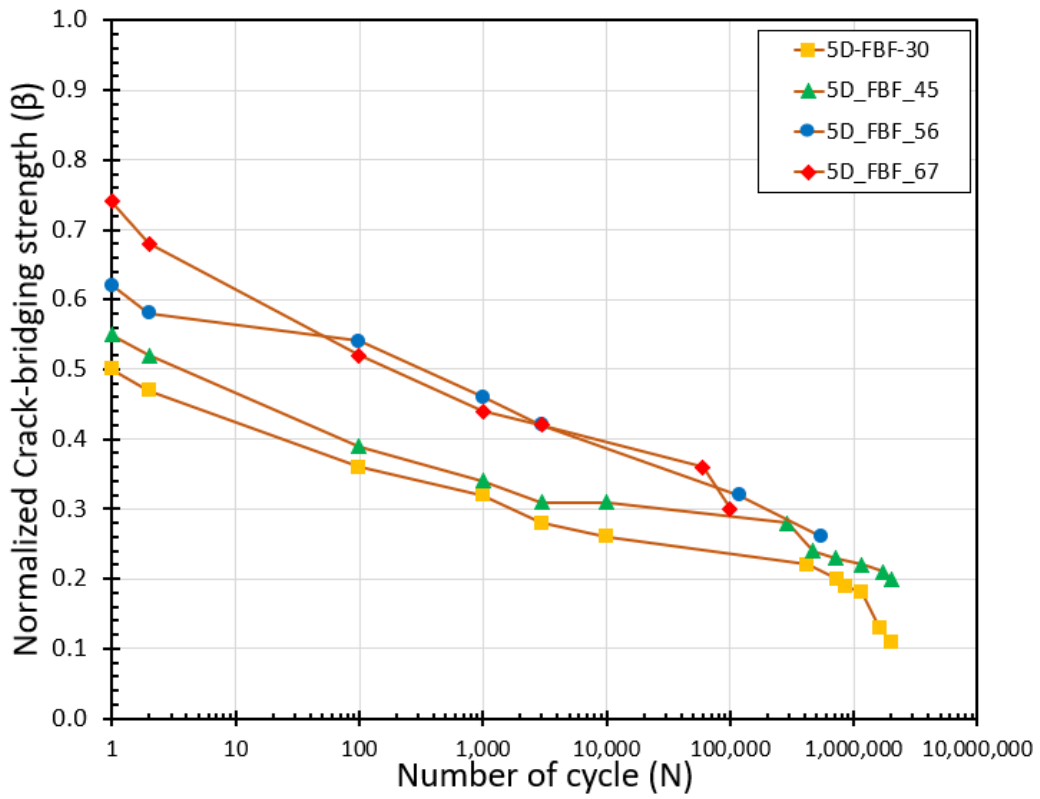


Fig. 7.61 Normalized crack-bridging strength degradation over the flexural fatigue life of the fourth series.

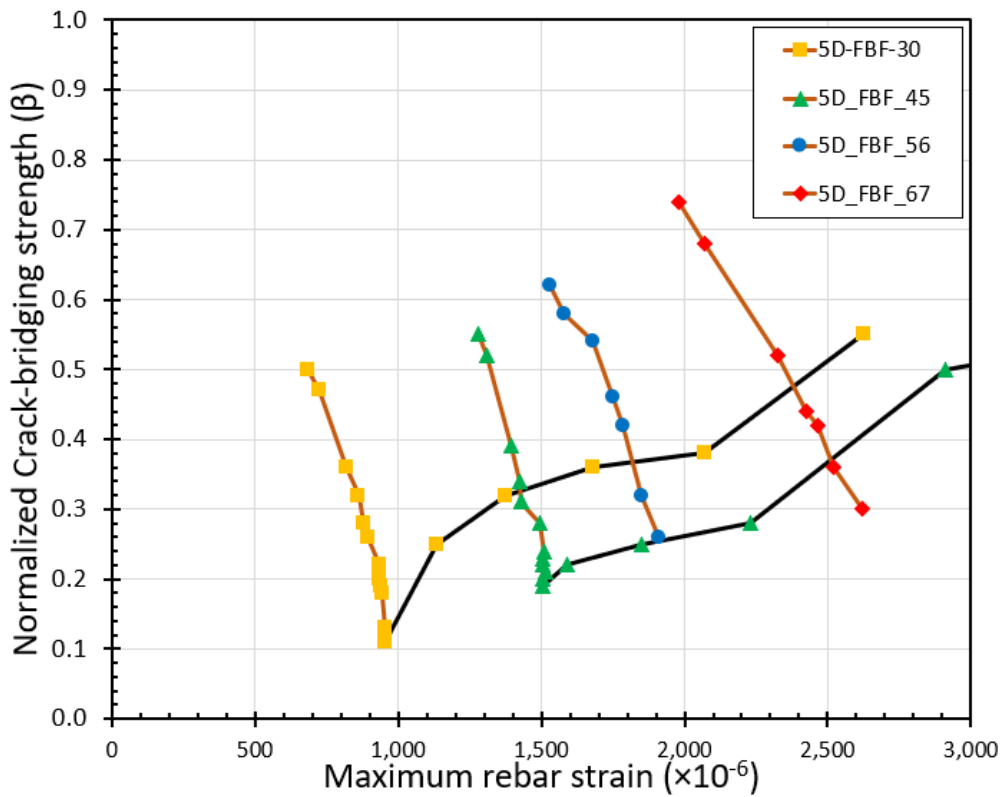


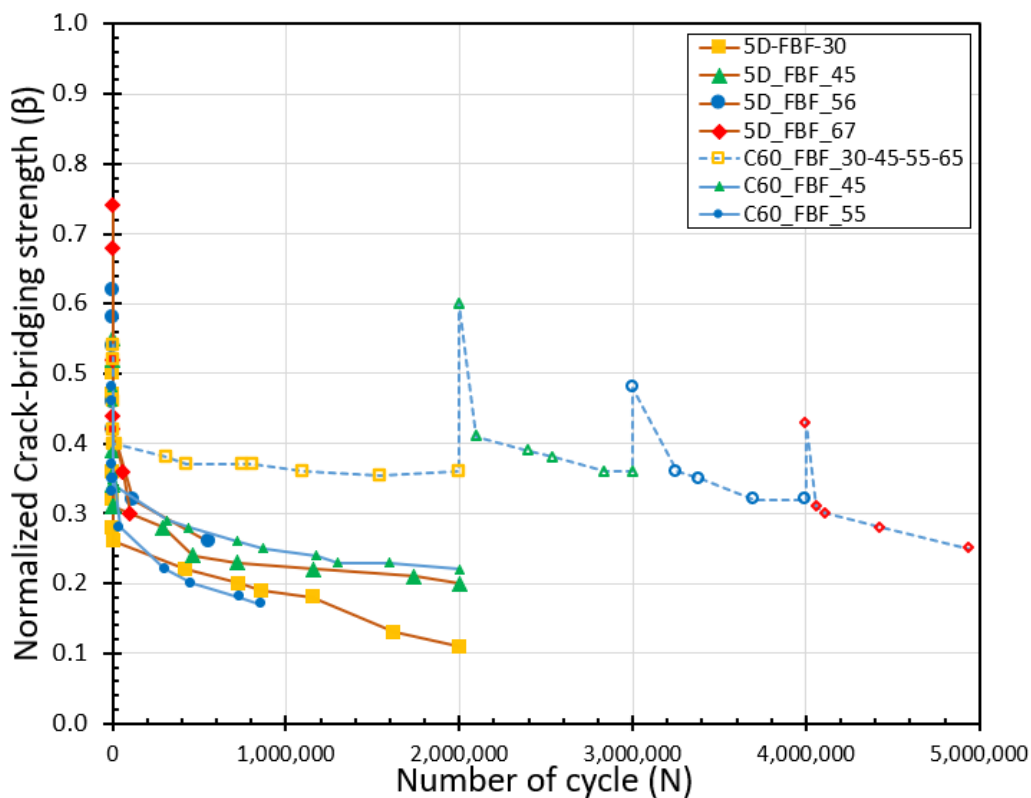
Fig. 7.62 Normalized crack-bridging strength degradation versus maximum rebar strain of the fourth series.

7.4.3 Evaluated Crack-bridging Strength of The fourth Series

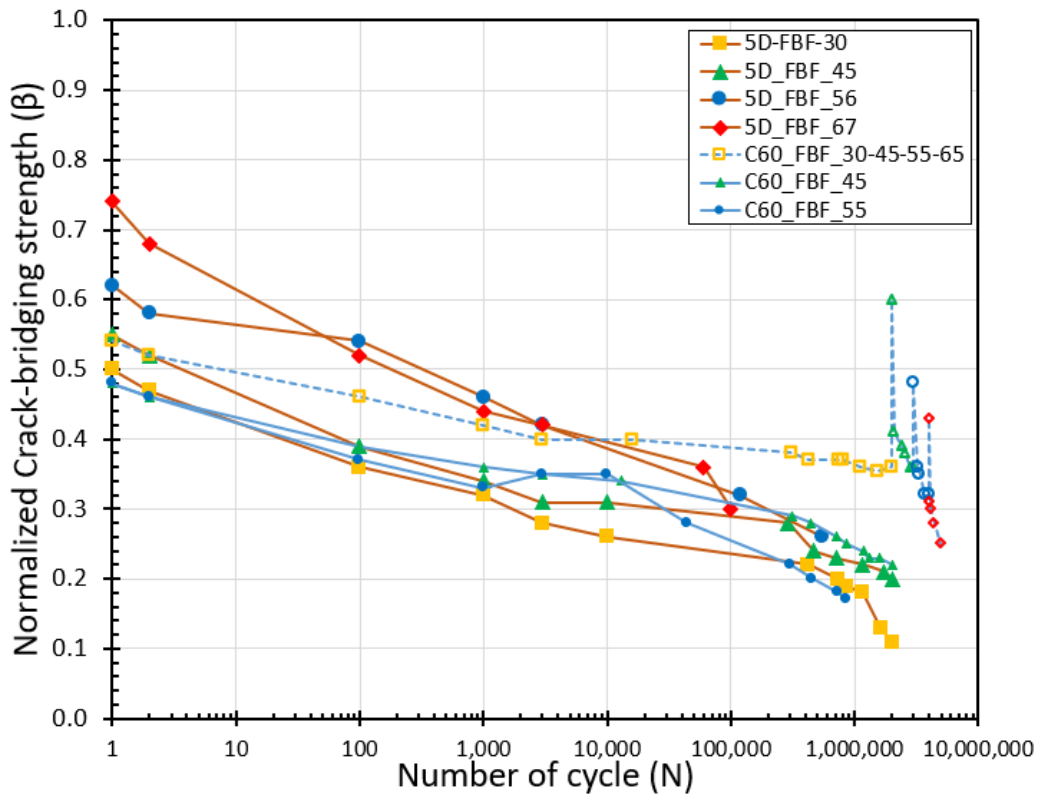
The normalized crack-bridging strength is derived using the inverse analysis calculation method for the fourth series and compared with the first and third series, testing the effect of higher concrete compressive strength with 1.0% volume fraction of double hooked-end steel fibers under single flexural fatigue load levels, illustrating the degradation of crack-bridging strength of the four SFRC structural beams – i.e. 5D_FBF_30, 5D_FBF_45, 5D_FBF_56, and 5D_FBF_67 – over the fatigue life and regarding the evolution of the maximum rebar strain level, as plotted in [Figs. 7.63, 7.64, 7.66, and 7.67](#). As well, the evolution process of the crack-bridging strength was captured while increasing the flexural load level monotonically after the end of the two million cycles. Besides, the crack-bridging strength degradation and evolution model derived from the fourth series was compared with the one derived from the first and third series, as shown in [Figs. 7.65, and 7.68](#). Finally, the proposed diagram of the crack-bridging strength degradation and evolution could be a useful relationship for the fatigue design and assessment of SFRC beams.

[Figures 7.63, 7.64, and 7.65](#) show a comparison of the evaluated crack-bridging strength degradation and evolution model over the fatigue life and regarding the evolution of the maximum rebar strain level between the SFRC structural beams for the fourth series, that using 1.0% volume fraction of the double hooked-end steel fibers with a higher concrete compressive strength, and the third series, that using 1.5% volume fraction of the single hooked-end steel fibers with a higher concrete compressive strength under the same fatigue load levels. The results show that SFRC beams of the fourth series have a higher degradation rate of the crack-bridging strength over the fatigue life under same various fatigue load levels, despite the higher tensile strength of the double hooked-end steel fibers, because of the lower volume fraction of the fibers at the tensile stress zone that resulting in the lesser contact surface between fibers and surrounding concrete and a faster loss of the bond at the fiber-matrix interface. However, at a higher fatigue load level – i.e. 5D_FBF_67 – where the maximum rebar strain level exceeds the yielding strain with a larger crack-width inside the constant moment region, the degradation rate became softer and it could be explained as the effect of the double level of the hooked that became more dominate at higher crack-width, as shown in [Figs. 7.64, and 7.65](#). Besides, the evolution rate of the crack-bridging strength did not change between the fourth and third series as it depends only on the damage level, as shown in [Fig. 7.65](#).

Figures 7.66, 7.67, and 7.68 show a comparison of the evaluated crack-bridging strength degradation and evolution model over the fatigue life and regarding the evolution of the maximum rebar strain level between the SFRC structural beams for the fourth series, that using 1.0% volume fraction of the double hooked-end steel fibers with a higher concrete compressive strength, and the first series, that using 1.5% volume fraction of the single hooked-end steel fibers with a normal concrete compressive strength under the same fatigue stress levels. The results show that SFRC beams of the fourth series have the same degradation rate of the crack-bridging strength over the fatigue life under various fatigue stress levels, despite the lower fiber's volume fraction of the double hooked-end steel fibers, because of the higher concrete compressive strength with a lower volume fraction of the fibers at the tensile stress zone that resulting in the same loss of the bond at the fiber-matrix interface during fatigue, as shown in Figs. 7.67, and 7.68. Besides, the evolution rate of the crack-bridging strength did not change between the fourth and first series as it depends only on the damage level, as shown in Fig. 7.65.



(a) Normal scale.



(b) Logarithmic scale.

Fig. 7.63 Normalized crack-bridging strength degradation over the fatigue life for the fourth and third series.

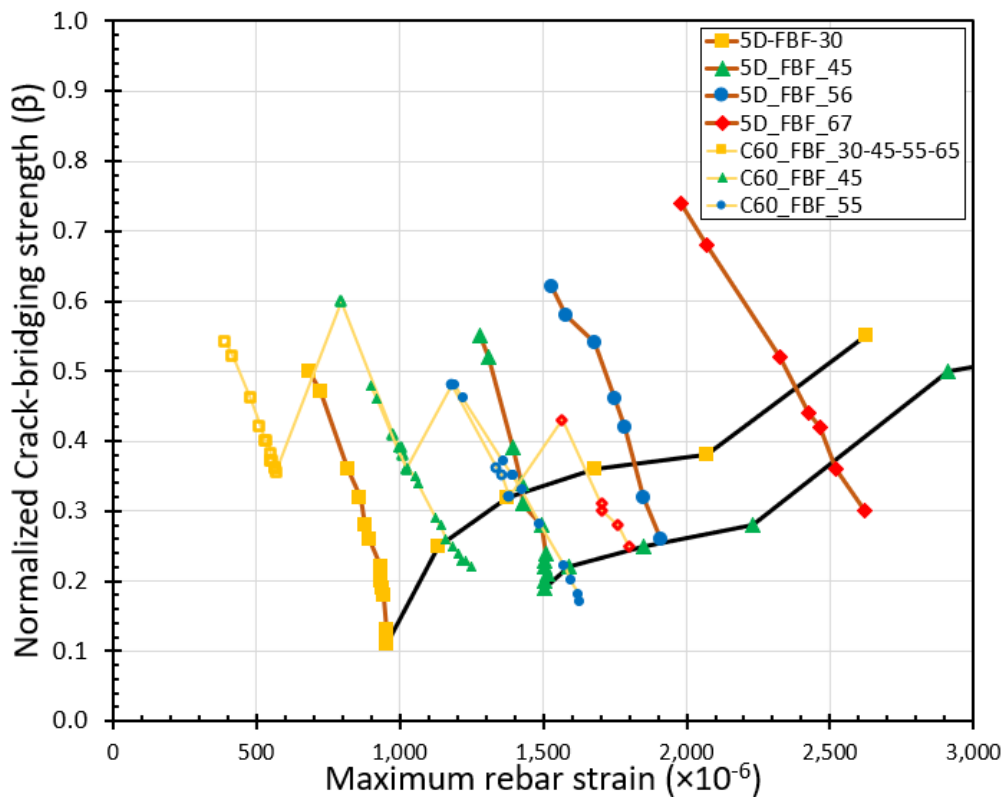


Fig. 7.64 Normalized crack-bridging strength degradation and evolution diagram versus maximum rebar strain for fourth and third series.

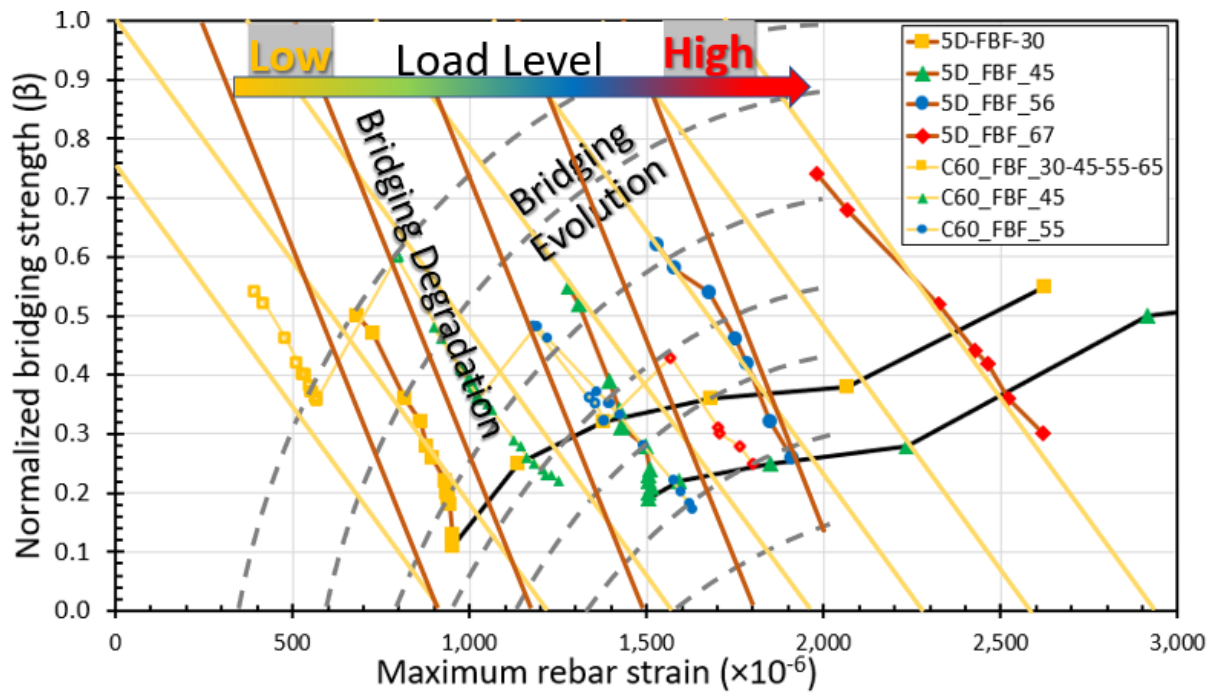
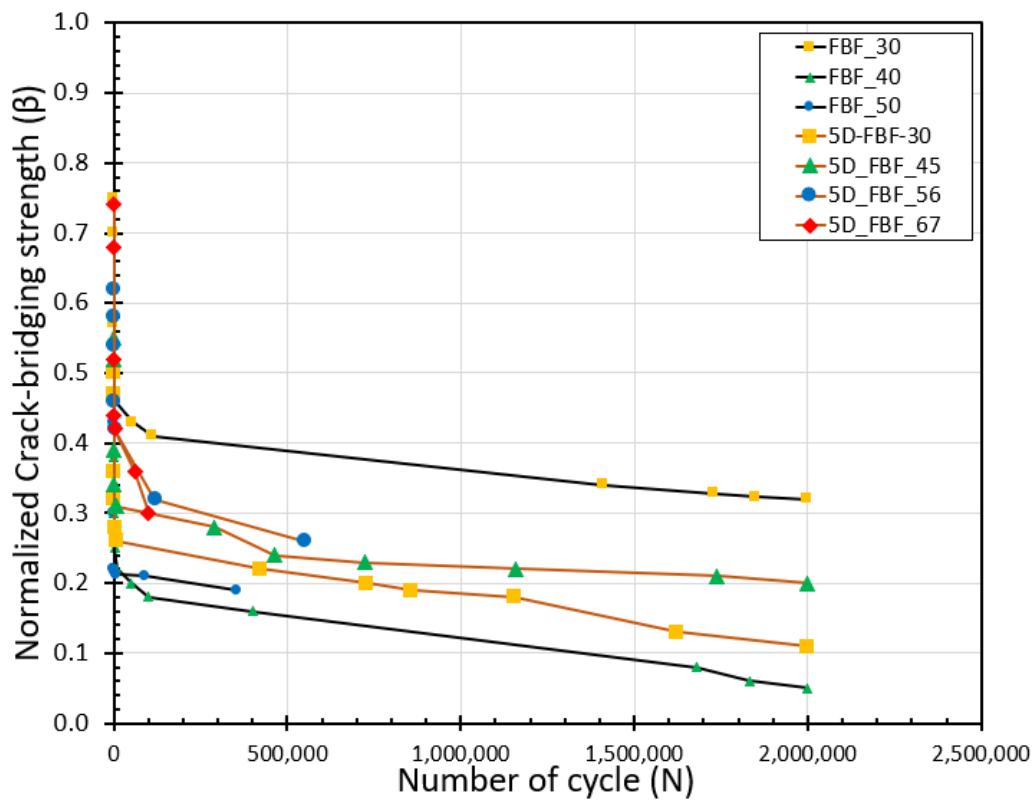
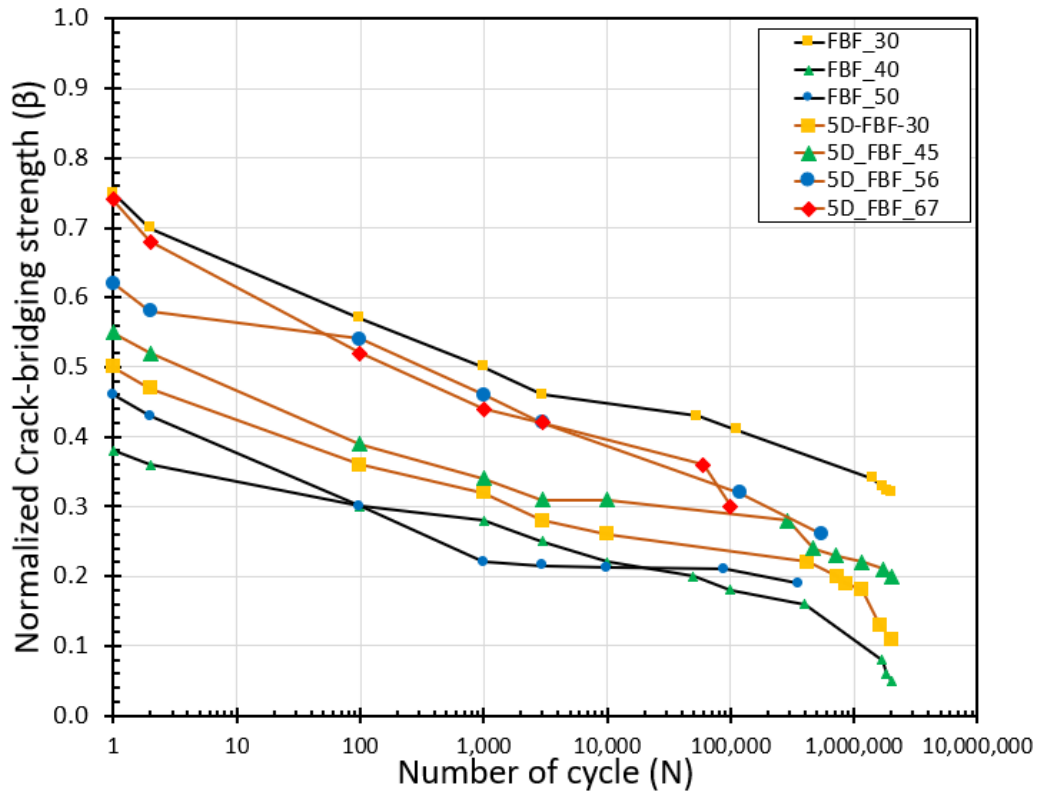


Fig. 7.65 Normalized crack-bridging strength degradation and evolution diagram versus maximum rebar strain for fourth and third series.



(a) Normal scale.



(b) Logarithmic scale.

Fig. 7.66 Normalized crack-bridging strength degradation over the fatigue life for the fourth and first series.

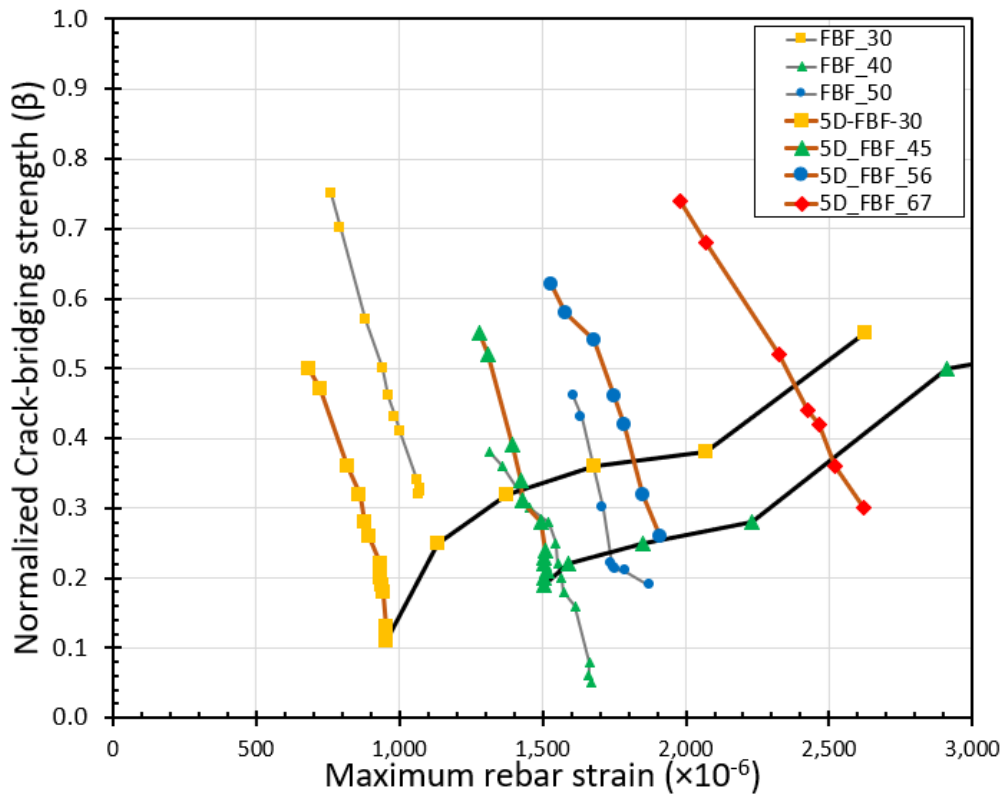


Fig. 7.67 Normalized crack-bridging strength degradation and evolution diagram versus maximum rebar strain for fourth and first series.

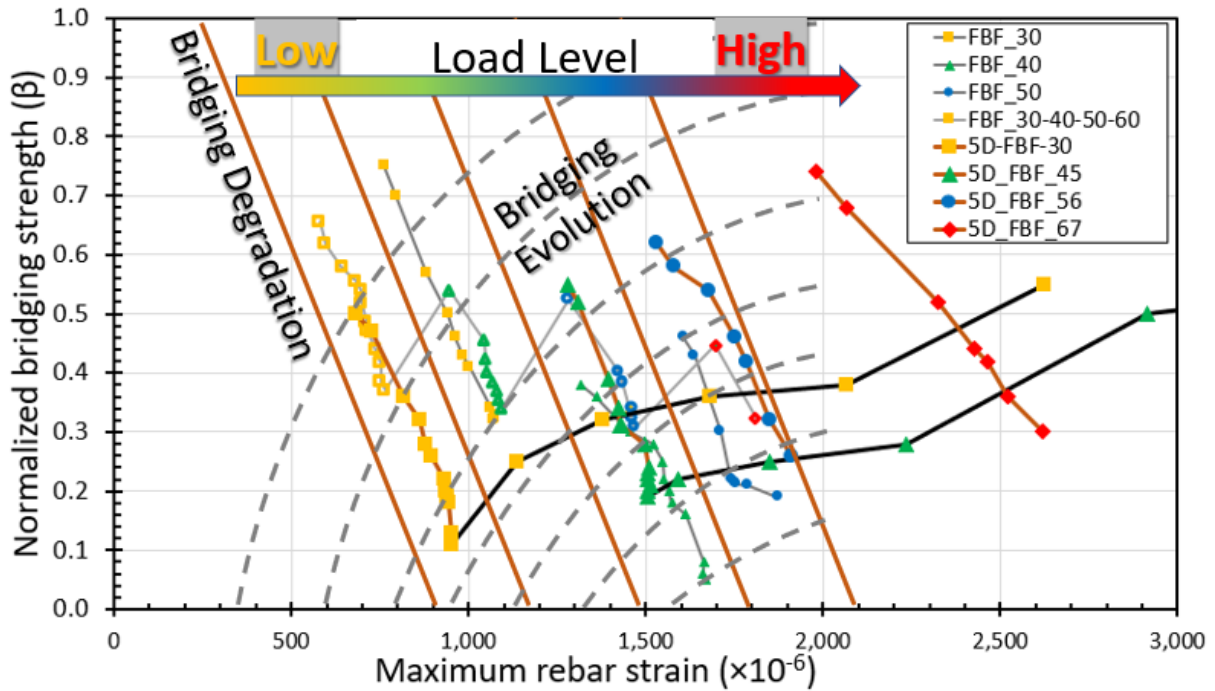


Fig. 7.86 Normalized crack-bridging strength degradation and evolution diagram versus maximum rebar strain for fourth and first series.

7.5 Conclusion

The research work of the fourth series presented in this chapter aimed at capturing the effect of double hooked-end steel fibers with a higher tensile strength using a higher concrete compressive strength on both static and fatigue flexural response of SFRC structural beams. Besides, the effect on the evaluated degradation and evolution crack-bridging strength model over the whole fatigue life of structural beams under cyclic loading with various flexural load levels until the end of the fatigue life was captured. An inverse analysis method is used to derive a degradation and evolution model for crack-bridging strength from the experimental fatigue response of SFRC structural beams. The degradation and evolution model was captured for a wide range of fatigue load levels and the main conclusions that can be drawn from this work are as follow:

1. An enhancement in the flexural static response of SFRC structural beams was achieved by incorporating 1.0% volume fraction of double hooked-end steel fibers with higher concrete compressive strength, resulting in a more ductile behavior and a greater load-bearing capacity, hence, lowering the mid-span deflection and stresses in the reinforcing bar and concrete.

2. Higher concrete compressive strength has a noticeable effect in the improvement of the bond strength at the fibers-matrix interface, thus leads to enhancement in the flexural static response having regard to the fiber's volume fraction and shape.
3. Incorporating a lower volume fraction of the double hooked-end steel fibers resulted in the same enhancement in the flexural static response as a higher volume fraction of the single hooked-end steel fibers because of the higher tensile strength and mechanical bond of double hooked-end steel fibers.
4. The good fit obtained with the proposed degradation and evolution model for the crack-bridging strength provided by double hooked-end steel fibers confirms the applicability of inverse analysis assuming a plane strain distribution since no strain redistributions in the compressive stress zone was observed.
5. The normalized crack-bridging strength was proposed for each different level of flexural fatigue stress of each SFRC structural beam during fatigue life, which monotonically changes by linearly degradation manner over the fatigue life and regarding the evolution of rebar strain level because of the loss of bond strength at fiber-matrix interface.
6. The normalized evaluated crack-bridging strength increased by increasing the flexural load level monotonically with the contribution of the new fibers in bridging the cracks inside the tensile stress zone and the contribution of the old fibers with the desired damage level, with almost the decreased inclination regarding the fatigue stress level and the bond damage level at the fiber-matrix interface.
7. The evaluated crack-bridging strength induced by a lower volume fraction double hooked-end steel fibers has a higher degradation rate over the fatigue life and regarding the evolution of the rebar strain level comparing to a higher volume fraction of single hooked-end steel fibers, emphasizing the effect of the fiber's volume fraction crossing the cracks in resisting the cyclic loading.
8. The evaluated crack-bridging strength induced by a lower volume fraction double hooked-end steel fibers with a higher concrete compressive strength has the same degradation rate over the fatigue life and regarding the evolution of the rebar strain level comparing to a higher volume fraction of single hooked-end steel fibers with a normal

concrete strength, emphasizing the balancing effect of the lower fiber's volume fraction with a higher concrete compressive strength that providing a higher bond strength at fiber-matrix interface.

9. Using the proposed degradation and evolution diagram of crack-bridging strength with the material constitutive laws based on direct sectional analysis calculations over of fatigue loading cycles, an accurate full design and assessment procedure for the whole fatigue life of SFRC beams under flexural fatigue loading is expected to be accomplished.

8 Conclusions

8.1 General Conclusions

This research focuses on the evaluation of the crack-bridging strength induced by steel fibers from the structural experimental response of SFRC beams subjected to cyclic loading using the sectional analysis calculations inversely. A review of the literature reveals that fatigue is a limiting design consideration for structures such as bridge girders, offshore installations, and railway sleepers. To enhance the fatigue performance of concrete, steel fibers appear to be a potential solution. A significant amount of research has been conducted with SFRC and it is acknowledged that steel fibers increase the fatigue performance of plain concrete; little was known, however, how steel fibers perform in structural members under fatigue loading. This research work aims to understand the degradation and evolution mechanism of the crack-bridging strength under a wide range of fatigue stress levels with constant and various amplitude cyclic loading through increasing or decreasing the maximum fatigue load levels over the whole fatigue life of SFRC structural beams with different material properties.

Despite its increased awareness in practice and research, however, SFRC has largely been limited to use in non-critical members such as in large warehouse slabs. For SFRC to be used regularly, a framework of material models identifying the key material parameters must be established. The most fundamental property when considering the design of a structural member manufactured with SFRC is its post cracking, or residual, tensile strength. After cracking, the behavior of SFRC can be most readily described in terms of its nominal stress versus crack opening displacement relationship describing how much fracture energy it had. However, this fracture energy was consumed during the application of the cyclic loading, that still an undiscovered area. The purpose of this research was to investigate a simplified flexural fatigue design and assessment recommendations of SFRC structural beams by proposing a

diagram for the crack-bridging strength degradation and evolution regarding the evolution of the rebar strain level over the fatigue life until the rupture fatigue failure of tested beams.

In chapter 3, a model for the evaluation of the crack-bridging strength degradation during cyclic loading is derived to obtain a rational understanding of the mechanical response of SFRC structural beams under flexural cyclic loading at each set of cycles over the whole fatigue life from the experimental fatigue response of SFRC structural beams. The basis of the model is inverse sectional analysis calculations using material and structural level tests. Material-level experimental tests are carried out to identify the mechanical and fracture properties of SFRC, with the results consequently used in the sectional analysis calculations. Also, structure-level experimental tests are carried out under fatigue bending loading, while simultaneously monitoring mid-span deflection, rebar strain, surface concrete strain, and neutral axis (N.A.) position. Finally, in the inverse analysis, certain levels of degradation in the crack-bridging strength in each set of cycles were derived during the fatigue life at maximum fatigue stress level through achieving a good fitting between the experimental and analytical fatigue response of SFRC beams.

In chapter 4, the influence of hooked-end steel fibers on the reinforced concrete structural beams subjected to flexural cyclic loading was examined, as well the inverse analysis method is used to evaluate the crack-bridging strength degradation over the fatigue life for SFRC structural beams. A degradation model for the crack-bridging strength is proposed over the fatigue life and also a model for that crack-bridging strength degradation is related to the evolution of the maximum rebar strain for several fatigue stress levels ranging from low, medium to high. The experimental program for the first series of NC and SFRC beams on material and structural scale under static and fatigue loading conditions is presented. The normalized crack-bridging strength, which is proposed for each different level of flexural fatigue stress of SFRC structural beams in the first series, monotonically linearly decreases with the evolution of rebar strain level for all fatigue stress levels, with almost same inclination regardless the fatigue stress level, that would be an interesting relationship simplifying the flexural fatigue design of SFRC beams.

In chapter 5, the influence of hooked-end steel fibers on the reinforced concrete structural beams subjected to flexural cyclic loading in bridging the crack's opening under several fatigue stress levels in an increasing or decreasing manner were examined. As well, this chapter aims

to understand the mechanism of crack-bridging strength evaluated from the inverse analysis calculation method based on changing the fatigue load levels in an increasing or decreasing manner. Furthermore, by the end of this chapter, a diagram of the crack-bridging strength degradation and evolution over the fatigue life of SFRC structural beams under flexural cyclic loading under several fatigue stress levels would be proposed based on inverse analysis calculation methods. The experimental program for the second series of two SFRC beams on the structural scale under fatigue loading conditions is presented.

On one hand, the results of the SFRC structural beam, that experienced increasing amplitude of the flexural cyclic loading by increasing the maximum flexural fatigue load level from low to high, was derived. The normalized crack-bridging strength tends to monotonically degrade under flexural fatigue loading over the fatigue life and decreases monotonically linearly regarding the evolution of rebar strain level for all fatigue stress levels, with almost the same inclination regardless of the fatigue stress level. The normalized evaluated crack-bridging strength increased by increasing the flexural load level monotonically with the contribution of the new fibers in bridging the cracks inside the tensile stress zone and the contribution of the old fibers with the desired damage level and with almost a decreased inclination regarding the fatigue stress level and the bond damage level at the fiber-matrix interface, resulting in an evolution model of crack-bridging strength.

On the other hand, the results of the SFRC structural beam, that experienced decreasing then increasing of the amplitude of the flexural cyclic loading by decreasing the maximum flexural fatigue load level from high to low then increasing again to high load level, was derived. The normalized crack-bridging strength tends to monotonically degrade under flexural fatigue loading over the fatigue life, except for if the SFRC beam was tested under a higher fatigue loading level in the fatigue loading history, where the crack-bridging strength tends to stabilize because of lower pullout force applied on fibers at the crack location with a higher damage level at the fiber-matrix interface, and with almost the same inclination regardless of the fatigue stress level. Further, The normalized evaluated crack-bridging strength increased by increasing the flexural load level monotonically, with decreased inclination regarding the fatigue stress level.

In chapter 6, the influence of changing material properties (i.e. concrete compressive strength and the beam's reinforcement ratio) on the flexural fatigue experimental response and the crack-bridging strength induced by hooked-end steel fibers on the reinforced concrete

structural beams subjected to a constant and increasing amplitude of flexural cycle loading were examined. As well, this chapter aims to understand the mechanism of crack-bridging strength evaluated from the inverse analysis calculation method based on changing the material properties under various fatigue load levels. Furthermore, by the end of this chapter, a diagram of the crack-bridging strength degradation and evolution over the fatigue life of SFRC structural beams under flexural cyclic loading regarding fatigue stress levels would be proposed based on inverse analysis calculation methods and to be compared with the one proposed in chapter 5. The experimental program for the third series of six SFRC beams on the structural scale under fatigue loading conditions is presented.

Increasing the concrete compressive strength enhanced the bond strength at fibers- matrix interface with lower mid-span deflection and rebar and concrete strain levels of SFRC structural beams under flexural cyclic loading over the fatigue life for a variable fatigue load levels. The increased concrete compressive strength resulted in a lower degradation rate of the evaluated crack-bridging strength regarding the evolution of maximum rebar strain. However, the evolution rate of the crack-bridging strength did not influence the increased concrete compressive strength.

Decreasing the ordinary bars reinforcement ratio degraded the structural stiffness of the tested beams with higher crack length at the cracked section and accelerated rate of rebar strain evolution of SFRC structural beams under flexural cyclic loading over the fatigue life for a variable fatigue load levels. The decreased reinforcement ratio resulted in a lower degradation rate of the evaluated crack-bridging strength regarding the evolution of maximum rebar strain. However, the evolution rate of the crack-bridging strength did not influence the decreased reinforcement ratio.

In chapter 7, the influence of double hooked-end steel fibers on the flexural static and fatigue experimental response was examined, and the crack-bridging strength induced by double hooked-end steel fibers with a lower volume fraction of 1.0 % and higher concrete compressive strength was evaluated on the reinforced concrete structural beams subjected to flexural static and cyclic loading under various fatigue stress levels. Furthermore, by the end of this chapter, a diagram of the crack-bridging strength degradation and evolution over the fatigue life of SFRC structural beams under flexural cyclic loading regarding fatigue stress levels was proposed based on inverse analysis calculation methods and to be compared with the one proposed for the second and third series in chapter five and six. As well, this chapter aims to

understand the mechanism of crack-bridging strength evaluated from the inverse analysis calculation method based on changing the fiber's shape and volume fraction under various fatigue load levels. The experimental program for the fourth series of six SFRC beams on the structural scale under static loading for two beams and fatigue loading with various constant amplitude for four beams is presented.

For the static loading conditions, an enhancement in the flexural static response of SFRC structural beams was achieved by incorporating 1.0% volume fraction of double hooked-end steel fibers with higher concrete compressive strength, resulting in a more ductile behavior and a greater load-bearing capacity, hence, lowering the mid-span deflection and stresses in the reinforcing bar and concrete. As, the higher concrete compressive strength has a noticeable effect in the improvement of the bond strength at the fibers-matrix interface, having regard to the fiber's volume fraction and shape. Further, incorporating a lower volume fraction of the double hooked-end steel fibers resulted in the same enhancement in the flexural static response as a higher volume fraction of the single hooked-end steel fibers because of the higher tensile strength and mechanical bond of double hooked-end steel fibers.

For the fatigue loading conditions, for the higher concrete compressive strength, the evaluated crack-bridging strength induced by a lower volume fraction double hooked-end steel fibers has a higher degradation rate over the fatigue life and regarding the evolution of the rebar strain level comparing to a higher volume fraction of single hooked-end steel fibers, emphasizing the effect of the fiber's volume fraction crossing the cracks in resisting the cyclic loading. Besides, the evaluated crack-bridging strength induced by a lower volume fraction double hooked-end steel fibers with a higher concrete compressive strength has the same degradation rate over the fatigue life and regarding the evolution of the rebar strain level comparing to a higher volume fraction of single hooked-end steel fibers with a normal concrete strength, emphasizing the balancing effect of the lower fiber's volume fraction with a higher concrete compressive strength that providing a higher bond strength at fiber-matrix interface.

Finally, after accomplishing this research work for a wide range of NC and SFRC under flexural static and fatigue loading varying the concrete compressive strength, ordinary bars reinforcement ratio, fiber's shape, and fiber's volume, the degradation and evolution diagrams of crack-bridging strength over the fatigue life were successfully proposed using the inverse analysis method based on the sectional analysis calculations. Using the proposed diagrams of crack-bridging strength with the material constitutive laws based on direct sectional analysis

calculations over of fatigue loading cycles, an accurate full flexural fatigue design and assessment procedure for the whole fatigue life of SFRC beams under flexural fatigue loading is expected to be accomplished.

8.2 Recommendations for the Further Study

Despite several decades of academic research, there are still a handful of challenges that lie ahead before SFRC can be used with confidence in routine design. Several key points stemming specifically from this study require further investigation.

It was observed that steel fibers improved the fatigue performance of reinforced concrete beams and the increase in fatigue performance is generally related to the increasing of the fiber's volume fraction, aspect ratio, material, and shape. This study was conducted at a specific volume fractions, and two steel fiber shapes, and a constant aspect ratio of steel fibers for a particular series of beams. To fully understand the crack-bridging strength degradation and evolution model of SFRC structural beams testing needs to be conducted. Further testing is recommended with variable reinforcing ratios, different fibers types, and varying fiber volumes fraction and aspect ratio.

Besides, it is well known that the brittleness of material may differ when the structural conditions change or when the elastic energy increases. The elastic energy is controlled by the volume of the structure. As such, larger structures are generally weaker, and their behavior is more brittle than geometrically scaled-down structures. This study was conducted at a specific structural beam size of steel fiber reinforced concrete for a particular series of beams. From the fracture mechanics point of view, it is imperative to understand the size's effect on the response of fiber in bridging the cracks during fatigue loading for cases of much larger scales of beams.

Furthermore, The research work was interested in the flexural fatigue behavior of the SFRC structural beams that were designed to fail in a ductile flexural failure mode and reinforced with only longitudinal steel bars without any shear reinforcement like stirrups. Hence, the practical industrial structural SRFC beams would have both upper and lower longitudinal bars and shear reinforcement also would fail in either flexural or shear or flexural-shear failure mode, which would affect the crack-bridging strength degradation and evolution mechanism induced by fibers at tensile stress zone during fatigue life. Further testing is recommended with a various

reinforcing arrangement using flexural and shear reinforcement, and varying the failure mode of the beams between flexural, shear, and flexural-shear failure.

Finally, the proposed diagram of the crack-bridging strength capturing the degradation and evolution mechanism induced by fibers over the fatigue life regarding the evolution of the rebar strain level would be a useful tool for the fatigue design and assessment of SFRC structures. As a result, for the design point of view, a validation work needs to be carried out by using such a simulation software i.e. finite element through modeling the tested beams under flexural fatigue and using the proposed diagram of the crack-bridging strength. As well, for the assessment point of view, a research work of the assessment of the rebar strain level inside the SFRC structure needs to be carried out from the surface concrete cracks width, which would be a helpful tool to connect the surface crack-width with the rebar strain level and the level of the crack-bridging strength level throughout the structural lifetime.

References

- Ali Amin, Tomislav Markic, R. Ian Gilbert, Walter Kaufmann. 2018. Effect of the boundary conditions on the Australian uniaxial tension test for softening steel fibre reinforced concrete. *Construction and Building Materials* 184: 215-28.
- Altun F, Haktanir T, Ari K. 2007. Effects of steel fiber addition on mechanical properties of concrete and RC beams. *Constr Build Mater*;21(3):654–61.
- Alwan, J.M., Naaman, A.E., and Guerrero, Z.A.P. 1999. Effect of mechanical clamping on the pullout response of hooked steel fibres embedded in cementitious matrices. *Concrete Science and Engineering* 1(1): 15-25.
- ASTM. ASTM C 1609. 2010. Standard test method for flexural performance of fiber-reinforced concrete: using beam with third-point loading. ASTM International, USA.
- Barnes RA, Mays GC. 1999. Fatigue performance of concrete beams strengthened with CFRP plates. *J Compos Constr*;3(2):63–72.
- Bentur A, Mindness S. 2007. *Fiber reinforced cementitious composites*. New York: Taylor & Francis.
- CEB, 1988. *Fatigue of concrete structures, state of the art report*, CEB Bulletin d'Information No. 188, Comité Euro-International du Béton, Lausanne.
- Charalambidi B, Rousakis T, Karabinis A. 2016. Fatigue behavior of large-scale reinforced concrete beams strengthened in flexure with fiber-reinforced polymer laminates. *J Compos Constr*;20(5):04016035-1–10.
- Denneman E, Kearsley EP, Visser AT. 2011. Splitting tensile test for fibre reinforced concrete. *Mater Struct*;44:1441–9.
- EN. EN 14651. 2007. Test method for metallic fibre concrete – measuring the flexural tensile strength (limit of proportionality (LOP), residual). European Committee for Standardization, B-1050 Brussels.
- Fib, 2013. “fib Model Code 2010”, fib Bulletin No. 65/66. Federation Internationale du Béton, Ernst & Sohn, Berlin, Germany, pp: 402.
- Gao L, Hsu TCC. 1998. Fatigue of concrete under uniaxial compression cyclic loading. *ACI Mater J*;95(5):575–81.

- Goel S, Singh SP. 2014. Fatigue performance of plain and steel fibre reinforced self compacting concrete using S-N relationship. *Eng Struct*;74:65-73.
- Gribniak V, Kaklauskas G, Kacianauskas R, Kliukas R. 2012. Improving efficiency of inverse constitutive analysis of reinforced concrete flexural members. *Sci Res Essays*;7:923-38.
- Heffernan PJ, Erki MA, DuQuesnay DL. 2004. Stress redistribution in cyclically loaded reinforced concrete beams. *ACI Struct J*;101(2):261–68.
- Holmen, J.O. 1982. Fatigue of concrete by constant and variable amplitude loading, *Fatigue of Concrete Structures*, ACI Special Publication 75, S.P. American Concrete Institute, Detroit, pp: 71-110.
- Horii H, Shin HC, Pallewatta TM. 1992. Mechanism of fatigue crack growth in concrete. *Cem Concr Compos*;14:83–9.
- JCI-S-001-2003. 2003. Method of Test for Fracture Energy of Concrete by Use of Notched Beam. Japan: JCI.
- Johansson U. 2004. Fatigue test and analysis of reinforced concrete bridge deck models. Stockholm, Sweden: Royal Institute of Technology.
- Kaklauskas G, Ghaboussi J. 2001. Stress-strain relations for cracked tensile concrete from RC beam tests. *J Struct Eng*;127(1):64–73.
- Kaklauskas G, Gribniak V. 2012. Deriving stress–strain relationships for steel fibre concrete in tension from tests of beams with ordinary reinforcement. *Eng Struct*;42:387–95.
- Kaklauskas G, Gribniak V. 2011. Eliminating shrinkage effect from moment-curvature and tension-stiffening relationships of reinforced concrete members. *ASCE J Struct Eng*;137:1460-9.
- Kaklauskas G. 2004. Flexural layered deformational model of reinforced concrete members. *Mag Conc Res*;56:575–84.
- Kolluru SV, O’Neil EF, Popovics JS, Shah SP. 2000. Crack propagation in flexural fatigue of concrete. *J Eng Mech*;126(9):891–8.
- Kolluru, S. V., O’neil, E. F., Popovics, J. S. and Shah, S. P. 2000. Crack propagation in flexural fatigue of concrete, *Journal of Engineering Mechanics*, ASCE, Vol. 126, pp: 891-898.
- Kormeling HA, Reinhardt HW, Shah SP. 1980. Static and fatigue properties of concrete beams reinforced with continuous bar and with fibers. *ACI J Proc*;77(1):36–43.
- Lee MK, Barr BIG. 2004. An overview of the fatigue behavior of plain and fibre reinforced concrete. *Cem Concr Compos*;26(4):299-305.
- Lee S, Cho J, Vecchio FJ. 2013. Tension-stiffening model for steel fiber-reinforced concrete containing conventional reinforcement. *ACI Struct J*;110:639–48.
- Lee SC, Cho JY, Vecchio FJ. 2011. Model for Post-Yield Tension Stiffening and Rebar Rupture in Concrete Members. *Eng Struct*;33(5):1723–33.

- Li, V.C. 2002. Large volume, high performance applications of fibres in civil engineering". *Journal of Applied Polymer Science*; 83: 660-686.
- Liu F, Zhou J. 2018. Experimental research on fatigue damage of reinforced concrete rectangular beam. *Ksce J Civil Eng*;1:1-12.
- Loo KYM, Foster SJ, Smith ST. 2012. Fatigue behaviour of carbon fiber-reinforced polymer-repaired corroded reinforced concrete beams. *ACI Struct J*;109(6):795–803.
- Mallet, G.P., 1991. *Fatigue of reinforced concrete*, Her Majesty's Stationery Office, London.
- Meda A, Minelli F, Plizzari GA. 2012. Flexural behaviour of RC beams in fibre reinforced concrete. *Compos Part B: Eng*;43(8):2930–7.
- Montaignac RD, Massicotte B, Charroon J. 2012. Design of SFRC structural elements: flexural behaviour prediction. *Mater struct*;45:623–36.
- Moss, D. S. 1982. Bending fatigue of high yield reinforcing bars in concrete, TRRL Report SR748. Transport and Road Research Laboratory, UK.
- Olivito RS, Zuccarello FA. 2010. An experimental study on the tensile strength of the steel fibre reinforced concrete. *Compos: Part B*;41(1):246-255.
- Otter DE, Naaman AE. 1988. Properties of steel fiber reinforced concrete under cyclic loading. *ACI Mater J*;85:254–61.
- Özcan DM, Bayraktar A, Şbahin A, Haktanir T, Türker T. 2009. Experimental and finite element analysis on the steel fibre-reinforced concrete beams ultimate behavior. *Constr Build Mater*;23(2):1064–77.
- Parvez A, Foster SJ. 2015. Fatigue behavior of steel-fiber-reinforced concrete beams. *J Struct Eng*;141(4):04014117-1–8.
- RILEM. RILEM TC 162-TDF. 2002. Test and design methods for steel fibre reinforced concrete, σ - ϵ design method. *Mater Struct*;35,:579–82.
- Rots, J.G., and de Borst, R. 1989. Analysis of concrete fracture in 'direct' tension. *International Journal of Solids and Structures* 25(12): 1381-1394.
- Schläfli M, Brühwiler E. 1998. Fatigue of existing reinforced concrete bridge deck slabs. *Eng Struct*;20(11):991–8.
- Singh SP, Ambedkar BR, Mohammadi Y, Kaushik SK. 2008. Flexural fatigue strength prediction of steel fibre reinforced concrete beams. *Elect J Struct Eng*;8:46-54.
- Singh, S. P., Mohammadi, Y. and Madan, S. K., 2006. Flexural fatigue strength of steel fibrous concrete containing mixed steel fibres, *Journal of Zhejiang University*, Vol. 7, No. 8, pp: 1329-1335.
- Su-Tae K, Yun L, yon-dong P, jin-Keun K. 2010. Tensile fracture properties of an ultra high performance fiber reinforced concrete (UHPFRC) with steel fiber. *Compos Struct*;92:61–71.
- Tejchman J, Kozicki J. 2010. *Experimental and theoretical investigations of steel fibrous concrete*. Berlin: Springer.

- Tilly, G. P. 1988. Durability of concrete bridges, *Journal of the Institution of Highways and Transport*, Vol. 35, pp: 10-19.
- Tong LW, Liu B, Qian QJ, Zhao XL. 2016. Experimental study on fatigue behavior of steel reinforced concrete (SRC) beams. *Eng Struct*;123:247–62.
- Van Mier, J.G.M. 1997. *Fracture processes of concrete: assessment of material parameters for fracture models*. CRC Press, Boca Raton, Florida, USA., 448 pp.
- Van Mier, J.G.M., 2013. *Concrete fracture-a multiscale approach*. Taylor & Francis, New York. pp. 22-28 and 161-162.
- Zanuy C, Fuente P, Albajar L. 2007. Effect of fatigue degradation of the compression zone of concrete in reinforced concrete sections. *Eng Struct*;29(11):2908–20.
- Zanuy, C., Albajar, L. and Fuente, P., 2009. Sectional analysis of concrete structures under fatigue loading, *ACI Structural Journal*, Vol.106, No. 5, pp: 667-677.
- Zhang J, Stang H, Victor C LI. 2000. Experimental study on crack bridging in FRC under uniaxial fatigue tension. *J Mater Civ Eng*;12(1):66–73.
- Zhou, B., Uchida, Y. 2013. Fiber orientation in ultra-high-performance fiber reinforced concrete and its visualization, *Proceeding of the 8th International Conference on Fracture Mechanics of Concrete and Concrete Structures (FraMCoS-8)*, 2013, pp.217-224.
- Zollo, R.F. 1997. Fiber-reinforced concrete: an overview after 30 years of development, *Cement and Concrete Composites* 1997, Vol. 19, No. 2, pp: 107–122.